

Detection of Perfluoroalkyl Compounds  
with Polyvinylidene Fluoride Coated  
Optical Fibre

**Fairuza Faiz**

**A thesis submitted in fulfilment of the  
requirement for the degree of Doctor of  
Philosophy**



**Institute for Sustainable Industries  
and Liveable Cities**

**Victoria University**

**October, 2019**

## Abstract

Perfluoroalkyl substances (PFAS) are a class of man-made chemicals with many uses from fire-fighting foams to surface coatings and other industrial applications. In recent years, PFAS have gained considerable attention within the scientific community and the global media alike. Due to their strong chemical bonds, PFAS are inherently non-biodegradable and therefore persist in the environment. Listed in the Stockholm Convention of Persistent Organic Pollutants, these chemicals have been linked to various health issues in both humans and animals, lately, which are resulting in millions of dollars' worth of expenses in health care and compensation for the governments of affected countries every year. In addition, the cost of cleaning up PFAS from the environment along with these human costs exceeds \$50 billion in Europe alone.

There is an urgent need for a portable sensing system to detect PFAS in the environment, including the most common types, perfluorooctanoic acid (PFOA) and perfluorooctane sulphonate (PFOS). At present, the methods available to accurately measure the concentration of PFAS in contaminated samples involve field sampling followed by laboratory-based, time consuming analytical techniques, such as liquid/gas chromatography and tandem mass spectrometry that are unsuitable for real-time field measurements. Existing portable systems have not yet attained the precision of the analytical methods and face challenges in field tests due to various limitations, including lack of specificity, cross sensitivity to environmental conditions and generation of toxic waste. Therefore, this research has focused on providing a proof of principle of a Fabry-Perot Interferometry (FPI) based optical fibre sensor for *in situ* detection of PFOA in aqueous solution. It has aimed at characterizing the potential of the envisioned PFAS

sensing technique to obtain accurate and real time measurements. The proposed research capitalised on the numerous practical advantages offered by optical fibre sensors and the ability of an integrated polyvinylidene fluoride (PVDF) coating at the fibre end-face to respond to the presence of PFOA. To the best of the author's knowledge, PVDF was experimentally shown to respond to the emerging contaminants for the first time in this work.

A novel approach of forming a thin PVDF film (or Fabry-Perot etalon) on an optical fibre end-face was developed and thoroughly characterized. The thermoplastic polymer PVDF, known for its many useful characteristics such as hydrophobicity, corrosion resistance and ferroelectricity, was considered a robust sensor material based on its performance related to water filtration membranes and other engineering applications. This work has reported the synthesis of optimized coating on optical fibres through the immersion precipitation technique and has discussed subsequent experiments with the fabricated PFAS detector that demonstrated reproducible changes in the FPI spectrum in the presence of PFOA.

Successful detection of analytes or their change in concentration was denoted by spectral shifts on the obtained FPI reflection spectra. A variation in the optical path difference (OPD) determined through numerical modelling provided a measure of sensitivity of the FPI based system to the different PFOA solutions. Analytical tests confirmed that PVDF adsorbs PFOA by measuring the concentration of PFOA in solution before and after a PVDF film was immersed for several hours. Visual evidence in the form of scanning electron microscopic images also displayed differences in the surface structures of PVDF thin films that were exposed to PFOA. These results supported the inference that the changes in OPD were due to the adsorption of PFOA on the PVDF coated optical fibre.

In addition to the solutions containing known amounts of PFOA, real industrial solutions containing residual fire-fighting foam from fire trucks were tested and showed successful detection at low levels. In this case, the solutions contained a mixture of PFOA and PFOS with a range of other PFAS compounds that are typically used in these foam formulations.

Further investigation involving alternative optical methods employing refractive index-based measurement utilizing an etched fibre Bragg grating (EFBG) and also a bare optical fibre, showed spectral response to change in PFOA concentration in solution. A shift in the EFBG spectrum due to change in PFOA concentration in the solution in which PVDF membranes had been soaked indicated that the analyte was adsorbed by the polymer. Similarly, a change in the reflection intensity of the signal obtained by a bare fibre end-face in the PFOA solution due to a change in its refractive index, indicated the adsorption of the fluoro surfactant on the PVDF thin film.

Following the confirmation of PFOA uptake by PVDF, functionalization of the polymer was also investigated, which revealed that the incorporation of zeolites into PVDF enables more PFOA from aqueous solution to be adsorbed onto the thin film. Fourier transform infrared spectroscopy was used to highlight structural differences in the doped coatings, whereas energy dispersive x-ray spectroscopy was used to show compositional differences between the doped and non-doped PVDF thin films. Thus, this research contributed to the prospect of developing a functionalized sensor for more efficient detection of PFAs while also creating opportunities for further research in water treatment.

A temperature characterization test, which was undertaken to eliminate possible signal cross-sensitivity effects, also indicated that the PVDF coated fibre can be considered for

thermometric applications due to its good repeatability and linearity of the measurements over a specified temperature range. More importantly, information gathered from the undertaken characterization test was used to optimize the PFOA sensing protocol in order to obtain reliable results.

This research has provided experimental evidence to support that a PVDF coated optical fibre can be used as a potential portable PFAS detector. It has demonstrated a novel and simple thin film fabrication and optimization process for selective detection of the emerging contaminant PFOA. Furthermore, by combining an interferometry type optical fibre sensing technology with aqueous PFAS detection this research has established the foundation for future studies that can lead to commercialisation of a portable PFAS sensor for wide-ranging environmental and engineering applications.

## **Acknowledgements**

I begin by acknowledging and thanking Allah, the Most Gracious and the Most Merciful for all His favours upon me. I would like to take this opportunity to express how truly grateful I am to my parents, teachers and friends for their incredible contributions in my life.

My utmost gratitude goes to my loving parents who gave me the best education and supported me in all my endeavours. After them, I would like to thank my supervisors, whose guidance was crucial for my success in obtaining the doctoral degree. My sincere gratitude goes to, Dr. Fotios Sidirolou and Dr. Marlene Cran for being the most amazing mentors. Their unwavering support and expert advice helped me pass through trying times with ease and provided the strength to achieve all the milestones for obtaining a PhD effortlessly. I am extremely thankful to Dr. Fotios Sidirolou for training me in the optics lab, his thorough evaluation of my work, constant encouragement and prompt feedback on any issue I presented him with. I am also obliged to him for all the sessional work opportunities he provided me over the years. At the same time, I am immensely grateful to Dr. Marlene Cran for helping me learn about different types of spectroscopic techniques, analytical methods and data interpretation processes among numerous other things including editing my thesis. Her expert suggestions were vital in achieving project goals and overcoming technical hurdles. I am truly grateful for all the assistance she has provided me in every aspect of my research work.

I would also like to thank Professor Stephen Collins and Professor Gregory Baxter for being my additional supervisors, and for their invaluable advice and feedback on my work, which helped me improve my research methods and writing skills. It was a great

pleasure to learn from them. Additionally, I would like to acknowledge Professor Collins for giving me the first break in sessional teaching.

I acknowledge Victoria University for the scholarship and financial support that I have received for undertaking this research and thank all the academic, technical and administrative staff who have facilitated my work and the successful completion of my thesis.

Last but not the least, I would like to thank my family, relatives and friends without whose unconditional support, love and prayers I would never have made it this far. I express my everlasting gratefulness to my loving parents, siblings and their wonderful spouses for selflessly supporting me and always being there when I needed them. I thank all my friends and colleagues in Australia and overseas, who wholeheartedly encouraged me to do my best and sincerely helped me whenever I needed any form of assistance. I also earnestly thank the family of my friend who helped me settle in Melbourne. In addition to this, I acknowledge the contribution of every single person who directly or indirectly motivated me to achieve my goals and facilitated my work.

## **Declaration by Author**

I, Fairuza Faiz, declare that the PhD thesis entitled “Detection of Perfluoroalkyl Compounds with Polyvinylidene Fluoride Coated Optical Fibre” is no more than 100,000 words in length including quotes and exclusive of tables, figures, appendices, bibliography, references and footnotes. This thesis contains no material that has been submitted previously, in whole or in part, for the award of any other academic degree or diploma. Except where otherwise indicated, this thesis is my own work.

Signature:



Date: 25.10.2019

## Nomenclature

Symbol	Name	Unit
$\theta_c$	Critical angle	°
$\lambda$	Wavelength	nm
L	Thickness of film	nm
I	Reflected intensity	dB
v	Velocity	m/s
B	Magnetic field	T
z	Charge	C
r	Radius	m
$\phi$	Phase difference	rad
$R^2$	Variance	-
T	Temperature	°C

## Abbreviations

AFFF	Aqueous Film Forming Foam
APCI	Atmospheric Pressure Chemical Ionization
APPI	Atmospheric Pressure Photo Ionization
Butvar	Polyvinyl butyral
CVD	Chemical Vapour Deposition
DMF	N,N-dimethylformamide
DoEE	Department of Environment and Energy
EFBG	Etched Fibre Bragg Grating
ESI	Electrospray Ionization
FBG	Fibre Bragg Grating
FFPI	Fibre Optic Fabry-Perot Interferometry (or Interferometric)
FPI	Fabry-Perot Interferometry, Fabry-Perot Interferometer
FTIR	Fourier Transform Infrared
GC-MS	Gas Chromatography-Mass Spectrometry

HEPA	Heads of Environment Protection Authority
HPLC	High Performance Liquid Chromatography
IP	Immersion Precipitation
LbL	Layer by layer
LC–MS	Liquid Chromatography Mass Spectrometry
MALDI	Matrix Assisted Laser Desorption Ionization
MEK	Methyl Ethyl Ketone
MIP	Molecularly Imprinted Polymer
MALDI	Matrix Assisted Laser Desorption Ionization
NEMP	National Environment Management Plan
OFS	Optical Fibre Sensor
OPD	Optical Path Difference
OSA	Optical Spectrum Analyser
OFS	Optical Spectrum Analyser
PEC	Photoelectrochemical
PFA	Perfluoroalkyl
PFAS	Perfluoroalkyls
PFOA	Perfluorooctanoic acid
PFOS	Perfluorooctane sulphonate
PTFE	Polytetrafluoroethylene
PVD	Physical Vapour Deposition
PVDF	Polyvinylidene fluoride
RI	Refractive Index
SEM	Scanning Electron Microscope
SMF	Single Mode Fibre
ToF	Time of Flight

# TABLE OF CONTENTS

<b>Abstract</b> .....	<b>i</b>
<b>Acknowledgements</b> .....	<b>v</b>
<b>Declaration by Author</b> .....	<b>vii</b>
<b>Nomenclature</b> .....	<b>viii</b>
<b>Table of Contents</b> .....	<b>x</b>
<b>List of Figures</b> .....	<b>xiii</b>
<b>List of Tables</b> .....	<b>xvi</b>
<b>List of Publications/Presentations</b> .....	<b>xvii</b>
<b>1 Introduction</b> .....	<b>1</b>
1.1 Prelude .....	1
1.1.1 PFAS Exposure .....	2
1.1.2 Current PFAS Detection Methods.....	5
1.2 Optical Fibre Sensors .....	11
1.3 Research Hypothesis and Significance .....	13
1.4 Research Aims and Objectives .....	15
1.5 Thesis Outline .....	17
<b>2 Literature Review</b> .....	<b>19</b>
2.1 Overview.....	19
2.2 Optical Fibres: General Information .....	19
2.3 Optical Fibres: Fabrication Process .....	23
2.4 Optical Fibres: Application.....	26
2.4.1 Types of Optical Fibre Sensors .....	27
2.4.2 Interferometry Type Optical Fibre Chemical Sensors.....	30
2.4.3 Fibre Optic Fabry-Perot Interferometric (FFPI) Sensors .....	33
2.5 PVDF for Optical Fibre FPI (FFPI) Based PFOA Sensor.....	41
2.5.1 Properties of PVDF and Sensitivity to PFOA .....	41
2.5.2 FFPI Fabrication with PVDF and Features of PVDF Coating .....	42
2.5.3 Potential Application of FFPI Based Sensor in PFAS Remediation .....	45
2.6 Competing Methods for the FFPI based PFAS/PFOA Sensor .....	47
2.6.1 Liquid Chromatography Mass Spectrometry .....	48
2.6.2 Ionization Processes in LC-MS .....	49
2.6.3 Mass Analysers in LC-MS .....	51
2.6.4 Time-of-Flight (TOF) Mass Analysers .....	53
2.6.5 Magnetic Sector Mass Analysers .....	53
2.6.6 Detectors in LC-MS .....	56
2.7 Chapter Summary .....	57
<b>3 Development and Optimization of PVDF Coated Fibres</b> .....	<b>58</b>
3.1 Overview.....	58

3.2	Coating Fabrication Technique using PVDF .....	58
3.2.1	Materials.....	59
3.2.2	Apparatus .....	60
3.2.3	Method of forming PVDF solution using MEK.....	61
3.2.4	Method of forming PVDF solution using MEK and Acetone .....	62
3.2.5	Method of forming PVDF solution using MEK and DMF.....	62
3.2.6	Method of forming PVDF solution using DMF .....	63
3.2.7	PVDF Coating Formation using Immersion Precipitation .....	63
3.2.8	Method of Identifying $\beta$ -Phase PVDF in Coating .....	63
3.2.9	PVDF Coating Optimization Process .....	64
3.3	General Discussion .....	70
3.4	Evolution of the Fabrication Process and Sensing Trials .....	71
3.5	Chapter Summary .....	78
<b>4</b>	<b>Temperature Characterization of PVDF Coated Fibre.....</b>	<b>79</b>
4.1	Overview .....	79
4.2	Materials and Methods.....	79
4.2.1	Chemicals.....	79
4.2.2	General Apparatus.....	80
4.2.3	Coating Fibre End-face .....	81
4.2.4	Coated Fibre Identification and Selection .....	82
4.2.5	Temperature Sensing .....	83
4.2.6	Influence of Heat on PVDF Coating .....	86
4.3	Results and Discussion .....	86
4.3.1	PVDF Coated Fibre Operating Principle.....	86
4.3.2	PVDF Coated Fibre Response to Temperature Variation .....	89
4.3.3	Performance Analysis of Coated Fibre.....	91
4.3.4	Effect of Heat Treatment on PVDF Coating .....	99
4.4	Chapter Summary .....	102
<b>5</b>	<b>PFOA Detection with PVDF Coated Optical Fibre .....</b>	<b>104</b>
5.1	Overview.....	104
5.2	Introduction.....	104
5.3	Materials and Methods.....	106
5.3.1	Materials.....	106
5.3.2	General Apparatus.....	107
5.3.3	Coating Composition Characterization using FTIR Spectroscopy .....	109
5.3.4	Coated Optical Fibre Testing and Selection .....	110
5.3.5	Coated Optical Fibre Temperature Sensitivity in Water .....	110
5.3.6	Coated Optical Fibre Sensitivity to PFOA in Aqueous Solution .....	111
5.3.7	Coated Optical Fibre Sensitivity to PFOA in Saline Water .....	113
5.3.8	Coated Optical Fibre Sensitivity to PFAS Wash Water .....	113
5.4	Results and Discussion .....	114

5.4.1	PVDF Coated Fibre PFOA Sensing Principle.....	114
5.4.2	FTIR Spectra of PVDF Coated Fibre .....	114
5.4.3	Coated Fibre Temperature Response in Water.....	115
5.4.4	Coated Fibre Response to PFOA Solution .....	119
5.4.5	Coated Fibre Response to PFOA in Saline Water .....	131
5.4.6	Coated Fibre Response to PFAS in Wash Water from Fire-fighting Trucks .....	133
5.5	Overall Performance of PVDF Coated Fibre .....	136
5.6	Chapter Summary .....	138
<b>6</b>	<b>Alternative Methods of PFOA Detection .....</b>	<b>139</b>
6.1	Overview.....	139
6.2	Background of Methods.....	140
6.2.1	Refractive Index Measurement .....	140
6.2.2	Analytical Test for Determining Chemical Concentration .....	142
6.3	Experimental Methods of PFOA Detection .....	143
6.3.1	Materials and Chemicals .....	143
6.3.2	Refractive Index Measurement Test with Bare Optical fibre .....	143
6.3.3	Refractive Index Measurement Test with Etched Fibre Bragg Grating .....	145
6.3.4	Quantification of PFOA Adsorption on PVDF Film.....	146
6.4	Results and Discussion .....	147
6.4.1	Refractive Index Measurement with Bare Optical Fibre .....	147
6.4.2	Refractive Index Measurement with Etched Fibre Bragg Grating .....	150
6.4.3	Quantification of PFOA Adsorption .....	155
6.5	Comparison of the Optical PFAS Detection Techniques .....	155
6.6	Chapter Summary .....	158
<b>7</b>	<b>Zeolite Doped Functionalized PVDF in PFAS Sensing.....</b>	<b>159</b>
7.1	Overview.....	159
7.2	Background on Zeolite Functionalized Membranes .....	159
7.3	Materials and Methods.....	160
7.4	Results and Discussion .....	162
7.4.1	FTIR Spectra of Zeolite Doped PVDF Thin Films .....	162
7.4.2	PFOA Adsorption by Zeolite Doped PVDF Thin Film.....	164
7.4.3	Response of Optical Fibre with Zeolite Doped Coating to PFOA .....	172
7.5	Chapter Summary .....	172
<b>8</b>	<b>Conclusions and Recommendations .....</b>	<b>174</b>
8.1	Thesis Summary .....	174
8.2	General Conclusions .....	175
8.3	Recommendations for Future Work.....	179
	<b>References .....</b>	<b>181</b>
	<b>Appendix A .....</b>	<b>200</b>
	<b>Appendix B.....</b>	<b>205</b>

## List of Figures

Figure 1.1 News articles discussing extent of PFOA/ PFAS contamination in Australia .....	3
Figure 1.2 Molecular structure of PVDF and PFOA. ....	16
Figure 2.1 Single and multimode fibre differences in refractive index profile.....	22
Figure 2.2 Single mode optical fibre configuration [96] showing composition .....	22
Figure 2.3 Optical fibre fabrication process [107].....	25
Figure 2.4 Classification of optical fibre sensors [138].....	29
Figure 2.5 Classification of optical fibre sensors by application in different categories showing overlap.30	
Figure 2.6 Light incident on a thin film.....	35
Figure 2.7: Schematic of FFPI sensor showing a normally incident ray on the etalon.....	36
Figure 2.8: Experimental setup for observing reflection spectrum from FFPI sensor .....	37
Figure 2.9 Shows transmission spectra of a low and a high sensitivity etalon .....	38
Figure 2.10 LC-MS system showing phase separation and mass analysis components [160]. ....	48
Figure 2.11 Mass spectrometer [193]. ....	49
Figure 3.1 Experimental set up for forming PVDF solution. ....	61
Figure 3.2 Sensor fabrication using immersion precipitation.....	64
Figure 3.3 Expected normalized reflection spectra from the FPI of a PVDF coating .....	66
Figure 3.4 Schematic showing fibrils that would form on non-optimized PVDF coatings.....	67
Figure 3.5 FTIR spectra of PVDF membranes formed from different solvents and polymer grades. ....	69
Figure 3.6 SEM image of PVDF coated fibre tip and cross section views .....	70
Figure 3.7 Pie chart summarizing the outcome of investigation. ....	77
Figure 4.1 Experimental set up for determining temperature response in air.....	80
Figure 4.2 Examples of (a) raw source and sensor spectra and (b) normalized sensor spectrum. ....	83
Figure 4.3 Temperature versus position inside the Carbolite tube furnace at a stabilized temperature .....	84
Figure 4.4 Spectral response of sample# 71 to temperature variation. ....	85
Figure 4.5 Spectral response of sample 74 to temperature variation showing peak wavelength shift. ....	85
Figure 4.6 Schematic of PVDF Coated fibre end-face. ....	87
Figure 4.7 Wavelength shift of sample#73 with temperature rise .....	90
Figure 4.8 Sample #73 fitted FFPI spectrum using Table Curve .....	92
Figure 4.9 Sample #73 fitted spectral data in Excel. ....	93
Figure 4.10 Correlation between fit in Excel and Table Curve. ....	93
Figure 4.11 (a-f) Curve fit of normalized spectra of sample #73 in Excel at various temperatures. ....	94
Figure 4.12 Shift in peak wavelength positions with temperature (sample #73).....	95
Figure 4.13 Variation in OPD with temperature. ....	96

Figure 4.14 Plot of OPD change vs temperature change with fit obtained using Table Curve. ....	98
Figure 4.15 FTIR spectra of the PVDF thin film at different temperatures.....	100
Figure 4.16 FTIR spectra of the PVDF thin film from 1250-1100 $\text{cm}^{-1}$ .....	101
Figure 4.17. FTIR spectra of the PVDF thin film from 900-750 $\text{cm}^{-1}$ .....	101
Figure 4.18 Normalized area under FTIR curves at different temperatures. ....	102
Figure 5.1 Experimental setup for PFOA detection. ....	109
Figure 5.2 FTIR spectra showing PVDF coating composition.....	115
Figure 5.3 PVDF Coated fibre response to temperature variation in water.....	116
Figure 5.4 Peak wavelength shift of PVDF coated fibre in water with change in temperature. ....	117
Figure 5.5 Change in OPD with temperature of a PVDF coated fibre in water. ....	117
Figure 5.6 Normalized spectral data of PVDF coated fibre response to change in PFOA concentration. ....	120
Figure 5.7 Simulated response of the PVDF coated fibre response to PFOA ....	120
Figure 5.8 (a) Magnified image of normalized and simulated spectra ....	121
Figure 5.9 (a-f) Curve fitting of spectral data of PFOA experiment in Excel. ....	124
Figure 5.10 (a-f) Curve fitting of spectral data of PFOA experiment in Table Curve (TC). ....	125
Figure 5.11 Plot of OPD vs PFOA concentration in (a) Excel and (b) Table Curve (TC) . ....	126
Figure 5.12 Correlation between OPD values obtained using Excel and Table Curve (TC). ....	127
Figure 5.13 (a) Variation of OPD (Excel) with PFOA concentration ....	129
Figure 5.14 PVDF coated fibre response to PFOA in the parts per billion (ppb) concentration range. ...	130
Figure 5.15 PVDF coated fibre's spectral response to PFOA in saline water.....	131
Figure 5.16 Variation in OPD with changing PFOA concentration in aqueous salt solution. ....	133
Figure 5.17 (a) PVDF coated optical fibre's spectral response to PFAS in wash water. ....	135
Figure 5.18 Variation in OPD with change in PFAS concentration in the parts per billion (ppb) range..	136
Figure 6.1 Experimental set up for observing wavelength shift using an etched FBG.....	144
Figure 6.2 Reflection intensity of bare fibre in different media. ....	148
Figure 6.3 Normalized area graph of different media. ....	148
Figure 6.4 Plot of reflection intensity in linear scale with changes in refractive index.....	149
Figure 6.5 Intensity vs. concentration graph of PFOA samples of different concentration.....	150
Figure 6.6 Wavelength shift of EFBG with change in refractive index of medium. ....	151
Figure 6.7 Normalized area of graph of EFBG ....	152
Figure 6.8 Response of EFBG to PFOA solution of varying concentrations. ....	152
Figure 6.9 Normalized area graph of intensity in PFOA solution of different concentrations. ....	153
Figure 6.10 Response of EFBG to PFOA solution in which PVDF membrane was soaked. ....	154
Figure 6.11 Normalized area graph of reflected intensity ....	154
Figure 6.12 Comparison of PFOA sensing technique of (a) EFBG and (b) bare optical fibre .....	157

Figure 7.1 FTIR spectra of Zeolite doped PVDF coating and a non-doped PVDF coating. ....	163
Figure 7.2 FTIR spectra of non-doped dry and PFOA soaked PVDF membranes.....	163
Figure 7.3 FTIR spectra of zeolite doped dry and PFOA soaked membrane. ....	164
Figure 7.4 SEM image of dry PVDF thin film surface.....	167
Figure 7.5 SEM image and EDX data of selected area on a dry PVDF thin film.....	167
Figure 7.6 SEM image of the surface of a PVDF thin film after it was soaked in PFOA solution. ....	168
Figure 7.7 SEM image and EDX data of selected surface area on a PVDF thin film exposed to PFOA. ....	168
Figure 7.8 SEM image of zeolite doped PVDF thin film surface texture in dry state. ....	170
Figure 7.9 SEM and EDX data of zeolite doped PVDF thin film exposed to PFOA. ....	170
Figure 7.10 EDX spectra showing composition of zeolite doped PVDF thin film exposed to PFOA. ....	171
Figure 7.11 Zeolite doped PVDF coating on optical fibre end-face showing spectral response .....	173
Figure 7.12 Optical fibre end-face with zeolite incorporated PVDF coating, in dry state.....	173

## List of Tables

Table 1.1 Comparison of techniques for PFOA/PFAS separation from different types of samples. ....	8
Table 1.2 Comparison of the conventional and non-conventional PFOA detection methods. ....	11
Table 2.1 Classification of intrinsic OFS .....	28
Table 2.2 Comparison of Mass Analysers .....	55
Table 3.1 Steps in forming PVDF solution .....	62
Table 3.2 Evaluation of PVDF coated optical fibres under different testing protocols. ....	74
Table 6.1 Comparison of PFOA sensing techniques utilizing OFS.....	156
Table 7.1 Perfluorooctanoic acid adsorption on rectangular PVDF thin film pieces. ....	166

# **List of Publications/Presentations**

## **Published Journals**

**F. Faiz, G. Baxter, S. Collins, F. Sidiroglou, and M. Cran, "Polyvinylidene Fluoride Coated Optical Fibre for Detecting Perfluorinated Chemicals," Sensors and Actuators B: Chemical, p. 128006, 2020.**

## **Conference Abstracts**

F. Faiz, M. J. Cran, G. Baxter, S. Collins, and F. Sidiroglou, "Perfluorooctanoic (PFOA) Acid Detection in Aqueous Medium using Polyvinylidene Fluoride (PVDF) Thin Film on Optical Fiber Endface," in Optical Sensors and Sensing Congress (ES, FTS, HISE, Sensors), OSA Technical Digest (Optical Society of America, 2019), paper EW4A.3.

## **Conference Proceedings**

Fabry-Perot Interferometric Fibre Optic Temperature Sensor with Polyvinylidene Fluoride (PVDF) Coating: accepted for publication in Proceedings of SPIE, 2019.

## **Journal Manuscripts under Review**

Polyvinylidene Fluoride Coated Fabry-Perot Interferometric Optical Fiber Temperature Sensor, submitted to Measurement Science and Technology.

# 1 Introduction

---

## 1.1 Prelude

The commercial production of fluoropolymers is a global multi-billion dollar industry and this is expected to grow significantly in the near future [1, 2]. Composed of per- and partially-fluorinated polymers like polytetrafluoroethylene (PTFE), Teflon-AF, Cytop, Hyflon, fluorinated-ethylene-propylene (FEP), perfluoro-alkoxy, polychloro-trifluoroethylene (PCTFE) and many others, the list of existing fluoropolymers contributing to global economy is a long one. The automotive [3], electronics [4, 5], construction [6], energy [1], chemical processing [7] and healthcare industries [8] among others, are some of the areas where fluoropolymers are in high demand. It has been reported that 20% of the fluoropolymers market belong to fluoroelastomers, fluorinated lubricants, and fluorosurfactants [1].

Perfluoroalkyl acids are fluorosurfactants that are used for the commercial production of other fluoropolymers, while the aqueous film forming foams (AFFFs) from the same group are the most effective flammable fire-fighting agents in the military [9], aviation, industry and domestic applications [1]. Recent concerns have emerged over non-biodegradation and bioaccumulation of fluorosurfactants like AFFF and their breakdown products, perfluorooctanoic acid (PFOA) and perfluorooctane sulphonate (PFOS) [10, 11] that have contaminated land and adjoining water bodies and aquifers [12, 13].

Environmental pollutants in land, water and air constantly threaten the safety and wellbeing of different species of life forms including humans [14-16]. The adverse health effects from these can manifest themselves over a short period of time [17] or a long one

[18]. Perfluoroalkyl substances (PFAS), such as PFOA and PFOS, are emerging contaminants, whose side effects are becoming evident gradually as a result of scientific investigations being carried out [19, 20]. Apart from fire-fighting foams, PFAS are commonly used in surfactants, aerosol propellants, insecticide, refrigerants, anaesthetics, plastics [21] etc., which put the users on the path of either direct or indirect harm.

### **1.1.1 PFAS Exposure**

In humans, studies have reported that certain PFAS related chemicals can adversely affect the growth of a foetus and can contribute to learning behaviour problems in children [22-24]. They can also decrease fertility, increase cholesterol, cause changes in the body's natural hormones, affect the immune system, and increase the risk of cancer [25]. Several studies on the population surrounding a chemical plant producing these chemicals have suggested that exposure to very high levels of PFOA may be correlated to kidney cancer, testicular cancer, ulcerative colitis, thyroid disease, hypertension and high cholesterol [26]. People affected by PFOA in some parts of Australia have reported using contaminated ground water for drinking, cleaning, gardening etc. [27]. News media tried to uphold the severity of PFAS/PFOA contamination across different Australian states and create more public awareness, as can be seen from the screenshots of some of the newspapers in Figure 1.1. Similar reports in other parts of the world, affected by the same problem [28], also created a growing concern over the usage of these toxic chemicals, however, to date scientists have not been able to clearly identify the exact impact on human health upon exposure to the contaminants at the level they are present in drinking water or food.

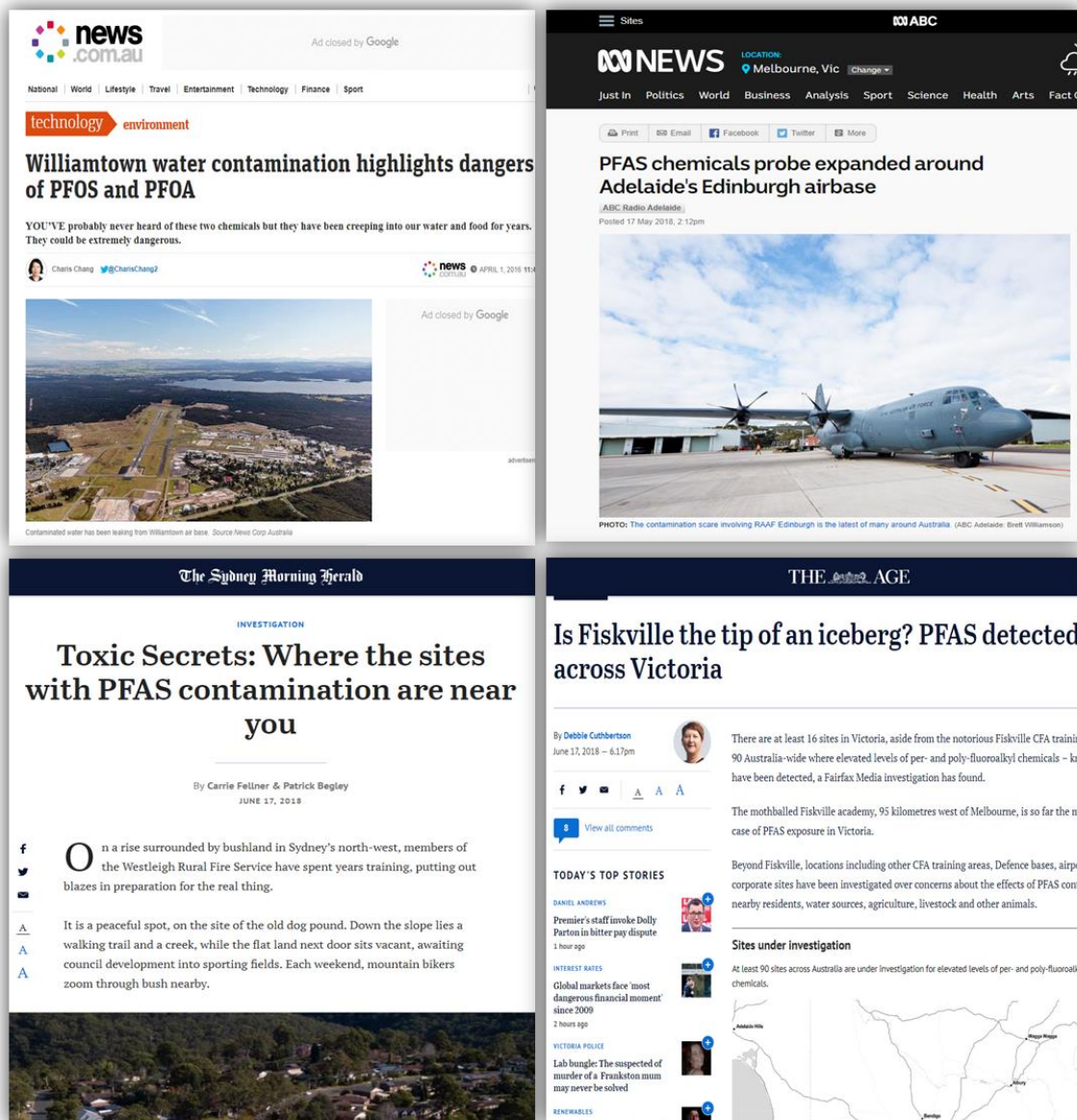


Figure 1.1 News articles discussing extent of PFOA/ PFAS contamination in Australia [29-32].

In 2016, Food Standards Australia New Zealand (FSANZ) has specified 70 ng/L (0.07 parts per billion (ppb)) of PFOS in drinking water to be the maximum level for human consumption [33]. For PFOA, FSANZ has specified a tolerable daily intake (TDI) value of 160 nanograms per kilogram of body weight per day and the drinking water quality value from 0.56 to 5 ppb (or 0.56~5 µg/L) [34]. In the USA, the levels of PFOA

concentrations under which adverse health effects are not expected to occur over a lifetime of exposure has been set at 0.07 ppb (70 ppt) by the Environment Protection Authority [35].

Around the world, 171 countries including the UK, Germany and China have agreed to ban the use of PFOS by listing it on the United Nations Stockholm Convention, whereas Australia has not yet agreed upon the phase-out [30]. In 2015, PFOA, its salts and PFOA-related chemicals were nominated for listing on the Stockholm Convention and in May 2019, it has been listed in Annex A of the treaty with certain exemptions [36, 37]. Meanwhile, \$13 million was provided by the Australian government for a PFAS Remediation Research Program for developing technologies to help investigate and remediate PFAS contaminated areas [38]. Recently, the Heads of Environment Protection Authority (HEPA), in Australia and New Zealand and the Australian Government Department of the Environment and Energy (DoEE) have collaborated to develop the PFAS National Environmental Management Plan (NEMP) to address environmental regulation of PFAS [37]. The NEMP discusses many important points and some of these are related to monitoring PFAS, assessment of PFAS in contaminated sites, containment, storage and disposal of contaminated items, re-use of contaminated soils and water as well as treatment and remediation. Therefore, there is a growing interest in the scientific community to develop an accurate and efficient *in situ* detection device and methods that would assist in determining the level of contamination at a site or in a sample instantaneously to help with the investigation, as the existing methods, which are discussed below, do not offer this facility.

### **1.1.2 Current PFAS Detection Methods**

The type and extent of PFAS contamination in soil or water is currently determined using analytical methods. The samples from the site are collected and sent to a laboratory for chemical analysis. Traditional analytical methods employed in this case include gas chromatography–mass spectrometry (GC–MS) [39], liquid chromatography–mass spectrometry (LC–MS) [40], and liquid chromatography–tandem mass spectroscopy (LC–MS/MS) [41], which often require complicated pre-treatment steps, expensive labour resources, and are inapplicable for in-situ measurements and analysis [42]. Some of these methods, such as GC analysis, require sample derivatization prior to analysis [43]. This is necessary when a compound such as PFOA has poor volatility and thermal stability, or may can be adsorbed in the GC injector. It involves chemically changing the compound, producing a new modified compound that has more suitable and amendable properties for the GC technique.

Perfluorooctanoic acid contaminated food items are currently only detectable in a reliable manner using LC-MS/MS and GC-MS, but very few reports of these are available [44]. Therefore, many assumptions have been made to derive exposure estimates of PFOA and other PFAS in humans. However, there is considerable evidence that its toxicity affects the natural environment, humans and animals.

Over the years many researchers have reported novel detection techniques, some of which involve the combination of the traditional analytical methods, while others include electrochemical detection or colorimetric visualization. A few examples are highlighted in the paragraphs below.

### *Conventional Methods of PFOA Detection in Water*

To measure organic fluorochemicals in drinking water and surface water in trace amounts Hansen, et al. [45], developed a solid-phase extraction method coupled with high-performance liquid chromatography (HPLC)-negative-ion electrospray tandem mass spectrometry. Their result from the analysis of PFOS and PFOA with a test sample from the Tennessee River showed good precision and accuracy down to 25-50 ng/L or 0.025-0.05 ppb. Takayose, et al. [46] devised a colorimetric detection method for the determination of PFOA. Gold nanoparticles modified with thiol-terminated polystyrene (AuPS) were used in this research. A colour change of the AuPS solution from red to blue-purple upon addition of PFOA was confirmed by the naked eye. Using several acids and fluorinated compounds, the detection system was shown to be selective for PFOA and tridecafluoroheptanoic acid, which suggests that both a highly acidic carboxyl group and a fluorocarbon group are required for the colour change. However, no conclusive evidence about the need for the carboxylic functional group for a colour change has been provided here and no direct proof has been given for the long fluorocarbon group encouraging fluorine-fluorine interaction and in turn the aggregation of the AuNPs.

Surface-assisted Laser Desorption/Ionization mass spectrometry (SALDI-MS) has also been investigated as a method of detecting PFOS and PFOA by many researchers [47-49]. However, SALDI-MS has been considered suitable only for perfluoro-alkylcarboxylic acids with chain lengths below C<sub>6</sub> (i.e. with a carbon-backbones having less than six carbon atoms). Matrix-assisted Laser Desorption/Ionization-Time of Flight Mass Spectrometry (MALDI-TOF-MS) is an enhanced quantitative analysis technique, which has been reported by Cao, et al. [49]. Not unlike the GC and HPLC techniques,

these methods are limited to the laboratory, require specialized personnel to execute the process and interpret results, and incur relatively high cost of operation. Therefore, none of these conventional methods are currently suitable for analysis in the field.

The analytical methods used in determining very low concentrations of PFAS compounds are mostly variations of the combination of chromatography and mass spectrometry techniques. Some of these are HPLC with UV and fluorescence detection, nuclear magnetic resonance (NMR), GC-MS, ultra-high-performance liquid chromatography–tandem mass spectrometry (UHPLC–MS/MS), capillary liquid chromatography–mass spectrometry (CLC–MS), negative ion electrospray tandem mass spectrometry and liquid chromatography coupled to time-of-flight MS. The choice of a technique can be influenced by the type of compound that needs to be quantified along with cost and time taken for analysis.

Several options exist to test PFAS compounds in water from various sources, and while literature reports of many, a few examples have been highlighted in the following paragraphs.

- A solid-phase extraction method coupled with HPLC-negative-ion electrospray tandem mass spectrometry has been used to identify fluorochemicals in drinking water and surface water [45] up to the limit of 25 ppt. The use of this same technique has also been reported in the detection of PFAS in estuarine water samples where it measured a PFOA concentration of 20.6 ng/L or 0.0206 ppb [50].

- Instrumental analysis using high-performance liquid chromatograph interfaced with a tandem mass spectrometry (HPLC-MS/MS) was used on river water that measured a concentration of 7.9–110 ng/L or 0.0079-0.11 ppb of PFOA [51].
- A solid-phase extraction followed by liquid chromatography coupled to a time-of-flight mass spectrometer (LC–ToF-MS) in surface, sewage and seawater has been reported with limits of quantification (LOQs) varying from 2 to 200 ng L<sup>-1</sup> [52].
- The use of liquid chromatography–ion trap mass spectrometry has been applied to water from rivers, effluents from waste water treatment plants, water from a lagoon, lakes and also coastal water [53, 54].

**Table 1.1 Comparison of techniques for PFOA/PFAS separation from different types of samples.**

Technique	Compound	Cost	Time	Reference
<b>GC-MS</b>	<ul style="list-style-type: none"> <li>• Environmental samples</li> <li>• Organic pollutants</li> <li>• Fire debris</li> <li>• Drugs</li> </ul>	Low	More time required for experiments	[55-57]
<b>UHPLC-MS/MS</b> <b>HPLC MS/MS</b> <b>LC-ToF-MS</b> <b>CLC-MS</b> <b>LC-MS</b>	<ul style="list-style-type: none"> <li>• Environmental samples</li> <li>• Biological fluids</li> <li>• Water samples</li> <li>• Food samples</li> <li>• Plant phenols</li> <li>• Proteins</li> <li>• Drugs</li> </ul>	High	Less time required for experiments	[52, 56-63]

### ***Non-Conventional Methods of PFOA Detection in Water***

A relatively recent on-site PFAS screening technique utilizing a smart-phone based monitoring tool has been reported by Fang, et al. [64]. The authors highlighted an easily

available and accessible method, with a sensing principle that involves detecting the colour of a specific cationic dye and converting it to a specific concentration of the PFAS being detected. It was reported that the technique does not differentiate between any anionic surfactants and the visual test gets affected adversely with changes in background illumination.

A photo-electrochemical (PEC) sensor by Gong, et al. [42] discusses a nanostructured probe made of molecularly imprinted polymer (MIP) modified AgI nanoparticles–Bismuth oxyiodide (BiOI) nanoflake arrays that act as the photoactive electrode in the detection of PFOA. This method requires a complicated fabrication procedure and employs an indirect photo induced electron transfer process. This is so since  $\text{TiO}_2$  and other oxidants of hydroxyl radicals show a poor reactivity with PFOA to support the conventional direct visible-light-responsive PEC strategy of detection.

A Molecularly Imprinted Polymer (MIP) which is able to bind to PFAS and utilizes an optical fibre platform working on the principle of surface plasmon resonance (SPR), has been presented in the work of Cennamo, et al. [65]. The authors reported a complex and time-consuming sensor fabrication protocol and reported that the MIP was designed to recognise  $\text{C}_4$  to  $\text{C}_{12}$  PFAS, indicating a lack of specificity. Moreover, no information was presented on the MIPs dependence on temperature or the overall sensitivity of the system to temperature or other possible environmental factors.

The descriptions provided above and the comparisons in Table 1.1 and Table 1.2 clearly show that the majority of these existing techniques of PFAS detection do not meet the requirements of an instrument that needs to be accurate, versatile, rugged, and quick to produce an outcome in a field test. Thus, a portable system that is lightweight and robust

in nature and capable of delivering instantaneous information about the level of PFAS contamination in any type of sample is a highly desirable technology. Compared to the GC-MS or LC-MS techniques it would be less expensive, robust and suitable for on-site real time measurements. Therefore, a strong motivation now exists to work towards the development of portable, handheld field instruments, not unlike the common digital multimeter, that would perform this envisioned sensing task. The proposed research, therefore, attempts to pursue this revolutionary idea of PFAS detection by providing a proof of principle for an optical fibre sensor-based system.

**Table 1.2 Comparison of the conventional and non-conventional PFOA detection methods.**

<b>Conventional Analytical Methods</b>	<b>Advantages</b>	<b>Disadvantages</b>	<b>References</b>
<b>GC-MS LC-MS</b>	Highly accuracy Good reliability	Time consuming preparation steps Requires bulky instruments Requires trained personnel Non-portable Complex data analysis technique Expensive	[56, 66-68]
<b>Non-Conventional Methods</b>	<b>Advantages</b>	<b>Disadvantages</b>	<b>References</b>
<b>Smartphone app SPR based detection with MIP Colorimetric visualization Photo-electrochemical detection</b>	Portable Economic Quick response	Complex sensor fabrication procedure Sensitivity and selectivity challenges Complex data analysis technique Low accuracy Toxic waste	[42, 46, 64, 65]

## **1.2 Optical Fibre Sensors**

Optical fibre sensors (OFSs) are a recent class of inventions that have unmatched performance and immense engineering benefits [69-71]. Sensors made from optical fibres have been applied in the study of physical parameters to develop energy efficient systems in different commercial sectors. Even though the optical fibre was initially designed for the telecommunication industry, for facilitating and optimizing data transmission, it quickly found practical applications in other areas such as process monitoring and data acquisition in harsh environmental conditions [72, 73]. The ease of handling their lightweight structure, coupled with their remote sensing capabilities, biocompatibility and immunity to electromagnetic interference have made them a very convenient tool for use

in underground sensing operations, structural monitoring and determining chemical concentration [74-78].

There can be three categories of OFS based on the location of measurement. Point sensors, which detect parameters at a specific position on the optical fibre. Quasi-distributed sensors that make measurements at multiple precise locations on the optical fibre and distributed sensors, which measure continuously over the length of the fibre cable. A bare optical fibre serves as the simplest OFS (point sensor). However, it is useful only for refractometric type of measurements. If a bare fibre end-face is coated with a material, then it turns into an interferometric point sensor that can be used for a wider range of selective applications.

A thin film formed at the fibre end-face acts like a Fabry-Perot interferometer (FPI). It helps to give rise to reflections at the boundaries between the surrounding environment and the outer surface of the thin film as well as the optical fibre end-face and the inner surface of the film [79]. These reflected light waves undergo interference to produce a resultant signal that propagates through the core of the optical fibre and can be observed using a detector such as an optical spectrum analyser (OSA). When there is a change in the thickness of the coating or its refractive index or both, then the wavelengths at which constructive or destructive interference occurs are affected. All of these phenomena cause a shift in the intensity maximum or minimum point on the monitored reflection spectrum to a different wavelength. Thus, the change in the reflection spectrum, as a result of a physical change in the FPI etalon, acts as an indicator for changes in the environment of the sensor. In this thesis, the term wavelength shift or spectral shift is often used for the

convenience of discussing the change in the maximum or minimum intensity positions as will be seen in later chapters.

### **1.3 Research Hypothesis and Significance**

The analysis of PFOA and other PFAS, using conventional analytical approaches like HPLC-MS and GC-MS techniques are not suitable for on-site applications since they need time-consuming preparation steps in addition to expert personnel to interpret the results among other things discussed earlier. Non-conventional methods including mobile apps, optical detection methods and potentiometric sensing techniques, based on molecularly imprinted polymers (MIP) that tried to address *in situ* measurement [64, 65, 80, 81] suffer from selectivity issues. Moreover, the recently developed smartphone based app is reported to be highly sensitive to weather conditions [64]. In addition, there is a lack of information when it comes to temperature sensitivity or cross-sensitivity of the existing MIP based portable sensors. Until now only one category of OFS relying on MIP, which works on the principle of surface plasmon resonance, has been examined in relation to the study of PFAS. No investigation has been done with any other type of OFS, especially one that involves a fibre optic Fabry-Perot interferometry (FFPI) based sensor, which is operational under water. So, a gap in the literature is found when it comes to the variety of OFS investigated for use as PFAS detector, to address *in situ* and real time measurement of the contaminants.

Apart from the above, there is also a strong interest to work towards the development of a handheld probe that can provide accurate results in real time, whenever it is dipped in a contaminated water body or inserted into a solid sample. This is because of the

tremendous advantages it would provide, that include, but are not limited to, affordability, ease of operation and handling.

Thus, in this thesis research has been undertaken to establish whether polyvinylidene fluoride (PVDF), as a polymer often used in water filtration, is able to absorb PFOA and therefore help in the development of a coating for a FPI based OFS for *in situ* measurement of the contaminant in its natural environment. Hence, the research has focused on demonstrating a proof of concept for an interferometry based optical fibre portable PFOA (or PFAS) detector and aimed at demonstrating the novelty of the PVDF coating in sensing PFOA (or PFAS).

To this end the thesis made an attempt at producing a hybrid probe combining the advantages of the PVDF membrane and fibre optic Fabry-Perot interferometric (FPI) sensing technique for detecting PFOA concentration in real time, to address the limitation of the conventional method. It adopted a dip coating technique for multiple layer formation to produce the PVDF coating on the fibre end-face.

This research has demonstrated that PVDF absorbs PFOA by the use of both analytical and optical methods. It has highlighted a potentially simple and convenient sensor fabrication process via immersion precipitation. In addition, this work has contributed to the design of a portable OFS based sensing system and provided information on PVDF's response and operational characteristics as a Fabry-Perot etalon for detecting PFOA or PFAS.

## 1.4 Research Aims and Objectives

Research into novel materials that have the capability to interact with the highly stable PFAS contaminants, to detect their presence or assist in their removal is an important part of scientific investigation that is constantly generating new information to improve water treatment procedures for safe consumption and usage. Although, PVDF has long been known in the water research community as an excellent nano- and micro-filtration membrane forming polymer, it has not been studied previously in relation to PFAS sensing.

Polyvinylidene fluoride (PVDF) is a thermoplastic polymer that is easy to process and has high chemical resistance and heat tolerance capacity with low permeability to most gases and liquids [82]. It is also known to be resistant to UV radiation and abrasion [82] and functionalized PVDF membranes are commonly used in waste water filtration to remove pesticides and medicine. As a natural ferroelectric material, this polymer has a spontaneous electric polarization which is reversible. A membrane rich in beta ( $\beta$ ) phase PVDF, which is one of the four polymorphic states the material can have, is more prone to display this characteristic along with the corresponding surface charge, when it is formed by the phase inversion process of immersion precipitation using some specific solvents [83]. Therefore, a PVDF membrane with the  $\beta$ -phase can resemble an ion exchange membrane, whereby it can attract particles and molecules to its surface due to the presence of dipoles or via hydrophobic interactions. There is considerable similarity in the molecular structure of PVDF and PFOA as can be seen from Figure 1.2. However, no research has been reported, which discusses how PVDF interacts with PFOA or outlines the sensitivity of the polymer to the contaminant. On the other hand, there is



- Examine a numerical modelling and graphical analysis technique to address some of the complexities of existing data interpretation process.
- To publish the results of the work done in the international literature, and therefore inform the community of the successes of the research.

Thus, this thesis has been organized in the following manner to reveal how the research aims have been fulfilled.

## **1.5 Thesis Outline**

**Chapter 2 Literature Review:** provides an overview of optical fibres and their operating principles. It highlights Fabry-Perot Interferometry (FPI) based Optical Fibre Sensors (OFS) in sensing chemical analytes and outlines different types of sensing techniques and sensors made using optical fibres. It also provides an insight into chemical sensing with OFS including techniques for detecting perfluoroalkyl compounds. In addition, general information about the conventional analytical methods of PFAS detection is also presented beside an overview of PVDF and FFPI sensor operating principle.

**Chapter 3 Development and Optimization of PVDF Coated Fibres:** discusses the immersion precipitation technique used in membrane development for the formation of the Fabry-Perot etalon with PVDF at the optical fibre end-face. In addition, it also provides the details of the coating and sensor optimization procedure.

**Chapter 4 Temperature Characterization of PVDF Coated Fibre:** describes the temperature sensitivity of the PVDF thin film developed on the optical fibre end-face. It provides details on performance analysis techniques using mathematical modelling and curve fitting procedures.

**Chapter 5 PFOA Detection with PVDF Coated Optical Fibre:** provides details of experimental methods used in determining the ability of the coated fibre to detect perfluorooctanoic acid (PFOA) in aqueous solutions. It discusses overall performance of the sensor by considering changes in the optical path difference (OPD) with variation in the measurand.

**Chapter 6 Alternative Methods of PFOA Detection:** discusses some general optical methods using bare optical fibre and fibre Bragg grating (FBG) based sensors that involve refractive index measurement of the analyte solution to determine concentration change. It provides supporting evidence of the findings of Chapter 5, compares and contrasts outcomes of the various optical sensing techniques used in this research.

**Chapter 7 Zeolite Doped Functionalized PVDF in PFAS Sensing:** provides information on the structural and compositional differences of the zeolite incorporated PVDF membranes with regards to the non-doped PVDF membranes. It presents findings from SEM images, FTIR and energy dispersive x-ray (EDX) spectroscopic data as well as the NATA accredited Method EP231X from an external lab (ALS). The chapter also reports on the variation in FPI spectra observed in a zeolite doped PVDF coated optical fibre.

**Chapter 8 Conclusions and Recommendations:** gives an overview of the research and its contribution and highlights the scope for further work in this area.

## 2 Literature Review

---

### 2.1 Overview

This chapter reviews the literature related to the concepts of optical fibres, optical fibre sensors (OFS), and the characteristics of the emerging PFAS contaminants alongside the prospect of an OFS to detect them. The following sections in this chapter thus provides further details on OFS, their classification, fabrication and applications with special emphasis on chemical sensing. Alongside these, the chapter also discusses characteristics of PVDF as a polymer coating material for a fibre optic FPI (FFPI) sensor and explains its principle of operation besides prospective application in areas of PFOA/PFAS detection. It also provides an in-depth review of the competing conventional PFAS detection techniques against the FFPI sensor.

### 2.2 Optical Fibres: General Information

Humans have tried to understand and utilize the true potential of light as a medium of information exchange since it was first used thousands of years ago by ancient civilizations [86]. Military communication using fire beacons and smoke were commonplace not only in ancient Greece and Rome but also Elizabethan England [87]. These signals, in most cases, were unidirectional and contained prearranged messages that the receiver had no difficulty in decoding. As civilizations evolved so did the modes of communication. Changes came slowly and the first attempt at using sunlight for transmission of a sound signal ensued in the 1880s. Alexander Graham Bell invented the Photophone [88], the first sophisticated voice transmission system using an optical beam, which was never commercialized. Almost eighty years later, a breakthrough invention in 1962, the semiconductor laser, paved the path of success for optical communications [89].

In September 1970, at the Corning Glass Works (now Corning Inc.), Robert Maurer, Donald Keck and Peter Schultz reported the first single-mode optical fibre with an attenuation of 17 dB/km [90, 91], which in conjunction with the discovery of the Erbium doped fibre amplifier (EDFA) in 1987 [92], formed the basis of optical fibre based communications that have revolutionised our world. Then in late 1997, the Global Cloud Exchange installed the infrastructure for high speed internet applications, the Fibre Optic Link Around the Globe (FLAG), for use in commercial telecommunication services. After that, in 2002, an intercontinental network of 250,000 km of submarine communications cable with a capacity of 2.56 Tb/s was completed by the telecommunications industry that formed part of a massive network of intercity and transoceanic fibre communication lines. All these and more have been accomplished using technologies utilising the optical fibre, which have emerged as a scientific breakthrough and revolutionized the message transfer process.

An optical fibre is a transparent, flexible cylindrical waveguide made of silica (glass) or plastic that carries light signals. It usually has a core surrounded by a cladding, both of which are transparent. In this construction, the cladding always has a lower index of refraction compared to the core. Light propagation in the fibre takes place by total internal reflection over both short and long distances. By solving Maxwell's equation [93], it is possible to provide descriptions of the characteristics of light, in terms of electric and magnetic fields, propagating in the fibre. The two most widely used optical fibres are the single- and multi-mode types. A fibre in which only the fundamental mode can propagate is called the single-mode fibre (SMF), whereas one in which multiple modes can propagate is called the multi-mode fibre (MMF). In more general terms, there is only one

path that a light wave can take through a SMF whereas there are multiple pathways through an MMF. The latter is characterized by a wider core diameter than the SMF. While the MMF can have a step or graded refractive index profile the SMF only has a step refractive index profile [94].

The schematic representation of geometric optics in Figure 2.1 portrays how the variation in the structure of the fibre affects mode propagation in the core and the confinement of light through total internal reflection. When a propagating wave strikes a medium boundary at an angle larger than a particular critical angle with respect to the normal it is completely reflected. For an optical fibre this critical angle, is calculated by using Snell's law as shown below:

$$\theta_c = \sin^{-1} \frac{n_{cl}}{n_{co}} \quad 2.1$$

where, ( $n_{co}$ ) is the refractive index of the core and ( $n_{cl}$ ) is the refractive index of the cladding.

Figure 2.2 shows the structure of a typical telecommunications single mode optical fibre cable, with the buffer and jacket as the protective layers over the core and cladding.

In fibre optics, the range of incident light angles, known as the acceptance angle,  $\theta$ , that allow light to be transmitted along the fibre is described by the numerical aperture:

$$NA = \sqrt{(n_{co}^2 - n_{cl}^2)} \quad 2.2$$

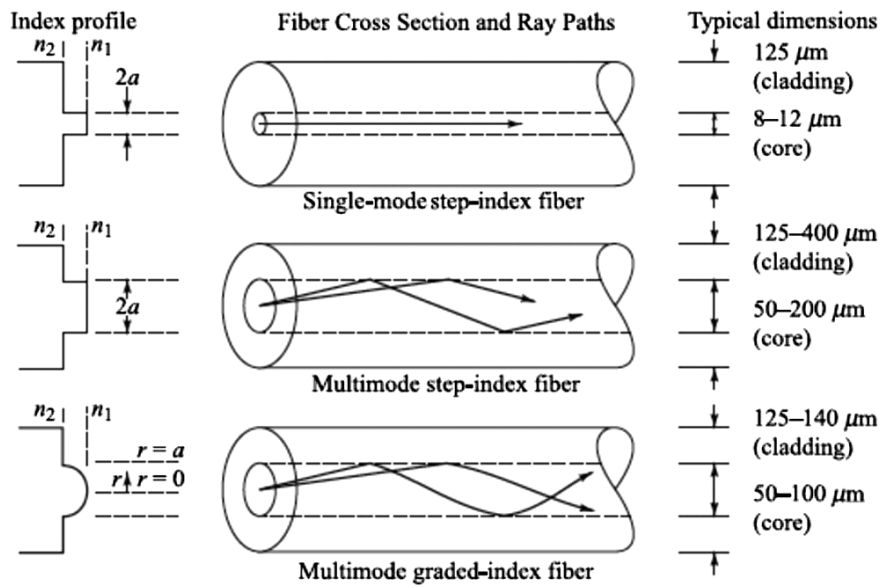


Figure 2.1 Single and multimode fibre differences in refractive index profile. Variation in core and cladding diameters and light propagation modes of different fibre types [95] . The letters  $n_1$  and  $n_2$  represent the core and cladding refractive index respectively and,  $r$ , the radius.

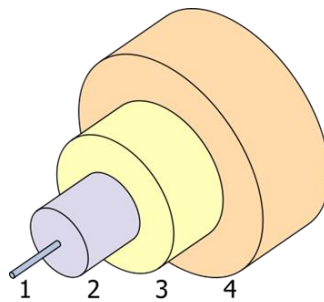


Figure 2.2 Single mode optical fibre configuration [96] showing composition Core 8–10  $\mu\text{m}$  (1), Cladding 125  $\mu\text{m}$  (2), Buffer 250  $\mu\text{m}$  (3) and Jacket 400  $\mu\text{m}$  (4)

Light entering the fibre at an angle greater than the acceptance angle experiences loss at the core cladding interface and so is attenuated and does not reach the other end. The normalized frequency or V number of an optical fibre is a dimensionless parameter, which acts as an indicator for the number of propagating modes within a step index fibre and is given by the equation:

$$V = \frac{2\pi a}{\lambda} \sqrt{(n_{co}^2 - n_{cl}^2)} \quad 2.3$$

Where 'a' is the fibre core radius and 'λ' is the wavelength of light in vacuum. For a step index fibre, the mode volume or number of bound modes is given by  $4V^2/\pi^2$ . A single mode fibre has  $V < 2.4048$  [97, 98]. Light waves that travel down a fibre are usually transverse electric, transverse magnetic or hybrid modes sometimes referred to as linearly polarized modes. Electric field distribution within the fibre results from the combination of the guided and radiation modes and helps to explain the energy variation along the fibre due to coupling of the waves that has implications for the information transferred. Since optical fibres are very different to conventional copper cables, they have some inherent advantages in terms of size, weight, cost, power loss, safety, immunity to electromagnetic interference, and security.

In silica fibres, both the core and the cladding material are made of silicon dioxide (SiO<sub>2</sub>, silica). The difference in their refractive indices is brought about by doping the core, or the cladding, or both with a suitable material [99-101]. Dopants such as germanium oxide, GeO<sub>2</sub>, and phosphorous pentoxide, P<sub>2</sub>O<sub>5</sub>, increase the refractive index of silica and are suitable for the core whereas dopants such as boron trioxide, B<sub>2</sub>O<sub>3</sub>, and fluorine decrease the refractive index of silica and are suitable for the cladding [102]. The major design issues are related to the refractive index profile, the amount of dopants, and the core and cladding dimensions for various applications [101, 102].

### **2.3 Optical Fibres: Fabrication Process**

Fabrication of telecommunication-grade silica fibres generally consists of two stages. The first stage uses a vapour-deposition technique to make a cylindrical preform with the

desired refractive-index profile, which is typically 1 m long and 2 cm in diameter and contains the core and cladding, while the second stage involves drawing the preform into a fibre by using a feed mechanism [102]. Other vapour deposition techniques also exist, including the outside vapour deposition (OVD) [103], vapour phase axial deposition (VAD or AVD) [104], plasma chemical vapour deposition (PCVD) [105]. Among these, PCVD and its upgraded versions (plasma impulse chemical vapour deposition (PICVD) and plasma-enhanced chemical vapour deposition (PECVD)) bear some resemblance to the modified chemical vapour deposition (MCVD) process, which was widely used in the 70's, while the others vary significantly in their method of preform preparation [106]. The following section discusses the general approach taken by MCVD type processes in the fabrication of silica optical fibres.

### **Stage 1: Preform Formation**

To form the preform, the gas produced by some chemical solution is directed into a hollow, rotating tube made of synthetic silica or quartz. The rotating tube is heated up to very high temperatures ( $\approx 1600$  °C) [106] that cause the gas to react with oxygen to form a fine soot of silica (i.e.  $\text{SiO}_2$  and possibly other substances like  $\text{GeO}_2$  depending on the composition of the gas). When the soot builds up to a desired thickness, which adhere to the inside of the rotating tube, it is put through various heat tests to remove moisture and bubbles followed by sintering [106-108]. By the end of this process, modification of the gas mixture gives rise to the precursor of the fibre core with higher refractive index and the tube is collapsed by heating it to  $\approx 2000$  °C [106].

## Stage 2: Fibre Drawing

The finished glass preform is installed at the top of a drawing tower [109], which supports various other devices used in the process, as shown in Figure 2.3. The process begins by lowering one end of the preform into an in-line furnace that produces heat in a range of 1871 to 2204 °C. Upon passing the preform through the furnace, the lower ends begin to melt and form a glob that is pulled downward by gravity. A thin strand of glass that trails behind this glob cools and solidifies quickly. The equipment operator threads this glass strand through the remainder of the devices on the tower, which include several buffer coating applicators and ultraviolet curing ovens and connects it to a tractor mechanism. The latter pulls the strand at a certain speed depending upon the feedback information it receives from a laser micrometre that continually measures the fibre's diameter. At the end of the run, the completed fibre is wound onto a spool.

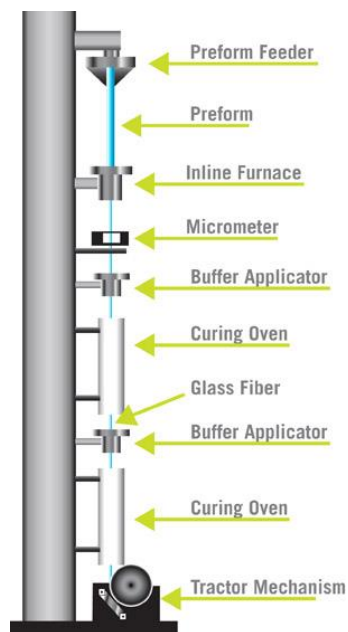


Figure 2.3 Optical fibre fabrication process [107].

## **2.4 Optical Fibres: Application**

Over the years optical fibres have emerged to find usage in diverse applications the most common of these being in the area of telecommunication and networking [90, 110, 111]. Transmission of voice, data, or video that covers distances of less than a metre to hundreds of kilometres has been achieved with optical fibres. Multinational firms can exchange financial information between buildings and computers and transfer data around the world in a secure and reliable way using fibre optic networks. Cable television companies use these waveguides for transmitting broadband signals, such as high-definition television (HDTV) telecasts [111]. Transportation systems, such as smart highways with intelligent traffic lights, automated tollbooths, and changeable message signs, use telemetry systems based on fibre optics.

In the biomedical industry, optical fibre systems are used in telemedicine devices for transmission of digital diagnostic images. Applications related to measurement of body temperatures [112], analysis of blood chemistry [113], and viewing of the interior of hollow organs in the body [114] have been accomplished with optical fibre sensing and data communication systems[115]. Furthermore, fibres are also used to transmit laser beams to stop bleeding or to burn away diseased tissue [116]. Optical fibre sensors rival more contemporary electrical detection methods in many areas because of their geometric versatility, non-interceptable data transmission capability, bio-chemical compatibility and immunity to electromagnetic interference [69, 117-120]. These attributes, which are inherent to optical fibres, provide the optical fibre based sensor with a high bandwidth and data transmission rate, low attenuation of signals and enhanced security[102, 119].

Thus, optical fibres are also seen in space, military, automotive, and industrial applications involving both sensor operation and data transmission [121, 122].

Military fibre optic applications are highly specific, usually with very distinct project requirements. The most promising application areas are in weapons, sensor and surveillance and computing systems and information transmission aboard vehicles [123]. Two high-profile projects on the Space Shuttle's flight, Space Transportation System 95, demonstrated successful use of fibre optic technology in strain and temperature sensing associated with the engine pitch actuator strut, and communication associated with detection of gaseous hydrogen in the shuttle aft area [124].

#### **2.4.1 Types of Optical Fibre Sensors**

A vast range of optical fibre based systems have been reported to date that can be classified based on the principle of their operation or their application [117, 118, 120, 125, 126]. Based on the interaction of the monitored optical signal with the environment, fibre optic sensors are broadly classified as 'intrinsic' or 'extrinsic' sensors. In applications where the optical fibre is used as the sensing element, it is called an intrinsic sensor and in places where the fibre acts as a relay medium by transferring signals from a sensor to the processing unit, it is called an extrinsic sensor.

Extrinsic OFS have been used to measure vibration, rotation, displacement, velocity, acceleration, torque, and temperature [127-130] with a considerable degree of overlap with intrinsic OFS between the areas of sensing. A major advantage of these sensors is that they can be used in places that are otherwise inaccessible or prohibitive for electrical signals.

Intrinsic OFS have been used in monitoring of strain, pressure, and temperature [131-134] besides flow rate and other parameters. For these OFS a perturbation of the measurand can change one or multiple fundamental elements of the wave field, which includes the intensity, phase, state of polarisation and wavelength. Intrinsic OFS are thus grouped into four broad categories based on the type of modulation they use [135]. Table 2.1 shows the different types and the parameters they detect.

**Table 2.1 Classification of intrinsic OFS**

<b>Intrinsic OFS Category</b>	<b>Parameters Detected by Sensor</b>	<b>Reference</b>
<b>Intensity-modulated</b>	Signal attenuation	[136]
<b>Polarisation-modulated</b>	Electric field Polarization state of light	[136]
<b>Phase-modulated</b>	Phase difference between signals	[136, 137]
<b>Wavelength-modulated</b>	Changes in optical spectrum	[136]

Fibre optic sensors can be further classified as grating based sensors, interferometric sensors or distributed sensors [117, 138] as shown in Figure 2.4, while the type of sensor application can also be categorized accordingly to illustrate their degree of overlap as shown in Figure 2.5. Intrinsic and extrinsic optical fibre based chemical sensors, falling in the sub-category of interferometric and grating based sensors, comprise a large group and is further discussed in detail in the following section.

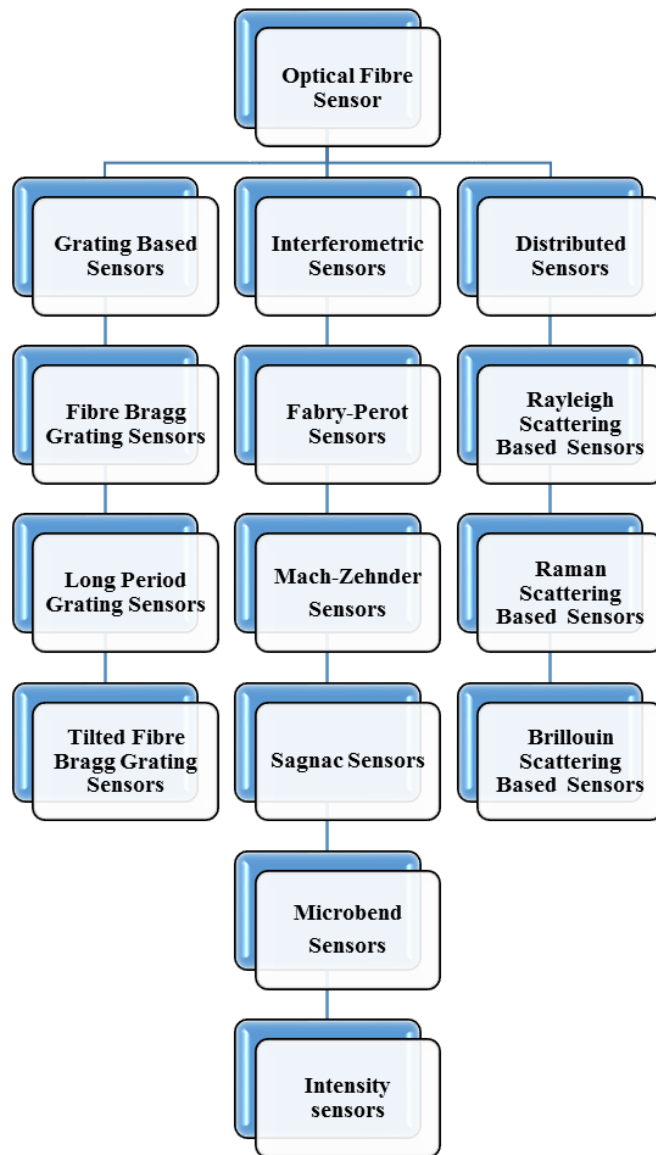


Figure 2.4 Classification of optical fibre sensors [138].

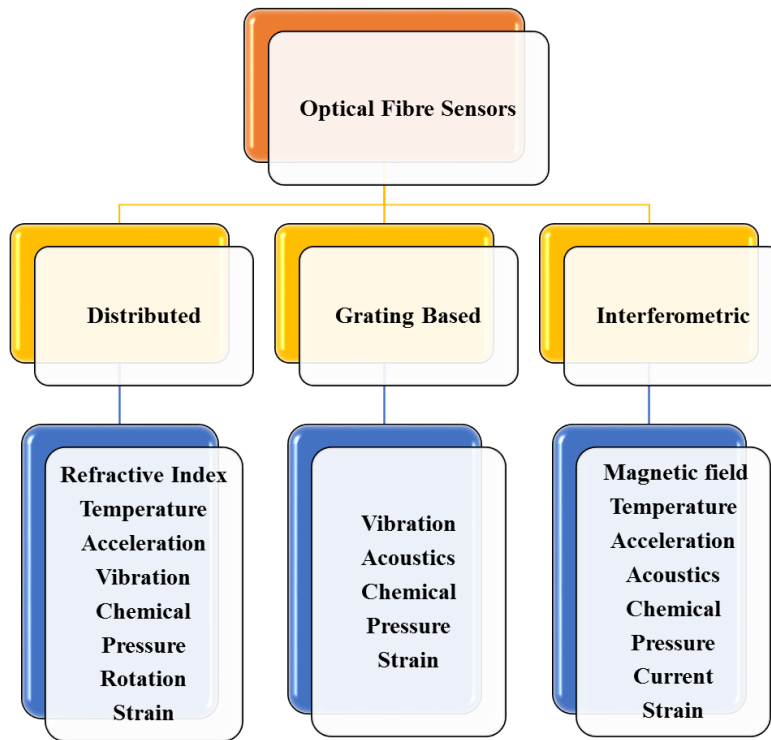


Figure 2.5 Classification of optical fibre sensors by application in different categories showing overlap.

#### 2.4.2 Interferometry Type Optical Fibre Chemical Sensors

Intrinsic OFS in chemical sensing applications utilize a chemical sensitive over-layer or coating that is placed on the optical fibre by removing the cladding. The ability of this sensitive layer to respond to changes in the physical properties of the analyte affects the guided mode's evanescent field. Thus, any variation in the optical property of detected light because of chemical absorption by the sensitive coating, reflectance, or fluorescence is interpreted as a change in the sensed parameter. Some extrinsic OFS that employ Fabry-Perot Interferometry (FPI) transmit light to an immobilized indicator, like a thin film deposited on the fibre end-face and monitor changes in the reflected light based on variation of the physical property of the particular chemical, which can be in a gaseous or a liquid state [139]. This method of determining the concentration of analytes using

OFS is very useful in places, which are difficult to reach by conventional electrical sensors or where fire hazard exists because of their use. The following paragraphs report some examples of chemical sensors from both the above mentioned categories that have been researched in the past few decades [140, 141].

Common contaminants in water are aluminium, ammonia, arsenic, barium, cadmium, chloramine, chromium, copper, fluoride, lead, nitrates/nitrites, mercury, perchlorate, radium, selenium, silver and uranium [142], apart from bacteria and viruses. These heavy metals increase the risk of certain types of cancer and organ failures in animals and humans if consumed above a certain accepted level. Trace amounts of chromium and nitrite concentrations in water ranging from 10 to 2000 ppb and from 1 to 1000 ppb, respectively, have been detected by an optical fibre sensor, based on evanescent wave absorption reported by Kumar, et al. [143]. Four types of Surface Plasmon Resonance (SPR) based sensing probes made using silver and indium tin oxide (ITO), which were further modified with a coating of pyrrole and chitosan composite have been discussed by Verma and Gupta [144] in the detection of  $\text{Cd}^{2+}$ ,  $\text{Pb}^{2+}$  and  $\text{Hg}^{2+}$  metal ions. Optical fibre sensors utilizing surface plasmon resonance have also been reported in relation to detection of some emerging water contaminants like the perfluoroalkyls [65].

Wu and Anslyn [145] mentioned a very sensitive Cu (II) detection system, which involves an optical fibre with an immobilized fluorophore-tagged Cu (II) binding protein. They reported that the system is capable of detecting 0.1 pM Cu (II) and is based on a fluorescence quenching and lifetime reduction approach [145]. A micro structured optical fibre based platform using the fluorescence indicator lumogallion has been reported in the literature for detecting aluminium ions [146] alongside a quinolin-8-ol-5-sulfonate

embedded ion-exchange resin coated trifurcated fibre-optic bundle, that is also able to detect magnesium (II), zinc (II) and cadmium (II) [147]. The *in situ* analysis of chlorinated hydrocarbons (CHCs) in water has been described in the work of Krska, et al. [148]. The authors discussed a silver halide fibre coated with low-density polyethylene (LDPE) and a Fourier transform infrared (FTIR) spectrometer utilizing an off-axis parabolic mirror and a fibre-detector coupling system, to measure concentrations of CHCs between 1 to 50 mg/L in water.

Numerous research projects have addressed sensing ammonia gas using OFS. Some have discussed evanescent wave absorption technique [149], while others described surface plasmon resonance [150] or fluorescence [151]. A chitosan thin film coated extrinsic OFS mentioned in the work of Sidirolou and Nguyen [152] explains detection of ammonia based on refractive index change of the natural polymer chitosan.

A FPI based sensor that utilizes a no-core fibre (NCF) spliced between single mode fibres functionalized with chitosan (CS)/poly acrylic acid (PAA) self-assembled polyelectrolyte layers have been reported by Raghunandhan, et al. [153] for detecting  $\text{Ni}^{2+}$ , a heavy metal ion, which has an adverse effect on skin and bones if one is exposed to an overdose.

There is currently, considerable room for exploring FPI based chemical sensors for environmental contaminant detection as well as industrial chemical sensing applications as mentioned earlier. Thus, the following section provides detailed discussion on fibre optic Fabry-Perot interferometry (FFPI) based chemical sensors and their fabrication methods.

### **2.4.3 Fibre Optic Fabry-Perot Interferometric (FFPI) Sensors**

Over the years extensive research has been performed on various types of fibre optic Fabry-Perot interferometric (FFPI) sensors [154, 155]. Like other fibre-based sensors FFPI are known for their ease of fabrication, low cost, versatility, high sensitivity, quick response, precision and immunity to environmental noise. It has been reported that single-mode FP interferometric sensors can sense temperature, mechanical vibration, refractive index, pressure, acoustic wave, alternating voltage and magnetic fields effectively [155, 156]. A FFPI temperature sensor developed by Tseng and Chen has been reported to distinguish between temperature rise and falls [157]; the ultrasonic wave sensing capability of an FFPI sensor embedded in epoxy and submerged in water has been discussed by Tseng and Chen [157], while a pressure sensor formed by micromachining technology has been described by Kim, et al. [158]. In addition to these, a chitosan-based miniature acoustic pressure sensor with a sensitivity of 0.002 V/mPa at 1kHz has been investigated in work by Chen, et al. [159]. A comprehensive review of the characteristics and application of FPI sensors can be found in the works of Rao [154], Rao, et al. [160] and Islam, et al. [156].

As mentioned above, there is a long list of optical fibre FFPI sensor in diverse applications, currently with room for further development to suit present and future needs in the commercial sector. However, after surveying existing reports it has become evident that there are few FFPI based chemical sensors compared to other OFS sensor categories. Thus, one area of research where FFPIs can contribute more is aqueous contaminant detection. Therefore, the following sections discuss the basic operating principle of the

FPI sensors and reviews their contribution in chemical sensing operations followed by their potential in PFAS detection.

### ***Fibre Optic FPI Sensor Working Principle***

Any layer of material with thickness in the nanometre to micrometre range is considered as a thin film. Light that strikes the film of thickness  $d$ , as shown in Figure 2.6, is both transmitted and reflected. The transmitted light reaches the bottom surface and gets partially transmitted or reflected again. When the light reflected from the top and bottom surfaces interfere the phase difference between the two waves control the extent of constructive or destructive interference that they undergo. This phase difference is dependent on the thickness and refractive index of the thin film as well as the angle of incidence ( $\theta_1$ ) of the original wave that strikes it. An additional phase shift of  $180^\circ$  or  $\pi$  radians is introduced upon reflection at a boundary when the refractive index of the medium the light travels through is less than the refractive index of the material it strikes (as in the case of ray  $R_1$  in Figure 2.6). In other words, if  $n_1$  is less than  $n_2$  (Figure 2.6) and the light is travelling from material 1 to material 2, then a phase shift occurs upon reflection. However, the reverse is not true i.e. when light travels from denser ( $n_2$ ) to lighter medium ( $n_3$ ) it does not undergo the  $\pi$  shift. The optical path difference between the reflected waves  $R_1$  and  $R_2$  is given by  $2n_2d\cos\theta_2$ , where  $\theta_2$  is the angle at which light travels in the thin film. The nature of interference (i.e. constructive or destructive) that these reflected rays undergo is a function of the wavelength of light,  $\lambda$ . When the incident angle  $\theta_1$  is  $0^\circ$  then the transmitted and reflected rays of light pass, normally (i.e. without bending) and  $\theta_2$  is also  $0^\circ$  (this is demonstrated in the case of the single mode fibre based FPI discussed below).

A Fabry–Perot interferometer operates on the same principle of Fresnel reflections that are used to explain thin film interference. A polymer coating in a FFPI can be assumed to be an etalon to understand the sensing principle.

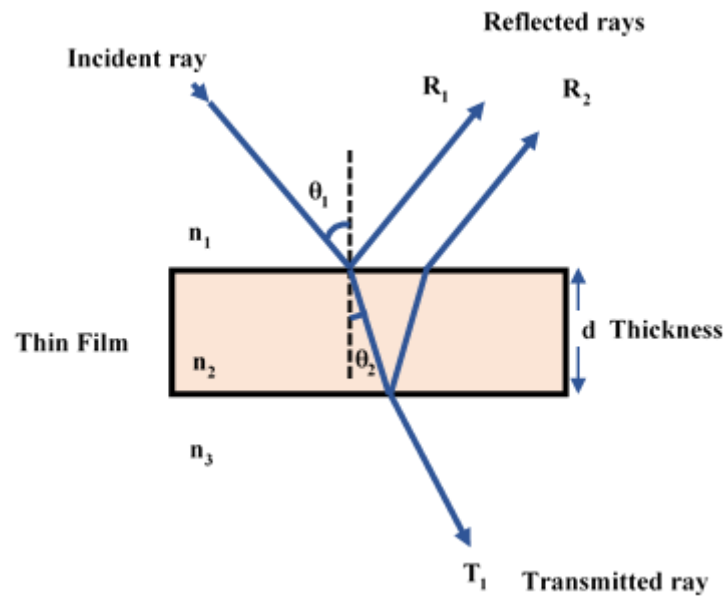


Figure 2.6 Light incident on a thin film

A Fabry-Perot Interferometer (FPI) or etalon is a device, which consists of two optical reflectors on either side of an optically transparent medium, for measuring small differences in the wavelength of light using interference. It is named after Charles Fabry and Alfred Perot, who developed the instrument in 1899 [161]. The phase of the light between the interferometer mirrors is modulated in response to changes in the effect being measured. Information about this phase change is obtained from the normalized reflected intensity. It has been reported that Fabry-Perot interference was first applied to fibre optic sensing in the 1980s [156].

The intensity of the resultant reflected spectrum from the Fabry-Perot etalon,  $I$ , can be calculated using the individual intensities of the reflected wavelength. The following

equation considers that  $I_1$  and  $I_2$  corresponds to intensities of the reflected rays  $R_1$  and  $R_2$ , shown in Figure 2.6.

$$I = I_1 + I_2 + 2\gamma\sqrt{I_1I_2} \cos\left(\frac{4\pi nL}{\lambda} + \phi_0\right) \quad 2.4$$

where  $\gamma$  is the degree of coherence  $\lambda$  is the wavelength of light in free-space, ' $nL$ ' is the optical path difference (OPD) and  $\phi_0$  is the initial phase difference of the reflected intensities. In the expression for OPD,  $n$ , represents the refractive index and  $L$  the length of the Fabry-Perot (FP) cavity or thickness of the etalon [160]. The cosine term in equation 2.4, is referred to as the overall or roundtrip phase shift ( $\Phi$ ) of the observed resultant reflection spectrum.

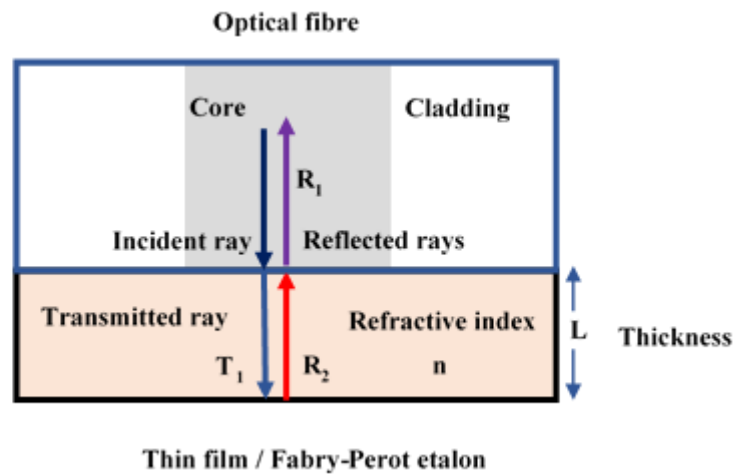


**Figure 2.7: Schematic of FFPI sensor showing a normally incident ray on the etalon and the corresponding transmitted and reflected waves at its boundaries.**

A cleaved fibre end-face has a reflectivity of 4% at the glass air boundary, which is affected by a change in the refractive index of the surrounding medium. When an FFPI is formed by coating the fibre end-face with a polymer the reflectivity at the glass-polymer boundary is less compared to the glass-air boundary, as the refractive index of the polymer is higher than that of air (Figure 2.7). However, the reflected intensity sweeps through

maximum and minimum interference effects depending on the amount of refractive index change of the material that forms the etalon or a change in the sensor cavity length due to perturbation. Early research findings have demonstrated that the amount of change in a parameter can be measured by comparing the information in a reflected spectrum with a known amount of perturbation to find a calibration constant for the FFPI sensor [162]. For carrying out such observations an experimental set up that is composed of a, light source, an optical spectrum analyser (OSA) and a fibre coupler as shown in Figure 2.8 may be used. Quantitative analysis of the parameter being sensed by the FFPI sensor can be done by measuring the phase shift ( $\Phi$ ) of the normalized reflection spectrum after data acquisition through such a set up.

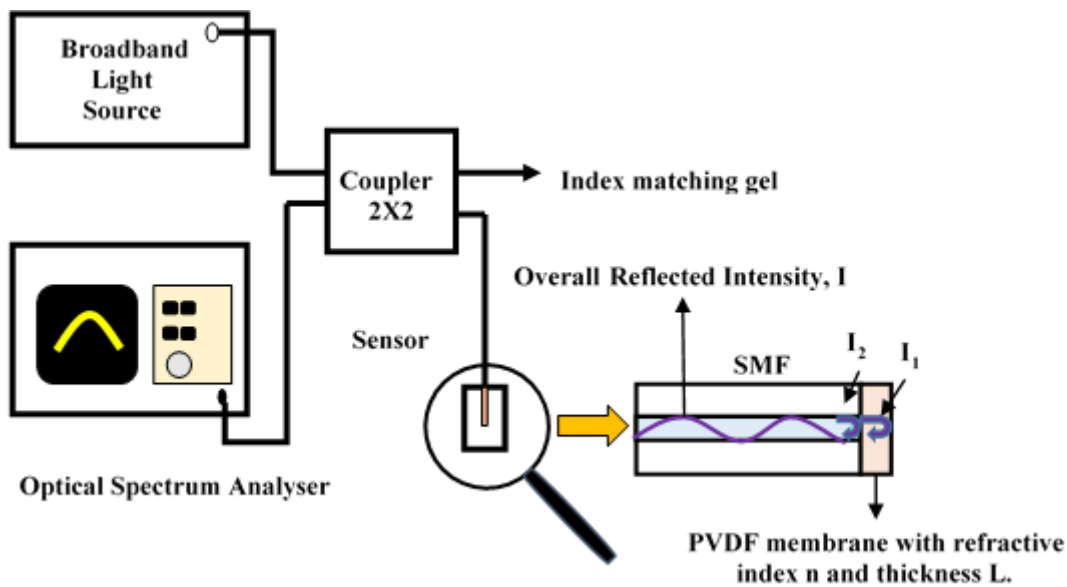


**Figure 2.8: Experimental setup for observing reflection spectrum from FFPI sensor consisting of a broadband light source, an optical coupler and an optical spectrum analyser.**

The free spectral range (FSR) or the spacing between adjacent interference peaks in the normalized spectrum, determines the finesse of the etalon, as can be seen in Figure 2.9. Finesse is a figure of merit and provides a measure of the interferometer's ability to

resolve closely spaced spectral lines that helps to understand the sharpness of the interference pattern. It has been reported in literature that a high finesse is characteristic of a high sensitivity FFPI sensor [155]. As shown in Figure 2.9, etalons with high finesse (red line) have sharper transmission peaks with lower minimum transmission coefficients,  $T_e$ , than a low-finesse etalon (blue line).

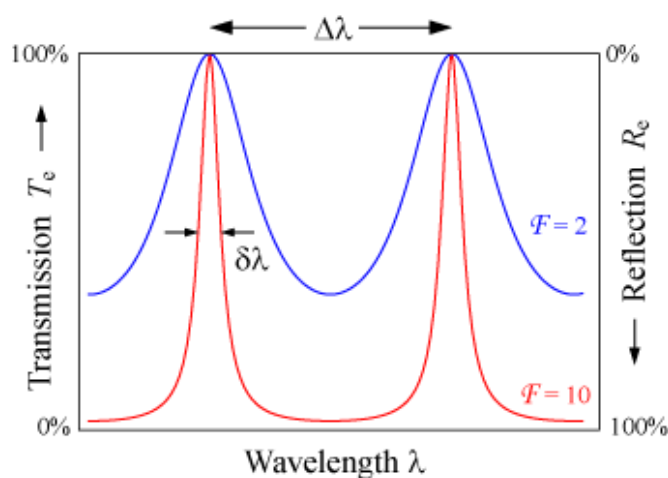


Figure 2.9 Shows transmission spectra of a low and a high sensitivity etalon as a function of wavelength where  $F=2$  (blue line) represents a low finesse and  $F=10$  (red line) represents a high finesse FFPI sensor. Percentage reflection from the low finesse FFPI sensor is more compared to that of the high finesse sensor.

### ***FFPI Based Chemical Sensors***

These OFS often make use of chemically selective spectrophotometric reagents that are held at the end of the fibre. In a FFPI based sensing system, functionalized polymeric materials are usually preferred as end-face coating substances for the detection of analytes. The following paragraphs present the range of research that has been investigated for humidity and gas or vapour detection using FFPI based sensors.

Arregui co-workers developed a FFPI humidity sensor using the ionic self-assembly monolayer (ISAM) process [163]. This method utilizes the electrostatic attraction between opposite charges of molecules to build multiple layers of coating on top of each

other. There are several steps in the ISAM process, which can be considered as a drawback when it comes to simplicity of the fabrication method. In the case of an optical fibre, the end-face is treated to create a surface charge. Then, it is alternately dipped into solutions of cationic and anionic polymers to create a multilayer thin film. The individual layer composition and thickness in this process can be controlled and works well on substrates made of metals, plastics, ceramics and semiconductors. However, disadvantages of this technique includes instability due to oxidation of the monolayers and defects arising from intrinsic and extrinsic factors related to cleanliness of substrates, purity of the adsorbates, methods of preparation or the thermodynamics of the monolayer formation [164, 165].

Maciak has reported a FFPI based hygrometer formed using standard multi-mode fibre for the measurement of relative humidity which utilizes a Nafion sensing film [166]. In a different experiment with the Nafion coated optrode, Pustelny, et al. [167] reported measurement of concentration of ammonia in a low and high relative humidity environment. The deposition of Nafion film at the fibre tip has not been explicitly discussed in this paper. However, Erwin [166] has referred to a layered structure for the formation of the Fabry-Perot cavity where polymethyl methacrylate (PMMA), polyethylene, polyisobutylene, chitosan and polyvinyl acetate have been mentioned as inhibitory layers deposited to attenuate the influence of humidity during ammonia sensing. The results of Pustelny's research have shown that the response to change in ammonia concentration is non-linear and a stable moisture level is required for good sensor performance.

A humidity sensor formed by splicing a single mode fibre to a hollow-core fibre, with a chitosan diaphragm has been reported by Chen, et al. [168]. In a hollow core fibre light is guided through the core (which may be filled with air or other gas) by virtue of the designed cladding that acts like mirrors by reflecting the light and confining it to the hollow core. It was not clear from the work of Chen, et al. [168] to what extent the design of their sensor caused it to be sensitive to both temperature and vibration besides humidity, for which appropriate laboratory conditions had to be maintained to obtain reliable data. In addition to these problems, the use of a delicate chitosan diaphragm as the hygroscopic material showed a lack of robustness in the sensor's structure.

Among FFPI based gas sensors, the fabrication of ammonia sensors by depositing thin films of zirconia ( $ZrO_2$ ) nanoclusters and poly (sodium-4-styrenesulfonate) salt on the cleaved ends of standard communications optical fibre using the electrostatic self-assembly method has been highlighted in the work of Galbarra, et al. [169]. In addition to monitoring the sensitivity of their sensor to ammonia the researchers have also recorded information that showed the sensor's insensitivity to certain other chemicals such as acetone, ethanol and dichloromethane.

A versatile sensor probe composed of a silver layer and a vapour-sensitive polymer layer that have been developed sequentially by depositing one layer over the other on the cleaved fibre end-face to form a FP cavity has been discussed in the work of Liu, et al. [79]. The combination of electro-less plating and dip coating utilized in their sensor fabrication method are not uncommon in the formation of thin-films and the preparation steps for the fabrication of the FPI are similar to the ISAM methods discussed earlier. Polyethylene glycol (PEG) 400 (RI=1.465-1.469) and Norland Optical Adhesive (NOA)

81 (RI=1.53-1.56) used by Liu, et al. [79] have shown different sensitivities to hexanol, methanol, and acetone vapours. This work introduced the concept that polar and nonpolar polymers have different response to vapour analytes for which reason it is very common for a gas sensor to incorporate a matrix of polymers to enhance the specificity of the probe.

While the choice of a suitable sensitive layer for a FFPI sensor depends on the measurand being sensed, the feasibility of sensor fabrication with it depends on the availability of the proper instruments and method. On this premise, a thin film developed on an optical fibre end-face with the polymer PVDF via the immersion precipitation technique is a novel and simple approach that can be adopted for fabricating a FPI sensor for carrying out instantaneous detection of a potential perfluoroalkyl compound like PFOA, PFOS and other perfluoroalkyls. There is a growing demand for a reliable, feasible and economic system for *in situ* measurement of these fluorosurfactants, due to the inapplicability of the conventional detection methods like HPLC or GC-MS for on-site, remote and real-time sensing, as discussed in Chapter 1. Hence the following section reviews the potential for developing FPI sensors based on polyvinylidene fluoride (PVDF) coating.

## **2.5 PVDF for Optical Fibre FPI (FFPI) Based PFOA Sensor**

### **2.5.1 Properties of PVDF and Sensitivity to PFOA**

A FPI based optical sensing method for detecting PFOA in aqueous solution can be cost effective and very user friendly compared to GC-MS or LC-MS besides being a very feasible portable solution. As mentioned in the earlier section, a possible way to optimize a FPI sensor to detect PFOA/PFAS in water is by coating it with a suitable polymer. Polyvinylidene fluoride is a fluoropolymer, similar in characteristics to Teflon (trade

name for polytetrafluoroethylene or PTFE), which has been hypothesised in this work to have the capacity to absorb PFOA [170]. PVDF is resistant to UV radiation and abrasion [82], has good heat tolerance capacity and is non-corrosive like PTFE, which makes it a robust sensor material. While there is a lot of similarity in the characteristics of PTFE and PVDF, the two polymers have considerable differences in their membrane formation techniques [171]. For instance, PVDF solution can be formed easily, with which membranes can be developed using the phase inversion process at room temperature, while PTFE cannot be processed in the same way. This gives PVDF an added advantage in thin film formation processes. Additionally, it is also a known ferroelectric material and exhibits pyro and piezoelectric properties, which have been utilized in many different sensor applications.

PVDF being a polymorph has the ability to exist in the  $\alpha$ ,  $\beta$ ,  $\gamma$ , and  $\delta$  phases and among these the  $\beta$ -phase is more popular in pyro and piezoelectric applications [172]. The pyroelectric property of PVDF which arises due to the  $\beta$ -phase, gives it the ability to generate a temporary voltage when it is heated or cooled, which is a feature of great technological importance, especially in sensor application [173, 174]. More information on the characteristics of PVDF thin film and their fabrication techniques is provided in the next section.

### **2.5.2 FFPI Fabrication with PVDF and Features of PVDF Coating**

The brittle nature of bare optical fibre is the most vulnerable aspect of this otherwise remarkable modern tool, which necessitates the use of a suitable coating for protection. Since a portion of bare fibre in the sensor may serve as a weak link, any stripped portion of the fibre also needs to be coated with PVDF for the formation of the FPI sensor.

Usually, the choice of a standard technique such as physical vapour deposition (PVD), chemical vapour deposition (CVD), spin coating, electrospinning, electrochemical deposition, electroless plating, nanolithography, Langmuir–Blodgett (LB) technique, layer-by-layer (LbL) electrostatic self-assembly etc., depends on a number of factors governing the application and the costs [175].

The immersion precipitation (IP) technique of membrane formation, a mechanism which can help form the FPI in a non-conventional and convenient way, bears some resemblance to the LbL technique, where thin films are formed by depositing alternating layers of oppositely charged materials with wash steps in between. The IP is a wet process like the LbL with quite different principles that govern the formation of the coating layer, but like LbL it is inexpensive, convenient and can be performed at room temperature. In LbL the pH, concentration, ionic strength, curing temperature, or ratio between the polyelectrolytes used, need to be controlled for forming multiple layers of coating. In immersion precipitation only the concentration of the solution and the number of dips need careful determination for the development of a desired coating with suitable thickness on an optical fibre, which makes it a very convenient process.

When a polymer solution is cast on the material to be coated and then submerged in a coagulation bath containing a non-solvent a porous coating results from the IP technique. Crystallization and liquid–liquid de-mixing have been considered by many researchers to be the processes that strongly influence the membrane morphology [176-181]. It has been reported that the membrane structure, which plays an important role in water influx, is determined by the composition of the solvent in the polymer solution and the composition of the non-solvent baths. Other studies have shown that the type of solvent used in the

formation of the polymer solution affects the formation of the  $\beta$ -phase rich PVDF [83]. In mixed solvent systems (e.g. tetrahydrofuran/DMF, methyl ethyl ketone/DMF or ethanol/DMF), it has been found that increasing the content of DMF facilitates the formation of  $\beta$ -phase [83, 182-184]. In addition, the choice of anti-solvent in IP has also been reported to play a key role in the synthesis of the  $\beta$ -phase and the effect has been demonstrated using ethanol and water as coagulation baths by Mago, et al. [185]. The thin film's characteristic electrical properties and hydrophobicity result from the polarity of alternating  $\text{CH}_2$  and  $\text{CF}_2$  groups on the polymer chain [186, 187] that affects the hydrophobic or dipole-dipole interaction with molecules. Generally, these PVDF membranes exhibit very good stability in harsh thermal, chemical, or ultraviolet conditions [187].

Lin, et al. [176] have reported that the polymer membrane formed by liquid-liquid demixing yields a dense skin with a porous bulk containing macrovoids. They also said that as the porosity of the skin increases the water flux also increases and the tensile strength of the membrane decreases. Buonomenna, et al. [188] suggested that even though concentration of the polymer solution has little effect on the overall morphology of the membrane, it plays a role in determining the resulting density of the skin layer.

Kuo, et al. [189] reported the development of highly hydrophobic membrane surfaces using alcohol as a coagulant via a wet immersion method. They used Kynar 760 and anhydrous N-methyl-2-pyrrolidinone (NMP) in their work, alongside a coagulation bath of alcohol (methanol, ethanol, n-propanol or n-butanol) for forming the polymer membrane. The results obtained have shown that microporous membranes with water

contact angles ranging from  $144^\circ$  to  $148^\circ$  can be achieved with their techniques, which are all higher than the ones obtained using only a water bath.

The existing literature show that water influx through PVDF membranes occur with a high trans-membrane pressure for membranes with dense pores on the surface [176]. Typical values of this pressure lie between 35 and 400 kPa. This helps assure that if a membrane is developed from a carefully designed solution of PVDF and appropriate coagulation bath, it will be able to protect the fibre end-face as well as the bare portion of the optical fibre in an aqueous environment. However, the deposition of a layer of polymer on the surface of a bare optical fibre using dip coating does not ensure a uniform thickness over its cylindrical shape or the end-face. The method only makes the process of coating less complex and allows some flexibility in controlling the thickness of the layer. Details about PVDF coating formation on the optical fibre end-face are provided in the next chapter (Chapter 3) and the potential application of the device in sensing contaminants in water is discussed below.

### **2.5.3 Potential Application of FFPI Based Sensor in PFAS Remediation**

From the information provided in the PFAS National Environmental Management Plan (NEMP) [37], it is apparent that there is a need for a portable sensor technology, which can provide quantitative data about specific PFAS concentrations and their forms instantaneously so that quick decisions can be taken regarding regulations around contaminated locations. A PVDF based FFPI sensor can contribute to the plan through appropriate functionalization processes.

The NEMP also emphasizes the treatment processes or remediation following the identification of the PFAS, which is required to be extremely thorough and involve: a

separation stage, an encapsulation procedure and a step for removal by destruction. These strict procedures are set to ensure that reusable items, such as water and soil, have a safe level of these contaminants for tasks such as irrigation, dust suppression, industrial processes, recharging of aquifers etc. [37]. A brief outline about these follows in the next paragraphs as these are important issues but more suited for discussion in an appropriate context other than this thesis.

The most common separation technique that is applied to segregate contaminants from water is filtration. In water treatment facilities filters are also referred to as membranes, where the surface is the main zone of particle separation. Some adsorption devices like activated charcoal and ion exchange resins which bring about separation of particles based on surface charge, are also known as filters commercially and are employed in the removal of PFAS in water. Ion exchange membranes, in particular, are known for their use in ultrafiltration and microfiltration processes [190], which appear in the first step of the treatment. Subsequent steps for total removal of PFASs can include the interim measures taken with granular activated carbon or polymer supported activated carbon [191] and ozofractionation [192]. Similarly chemical oxidation can be used for the remediation of some PFAS just like electrochemical oxidation, but with a resultant short chain PFAS or undesirable by products [192]. Additionally, sonolysis, another potentially destructive technology, can be used but it faces challenges during scale up. Apart from this, there are thermal technologies to treat PFAS in soil with a plethora of other technologies still in the development stage, which can manage PFAS and are evolving to meet current needs.

The role of an optical fibre sensor utilising a PVDF coating as a sensing material, in determining the correct remediation technique, is an indirect one. The absorbance of specific PFAS on the polymer thin film and the concentration of the contaminant detected by the OFS can be considered to choose a particular remediation process. If the PVDF coating is functionalized with a certain nanoparticle or adsorbent material to detect a specific PFAS from aqueous solution, then depending on the optical response the applicability of that chosen adsorbent or nanoparticle can be considered in the remediation process. If a direct link can be formed between the absorbance of the material and the optical signal it will be a more convenient technique for determining the suitability of the adsorbent material in PFAS remediation process compared to the traditional GC-MS or LC-MS techniques that are currently the primary methods of analysing PFAS concentration in test samples. The following section provides a detailed description of this technology.

## **2.6 Competing Methods for the FFPI based PFAS/PFOA Sensor**

Analytical methods involving GC-MS and LC-MS rely on physical separation and mass analysis of the substance under investigation. In order to understand the differences in the techniques mentioned along with their complexity and inapplicability for *in situ* detection, a basic understanding of the elements present in LC-MS and mass analysers are required. So, a brief account of the separation and detection procedures, ionization processes and types of mass analysers is provided below with a general diagram of the set up in Figure 2.10 to demonstrate the desirability for a cost effective, quick and portable PVDF based FPI sensor mentioned above.

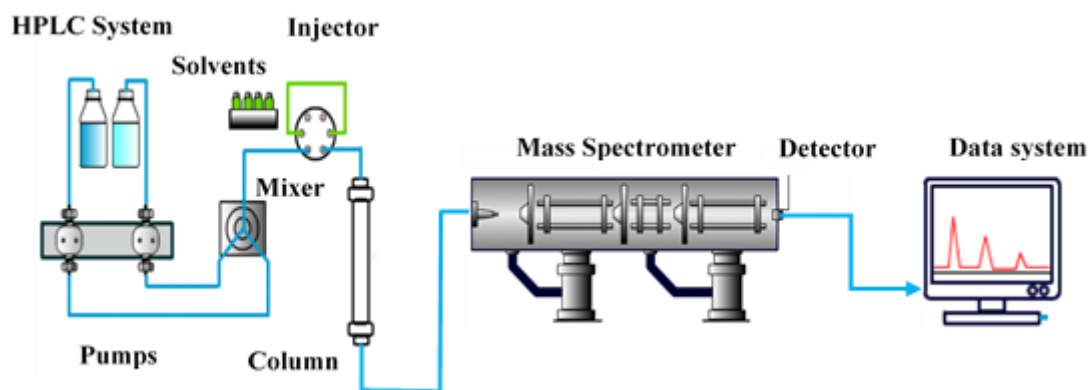


Figure 2.10 LC-MS system showing phase separation and mass analysis components [160].

### 2.6.1 Liquid Chromatography Mass Spectrometry

Liquid Chromatography (LC) is a technique used in analytical chemistry to separate, identify and quantify components in a mixture. In HPLC the analytes are differentially segregated between the mobile phase (eluent) and the stationary phase (adsorbent packed into a column) based on hydrophobic interaction, ion-exchange, ion-pair, surface localization, etc. In this process the analyte is prepared from and is soluble in the solvents used in the mobile phase [193]. As the solvent molecules "elute", or pass down the chromatography column, they go through the adsorbent/analyte complex and in the process displace the analyte by binding to the adsorbent in its place. After the analyte has been displaced, the mobile phase is carried out of the column for analysis. In the HPLC-MS technique, as shown in Figure 2.10, it typically flows into an ionization chamber to be converted into ions in the gas phase, which are then passed down to the mass spectrometers for detection according to their mass to charge ratio. The next section discusses the various ionization techniques used in mass analysers in the LC-MS methods.

## 2.6.2 Ionization Processes in LC-MS

A mass spectrometer (MS) is an analytical instrument that ionizes (adds or removes electrons to) atoms or molecules and sorts the gas phase ions based on their mass-to-charge ( $m/z$ ) ratio value. Strong electric fields are used to bring about ionization in the vapour or condensed phase. When this is done under atmospheric pressure condition, the process is referred to as Atmospheric Pressure Ionization (API). The forms of ionization, which are commonly used in LC-MS include:

- Electrospray Ionization (ESI)
- Atmospheric Pressure Chemical Ionization (APCI)
- Atmospheric Pressure Photo Ionization (APPI)
- Matrix Assisted Laser Desorption Ionization (MALDI)

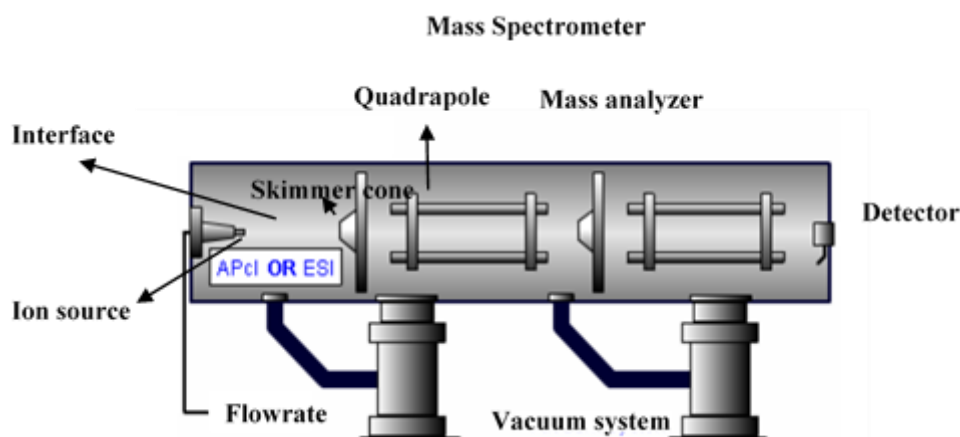


Figure 2.11 Mass spectrometer [193].

Figure 2.11 shows the different sections of a mass spectrometer. Only preferentially sampled gas ions pass through the skimmer cone, a specially designed orifice, into the mass analyser. Quadrupoles in the chamber, which are an arrangement of rods through which oscillating electric fields can pass, separate the ions according to their charge. In

tandem mass spectrometry ions emerging from the first mass analyser are further fragmented in a collision chamber before being passed onto the next mass analyser.

The ionization process starts with the desolvation or removal of the solvent molecules from the analyte in the eluent, which enters the interface through the ion source or capillary. It is then followed by charging of the analyte molecule or derivatives in the interface. In electrospray ionization (ESI) the analyte ions are pre-formed in the mobile phase before they enter the interface, whereas in atmospheric pressure chemical ionization (APCI), they are formed in the interface via the charge transfer process in the gas phase [193].

The pH in the eluent influences the analyte ion formation before or after it passes through the HPLC column in ESI, thus, ionization is carried out in the liquid or condensed phase. The charged droplets undergo evaporation by a heated gas as a desolvation process to yield the gas phase analyte ions.

In the APCI process the eluent molecules form aerosols when they emerge out of the capillary into a heated interface region filled with an inert nebulizing gas. An electric discharge from a pin connected to a high potential causes the elute molecules to become ionized, which then ionizes the analyte molecule via charge transfer reactions or molecular interaction [193]. Both the APCI and the ESI process form pseudo-molecular ions characteristics of which are regulated by the nature of proton affinity of the analyte molecule.

Atmospheric pressure photo ionization (APPI) is the ionization process mostly used in the case of non-polar or low polarity compounds which cannot be easily ionized by ESI

or APCI [193]. Here the aerosol of the eluent droplets is ionized by photo-irradiation. Ultraviolet lights are used in direct APPI processes to form radical cations. When the photons energy exceeds the ionization potential of the analyte molecule, it causes the loss of an electron to create a radical cation. In dopant assisted APPI, the dopant molecules are ionized directly by the UV photons. Since the dopant molecules are greater in number than the analyte molecules, due to increased collision rate, more dopant ions are formed. These dopant ions then donate a proton to the analyte molecule or receive an electron from the analyte molecule to form radical cations or anions respectively. This technique heats up the analyte samples to high temperatures for which it is unsuitable for molecules prone to thermal degradation [194].

Matrix assisted laser desorption ionization (MALDI) is a method of ionization in which the sample is ionized with a laser with minimal fragmentation. Like the APPI technique, the sample is mixed with a matrix that absorbs the laser radiation and transfers a proton to it. The laser is always pulsed, and typically in a vacuum [195].

The next step after ionization is the analyte fragment separation process according to the mass to charge ratio, which is done in the mass analyser. The following section briefly discusses the different mass analysing techniques.

### **2.6.3 Mass Analysers in LC-MS**

There are many different mass analysers which are commonly used in association with liquid chromatography mass spectrometry that differ in their fundamental way of separating a species based on its mass to charge ratio [193]. These are the:

- quadrupole and ion trap mass analysers

- time of flight mass analysers
- magnetic sector mass analysers

Quadrupole and ion trap mass analysers: as the name implies are composed of four cylindrical/ hyperbolic metal rods or poles, set parallel to each other. Two opposite rods have positive potential and the other two have a negative potential. The applied voltages affect the trajectory of the ion fragments traveling through the space between the poles. For a given direct current (DC) and alternating current (AC) voltages, only ions of a specific mass-to-charge ratio ( $m/z$ ) pass through the central axis of the quadrupole. A mass spectrum is obtained by monitoring the ions passing through the quadrupole as the ac and dc voltages on the rods are varied. By a suitable choice of the voltage ratio a mass filter is formed which resolves ions with low and heavy atomic masses.

Ion trap mass analysers use a combination of electric or magnetic fields to capture charged particles. It may incorporate a Penning trap [196], Paul trap [197] or the Kingdon trap [198]. It is common for mass spectrometers to use a linear quadrupole ion trap as a selective mass filter. A Paul trap is a type of quadrupole ion trap that uses static DC and AC electric fields to trap ions. The amplitude of both the AC and DC voltages can be varied to selectively trap an ion of specific  $m/z$  ratio and provide a path to the non-selected ions to exist the trap. Trapping instruments are capable of performing multiple steps of analysis, which can be presented as MS to the power of  $n$ . In most cases the number of steps,  $n$ , is not indicated, but sometimes the value might be specified to indicate the stages of separation; for example,  $MS^3$  would refer to mass analysis using a three-step process of separation. The spectra acquired using this technique is different from those obtained using other techniques.

#### **2.6.4 Time-of-Flight (TOF) Mass Analysers**

In these instruments, the measurement technique is quite simple. The ions are accelerated by a predetermined electric field which causes the ions with the same charge and mass to have the same kinetic energy. The velocity of the ion depends on the mass to charge ratio and does not change after acceleration when it is moving through the field-free region. It can be calculated by dividing the length of the path of flight of the ion by the time taken by that ion to reach a detector. This time is a measure of the ion's mass-to-charge ratio, which causes different ion fragments to have different velocities. It has been seen that heavier ions of the same charge have lower speeds and ions with higher charge have higher velocity.

#### **2.6.5 Magnetic Sector Mass Analysers**

These types of analysers, like the TOF analysers mentioned above, accelerate ions through a flight tube, where they get separated by charge to mass ratios ( $z/m$ ) by a magnetic field instead of an electric field like the former analyser. As a charge enters the magnetic field, it is deflected in a circular motion with a unique radius in a perpendicular direction to the applied magnetic field. The radius ( $r$ ) of this arc depends upon the momentum of the ion, the charge of the ion ( $z$ ) and the magnetic field strength ( $B$ ). Thus, ions in the magnetic field, which experience a centripetal force has a velocity ( $v$ ) given by the following equation:

$$v = \frac{Bzr}{m} \quad 2.5$$

The  $m/z$  value can be determined using the velocity equation shown above if both the magnetic field magnitude, and the potential difference ( $V$ ) in the accelerator are kept

constant. As the electric potential energy of the ion gets converted to its kinetic energy the  $m/z$  can be calculated by equating the two as shown below:

$$\frac{m}{z} = \frac{B^2 r^2}{2V} \quad 2.6$$

When two or more mass spectrometry methods are combined for the analysis of a species it is called tandem mass spectrometry (MS/MS) [193]. In this process, ions are formed and separated, based on their  $m/z$  ratio, in the first stage of mass spectrometry (MS1). After that, ions of a specific  $m/z$  ratio are selected and fragmented to form the product ions, by collision-induced dissociation, ion-molecule reaction, photo dissociation, or other processes and then the resulting ions are further separated and detected in a second stage of mass spectrometry (MS2). The process can be divided into the following categories:

- *Tandem in space*: the separation elements are physically separated and distinct and can be a sector mass analyser, transmission quadrupole mass analyser, or time-of-flight mass analyser.
- *Tandem in time*: the separation is brought about by ion trap instruments, which uses ions, trapped in the same place, with multiple separation steps taking place over a period of time. A quadrupole ion trap instrument can be used for such an analysis.

Tandem mass spectrometry is preferred when high selectivity and sensitivity is required for quantitative analysis. As with any analytical method the process ends with the detection of the chemical species. Therefore, a brief account of the detectors follow this section after Table 2.2, which lists the advantages and disadvantages [67,

199-201] of the different mass analysers. Parameters related to size, cost, resolution and ionization techniques are used as a measure of comparison in the table.

**Table 2.2 Comparison of Mass Analysers**

<b>Mass Analyser</b>	<b>Advantage</b>	<b>Disadvantage</b>
<b>Quadrupole</b>	<ul style="list-style-type: none"> <li>• Both positive and negative ions can be detected easily</li> <li>• Good reproducibility</li> <li>• Comparatively small size</li> <li>• Low-cost</li> <li>• Uses low-energy collision-induced dissociation</li> </ul>	<ul style="list-style-type: none"> <li>• Low resolution</li> <li>• Low mass range</li> <li>• Depends strongly on energy, collision gas, pressure, and other factors</li> <li>• Poor compatibility with MALDI</li> </ul>
<b>Ion Trap</b>	<ul style="list-style-type: none"> <li>• Medium resolution</li> <li>• Good compatibility with pulsed ionization methods such as MALDI</li> <li>• Applies non-destructive ion detection technique</li> <li>• Good compatibility with tandem in time spectrometry (MS<sup>n</sup>)</li> <li>• Simple design and small size</li> <li>• Low cost</li> <li>• Easy to resolve both positive and negative ions</li> </ul>	<ul style="list-style-type: none"> <li>• Limited mass range</li> <li>• Strict low-pressure requirements make the use of an external source necessary for most analytical applications</li> <li>• Ion molecule reactions and space charge affect the outcome</li> <li>• Harmonics and sidebands are present in the mass spectra</li> <li>• Depends on collision energy, collision gas, and other parameters</li> </ul>
<b>Time of Flight</b>	<ul style="list-style-type: none"> <li>• Fastest MS analyzer</li> <li>• Works well with pulsed ionization methods (or MALDI)</li> <li>• Simple design</li> <li>• Low cost</li> <li>• Highest mass range</li> <li>• High resolution</li> </ul>	<ul style="list-style-type: none"> <li>• Low resolution</li> <li>• Not compatible with electrospray ionization method</li> <li>• advanced designs have limited mass range</li> </ul>
<b>Magnetic Sector</b>	<ul style="list-style-type: none"> <li>• Very high reproducibility</li> <li>• Best quantitative performance among analysers</li> <li>• Capable of high resolution, sensitivity and dynamic range</li> <li>• Good reliability (manufacturer dependent)</li> </ul>	<ul style="list-style-type: none"> <li>• Not well-suited for pulsed ionization methods (e.g. MALDI)</li> <li>• Expensive.</li> <li>• Massive size</li> <li>• Slow scanning</li> </ul>

### 2.6.6 Detectors in LC-MS

Detectors are an important component of mass spectrometers. They convert the selectively separated ions from the mass analysers into usable electrical signals. An ion detector can be thought of as two metal grids separated by air with opposite charges on them. An electric potential difference (voltage) exist between the two grids. When an ionized species enters the region between these two grids it causes a current to pass from one to the other. This current is amplified and used as a signal.

The higher the concentration of the chemical analyte, the greater the number of ions generated, and in return the greater is the current. The detectors can be point type or array type. In point type detectors the ions are temporally and sequentially resolved, whereas in array type detectors the ions are spatially resolved and detected simultaneously.

Thus, all the discussion about the methods and instruments used in the conventional detection techniques, has shown why the LC-MS or GC-MS processes are time consuming, complex and unsuitable for *in situ* measurement and analysis of PFOA/ PFAS in the natural environment. It is evident from the information found in the existing literature that a reliable, cost effective and portable system to detect PFOA/ PFAS does not exist. Furthermore, a Fabry-Perot interferometry based optical fibre sensor has never been utilised for the purpose of sensing a perfluorinated compound prior to the proposed project. Therefore, in light of the gap in the market, the weaknesses of conventional systems and the capabilities of optical fibre sensors, this research aims to demonstrate that the PVDF coated fibre has the potential to address *in situ* measurement of PFOA in aqueous solutions. As stated in section 1.4, this objective would be met by undertaking a comprehensive sensor fabrication and characterization protocol that would help provide

proof of concept, while considering effect of cross-sensitivity to temperature and other environmental conditions.

## **2.7 Chapter Summary**

This chapter has provided an overview of the characteristics of optical fibres and their sensors. In addition to discussing the different OFS categories it has reviewed the details of FFPI based chemical sensors and provided an understanding of the gap in literature with regards to the lack of OFS in PFAS sensing. Following this, the chapter has also highlighted the features of PVDF as FFPI sensor material and discussed how it can contribute to the PFAS detection process. It has given an account of the existing analytical methods that the FFPI would have to compete against in order to emerge as a standalone superior technology. This chapter has therefore, formed the basis for discussing sensor fabrication through PVDF membrane synthesis in the following chapter.

## **3 Development and Optimization of PVDF Coated Fibres**

---

### **3.1 Overview**

In the previous chapter, a general literature review was presented leading to the concept of developing a PVDF coated optical fibre sensor for PFOA. In this chapter, the PVDF thin film formation process via the immersion precipitation (IP) technique and optimization of the coating for sensing operations is discussed in addition to the transformations that the fabrication and detection process underwent before they were optimized to deliver functional PVDF coated fibres. This chapter also highlights that a smooth, even coating that enabled the coated fibre end-face to produce a sinusoid like reflection pattern was preferred from a data analysis perspective. Therefore, it provides the details of how it was achieved through optimization in the fabrication procedure after a large number of trials and testing of coated fibres using an optical spectrum analyser.

### **3.2 Coating Fabrication Technique using PVDF**

The formation of a PVDF membrane using the Immersion Precipitation (IP) technique, on the cleaved end-face of an optical fibre requires the structure to be dipped in the polymer solution followed by submergence in a coagulation bath. The IP technique is a standard procedure for forming microporous flat and tubular membranes used in filtration tasks. Since the bare optical fibres are extremely delicate and cylindrical in shape, the conventional casting technique, which involves spreading the solution with a casting blade, is not a suitable method for depositing the polymer solution as it can cause permanent damage by breaking the structures. For this reason, the dip coating procedure has been followed in this research to coat optical fibre end-faces. A trial and error method

for developing a coating of desirable thickness to produce satisfactory Fabry-Perot interference effect has been explored.

It was observed during previous trials that a viscous PVDF solution works better in forming a membrane or layer of coating on the bare optical fibres. The following section provides a description of the procedures adopted in this research to form PVDF solutions using the solvents methyl ethyl ketone, acetone and N, N-dimethylformamide separately to determine the best combination for a membrane that exhibits satisfactory Fabry-Perot Interference (FPI) and displays good adhesion to the bare glass optical fibre.

### **3.2.1 Materials**

Two types of PVDF polymer were used: Solef 1015 from Solvay with very high molecular weight and density between 1.75-1.8 g/mL and powdered poly (vinylidene fluoride) from Sigma-Aldrich, having an average molecular weight,  $M_w=534,000$  and density 1.74 g/mL. Solvents Methyl Ethyl Ketone (MEK), Acetone and N, N Dimethylformamide (DMF) were obtained from Sigma-Aldrich. The resin polyvinyl butyral (Butvar) was purchased from Sigma-Aldrich. Ultrapure water used as coagulation bath was generated using a Millipore system. All the materials for the experiments have been used in their original form.

Four techniques for forming the polymer solution with the two PVDF grades were investigated using various combinations of MEK, acetone and DMF to determine which process results in the formation of a desired coating on the optical fibre end-face. The presence of the desirable  $\beta$ -phase of PVDF in the developed coating was observed using FTIR spectroscopy. A Fourier-transform infrared (FTIR) spectrum represents a fingerprint of a sample with absorption/ transmission peaks that correspond to the

frequencies of vibrations between the bonds of the atoms, which make up the material [202]. As different materials have different combination of atoms, no two compounds produce an identical infrared spectrum and thus each spectrum is unique. Therefore, infrared spectroscopy results in a positive detection of a specific material and its composition. In addition, the size of the peaks in the absorption spectrum is a direct indication of the amount of material present [202]. A general description of the apparatus used in the trials have been provided below. Alongside this a table which shows the steps followed in making the polymer solutions is provided for ease of understanding. The differences in the individual techniques are highlighted in the respective paragraphs that discuss them in the following section.

### **3.2.2 Apparatus**

The experimental set up used in the formation of PVDF solution included a hot plate with magnetic stirrer, a beaker, retort stand and clamp for support and thermometer for monitoring temperature, as shown in Figure 3.1.

A Perkin Elmer Frontier Fourier-transform infrared (FTIR) spectrophotometer with a diamond attenuated total reflectance accessory was used to obtain information on any composition of PVDF membranes.

A Hitachi TM3030 Plus Tabletop Scanning Electron Microscope (SEM) using an accelerating voltage of 15 kV in backscattering mode was used for obtaining the image of the membranes, coated fibre end-faces and cross sections.

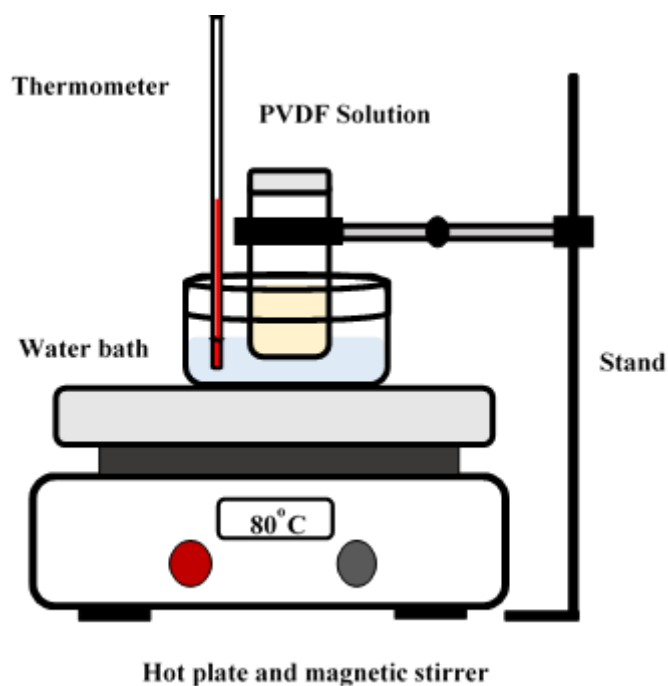


Figure 3.1 Experimental set up for forming PVDF solution.

### 3.2.3 Method of forming PVDF solution using MEK

A clear viscous PVDF solution, which worked better, compared to a dilute solution in forming a sustainable coating, required dissolving the PVDF powder in MEK under continuous heating and stirring at a constant temperature of 76 °C for 15-30 minutes. Mass fraction of the solute and solvent determined the solubility of the polymer in the solvent at a certain temperature for which predetermination of the quantities of PVDF powder and MEK was required. The optimum ratio for this was finalized through a trial and error method. Table 3.1 describes how a clear PVDF solution was formed:

**Table 3.1 Steps in forming PVDF solution**

<b>Step No.</b>	<b>Experimental Process</b>
1	A known volume of the solvent (<20 mL) is transferred into a beaker.
2	The beaker is then placed in a water bath maintained at a constant temperature using a heating plate and under continuous stirring.
3	A known mass of PVDF powder (<2 g) is weighed and transferred into the beaker in small portions.
4	The PVDF is dissolved under continuous stirring for up to 60 minutes to produce a clear solution.

### **3.2.4 Method of forming PVDF solution using MEK and Acetone**

The steps, which have been followed to form this solution, are quite like the ones used for forming the PVDF solution using only MEK discussed in Table 3.1. The differences are in the temperature at which the mixture was heated, and the proportion of solvent used. Since Acetone has a boiling point of 56 °C and MEK has 80 °C the combined solvent mix was heated at 55 °C and not beyond 60 °C to prevent boiling and vaporization of the solvent and consequently a change in concentration of the solution. The combination used for good adhesion from this trial consisted of a mixture of 9 mL Acetone and 5 mL MEK for 1.14 g of the PVDF grade from Sigma-Aldrich.

### **3.2.5 Method of forming PVDF solution using MEK and DMF**

The PVDF powder from Sigma-Aldrich has a high solubility in this solvent mixture and a clear solution was easily formed in the 60-70 °C temperature range using the steps mentioned in Table 3.1. A MEK and DMF mixture in a 9:5 ratio was used to form a viscous solution that would form a sustainable coating on the bare optical fibre end-face.

### **3.2.6 Method of forming PVDF solution using DMF**

It was seen that the solvents Acetone and MEK could not dissolve the PVDF grade from Solvay (Solef 1015) to form a solution even with heating, only DMF could. Therefore, in this trial, 1.67 g of Solef 1015 was dissolved in 14 mL DMF to obtain a polymer solution by heating for one hour in a water bath at 80 °C.

### **3.2.7 PVDF Coating Formation using Immersion Precipitation**

The PVDF coating on the cleaved single mode fibre end-face was developed using the Immersion precipitation (IP) technique; i.e. by dipping the fibre tip in the polymer solution and then submerging it in ultrapure water. The novel sensor fabrication process, is depicted in Figure 3.2. The coating steps were repeated several times to obtain a PVDF thin film thickness in the 10-50 µm range on the fibre end-face, for observing Fabry-Perot interference (FPI).

### **3.2.8 Method of Identifying β-Phase PVDF in Coating**

The polymer solutions formed using the four techniques mentioned above were used to develop flat films which were examined using the Perkin Elmer FTIR spectrophotometer. The FTIR spectrum was scanned for a peak at 840 cm<sup>-1</sup>, which was indicative of the β-phase of PVDF. When the peak was identified its corresponding normalized absorbance was noted. A greater value of normalized absorbance was suggestive of a greater abundance of the identified phase in the polymer.

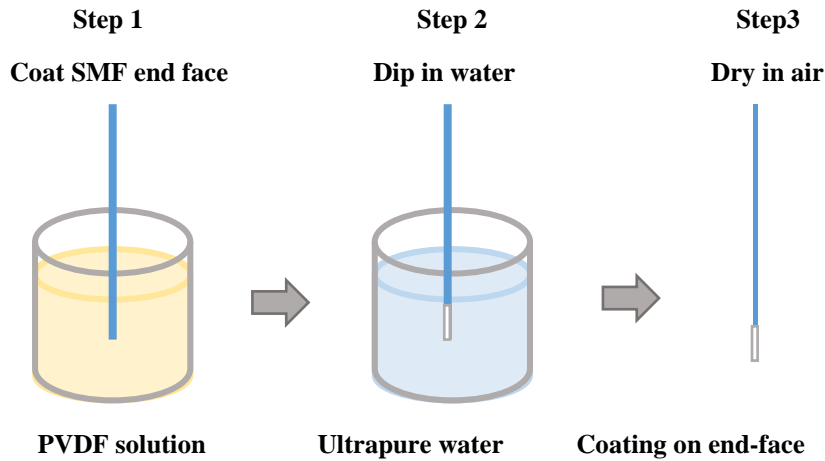


Figure 3.2 Sensor fabrication using immersion precipitation.

### 3.2.9 PVDF Coating Optimization Process

As discussed in the previous section, the expectation from a PVDF coating on an optical fibre end-face was to demonstrate Fabry-Perot interference through which PFOA/PFAS detection test could be carried out. Several factors played important roles in determining the quality of the coating and the corresponding FPI. Among them, the most important or primary factors were concentration of the PVDF solution, number of dips (for controlling thickness of the coating), surface morphology or structure (defined by density, size of pores and roughness) and adhesion of the coating to the fibre's glass surface. Secondary factors that directly or indirectly affected the primary factors included the polymer grade and solvent combination used in the PVDF solution mixture and the presence or absence of cross-linking reagents or adhesives in the polymer solution.

It is known from literature sources [83] that use of some specific solvent and polymer combinations determine the formation of the  $\beta$ -phase of PVDF, which plays an important role in sensing. On the other hand, use of a suitable cross-linker assists in the bonding of

the polymer with the fibre's glass. Based on these reported observations the undertaken experiments for the optimization of the coating involved:

- varying the concentration of PVDF solution and the subsequent number of dipping
- testing combination of solvents and polymer grades
- determination of the presence of the  $\beta$ -phase (using Fourier Transform Infrared (FTIR) spectroscopy)
- inspection of surface morphology of the coating (using Scanning Electron Microscopy)
- analysis of the effect of the adhesive resin polyvinyl butyral (Butvar) on glass-polymer coupling and Fabry-Perot interference

The following paragraphs discuss the ways in which the coating development was optimized.

The quality of interference pattern, which was obtained from a coated optical fibre, was given priority to find a trade-off between the concentration of the PVDF solution and the number of dips required to form the thin film on the fibre end-face. A normalized FPI reflection spectrum (Figure 3.3), which resembles a sinusoid like shape with multiple peaks, provides ease of data analysis.

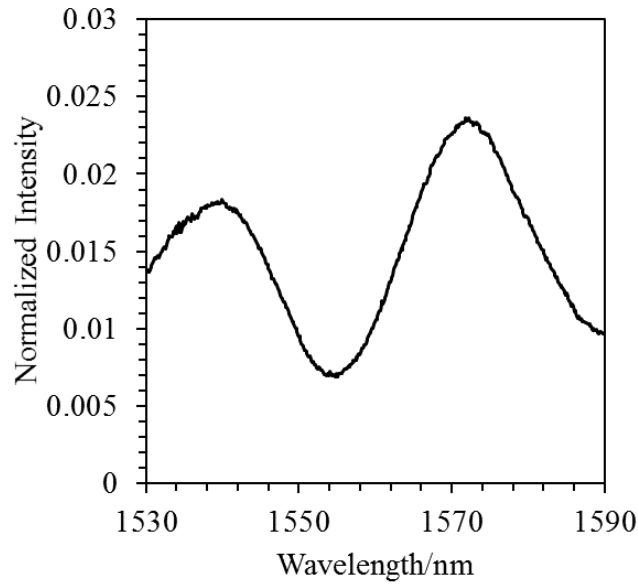


**Figure 3.3 Expected normalized reflection spectra from the FPI of a PVDF coating on an optical fibre end-face showing a sinusoid like shape with multiple peaks and troughs.**

Hence, equation 2.4, from Chapter 2, was used to obtain some idea about the thickness of the coating on the fibre end-face and its relation to the number of peaks in the interferogram. It showed that with an increase in the thickness,  $L$ , the number of peaks in the reflection spectrum increased. Therefore, as it was desirable to have interference patterns with multiple peaks, the thin film was formed with approximate thickness in the 10-50  $\mu\text{m}$  range from 5-10 dips in a PVDF solution having a concentration of 11% by mass, i.e.

$$\text{Concentration of PVDF Solution} = \frac{\text{Mass of PVDF} * 100 \%}{\text{Mass of Solvent} + \text{Mass of PVDF}} \quad 3.1$$

Coated fibres were tested using a similar set up to that shown in Figure 2.8 and curve fitting was done on the acquired interference spectrum of a good sensor to estimate the PVDF thin film thickness. MATLAB and Excel functions were used to generate these simulated waveforms, using equation 2.4. When a desired fit was found, the

corresponding thickness was noted along with the number of dips from which the sensor coating was formed for future reference to assist in repeating the coating process. This was done since the PVDF thin film formation procedure was not automated to regulate the coating thickness or its uniformity.

The initial PVDF coated fibres formed without any coupling agent were not able to demonstrate good reversibility due to problems with adhesion. In other words, this means that the normalized spectra would become distorted upon being kept in water for an extended time and would not regain its initial sinusoid like pattern. In addition to this, the coatings developed with the PVDF grade from Sigma-Aldrich and the solvent MEK and Acetone formed rough outer surface with fibrils (string like structures protruding outwards from the surface (Figure 3.4)), which were undesirable as they made the surface more non-uniform and also because they did not contribute to the FPI. The presence of the fibrils meant that some amount of the contaminant (PFOA/PFAS) would be absorbed/adsorbed on to them, which would not bring about any change in the FPI and hence lead to an inaccurate analysis of the measurand being detected by the sensor.

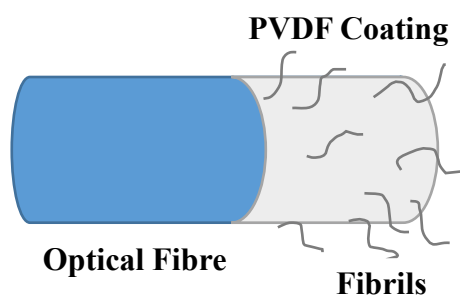


**Figure 3.4 Schematic showing fibrils that would form on non-optimized PVDF coatings.**

The coatings developed with the PVDF grade from Sigma-Aldrich and the solvent MEK and Acetone, were found to be lacking in the  $\beta$ -phase (indicated by the peak at  $840\text{ cm}^{-1}$

in Figure 3.5), which imparts a surface charge to the PVDF coating that has been assumed to help in electrostatic/hydrophobic interactions with molecules. Therefore, PVDF solution made from the PVDF grade from Solvay (Solef 1015) and DMF enriched with Butvar was used for forming the polymer membrane to enhance glass-polymer bonding and also to promote  $\beta$ -phase formation. The resin (adhesive polymer or cross-linker) Butvar, was first dissolved in chloroform and then mixed with the PVDF solution. The prepared fibres (i.e. stripped, cleaved and cleaned bare optical fibres), were then coated using this mixture to form the PVDF coating on the fibre end-face. Butvar promoted good adhesion between the optical fibre glass surface and the polymer and resulted in the formation of a very durable coating. FTIR studies have indicated that PVDF thin films synthesized from a polymer solution made using the solvent N, N dimethylformamide (DMF) has a greater abundance of the  $\beta$ -phase compared to those formed from the solvents acetone, methyl ethyl ketone (MEK) or their combination. The use of Solef 1015 and DMF displayed an enhanced presence of the  $\beta$ -phase in FTIR spectra, shown in Figure 3.5, compared to other PVDF grade and solvent combinations. Thus, optimization of the coating was carried out through trial and error to form a sensor to detect PFOA.

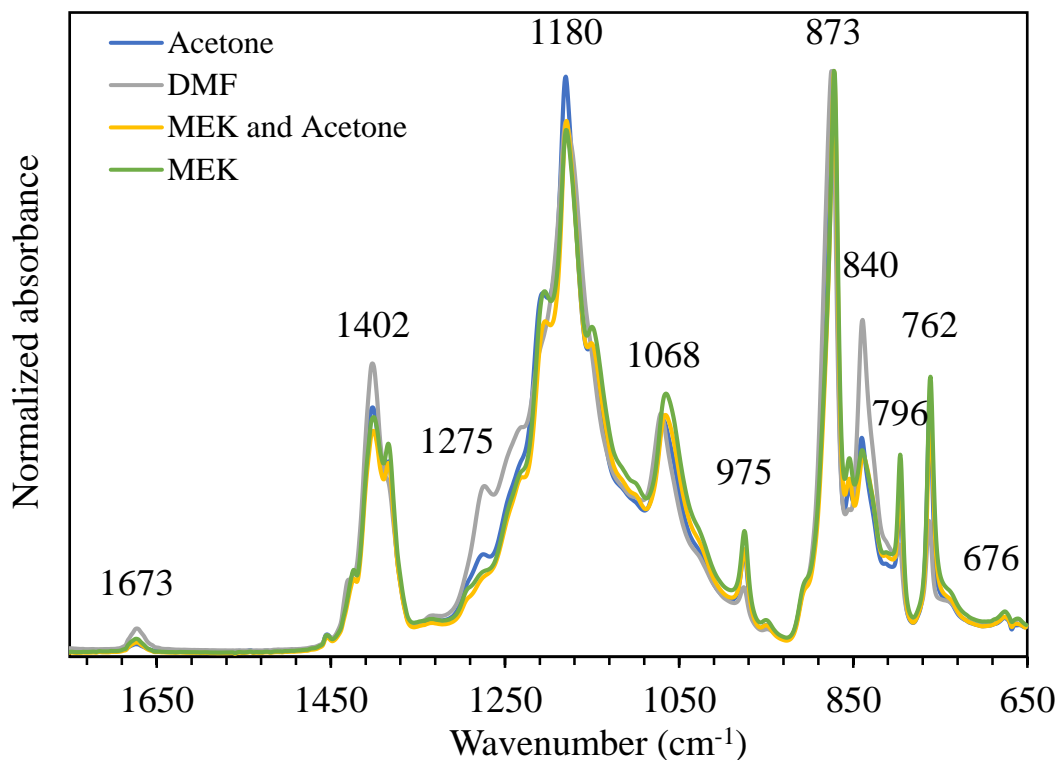
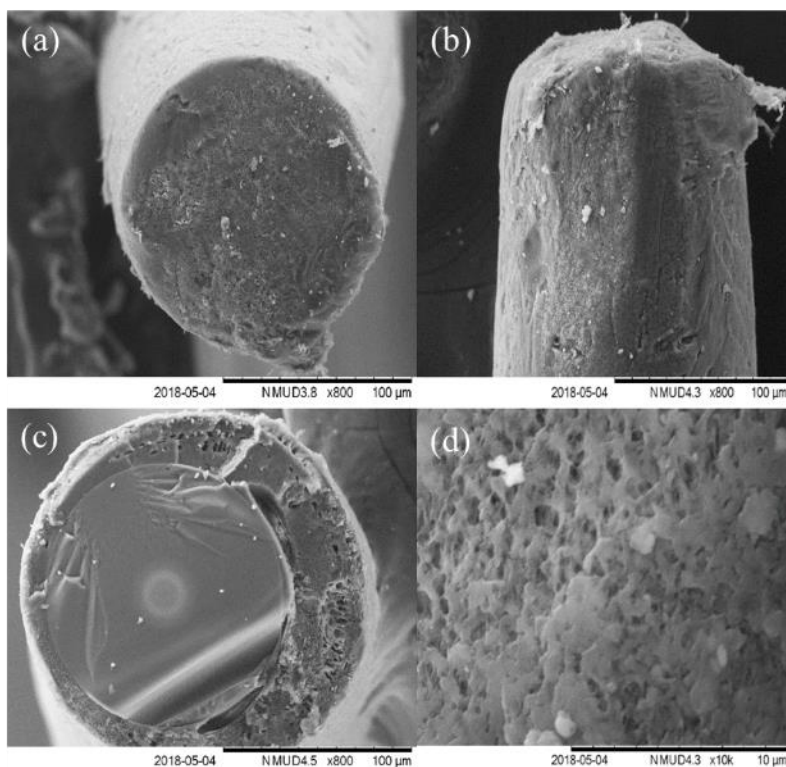


Figure 3.5 FTIR spectra of PVDF membranes formed from different solvents and polymer grades.

Figure 3.6 shows the SEM image of a coated optical fibre end-face, the texture of the membrane and the cross section of a cleaved coated fibre. The samples were imaged using a Hitachi TM3030 Plus Tabletop SEM using an accelerating voltage of 15 kV in backscattering mode. It is noteworthy that the membrane has a dense outlook with the biggest pore size approximately equivalent to 1 $\mu$ m in diameter. A pressure differential is required to force water through the microporous membrane, but it is known from the datasheet [203] that Solef 1015 absorbs less than 0.04% water at 23 °C over a period of 24 hours. However, when the membrane is soaked in 100% ethanol, methanol or isopropanol it is hydrated or wetted. As adsorption of PFOA to PVDF is affected by wetting with possible impact as the agent on the FFPI spectrum, use of the aforementioned

chemicals, especially methanol, was avoided to clean the membrane or for producing the PFOA solution.



**Figure 3.6 SEM image of PVDF coated fibre tip and cross section views**  
(a) coated fibre tip (b) side view of coated fibre (c) cross section of cleaved coated fibre showing bare tip and thickness of PVDF layer surrounding it (d) surface morphology.

### 3.3 General Discussion

It is evident from the coating trials via immersion precipitation that the combination of DMF, Butvar and the PVDF grade Solef 1015 from Solvay forms the smoothest coating on the single mode fibre end-face besides demonstrating a significant presence of the  $\beta$ -phase in the polymer as shown by the FTIR spectrum (Figure 3.5). It has also been observed that the chosen concentration yields coatings or membranes with dense pores in the micrometer range (Figure 3.6 (d)), which plays an important role in the number of binding sites. It has been assumed that the microporous structure of the coating acts like

a sponge to capture more PFOA unlike a smooth and even surface. Thus, it has been speculated that porosity might have some impact on how quickly the coating becomes saturated due to binding or trapping of specific contaminants. However, it was not the scope of this study to investigate this phenomenon.

The coating optimization process adopted by regulating the concentration of the polymer solution, the number of dips and the use of cross-linker enabled formation of a PVDF thin film with desirable FPI reflection spectrum characteristics, suitable for observing sensor performance. After applying the optimized coating techniques, a large majority of the normalized reflection spectrum obtained from PVDF coated optical fibre end-faces showed a peak and a trough. However, in most cases the exact coating thickness, which resulted in these satisfactory FPI patterns could not be ascertained with certainty and SEM images of coated fibres identified as good sensors (Figure 3.6) were utilized to estimate the values.

It was a lengthy process of determining the appropriate fabrication protocol and optimization techniques. Therefore, the discussion in the next section has tried to capture the essence of this journey from the PVDF coating development stage to the PFOA/ PFAS sensing stage.

### **3.4 Evolution of the Fabrication Process and Sensing Trials**

Information provided in the previous sections indicated that several attempts were made at perfecting the coating using various combinations of solvents and PVDF polymer grades until one proved to be useful. Alongside these, numerous coated fibres were tested for FPI spectra until a good relationship was found between the coating thickness and the number of peaks and troughs in the sinusoid like reflection spectra. All these show that

this research has undertaken numerous trial-and-error based experiments to determine the optimum method for developing the PVDF thin film on optical fibres for detecting PFOA with high accuracy.

As such, a large number of coated fibre samples were produced and tested before the best thin film formation technique and protocol for sensing was finalised. Several attempts were made at identifying a functioning coated fibre appropriate for carrying out the PFOA detection experiments to provide the necessary proof of concept in support of a PVDF based OFS. The successful experiments and results reported in the following chapters were obtained only after all identified sources of ambiguity and error were eliminated over a course of time through critical analysis of the outcome of the trials. It was not until the 70th sample was tested that a good idea about all the potential sources of error in measurement had been obtained. Experiments were repeated multiple times before the observations were confirmed. Extensive measures were taken to ensure reliability of the acquired data. In addition to the data analysis technique, this effort is reflected in the experimental set up, where the use of an incubator during PFOA/PFAS detection test ensured a constant temperature environment.

The following table provides information related to different aspects of optimization, which has been considered for categorizing the tested fibres. Table 3.2 highlights the categories tested and show the legend for clear understanding of the list of the coated fibres that have been investigated during the research to provide the proof of concept that a PVDF coated optical fibre can respond to PFOA concentration change in aqueous media. The unsuccessful samples in each of the categories shown in Table 3.2 have been denoted by red colour whereas the successful ones have been presented with a green

colour. Any sample which did not conform to the test has been denoted by a grey colour as shown in the legend provided.

In Table 3.2, the information that each heading imparts is listed below:

- Sample #: refers to the PVDF coated fibre number that has been studied in the research.
- Coating optimized: informs the reader which fibre had the well-formed PVDF coating that is desirable in sensing.
- Temperature influence: points out whether the coated fibre was used in a controlled environment during the experiment or not.
- FTIR spectra: tries to indicate to the reader how good the tested sample was in producing a FPI, to be deemed suitable for a sensing experiment.
- Detects PFOA: show whether the PVDF coated fibre is able to detect PFOA in different aqueous media.
- Sensing protocol: indicates how many of the coated fibres which were used in the PFOA detection test followed an optimized protocol during sensing.

From the information provided in Table 3.2 it can be seen that in the beginning, experiments were performed under non-optimized conditions i.e., without considering the impact of temperature influence and sensitivity of the polymer coating to chemicals such as methanol and other alcohols. As a result, data on PFOA sensitivity obtained from trials where the analyte solution was made in 1.25% methanol solution or where constant temperature was not maintained were ignored because of the bias. Some tested fibres did not have the optimized coating and apart from all these a suitable protocol was also missing. For example, the coated fibre was being taken out of different solutions and

dipped in others to observe the spectral shift instead of being stabilized and kept submerged in water throughout the entire time, while the concentration of the contaminant in the solution was adjusted gradually. This caused significant measurement errors and delivered unreliable results. Convenient procedures like automated data acquisition were put in place after several experiments were performed manually. There are some missing sample/fibre numbers in the table due to corruption of results for which the outcome could not be analysed or because the sample was not used for data collection.

**Table 3.2 Evaluation of PVDF coated optical fibres under different testing protocols.**

Legend	Criteria met	Criteria not met					Not Tested
Sample #	Coating Optimized	Temperature Influence: Present	FPI Spectra: Good	Detects PFOA: Non-Saline Water	Detects PFOA : Saline Water	Detects PFOA : Wash Water	Sensing Protocol : Optimized
1							
2							
3							
7							
8							
9							
10							
12							
13							
14							
15							
16							
17							
18							
19							
20							
21							
22							
23							
24							
25							

<b>Legend</b>	<b>Criteria met</b>	<b>Criteria not met</b>	<b>Not Tested</b>
---------------	---------------------	-------------------------	-------------------

Sample #	Coating Optimized	Temperature Influence: Present	FPI Spectra: Good	Detects PFOA: Non-Saline Water	Detects PFOA : Saline Water	Detects PFOA : Wash Water	Sensing Protocol : Optimized
26	Green	Red	Green	Grey	Grey	Grey	Red
27	Green	Red	Red	Grey	Grey	Grey	Red
28	Green	Red	Red	Grey	Grey	Grey	Red
29	Green	Red	Green	Grey	Grey	Grey	Red
30	Green	Red	Red	Grey	Grey	Grey	Red
31	Green	Red	Red	Grey	Grey	Grey	Red
32	Green	Red	Red	Grey	Grey	Grey	Red
33	Green	Red	Green	Grey	Grey	Grey	Red
38	Green	Red	Red	Grey	Grey	Grey	Red
39	Green	Red	Red	Grey	Grey	Grey	Red
40	Green	Red	Red	Grey	Grey	Grey	Red
41	Green	Red	Red	Grey	Grey	Grey	Red
42	Green	Red	Red	Grey	Grey	Grey	Red
43	Green	Red	Green	Green	Grey	Green	Red
53	Green	Red	Red	Green	Grey	Grey	Red
54	Green	Red	Green	Green	Grey	Grey	Red
56	Green	Red	Green	Green	Grey	Grey	Red
57	Green	Red	Green	Green	Grey	Green	Red
58	Green	Red	Green	Green	Grey	Grey	Red
59	Green	Red	Red	Green	Grey	Grey	Red
62	Green	Red	Green	Grey	Grey	Grey	Red
63	Green	Red	Green	Green	Grey	Grey	Red
64	Green	Red	Green	Grey	Grey	Grey	Red
65	Green	Red	Green	Green	Grey	Grey	Red
66	Green	Red	Green	Green	Grey	Grey	Red
68	Green	Red	Green	Green	Grey	Grey	Red
69	Green	Red	Green	Green	Grey	Grey	Red
71	Green	Green	Green	Grey	Grey	Grey	Green
73	Green	Green	Green	Grey	Grey	Grey	Green
74	Green	Green	Green	Grey	Grey	Grey	Green
75	Green	Green	Green	Grey	Grey	Grey	Green
77	Green	Green	Green	Green	Grey	Grey	Green
78	Green	Green	Green	Green	Grey	Grey	Green
79	Green	Green	Green	Green	Grey	Grey	Green
80	Green	Green	Green	Grey	Grey	Grey	Green
81	Green	Green	Green	Grey	Grey	Grey	Green
82	Green	Green	Green	Grey	Grey	Green	Green

<b>Legend</b>	<b>Criteria met</b>	<b>Criteria not met</b>	<b>Not Tested</b>
---------------	---------------------	-------------------------	-------------------

<b>Sample #</b>	<b>Coating Optimized</b>	<b>Temperature Influence: Present</b>	<b>FPI Spectra: Good</b>	<b>Detects PFOA: Non-Saline Water</b>	<b>Detects PFOA : Saline Water</b>	<b>Detects PFOA : Wash Water</b>	<b>Sensing Protocol : Optimized</b>
84							
85							
87							
88							
89							
90							
91							
94							
95							
96							
97							
98							
99							
100							

The overall outcome of success of the 100 coated fibre samples prepared and tested is summarized in Figure 3.7. The chart depicts that the number of coated fibres tested during the trial-and-error process is greater than the number of coated fibres actually used for sensing or which got rejected, highlighting the significant amount of time dedicated in perfecting the fabrication process. The ratio of accepted data to the rejected ones are almost equal. This shows that out of every two coated fibre samples tested, one provided a desirable outcome whereas the other did not. A considerable amount of time was invested in testing the coated optical fibres for suitable Fabry-Perot interference after they were formed in large batches over a short duration. Thus, it is worth noting that while the coating formation on the fibre end-face was a quick process the rigorous testing and analysis followed by data acquisition was not.

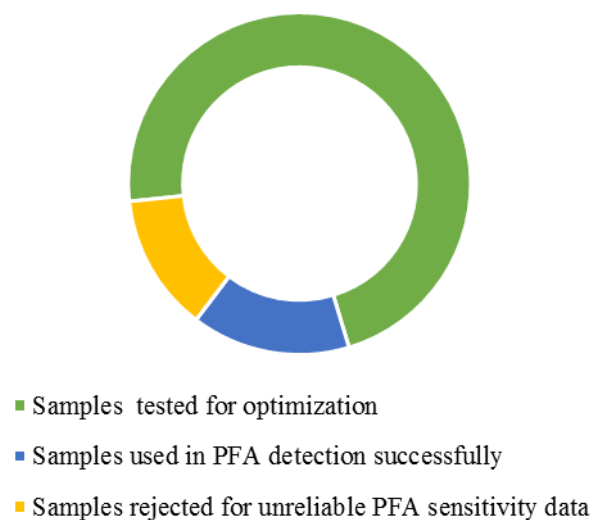


**Figure 3.7 Pie chart summarizing the outcome of investigation.**

At the initial stage when the sensing protocol was being optimized, each PVDF coated fibre was allowed approximately a day to stabilize in water. When the FPI data appeared to become consistent within a couple of minutes, gradually the time for stabilization was reduced. Although these fibres stabilized within 15-30 minutes, a minimum of 90 additional minutes were allowed for stabilization to remove any source of ambiguity from the acquired spectra before the actual PFOA/PFAS tests were performed. However, during the concentration measurement tests, approximately 15-20 minutes were allowed at each reading for the coated fibre to stabilize before the data was recorded. Moreover, the experiments were all repeated to confirm the observations.

As measuring the response time was not crucial to this research, the considerable time allowed for stabilization at different stages did not adversely affect the aim of the project that was related to demonstrating a proof of concept that a PVDF coated fibre can detect PFOA in aqueous solutions.

### **3.5 Chapter Summary**

This chapter described the thin film formation process using the immersion precipitation technique and outlined the optimization procedure for developing a desirable coating on the fibre end-face to form the Fabry-Perot etalon or the PFOA detector. In addition, it discussed the evolution of the sensing protocol and the extent to which a thorough characterization process of the coated fibres was performed and provided a good idea about the effort put into the experiments to obtain accurate measurements.

The outcome of the PVDF coated fibre in PFOA sensing and further information regarding sensitivity of the material and data analysis technique follows in the next chapter.

## 4 Temperature Characterization of PVDF Coated Fibre

---

### 4.1 Overview

The PVDF thin film formed by the phase inversion process via immersion precipitation, at the freshly cleaved end-face of a single mode telecommunications optical fibre, discussed in the previous chapter, was exposed to temperature variation in air and its response was observed. Sensitivity was demonstrated by shifts of the FPI reflection spectra and its performance was analysed through measurement of optical thickness or path difference with temperature variation.

After identifying a suitable PVDF coated fibre, its response to temperature was examined in order to design the protocol for carrying out the PFOA test by eliminating the influence of temperature variation. The temperature response of a PVDF coated optical fibre was investigated in both air and water but the following section outlines the pre-PFOA detection experiment that was carried out to examine the temperature sensitivity of the PVDF coated fibre in air only. This is to provide general information about the polymer's temperature sensitivity in a dry environment. The temperature response in water is discussed in the next chapter where its mention appears more appropriate.

### 4.2 Materials and Methods

#### 4.2.1 Chemicals

As discussed in Chapter 3, powdered PVDF (Solef 1015) obtained from Solvay (Australia), N,N-dimethylformamide (DMF), polyvinyl butyral (Butvar) and chloroform obtained from Sigma-Aldrich (Australia) and ultrapure water were used in coating development. All reagents were used without modification.

#### 4.2.2 General Apparatus

The equipment used in the temperature detection test, as shown in Figure 4.1, included a Carbolite GHC 1200 Degree Celsius horizontal tube furnace, a thermocouple and Fluke 54IIB thermometer for calibration. Reflection spectra were recorded using an ANDO AQ6317B optical spectrum analyser (OSA) capable of operating over a wavelength range between 600 to 1750 nm. An Erbium Broadband Source (EBS 7210) from MPB Communications Inc. emitting over the wavelength range between 1520 to 1620 nm was the light source of choice for these series of experiments. A 2 x 2 bidirectional single mode optical fibre coupler with a maximum insertion loss in the order of 3 dB and a 50/50 ratio at 1550 nm was used to connect the OSA, OFS and the light source. The broadband source and OSA were connected to port 1 and 4 of the coupler respectively, while the PVDF coated single mode optical fibre was connected to port 2. Port 3 of the coupler was terminated and inserted into index matching liquid to remove unwanted reflections as shown in Figure 4.1. Automated continuous data acquisition was achieved using LabVIEW via a GBIP interface so that the raw spectra could be saved to a computer for further analysis.

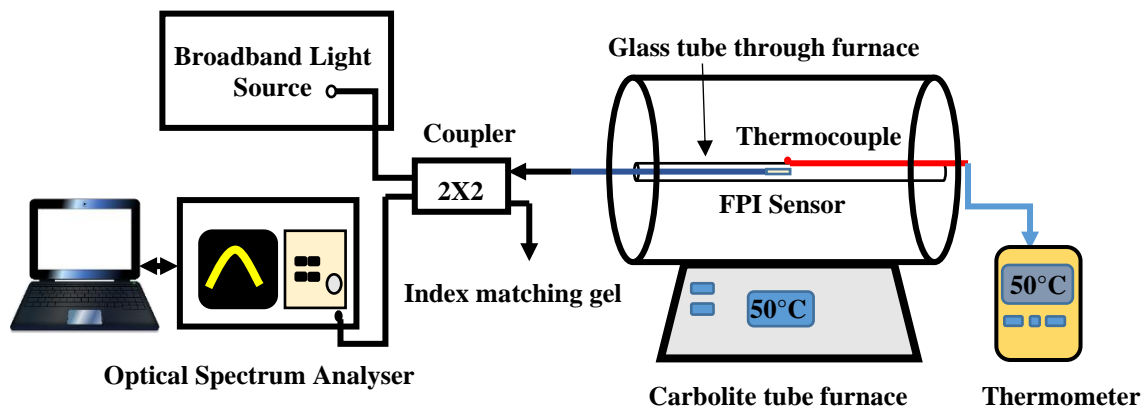


Figure 4.1 Experimental set up for determining temperature response in air.

A Perkin Elmer Frontier Fourier-transform infrared (FTIR) spectrophotometer with a diamond attenuated total reflectance accessory was used to obtain information on any changes in PVDF membranes following heat treatment. Apart from this a Hitachi TM3030 Plus Tabletop SEM using an accelerating voltage of 15 kV in backscattering mode was used for obtaining images of the coated fibre end-face.

### **4.2.3 Coating Fibre End-face**

The PVDF solution for developing the coating was formed by heating 1.67 g of Solef 1015 in 14 mL of DMF at 80 °C for one hour. The cross-linker, Butvar (0.03 g), was dissolved in 2 mL of chloroform, added to the homogenous PVDF solution mixture at 80 °C, and mixed thoroughly under continuous stirring. The polymer solution was allowed to cool to room temperature before dipping the freshly cleaved SMF fibre tips. The polymer coated tips were immediately dipped in ultrapure water to form the final coating layer. To obtain a satisfactory thin film thickness (roughly between 20-50 µm) on the fibre end-face, the alternating dipping procedure in PVDF solution and water was repeated several times allowing enough time for a coated layer to dry in between steps. The samples were dried at room temperature for at least two hours before they were tested and characterized for temperature measurements. Figure 3.6 in the previous chapter shows the image of a PVDF coated fibre obtained using a SEM. To obtain the images, some coated fibre samples which displayed good FPI reflection spectra, were air dried for 24 h, before small sections, 3 x 3 mm, were cut and mounted on aluminium stubs with double-sided conductive carbon tape. The samples were then coated with iridium using a Cressington 208HR sputter coater and later imaged using a Hitachi TM3030 Plus Tabletop SEM using an accelerating voltage of 15 kV in backscattering mode.

#### **4.2.4 Coated Fibre Identification and Selection**

The experimental results obtained in this work were acquired through the set up shown in Figure 4.1. During data collection, the OSA resolution was set at 0.1 nm, the sweep width at 11 nm and the centre wavelength at 1565 nm. The sensitivity was maintained at the high-level range and the sampling rate was set at 1001 points covering a 110 nm scanning bandwidth to ensure that the wavelength resolution (110 nm /1001) was in the same order (0.1 nm) as the chosen OSA resolution. Spectra were recorded in real time and saved on a computer through a GPIB card and LabView interface. Software including MATLAB, Excel and Table Curve were used for further data processing, curve fitting and simulation.

The raw spectral data obtained using the experimental set up were initially normalized against the reflection spectrum of a cleaved fibre end-face otherwise referred to as the ‘Source’ in Figure 4.2 (a), which was taken before splicing the coated fibre (referred to as the sensor in the figure) to the system. The normalization procedure produced an interferogram free of source modulation effect and one showing a sinusoidal-like curve, as shown in Figure 4.2 (b), was considered an indication of a good sensor from the perspective of data analysis. So, only coated fibres that displayed such characteristics in their normalized spectra were chosen for subsequent temperature monitoring experiments.

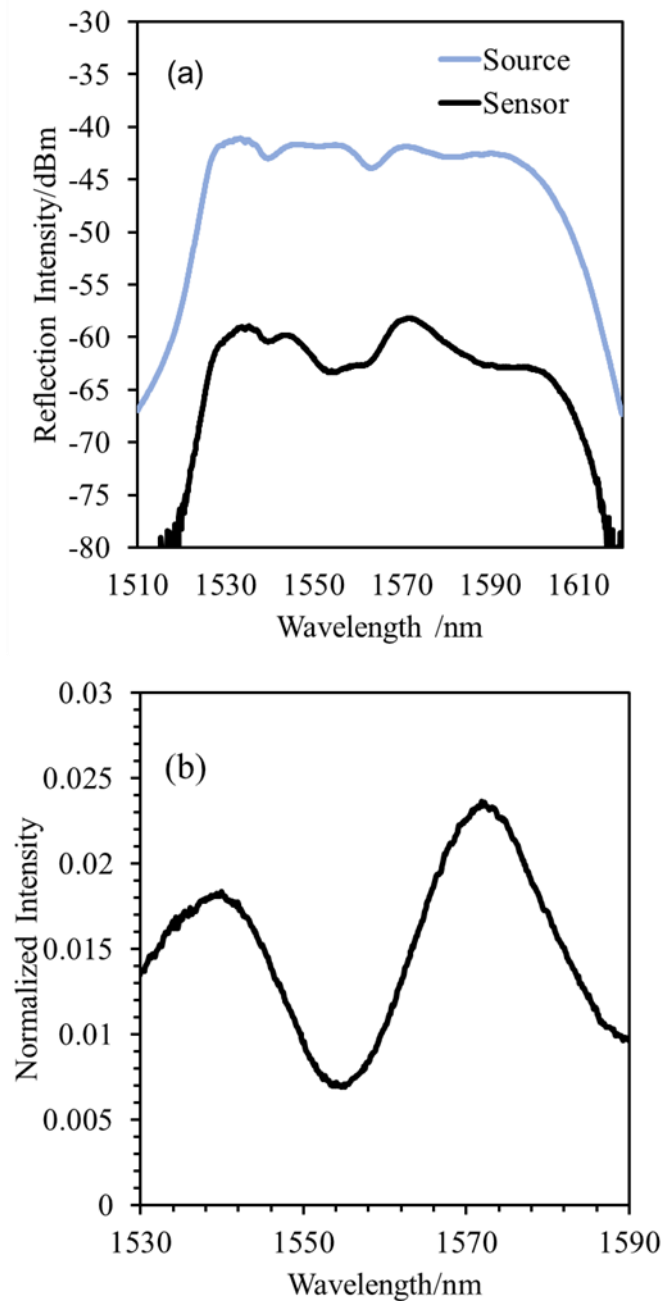
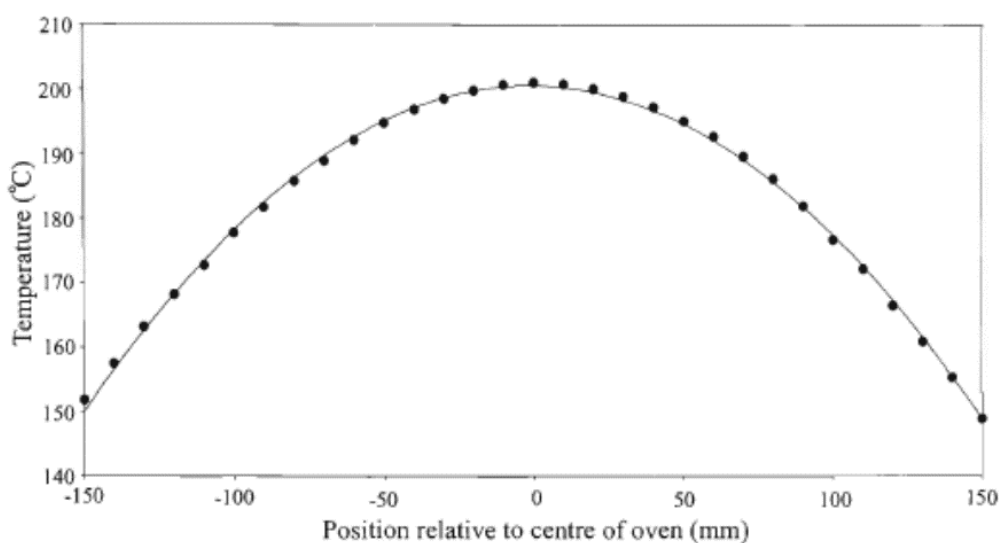


Figure 4.2 Examples of (a) raw source and sensor spectra and (b) normalized sensor spectrum.

#### 4.2.5 Temperature Sensing

An adequately coated fibre, identified and termed as a “good sensor” for simplicity (sample # 73), was exposed to temperature variations between 21 to 160 °C using the set up shown in Figure 4.1. The coated fibre tip was placed at the centre, inside the Carbolite

oven, since this location of the furnace exhibited the most stable temperature profile. A complete temperature characterization process of the Carbolite tube furnace has been provided in the work of Trpkovski [204]. The following diagram (Figure 4.3) shows the temperature versus position profile obtained from this study and thus, the PVDF coated optical fibre was placed at the centre of the oven.



**Figure 4.3 Temperature versus position inside the Carbolite tube furnace at a stabilized temperature of 200 °C showing minimum deviation of the value at the centre of the furnace.**

The temperature was first increased in steps of 10 °C and then decreased in the same way. Approximately 15 minutes were allowed for the temperature to stabilize at each level before the data was recorded. Additional information from the subsequent temperature characterization of other suitable fibre samples (#71 & 74) was used to further verify the temperature effect on PVDF coated optical fibres. Since each coated fibre is unique a common plot was not used to compare the response, rather the similarity in their spectral shift was monitored for assessment before confirming the outcome. Figure 4.4 and Figure

4.5 show the spectral response of coated fibre samples # 71 and 74. The following results and discussion section only describes the outcomes for sample #73.

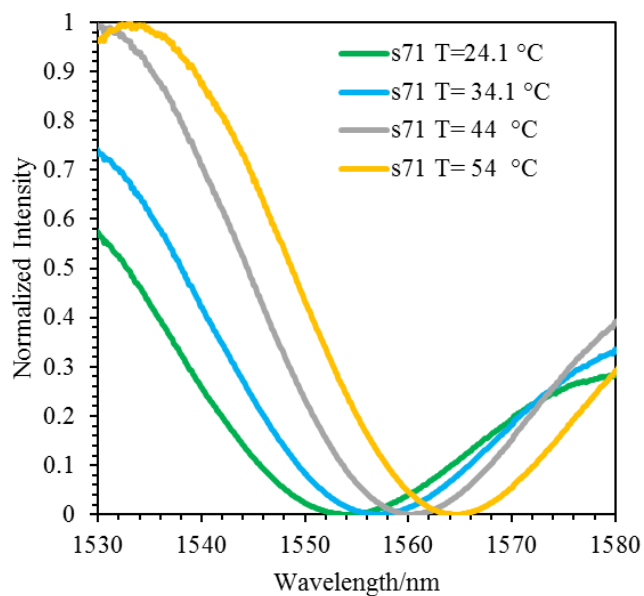


Figure 4.4 Spectral response of sample# 71 to temperature variation.

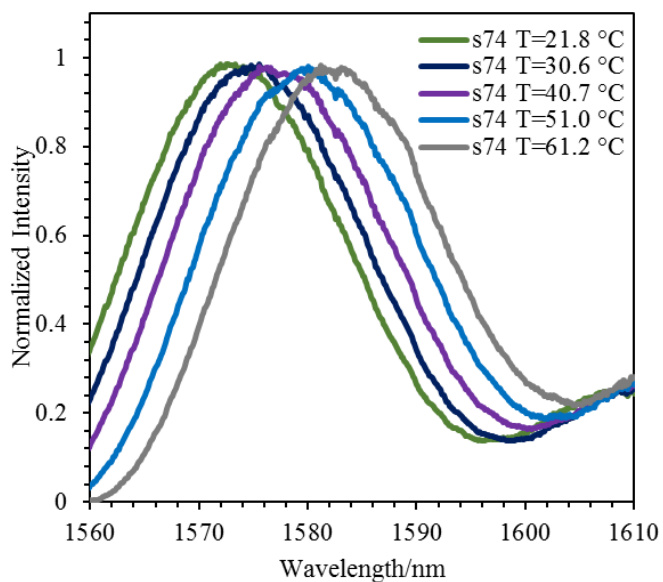


Figure 4.5 Spectral response of sample 74 to temperature variation showing peak wavelength shift.

#### **4.2.6 Influence of Heat on PVDF Coating**

A flat piece of PVDF film formed using the immersion precipitation technique was subjected to temperatures ranging between 40 and 160 °C at 40 °C increments in a Cole-Parmer stable temperature programmable muffle furnace (John Morris Group, Chatswood NSW). The FTIR spectra of the membrane pieces approximately 2 x 2 cm, were obtained before placing them in the muffle furnace muffle furnace for 10-15 minutes. A Perkin Elmer Frontier Fourier-transform infrared (FTIR) spectrophotometer with a diamond attenuated total reflectance accessory was used to record the spectra of the samples. The purpose of this experiment was to demonstrate any deformation to the physical and chemical structures of the PVDF thin film upon being heated to considerably high temperatures, close to its melting point. The FTIR spectra of the samples following heat treatment and after the samples had cooled were recorded again and compared with the initial spectra to observe any sign of change to the thin film structure. The total area under the FTIR spectra were obtained by integration and the values normalized to the unheated sample for comparison. The spectra were recorded in triplicate following each treatment.

### **4.3 Results and Discussion**

#### **4.3.1 PVDF Coated Fibre Operating Principle**

Figure 4.6 shows a schematic of what a low finesse FFPI sensor would look like after dipping a cleaved single mode fibre (SMF: 8 nm/125 nm) end-face first in the solution of PVDF and resin mixture and then in ultrapure water at room temperature. The boundaries of the PVDF coating with the glass fibre and the surrounding form the mirror surfaces that reflect light, which interferes inside the optical fibre core. A change in temperature

brings about a phase difference between the reflected beams from the inner and outer surface of the FP etalon due to a change in the optical path difference (OPD) caused by the change in physical thickness and refractive index of the thin film on the fibre end-face. The result appears on the reflectance spectrum in the form of a wavelength shift and can be observed using an OSA and the set up shown previously in Figure 4.1. Hence, the performance of the PVDF coated optical fibre in this work has been analysed by monitoring the wavelength shift in the resultant reflection spectrum and the corresponding change in OPD with temperature change.

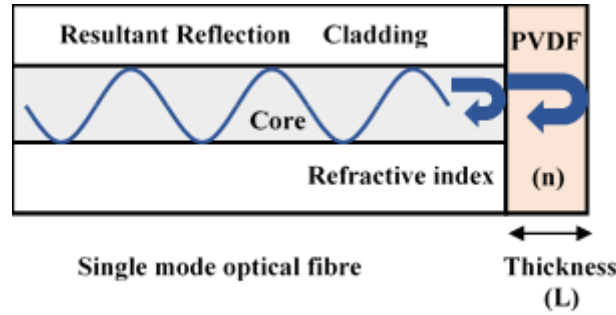


Figure 4.6 Schematic of PVDF Coated fibre end-face.

As discussed in Chapter 2, equation (2.4), also shown below, represents an expression of overall reflected intensity on two beam interference model that is representative of the reflection from the coated fibre end. This can be used as a tool for analysing normalized reflection spectra and curve fitting to determine OPD.

$$I = I_1 + I_2 + 2\gamma\sqrt{I_1 I_2} \cos\left(\frac{4\pi nL}{\lambda} + \phi_0\right) \quad 2.4$$

In equation 2.4,  $n$  is the refractive index of PVDF and  $L$  is the thickness of the PVDF thin film, the product of which is the OPD that can be determined from coefficients of the fitted curve representing the two parameters.

Equation (4.1) is a simpler version of equation (2.4) and has been used here for curve fitting to obtain the OPD measurements. As the FPI effect observed in the spectral response is brought about by a phase shift caused by the OPD change, the simpler mathematical model prioritizes the impact of  $n$  and  $L$  and assigns variables to these for generation of solutions through computation. Since the reflected powers  $I_1$  and  $I_2$  from the thin film boundaries do not influence the phase shift directly but rather determine the resultant wave amplitude, their individual impact is ignored and replaced by a collective term for analysis, in this equation.

$$I = A * \cos\left(\frac{4\pi * B * C}{\lambda} + D\right) + E \quad 4.1$$

The letters A to E in equation (4.1) are custom defined variables in the curve fitting function. Their relation to the physical parameters mentioned in equation (2.4) are:  $A = 2\gamma\sqrt{I_1 I_2}$ ,  $B = n$ ,  $C = L$ ,  $D = \phi_0$  and  $E = I_1 + I_2$ . Analysis based on this model can be performed using the software Table Curve and Excel, for determination of OPD. While a method of least squares is used by Table Curve to generate fits to spectra with suitable starting parameters for this model, Excel only uses direct user inputs for the variables to produce the spectrum.

The products of the software generated parameters B and C can be used to determine the OPD values corresponding to temperature. Then the most appropriate results can be chosen through comparison of the generated OPDs with an expected value determined through study of an SEM image of a cleaved coated fibre cross-section and a calculated value of  $L$  determined by considering the phase difference between two consecutive

peaks or troughs on the normalized spectrum using equation (4.2), where  $\lambda_1$  and  $\lambda_2$  are wavelengths of consecutive peaks or troughs:

$$\left(\frac{4\pi nL}{\lambda_1} + \phi_0\right) - \left(\frac{4\pi nL}{\lambda_2} + \phi_0\right) = 2\pi \quad 4.2$$

The variation in OPD with temperature change can be determined to produce a graph to further demonstrate the performance of the PVDF coated fibre or sensitivity in terms of OPD change per °C respectively.

The nature of the curve fit in Table Curve and Excel has different limitations and the outputs obtained using them are not sometimes ideal even though the mutual correlation can be very high ( $R^2=0.98$  in Figure 4.9). Thus, the appropriate fitted spectra for OPD analysis was chosen based on its correlation to the actual normalized spectra and also the closeness of match of the value of L to the expected value generated by equation 4.2. The following sections discuss OPD variation examined in this work on a case by case basis with regard to the experiments that have been discussed in the earlier sections.

#### **4.3.2 PVDF Coated Fibre Response to Temperature Variation**

The raw spectral data were initially normalized against the reflection spectrum of a cleaved fibre end-face and then self-normalized to values ranging between 0 and 1. The lowest value in the obtained data-set was considered 0 while the highest was considered 1. Figure 4.7 (a) shows the normalized spectra obtained from raw data. These closely resemble the spectra obtained using mathematical modelling and curve fitting in Excel as shown in Figure 4.7 (b). The correlation for an individual spectrum and fitted data has been seen to vary from 0.57 to 0.98. This is because in some spectra, the reflection pattern was distorted at certain wavelengths for which the mathematical model could not generate

a close match. It can be observed more clearly in the figures provided in the next section, where the individual fits have been compared.

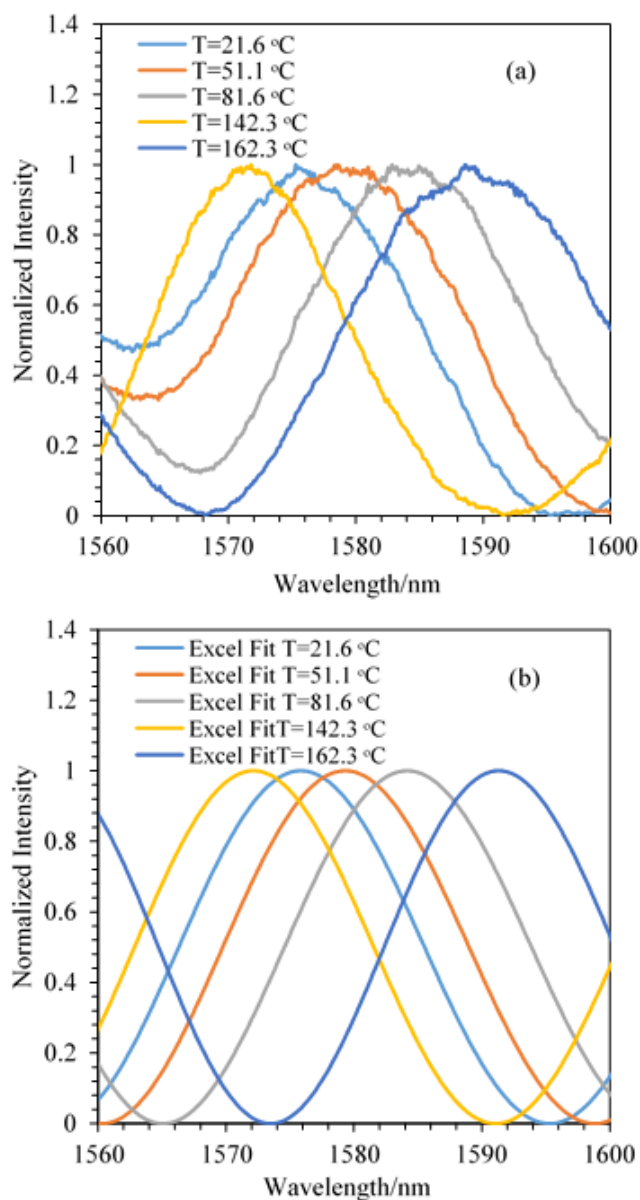


**Figure 4.7 Wavelength shift of sample#73 with temperature rise**  
(a) actual spectra (b) simulated spectra.

The overall results from Figure 4.7 show that the peak wavelength positions shift towards the right as the temperature increases. This shift is assumed to be primarily due to a change in the physical thickness of the PVDF thin film with temperature change. The

OPD change is intrinsically related to the thermo-optic coefficient and the thermal expansion coefficient of the sensing material and the combined effect of this is seen in equation (4.3) discussed in the following section where the performance analysis has been done.

### **4.3.3 Performance Analysis of Coated Fibre**

Curve fitting was performed on the normalized spectra shown in Figure 4.7(a) using equation (4.1) and the values of  $n$  and  $L$  were determined in accordance with the generated fit parameters to calculate the OPD. There was good correlation (0.989) between the fit generated in Table Curve and the simulated result obtained using the same mathematical model in Excel. Figure 4.9 illustrates the nature of the fit based on the method of least squares produced by Table Curve and Excel. All the individual parameters in equation (4.1) could be manually varied in both Table Curve and Excel to obtain a best fit. However, in Table Curve the user input was only used as a starting point to obtain the best fit parameters whereas for Excel it was taken as the final defining parameter for the spectra. Due to this reason, the final value of the parameters generated by Table Curve varied significantly in some cases, compared to those of Excel. That is why a slight difference in appearance can be seen between the two results shown in Figure 4.8 and Figure 4.9.

Since the fits generated by each of the software package had high correlation to the normalized spectral data, as indicated by the  $R^2$  values on the figures and also Figure 4.10, to select the more appropriate data-set for calculation of OPD a comparison of the  $L$  values from the fits were done with the expected value of  $L$ . In addition to it, the curve fit values were also compared against the range of possible thicknesses (20-40 $\mu$ m)

suggested by the SEM image of a cleaved coated fibre cross section, shown in Figure 3.6 in Chapter 3, to verify their reliability. The expected value of  $L$  was generated from the normalized spectral data using equation (4.2). It was seen that if the value of  $n$  is assumed to be at 1.42 for the PVDF thin film,  $L$  has a value of 23499 nm at 142.3 °C. The  $L$  value generated by Excel and Table Curve at 142.3 °C are approximately 23250 nm and 24399 nm respectively which correspond to a percentage difference of 1% and 3.8 % with the expected value generated using equation (4.2). Therefore, the data generated in Excel was chosen because of its closeness to the theoretical value of  $L$  for performance analysis of the coated fibre.

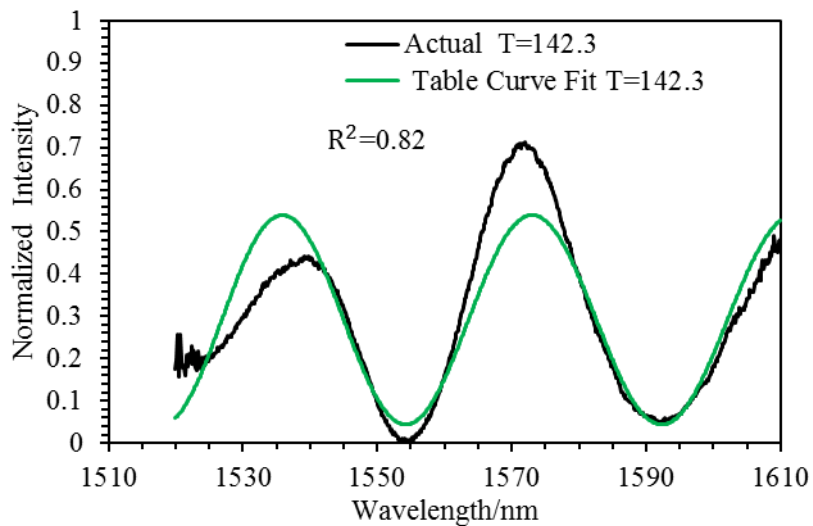


**Figure 4.8 Sample #73 fitted FFPI spectrum using Table Curve**

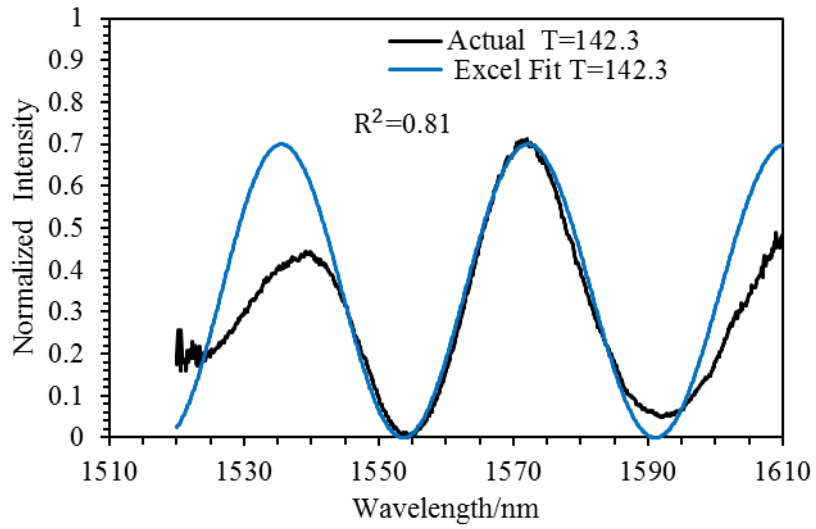


Figure 4.9 Sample #73 fitted spectral data in Excel.

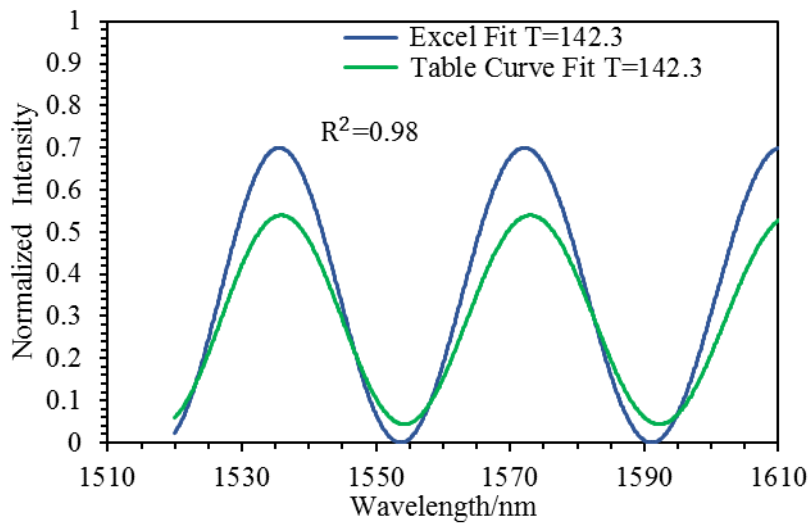


Figure 4.10 Correlation between fit in Excel and Table Curve.

The nature of individual fits in Excel are shown below (Figure 4.11). The closeness and goodness of fit are shown by the  $R^2$  value. The closer the value is to 1 the better the fit.

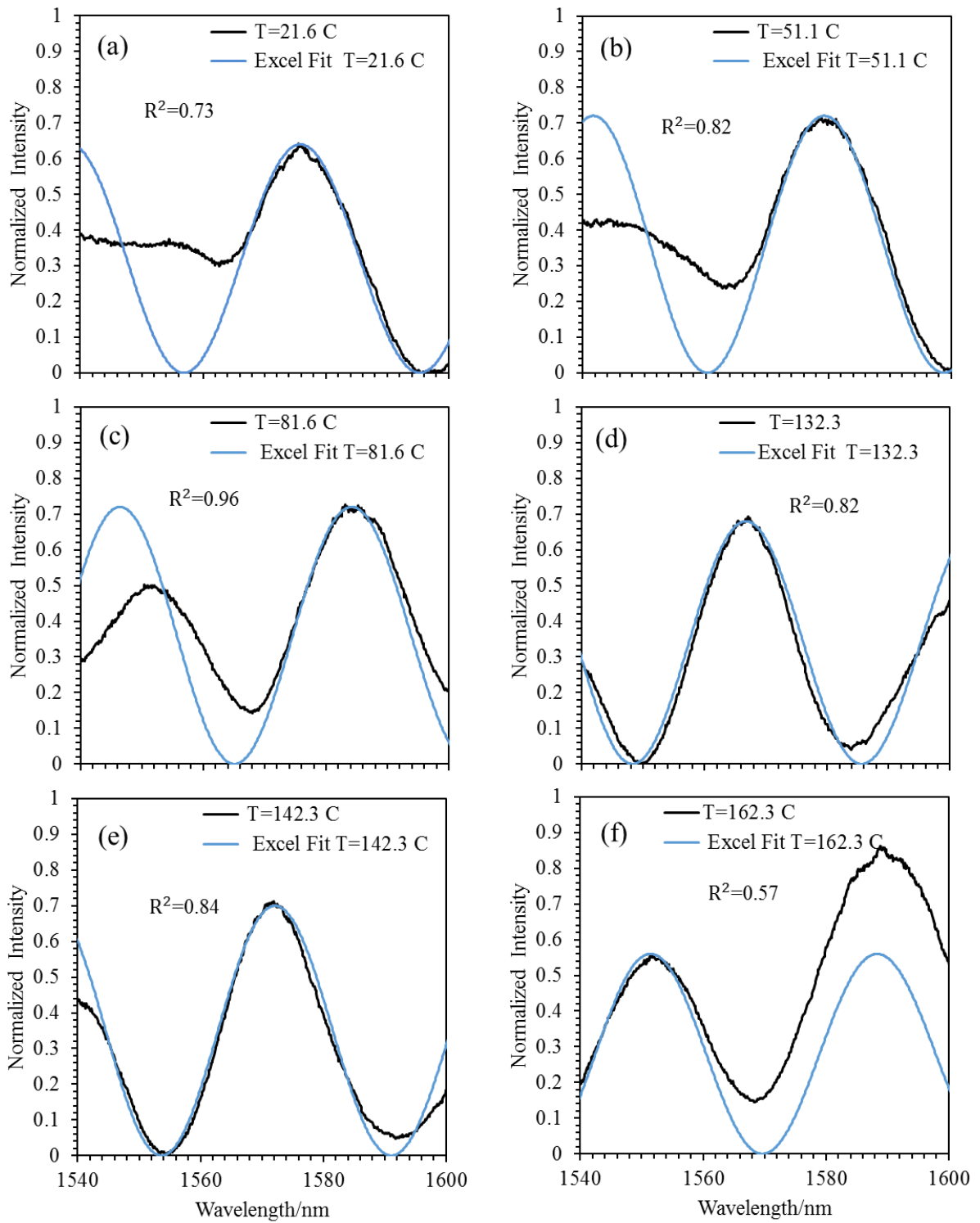


Figure 4.11 (a-f) Curve fit of normalized spectra of sample #73 in Excel at various temperatures.

Performance analysis of the PVDF coated fibre can be done by measuring the peak or trough wavelength shift with variation in temperature. The maximum or minimum point whose shift is to be observed, can be identified by the data call out function on the graph in Excel. The peak value from the normalized spectra at specific temperatures can be noted and the corresponding graph of peak wavelength against temperature can be plotted as shown in Figure 4.12. A non-linear wavelength shift of the PVDF coated fibre over the 20-160 °C temperature range is shown in the figure with a good correlation between the data during the rise and fall cycle, provided by the  $R^2$  value. Standard deviation of the peak wavelengths of the rise and fall cycle were measured at each temperature interval and the standard error was calculated by dividing this value with the square root of the total data points considered in the measurement. Thus, the uncertainty in the peak positions have been denoted by the error bars as shown in Figure 4.12.

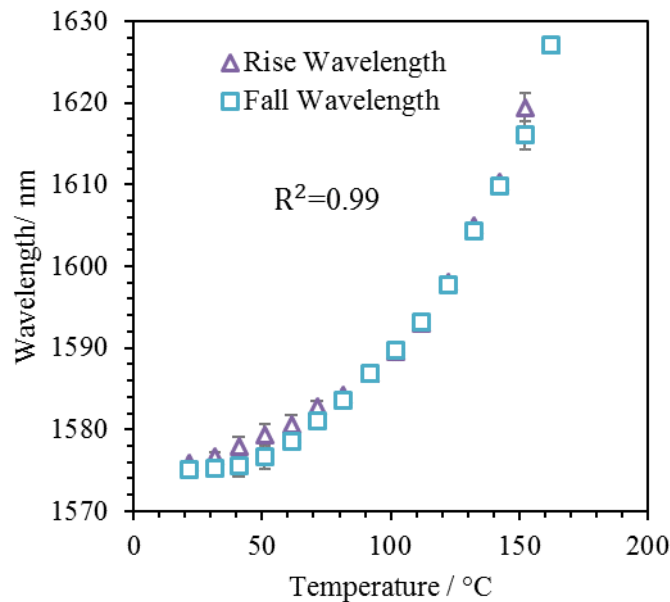
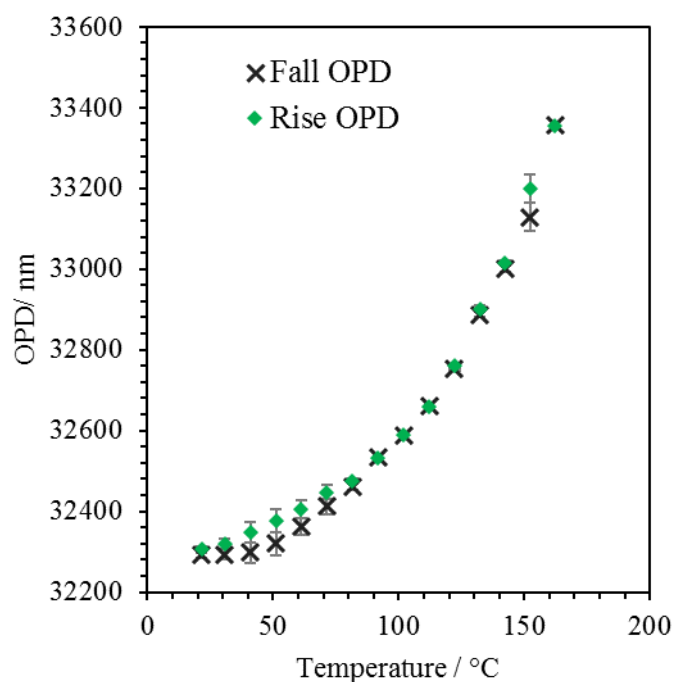


Figure 4.12 Shift in peak wavelength positions with temperature (sample #73).

Similarly, the OPD derived from the fit parameters generated by Excel show a non-linear response in Figure 4.13, with a good correlation in the order of 0.99. The uncertainty in the measurement of OPD shown in the graph was calculated following the same procedure mentioned above.



**Figure 4.13 Variation in OPD with temperature.**

The non-linear response, which can be seen in the plots of Figure 4.12 and Figure 4.13, might be attributed to the non-linear change in thermal expansion coefficient of PVDF [205]. In Figure 4.12, the wavelength shift during the heating (rise) and cooling (fall) phase indicate good repeatability and low hysteresis. However, it was also observed that the repeatability is affected by the amount of time the coated fibre head is exposed to relatively high temperatures that are close to the polymer's melting point of 154-184° C. The prolonged exposure to heat followed by slow cooling or in other words the annealing

process, affects the elasticity of the PVDF thin film causing an irreversible change in the physical structure that has an adverse effect on replication of measurements. The evidence of this can also be seen in the FTIR spectrum shown in section 4.3.4 below, which also supports the finding that permanent deformation of the membrane that influences sensing capabilities of the PVDF coated fibre is not observed at temperatures below 100 °C even under continuous exposure for extended duration. Figure 4.13, which shows the OPD values generated by simulation also relay the same information as that of Figure 4.12.

Further analysis of the OPD plot was done to examine the sensitivity of the PVDF coated fibre to temperature. The change in OPD (in nm) as a function of temperature change was obtained and its mathematical expression was determined by curve fitting as shown in Figure 4.14. The resulted fit shown by equation (4.3) represents a measure of the sensitivity of the PVDF coated fibre used in this work. The values of thermal expansion coefficient and the thermo-optic coefficient of the PVDF appears in the exponent.

$$\Delta\text{OPD} = e^{1.708+0.443\Delta T^{0.5}} \quad (4.3)$$

The coated fibre displayed a varying sensitivity ranging between 1.6 and 7.5 nm/°C over the temperature range of 21 to 160° C. The reason for this variation was assumed to be the nonlinear expansion of the PVDF thin film with temperature rise or fall, whereby a change in physical thickness and refractive index facilitates the change in the optical thickness during the experiment. Initially, when the temperature difference between the reference (room temperature) and the test temperature was small, the expansion of the thin film was also small and corresponded to a small wavelength shift and OPD value that was associated with low sensitivity.

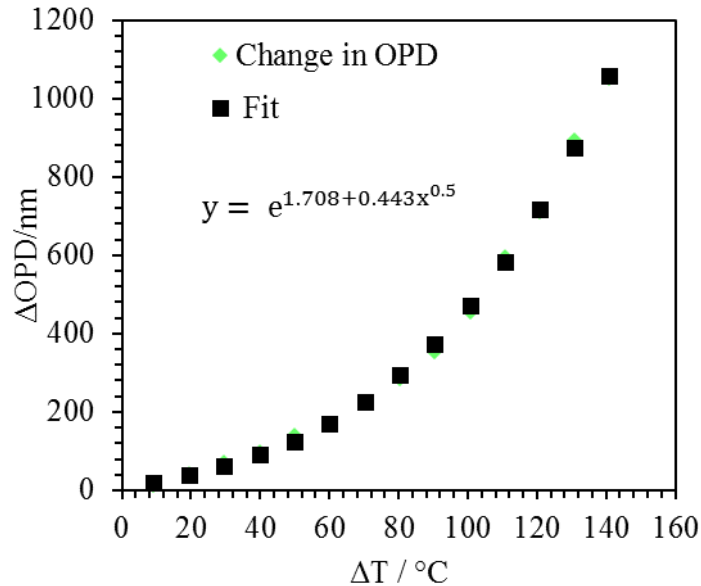


Figure 4.14 Plot of OPD change vs temperature change with fit obtained using Table Curve.

As the temperature increased, the relative temperature difference also increased along with the corresponding OPD value and sensitivity. Since the nature of expansion was non-linear, the wavelength shift between equal temperature intervals was not constant and the OPD change was also not uniform, for which the sensitivity of the PVDF coated fibre resulted in the exponential curve that can be seen in Figure 4.13. At the highest resolution of the OSA, which is 0.01nm for the AndoAQ6317B, the temperature resolution was calculated to be approximately 0.006 °C and 0.001 °C respectively at the lowest and highest sensitivity levels (i.e. temperature resolution is the resolution of the OSA divided by the sensitivity). Thus, based on these outcomes it can be suggested that there is a prospect for this PVDF coated optical fibre to work as a standalone temperature sensor.

Temperature measurements are crucial across a wide range of applications in industry and scientific studies, where in areas involving food processing, water treatment and

invasive medical procedures, there is the added demand that the sensing probe exhibits high chemical inertness for producing reliable data. Due to the PVDF coated optical fibre having multiple desirable properties including bio-chemical resistance, small size, high sensitivity, and immunity to electromagnetic interference [117, 122, 125], it can counteract problems that are faced by conventional electrical sensors. Further analysis of heat treatment of the coating material has provided the suitable range of operation of the polymer which has been discussed in the next section.

#### **4.3.4 Effect of Heat Treatment on PVDF Coating**

The FTIR spectra of the PVDF thin film depicted in Figure 4.15, which is representative of the actual coating on the fibre end-face, shows only subtle differences among the curves obtained over the 40-160 °C temperature range. This suggests that the structure of the coating remains relatively unchanged and is almost unaffected by temperature variation over the range of temperatures tested. At 160 °C, however, slightly broader peaks are evident for some peaks whereas others are slightly shifted. For example, the C-F peak centred 1179  $\text{cm}^{-1}$  [206] broadens slightly after heating at the highest temperature (Figure 4.16). The peaks at 840 and 796-762  $\text{cm}^{-1}$ , which are attributed to the  $\beta$  and  $\alpha$  phases of PVDF respectively [185], are also shifted with increased intensities following heating at 160 °C, suggesting that some morphological changes in the PVDF structure have occurred (Figure 4.17). It is also evident from the calculation of the total area under the FTIR curve, which was obtained through integration and normalization of the values to the unheated sample for comparison (Figure 4.18). The bar chart illustration in Figure 4.18 shows that there are noticeable differences in the areas of the unheated sample and the one which has been heated at 160 °C. A significant increase in the total

area (height of the bar) is observed in the case of the heated sample, which has been assumed to be caused by the broadening of the signal spectrum and the increase in intensity levels due to structural changes of the material. Compared to the rest of the sample data of heat treatment between 40 and 120 °C, the data for 160 °C shows a noticeable change in the total area with respect to the unheated sample data, which suggests that the PVDF coated fibre may be suitable for temperature measurements up to about 120 °C. As it can be seen that PVDF does not undergo significant change in its phase composition within the stated ideal range of operation, the polymer is deemed to be suitable also for temperature detection.

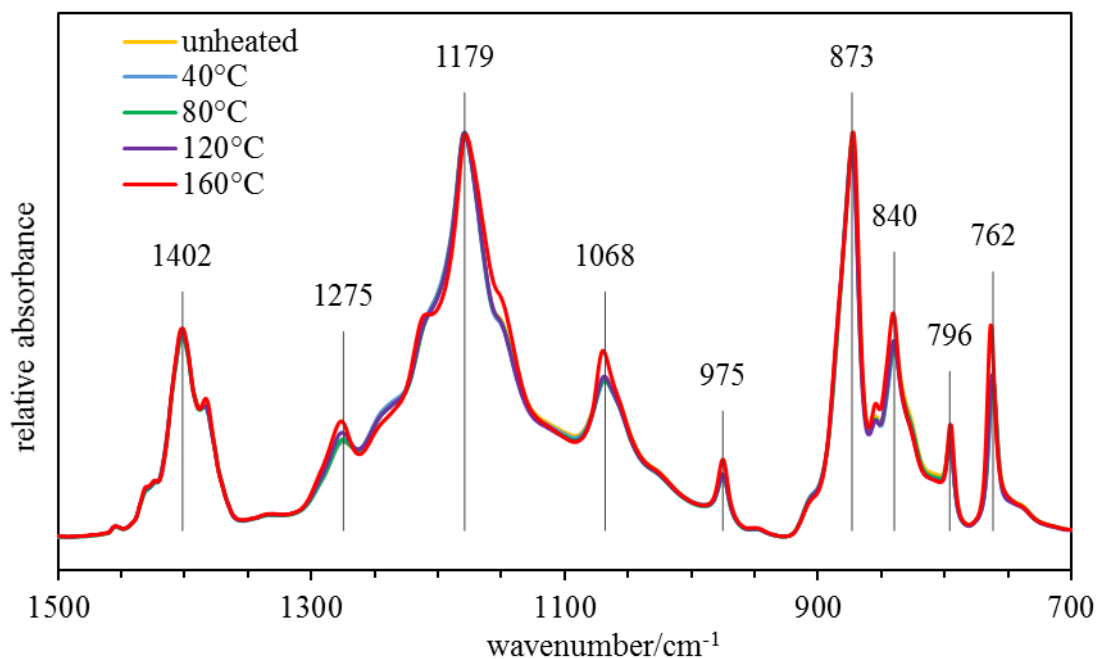


**Figure 4.15 FTIR spectra of the PVDF thin film at different temperatures over the range 1500-700 cm<sup>-1</sup>.**

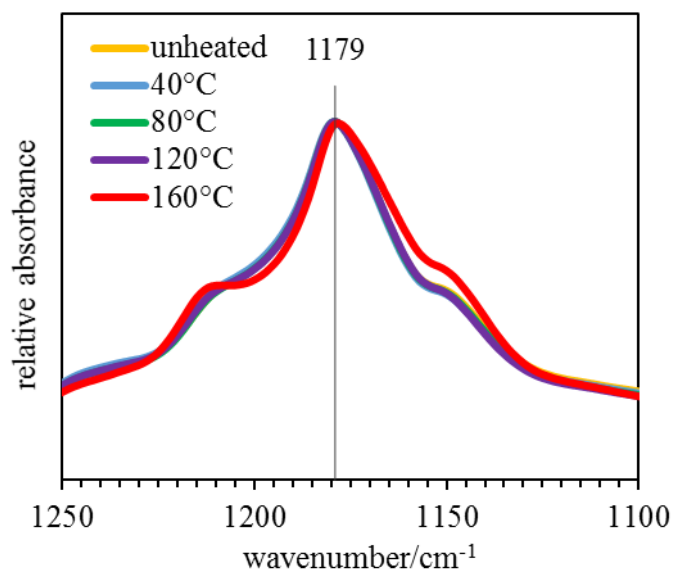


Figure 4.16 FTIR spectra of the PVDF thin film from 1250-1100  $\text{cm}^{-1}$ .

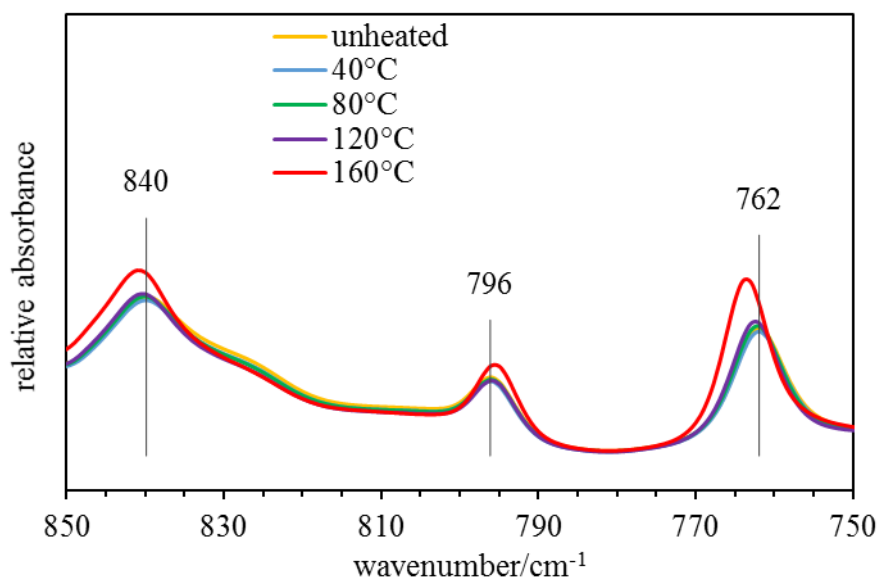


Figure 4.17. FTIR spectra of the PVDF thin film from 900-750  $\text{cm}^{-1}$ .

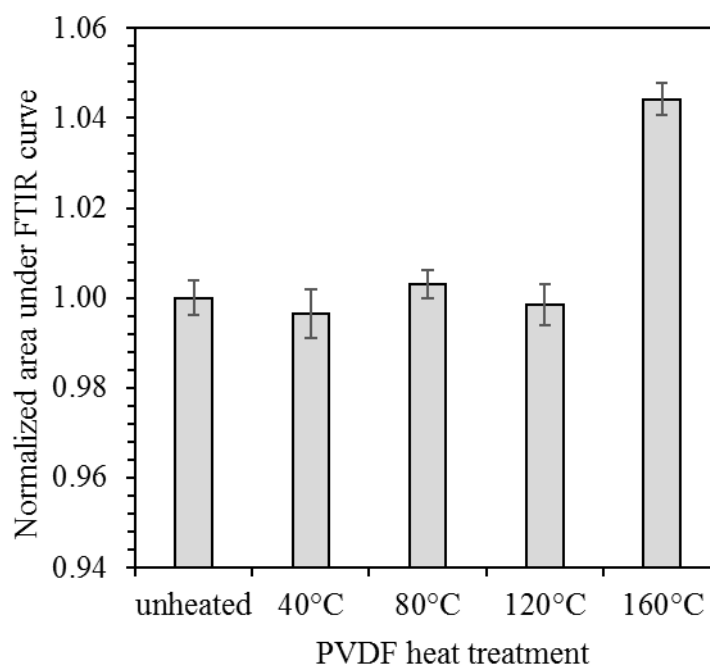


Figure 4.18 Normalized area under FTIR curves at different temperatures.

#### 4.4 Chapter Summary

This chapter has provided information on temperature response of the PVDF coated fibre formed using the immersion precipitation technique. It was demonstrated that the designed OFS responded to temperatures between 21 and 160 °C with high precision, low hysteresis and a sensitivity range between 1.6 and 7.5 nm/°C. As the envisaged sensor was expected to operate in the 3-40° C range, it was critical to find a coating that can operate in this window. Therefore, when PVDF was chosen, thin films formed from it were subjected to heat treatment and their FTIR spectra were recorded to ascertain any change in the signature FTIR spectra of the thin film, that would explain the corresponding physical change due to heat. It was observed that PVDF is not affected adversely by temperature variation over the 40 to 120 °C temperature range, which implies that it can be a potentially robust sensing material for a sensor. The next chapter considers these findings to discuss a protocol for sensing PFOA in aqueous solution. A

further investigation of the PVDF coated fibre temperature sensitivity in water is also provided in the next chapter

## 5 PFOA Detection with PVDF Coated Optical Fibre

---

### 5.1 Overview

This chapter provides a brief account of PFAS contamination and reviews the limitations of existing detection systems. It discusses the evolution of the experimental methods and techniques employed to determine the ability of the PVDF coated fibre to detect PFOA in an aqueous environment. It also highlights the performance of the Fabry-Perot interferometry-based sensing system in salt water and PFAS wash water from fire-fighting trucks and reports PFOA sensitivity in different aqueous media alongside the overall system performance. While this chapter presents the recommended acceptable limit for human consumption and sets the expectation to detect a concentration of PFOA in the 0.5 ppb range, it also indicates that the actual measured sensitivity of the PVDF coated fibre is different in different types of aqueous solutions, where the concentration can range between parts per billion to parts per million in each case. As such, this chapter provides an account of the capability of the PVDF coated fibre to detect changes in concentration in real PFAS solutions from fire-fighting trucks in the ppb range and lab-prepared PFOA in the ppm range, while considering the effect of temperature variation. Therefore, this chapter indicates temperature as an important parameter that can influence sensitivity and subsequently addresses this possible cross sensitivity issue, which other prior research had not considered before this work.

### 5.2 Introduction

Surface and ground water as well as adjoining land areas in many parts of the world have been reported to be affected by per or polyfluoroalkyl (PFAS) containing compounds

[207, 208], which have received recent attention for their persistence in the environment [209]. The discovery of these fluorochemicals in human serum and the environment has initiated research to study the effects and the extent of their presence in the environment [45, 210]. Recent reports have shown that locations of PFAS contaminated land, ground water or reservoirs are usually close to manufacturing plants or near military bases/airports or firefighters' training grounds that have a history of using a specific fire retardant manufactured by 3M called the Aqueous Film Forming Foam (AFFF) [11, 12]. Run-offs from military training exercises or actual fire extinguishing events have been suspected to be the cause of the environmental pollution. Investigation of human health in areas close to contaminated sites has shown the adverse impact of PFAS usage [10, 25].

Therefore, Environment Protection Agencies (EPA) around the globe have expressed the need to monitor these contaminants, while addressing issues regarding regulation and development of adaptive frameworks like the National Environment Management Plan (NEMP) [37] to respond to emerging research and knowledge. Based on scientific reports and evidence, Food Standards Australia New Zealand (FSANZ) in 2016 has considered 0.56 to 5 parts per billion (ppb) of PFOA and 70 ng/L~ 0.07 ppb of PFOS, in drinking water, to be the maximum safe level for human consumption [33] as discussed earlier. In addition to this, in 2017, FSANZ [34], also recommended the tolerable daily intake (TDI) values for PFAS, including PFOS and PFOA to be 160 nanograms per kilogram of body weight per day [34].

As discussed in Chapter 2 current detection methods for PFOA and PFOS contaminants in water reservoirs are based on conventional techniques such as liquid chromatography

mass spectrometry (LC-MS), liquid chromatography tandem mass spectroscopy (LC-MS/MS) [40, 41] or gas chromatography–mass spectrometry (GC–MS) [39]. All these techniques, which are laboratory based are costly and time consuming processes that often require complicated pre-treatment steps, expensive labour resources, and are inapplicable for *in-situ* measurements and analysis [42]. Non-conventional methods like the recently reported molecularly imprinted polymer (MIP) based portable sensors are unable to differentiate between different types of PFAS and require long fabrication times [64]. On the other hand, the smartphone based app that was also proposed, is susceptible to variation in weather conditions [64]. In addition to these limitations, there is a lack of information when it comes to the effect of temperature on sensitivity of these portable sensors and their cross-sensitivity to other contaminants.

Therefore, this work addressed the persisting problems of real time monitoring of PFOA in aqueous solutions with a PVDF coated fibre optic Fabry-Perot interferometry (FPI) based sensing system. It used constant temperature conditions to ensure that the changes observed in the FPI spectra are due to the changes in PFOA concentrations only and not changes in the morphology or thickness due to possible temperature variations. Thus, the work avoided temperature influence to a great extent unlike any of the other reported methods proposed for PFAS sensing.

## **5.3 Materials and Methods**

### **5.3.1 Materials**

The PVDF grade Solef 1015 from Solvay (Australia), N, N dimethylformamide (DMF), polyvinyl butyral (butvar) and chloroform from Sigma-Aldrich (Australia) has been used in the polymer film formation process. PFOA crystals from Sigma-Aldrich (Australia)

and ultrapure (Milli Q) water were used for forming the stock solution of the analyte. Pre-treated PFAS wash water from MFB fire-fighting trucks (Melbourne, Australia) and sodium chloride (NaCl) from J. T Baker (Australia) have been used for cross sensitivity measurement tests. No chemical reagent was modified prior to its usage.

### **5.3.2 General Apparatus**

Reflection spectra of the PVDF coated optical fibre for obtaining information on PFOA concentration were recorded using an ANDO AQ6317B optical spectrum analyser (OSA) capable of operating over a wavelength range between 600 to 1750 nm. An Erbium Broadband Source (EBS 7210) from MPB Communications Inc. emitting over the wavelength range between 1520 to 1620 nm was the light source of choice for these series of experiments. A three-port fibre optic circulator from AFW Technologies was used to connect the OSA, OFS and the light source. As shown in Figure 5.1 the broadband source and OSA were connected to port 1 and 3 of the circulator respectively, while the PVDF coated single mode optical fibre sensor head was connected to port 2. The transmitted signal from the light source went from port 1 to port 2 and the reflected signal from port 2 to port 3. The use of a circulator provided a better signal to noise ratio compared to a coupler, as it had a low insertion loss (<0.8 dB). Furthermore, the signal obtained using the circulator was at least 6 dB better since the 3 dB loss encountered by the signal upon passing through the coupler every time was not present in the circulator (i.e. 3 dB loss in going from light source to the PVDF coated fibre and another 3dB loss on returning trip from the coated fibre end to the OSA was avoided through the use of the circulator).

The experimental set up also included a Thermoscientific tabletop incubator for maintaining a constant temperature of the environment surrounding the sensing probe.

Temperature readings in the proximity of the coated fibre tips in aqueous solutions, were acquired using a K-type thermocouple connected to a Fluke 52 II electronic thermometer.

Automated continuous data acquisition was achieved using LabVIEW via a GPIB interface so that the raw spectra could be saved to a computer for further analysis. During data collection, the OSA resolution was set at 0.1 nm, the sweep width at 11 nm and the centre wavelength at 1565 nm. The sensitivity was maintained at the high-level range and the sampling rate was set at 1001 points covering a 110 nm scanning bandwidth to ensure that the wavelength resolution ( $110 \text{ nm} / 1001$ ) was in the same order (0.1 nm) as the chosen OSA resolution.

A Perkin Elmer Frontier FTIR spectrophotometer with a diamond attenuated total reflectance accessory was used to obtain information on any changes in PVDF membranes following heat treatment. The FTIR presented a fingerprint of a sample with absorption peaks that corresponded to the frequencies of vibrations between the bonds of the atoms which made up the PVDF membrane.

Some PVDF coated fibre samples were imaged using a Hitachi TM3030 Plus Tabletop SEM using an accelerating voltage of 15 kV in backscattering mode.

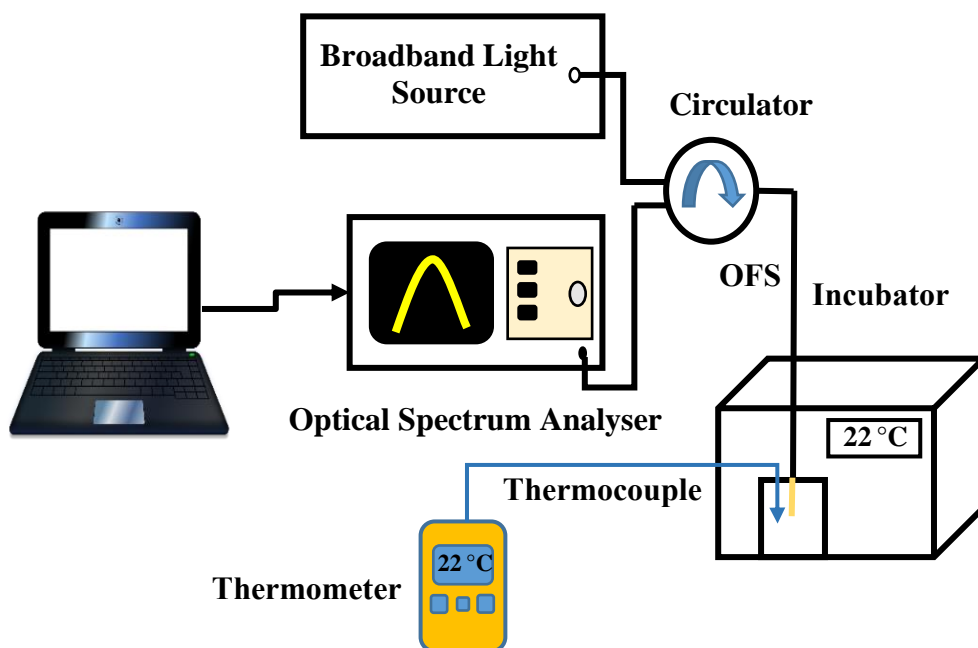


Figure 5.1 Experimental setup for PFOA detection.

### 5.3.3 Coating Composition Characterization using FTIR Spectroscopy

A Perkin-Elmer Frontier Fourier transform infrared (FTIR) spectrometer with a diamond attenuated total reflectance accessory was used to record the spectra of the coating/membrane samples developed from the solvent DMF and the polymer grade from Solvay, Solef 1015. The test involved analysing the presence of the  $\beta$ -phase of the PVDF membrane by looking at the intensity of the peaks at  $840\text{ cm}^{-1}$  and  $1275\text{ cm}^{-1}$  on the normalized absorbance spectrum as mentioned in Chapter 3. These wavenumbers correspond to wavelengths of  $11904.76\text{ nm}$  and  $7843.14\text{ nm}$  respectively. The wavenumber, as used in spectroscopy and most chemistry fields, is defined as the number of wavelengths per unit distance, typically reciprocal centimetres ( $\text{cm}^{-1}$ ) for which the same protocol has been adopted here.

### **5.3.4 Coated Optical Fibre Testing and Selection**

The raw spectral data obtained from a PVDF coated optical fibre, using the experimental set up shown in Figure 5.1 were normalized against the reflection spectrum of a cleaved fibre end-face in water, and taken before splicing the coated fibre to the system. A normalized spectrum, free of source modulation effects that showed a sinusoidal curve (as shown in Chapter 4 section 4.2.4) was considered an indication of a good sensor from the perspective of data analysis. So, only coated fibres that displayed such characteristics in their normalized spectra were chosen for further experimentation.

### **5.3.5 Coated Optical Fibre Temperature Sensitivity in Water**

The experimental setup of Figure 5.1 was used for this work. The incubator thermostat setting was changed to vary the temperature of water in which the PVDF coated fibre was submerged. They were kept steady until the temperature of the water stabilized to that value and data acquisition was completed. The PVDF coated fibre was first stabilized at a temperature close to the room temperature for several hours and then subjected to the actual temperature variation test. Like the previous experiments performed in air discussed in Chapter 4, the temperature was increased or decreased in steps of 10 °C but the range was limited between 22 °C to 60 °C, dictated by the operating range of the equipment.

The incubator used operated in the range 20-60 °C, which was representative of the experimental temperatures that could be tested in the field. However, temperatures below 20 °C were not investigated. The average temperature in Australia can be 3 °C in winter and 35 °C in summer. On a typical hot summer day in Melbourne, the incubator's lowest temperature would be the ambient temperature, which in most cases was observed to be

higher than 20 °C. Moreover, the incubator would not go below 20 °C to a lower temp because of its built structure and internal settings. Therefore, the experiments were performed between the stated range above.

The measurements at specific intervals were taken when the coated fibre had stabilized and the temperature reading on the thermometer was steady. Very high temperature response in water was ignored mainly to avoid added uncertainties in physical length, thickness or surface morphology due to deformation of the PVDF coating, which occurs upon thermal expansion. As mentioned earlier the research did not consider low temperatures and thus did not investigate the effect on spectral response of the PVDF coated fibre due to contraction.

### **5.3.6 Coated Optical Fibre Sensitivity to PFOA in Aqueous Solution**

A 100 mg/L or 100 ppm PFOA stock solution was prepared by dissolving PFOA (0.01 g) crystals in ultrapure water (100 mL) by heating at 80 °C for 10 minutes. Concentrations ranging between 10 to 60 ppm were derived subsequently from it through dilution. The PVDF coated fibre was stabilized in a known volume of ultrapure water (20 mL), at a temperature of 23.8 °C simultaneously with the PFOA solution to be tested. This was done to avoid cross sensitivity to temperature differential during sensing operation. After the coated fibre was stabilized, data acquisition was undertaken and the spectral response in water was observed using the set up shown in Figure 5.1. Following this, a known volume of the PFOA stock solution was added to the water in which the PVDF coated fibre was submerged and stabilized, to form a desired concentration, which was calculated using the following equation:

$$C_1V_1 = C_2V_2 \quad 5.1$$

where,  $C_1$  is the concentration of the PFOA stock solution,  $V_1$  is the volume of stock solution used,  $C_2$  is the final concentration of the diluted solution and  $V_2$  is the final volume of the diluted solution in the beaker. Data collection commenced after further stabilization of the coated fibre in the PFOA solution for approximately 10 minutes. This ensured that the temperature of the incubator in the immediate vicinity of the PVDF coated fibre tip was steady and molecular interaction between PFOA and PVDF was complete. Ideally, the response from the coated fibre is instantaneous if temperature is compensated for. Since simultaneous measurement of temperature was not in the scope of this work, the significant amount of time which was allowed for stabilization made sure that temperature sensitivity did not affect PFOA sensitivity as discussed earlier. The steps of taking measurements at different concentration levels were repeated following the same protocol.

To test the consistency of the results, the exact experimental procedures were repeated several times with different freshly prepared coated fibres (see Appendix A spectra of sample# 89). An attempt was also made to test the repeatability of each used fibre by first developing a cleaning protocol that would reset it to its original condition. Since the use of isopropyl alcohol and methanol during the cleaning procedure had an impact on the reflection spectra when they were used to remove residues of PFOA from the surface of the PVDF thin film (see Appendix A spectra of sample# 43 and 57), this protocol was discontinued.

### **5.3.7 Coated Optical Fibre Sensitivity to PFOA in Saline Water**

A stock solution of 100 ppm sodium chloride (NaCl) solution was prepared using the salt crystals (0.01 g) and ultrapure water (100 mL) and was subsequently diluted to produce the required concentrations. The PVDF coated fibre was stabilized in a known volume of ultrapure water (20 mL) at a constant temperature of 24.5 °C before NaCl solution was added to it. Data acquisition was performed using the set up shown in Figure 5.1 following stabilization. After that PFOA solution of known concentration (100 ppm) and volume was added to the stabilized coated fibre and the spectral data were collected. Subsequent concentration measurement followed in the same order and the experiment was repeated with a different sample fibre (see Appendix A spectra of sample# 99).

### **5.3.8 Coated Optical Fibre Sensitivity to PFAS Wash Water**

Perfluoroalkyl (PFAS) containing wash water sample that was obtained from Australian fire-fighting trucks was used in this test. The concentration of this PFAS wash water solution, which was composed of perfluoroalkyl sulfonic acids, perfluoroalkyl carboxylic acids, fluorotelomer sulfonic acids, was 1.14 ug/L or ppb as confirmed by an external analytical lab (Appendix B). The PVDF coated fibre was stabilized in a known volume of ultrapure water (20 mL), at a constant temperature of 23.3 °C. Following this, a known volume of the PFAS wash water was added to it and further stabilization was done. Data were collected after this using the set up shown in Figure 5.1. Like the previous method, the steps of PFAS addition and data acquisition were repeated for subsequently diluted concentrations.

## **5.4 Results and Discussion**

### **5.4.1 PVDF Coated Fibre PFOA Sensing Principle**

The operating principle of the PVDF coated fibre was previously described in relation to temperature sensitivity, by the schematic shown previously in Figure 4.6. It was explained how an increase in temperature primarily causes a change in the physical thickness through thermal expansion and alters the OPD to produce a shift in the reflection signal.

Here, the spectral shifts due to adsorption of PFOA (at constant temperature) is discussed.

In the presence of PFOA, assuming negligible refractive index variation, adsorption of the chemical analyte to the surface of the thin film induces a change in the physical thickness of the PVDF coating. This in turn causes a phase difference between the reflected beams from the inner and outer surface of the Fabry-Perot etalon by altering the OPD between them and leads to the resultant interferogram being shifted. The same data analysis technique involving equations 4.1 and 4.2 used to determine OPD in Chapter 4 was also used for these experiments.

### **5.4.2 FTIR Spectra of PVDF Coated Fibre**

The FTIR spectra of a PVDF membrane formed using DMF and Solef 1015, shown in Figure 5.2, depicts the peaks which are representative of the electroactive  $\beta$ -phase. These are typically at the wavenumbers  $840\text{ cm}^{-1}$  and  $1275\text{ cm}^{-1}$  [211]. The presence of the  $\beta$ -phase at the aforementioned wavenumbers support the presence of the surface charge on the PVDF coating which has been considered to play an important role in selectively attracting the PFOA molecules in solution to the binding sites on the coating.

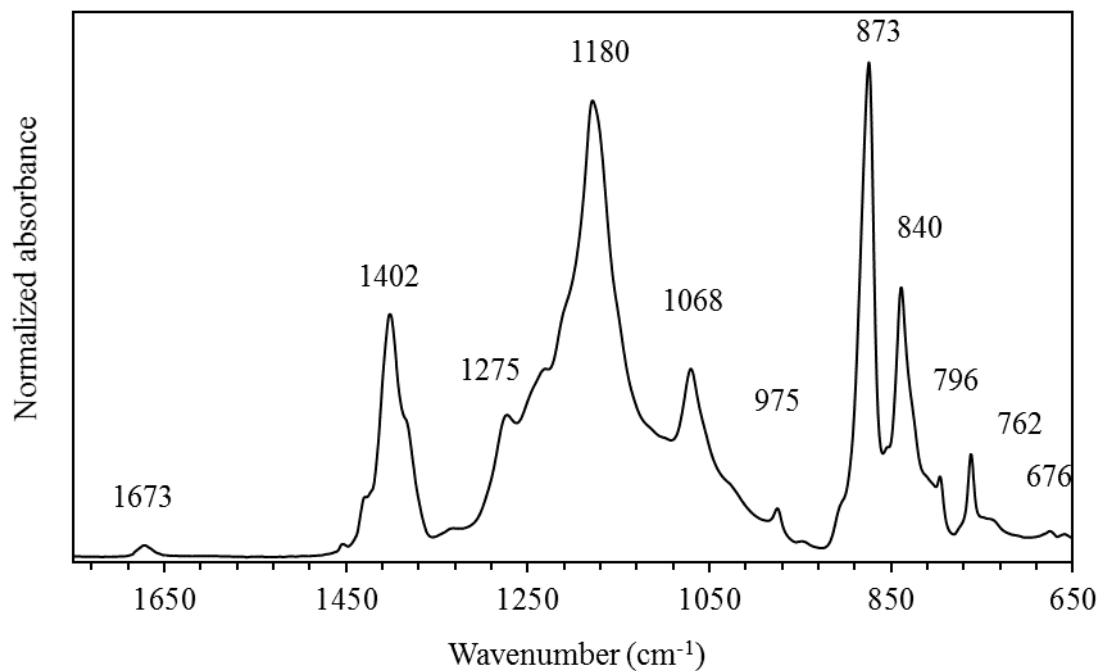


Figure 5.2 FTIR spectra showing PVDF coating composition.

#### 5.4.3 Coated Fibre Temperature Response in Water

The reflection spectra exhibit a redshift or peak wavelength ( $\lambda_p$ ) shift towards the higher wavelength region, as shown in Figure 5.3, with increasing temperature in water. This implies that the changes in OPD are primarily the result of changes in physical thickness due to thermal expansion. There is an added effect of a changed refractive index of the surrounding medium, which creates an impact on the wavelength shift and cause the final spectrum to be different from that in air. In other words, the spectral wavelength shift is dependent on the optical thickness which is linked to the characteristics of the ambient medium in the immediate vicinity of the PVDF coated fibre.

It is known that the particular grade of PVDF used in the coatings (Solef 1015) absorbs a certain percentage of water at a specific temperature [203]. This may also have influenced

the refractive index of the material and the physical thickness to ultimately affect light propagation through it, and further induce a change in the recorded interference spectrum.

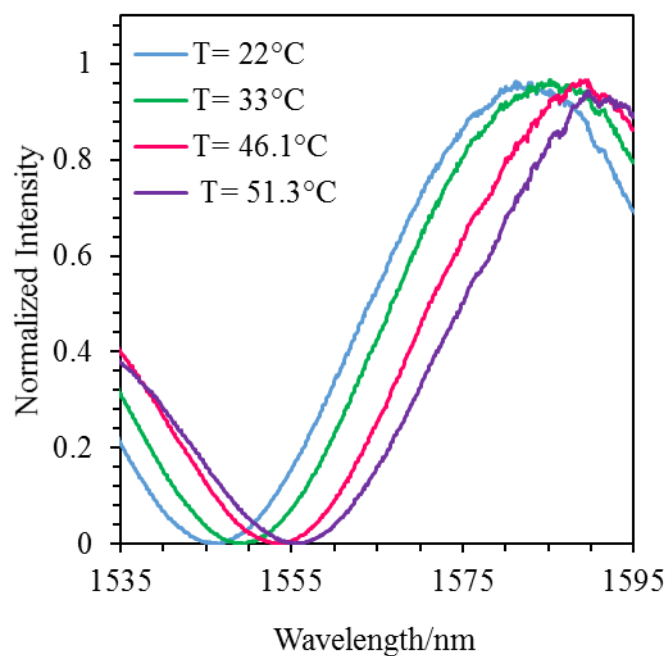


**Figure 5.3 PVDF Coated fibre response to temperature variation in water.**

The information presented in the normalized reflection spectrum of Figure 5.3 has been used to determine the relationship of peak wavelength shift and OPD with temperature variation as shown in Figure 5.4 and Figure 5.5 respectively.

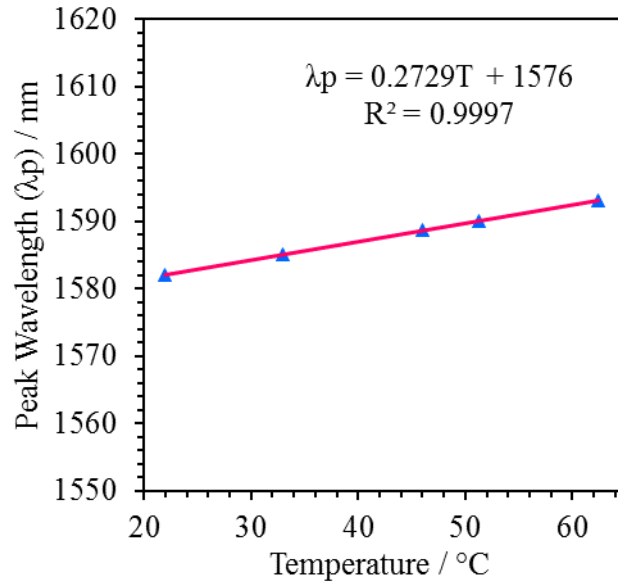


Figure 5.4 Peak wavelength shift of PVDF coated fibre in water with change in temperature.

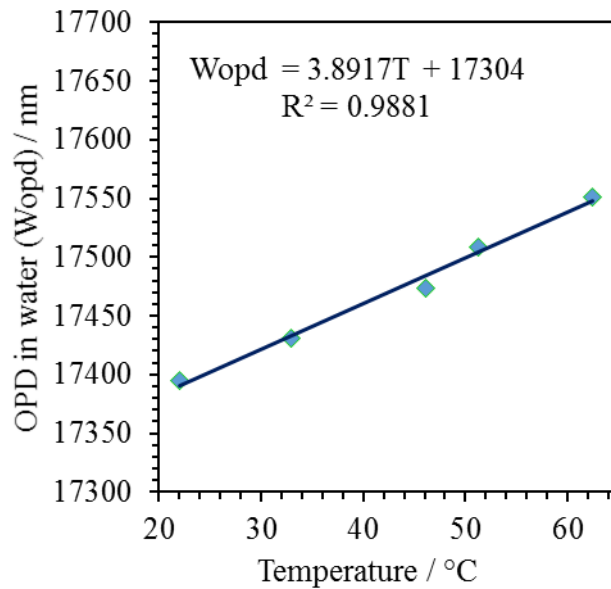


Figure 5.5 Change in OPD with temperature of a PVDF coated fibre in water.

Both the peak wavelength shift and OPD exhibit a linear response over the chosen temperature range of 20-60 °C. Furthermore, the temperature sensitivity indicated by the gradient of the fitted curve in Figure 5.5 is seen to be 3.9 nm/°C. This indicates that, outside of the controlled laboratory set up, the OPD change for temperature variation

needs to be compensated in order to correctly determine the PVDF coated fibre's response to PFOA. The issue of temperature cross sensitivity for field sensing applications can be addressed by using a rare earth doped fluorescence intensity ratio based optical fibre temperature sensors [212-214] in conjunction with the PVDF coated fibre. Fluorescence intensity ratio based temperature sensing has been shown to be one of the most successful in the past demonstrating a sensitivity in the order of 1.1 to 1.6 % change in the measurand per degree Celsius, which is much higher than that of the FBG ( $7 \times 10^{-4} \text{ \%}/^\circ\text{C}$ )[215]. If an all optical system is desired any of the above mentioned OFS or their suitable combination can be tried for temperature sensing [216, 217]. The PFOA sensitivity and temperature can be measured as a function of intensity change and wavelength shift in the FBG's reflection spectrum, respectively, as discussed in reference [218]. However, alternative options may also be used and can include different data analysis procedures and use of electrical temperature sensors like thermistors or ICs type semiconductor sensors like AD590 and LM35. An information bank consisting of the OPD response of the PVDF to different concentrations of PFOA can be created for a specific range of temperatures. High resolution thermistors or IC type sensors which are cheap, efficient and fast can be synchronised with the optical fibre-based sensor system to log temperature continuously and simultaneously with spectral data at a known concentration of PFOA. When data is acquired in a field test, appropriate algorithms can then be developed to find the closest match of the acquired spectral data from the data bank on the spot to provide a suggestion for the possible concentration range. For this it has to be ensured that the coating thickness on the fibre end-face is the same on all the fibres and that they have similar looking normalized spectra to ensure reliability of data

set. An additional task may involve ensuring absence of electromagnetic interference during measurements with electrical sensing devices.

The scope of this research was to provide a proof of concept that a PVDF coated fibre can detect PFOA in aqueous media, rather than to produce a viable PFOA field sensor. Thus, to eliminate the effect of temperature sensitivity from the PFOA detection test in this work, experiments with the PVDF coated fibre were performed under constant temperature conditions maintained strictly and following the procedure discussed previously in section 5.3.6. Based on the developed protocol utilising a stable temperature environment for carrying out the PFOA sensitivity test of the PVDF coated fibre, it was assumed that the OPD change observed is only due to the change in PFOA concentration and not due to any temperature effect. As it was seen that the OPD varies linearly with temperature change in water over 20-60 °C it was anticipated that the initial values of OPD for PVDF coated fibres stabilized at slightly different room temperatures on different days, would be different. However, once stabilized at a specific temperature, the OPD was not expected to change. Therefore, the PFOA test could be performed with confidence in the reliability of the outcome, assuming that the PVDF coated fibre's temperature sensitivity has been adequately compensated or corrected.

#### **5.4.4 Coated Fibre Response to PFOA Solution**

The normalized reflection spectra of the PVDF coated fibre submerged in PFOA solution of different concentrations at a constant temperature of 23.8 °C is shown in Figure 5.6 and the simulated spectra is shown in Figure 5.7. The raw spectral data obtained using the experimental set up shown in Figure 5.1, were initially normalized against the reflection spectrum of a cleaved fibre end-face in water. After that each data set was

normalized to itself. The highest value in each data set was considered 1 and the lowest was considered 0. The Excel fit was obtained on these spectra.

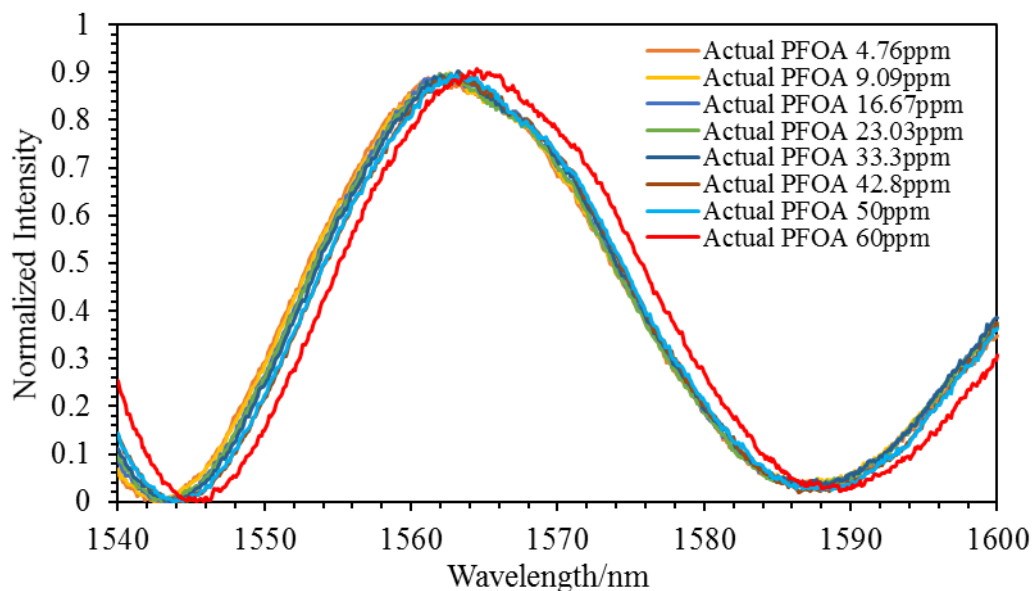


Figure 5.6 Normalized spectral data of PVDF coated fibre response to change in PFOA concentration.

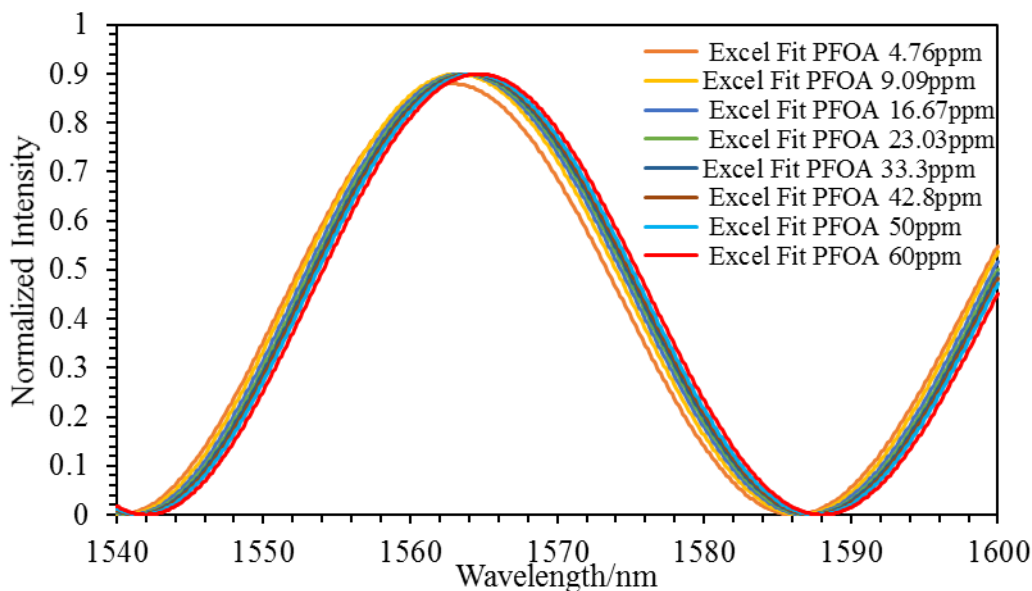
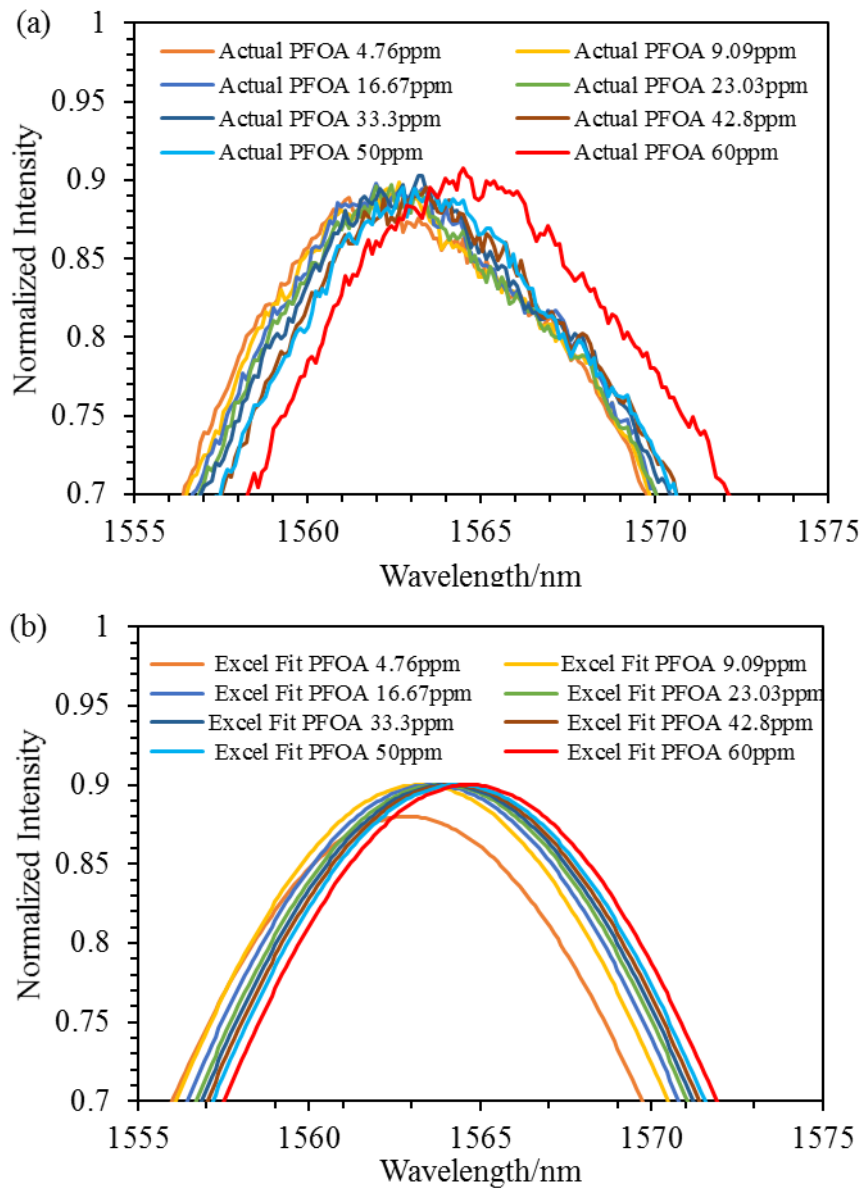


Figure 5.7 Simulated response of the PVDF coated fibre response to PFOA obtained through Excel fit of the normalized data shown in Figure 5.6.

When a certain section of Figure 5.6 and Figure 5.7 are magnified, as in Figure 5.8, the shift in peak positions with change in PFOA concentration can be seen more clearly. The

closeness between the normalized spectra and the Excel fit is discussed in more detail in the following sections.



**Figure 5.8 (a) Magnified image of normalized and simulated spectra of Figure 5.6 and (b) Magnified image of Figure 5.7 illustrating, shift in peak positions.**

The method of PFOA detection based on Fabry-Perot interference, involved observation of wavelength shifts, using the set up shown in Figure 5.1, and the measurement of OPD from individual spectral data with the software Table Curve and Excel using equation 4.1

described in Chapter 4 (also shown below). As mentioned earlier, in equation 4.1 the product of B and C provides the value of OPD.

$$I = A * \cos\left(\frac{4\pi * B * C}{\lambda} + D\right) + E \quad 4.1$$

Curve fitting in Excel was performed by setting appropriate constant values of the parameters A, B, D and E, which correspond to the amplitude, refractive index of PVDF (1.42), initial phase and vertical shift of the spectrum, and then varying C, which represents the coating thickness **L** on the fibre end-face. In the Table Curve program, the initial values of the parameters from A to E were provided only and the software generated the fit automatically based on the method of least squares. The final values of B and C were very different in most cases based on the starting values chosen for the fit. However, the OPD for a particular data set was the same irrespective of the difference in the values of B and C. The differences in the method by which the fits are generated by Excel and Table Curve have been discussed in detail in Chapter 4 section 4.3.1.

On average, correlation between the normalized spectral response and the Excel and Table Curve fits were both found to be in the order of 0.98. However, despite this, it was seen that the difference between the lowest and highest value of thickness **L** generated by Table Curve, at the lowest and highest concentration of PFOA respectively, was significantly large compared to the value generated by Excel. Such a difference is unexpected over the concentration range chosen, according to calculations performed on the actual normalized spectra using equation 4.2. The reason behind this noticeably large variation has been thought to be caused by the software's inherent technique of curve fitting. Since Table Curve alters the value of B (refractive index of PVDF) to a great

extent, in most cases, it falls outside the acceptable range of 1.41~1.42, and the corresponding value of L that it generates compensates for it to obtain a suitable fit. More information about the specific differences in Excel and Table Curve data is provided below after Figure 5.9 (a-f) and Figure 5.10 (a-f), where the curve fits are illustrated. In all the figures from a-f, the correlation of the fits is depicted by  $R^2$ , the coefficient of determination, which is a statistical measure in a regression model that represents the proportion of the difference or variance in statistical terms. The closer the value is to 1, the better the fit, or relationship, between the two factors. The  $R^2$  values shown in the individual figures from a to f, were generated using an Excel function by comparing the fitted data with the normalized spectral data. The curve fits in Excel and Table curve are followed by the OPD plots. Their correlation has also been determined using the same function in Excel and is discussed below. The presence of the error bars indicate uncertainty in the OPD values obtained by using the concept of standard error, discussed in Chapter 4.

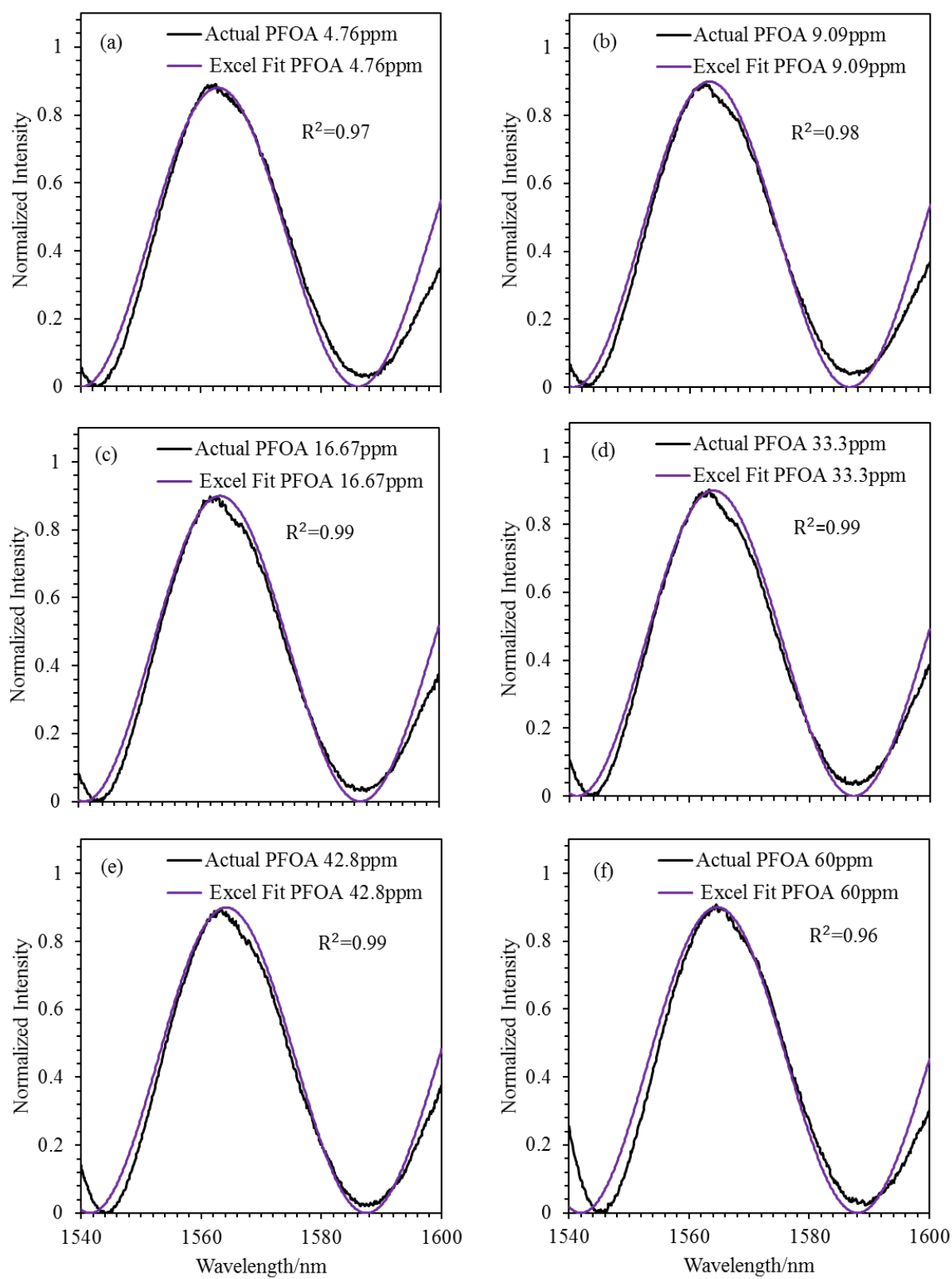


Figure 5.9 (a-f) Curve fitting of spectral data of PFOA experiment in Excel.

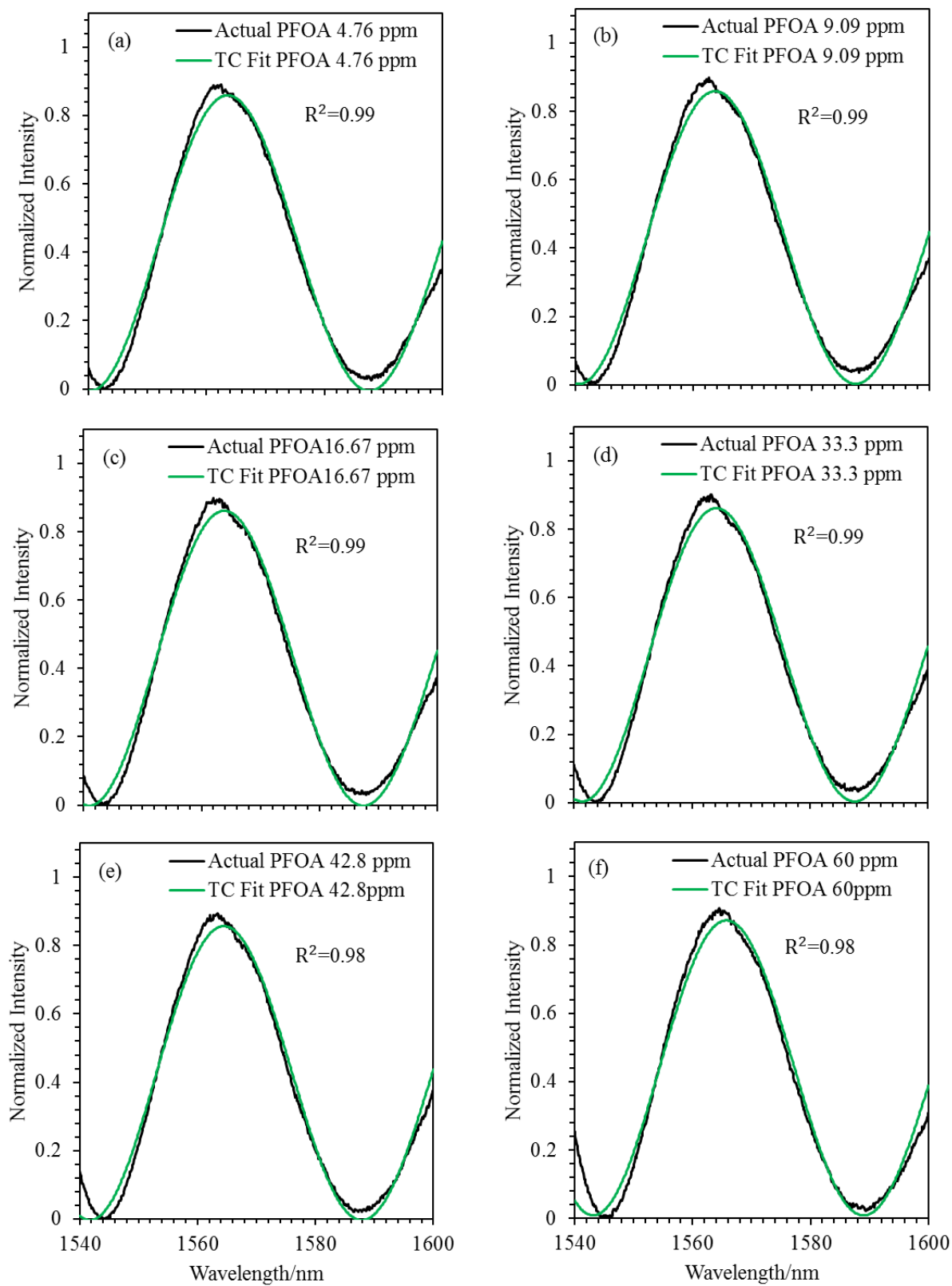


Figure 5.10 (a-f) Curve fitting of spectral data of PFOA experiment in Table Curve (TC).

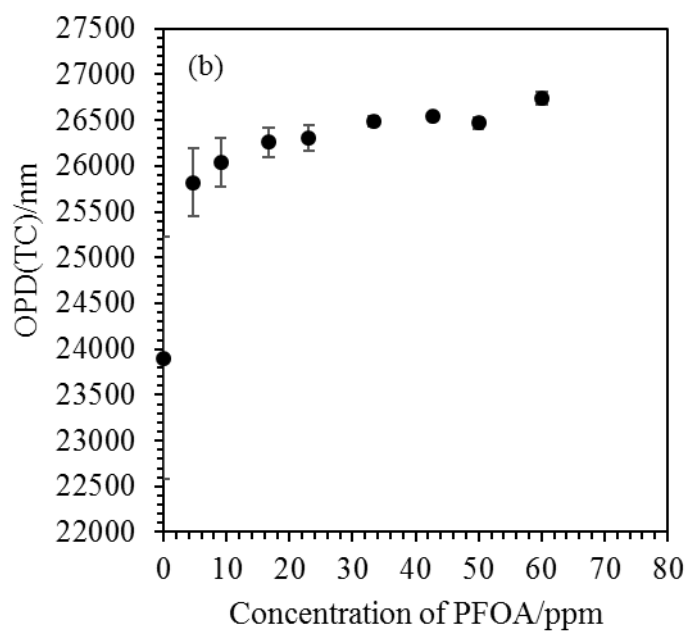
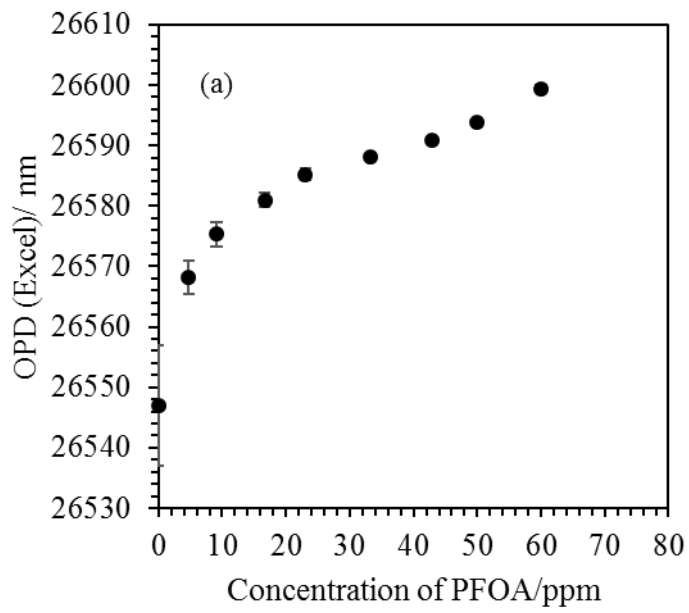


Figure 5.11 Plot of OPD vs PFOA concentration in (a) Excel and (b) Table Curve (TC) .

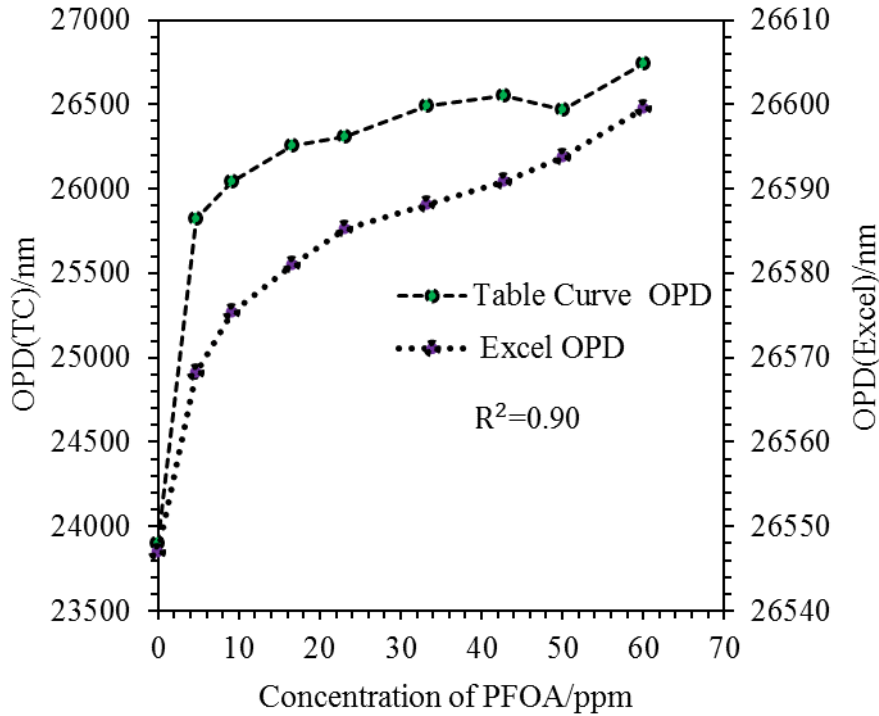


Figure 5.12 Correlation between OPD values obtained using Excel and Table Curve (TC).

Figure 5.11 shows the OPD values obtained from the fits in Excel and Table Curve, while Figure 5.12 shows the correlation between them. As can be seen, the OPD varies in a non-linear way in both the cases and the correlation between the two data sets is approximately 0.90. To identify which simulated data set is a more accurate representation of the PVDF coated fibre's performance, a comparison was done with the expected value of  $L$  generated from the spectral data using equation 4.2 discussed in Chapter 4. It was seen that if the value of  $n$  is kept constant at 1.42 for the PVDF thin film,  $L$  varies roughly from 18333 nm to 18380 nm when the concentration of PFOA is changed from 4.76 ppm to 60 ppm. Thus, the difference between the highest and lowest value was calculated to be approximately 47 nm. The corresponding OPD value difference was calculated to be approximately 68 nm. It has been seen that the difference between the highest and lowest

values of OPD generated by Excel and Table Curve are approximately 31 nm and 920 nm respectively.

As the OPD data generated in Excel was closer to the calculated value of L obtained using equation 4.2, the Excel fits were chosen for performance analysis of the coated fibres. The plot of OPD (Excel) versus PFOA concentration is depicted in Figure 5.13 (a). To determine the tested fibre's performance from the information in Figure 5.13 (a), a graph of OPD change with respect to PFOA concentration change was plotted (Figure 5.13 (b)), and a fit equation was generated. Figure 5.13 (b) shows equation (5.2) from the fit that has been used here for determining the sensitivity (i.e.  $\Delta\text{OPD}/\Delta\text{PFOA}_{\text{conc}}$  in nm/ppm) of the PVDF coated fibre to PFOA concentration in water.

Depending on the nature of OPD variation seen in Figure 5.13 (b), it was assumed that PFOA adsorption on the surface of the PVDF membrane increases with increasing concentration of PFOA until all the binding sites are occupied and the membrane is saturated. Although the graph shown in Figure 5.13 (b) does not show complete saturation, the trend observed suggests decreasing sensitivity with increasing PFOA concentration.

The development of a layer of PFOA was thought to cause a change in the apparent thickness of the PVDF membrane and influence its refractive index to bring about a change in the OPD value.

$$\Delta\text{OPD} = 13.23\Delta\text{PFOA}_{\text{conc}}^{0.33} \quad (5.2)$$

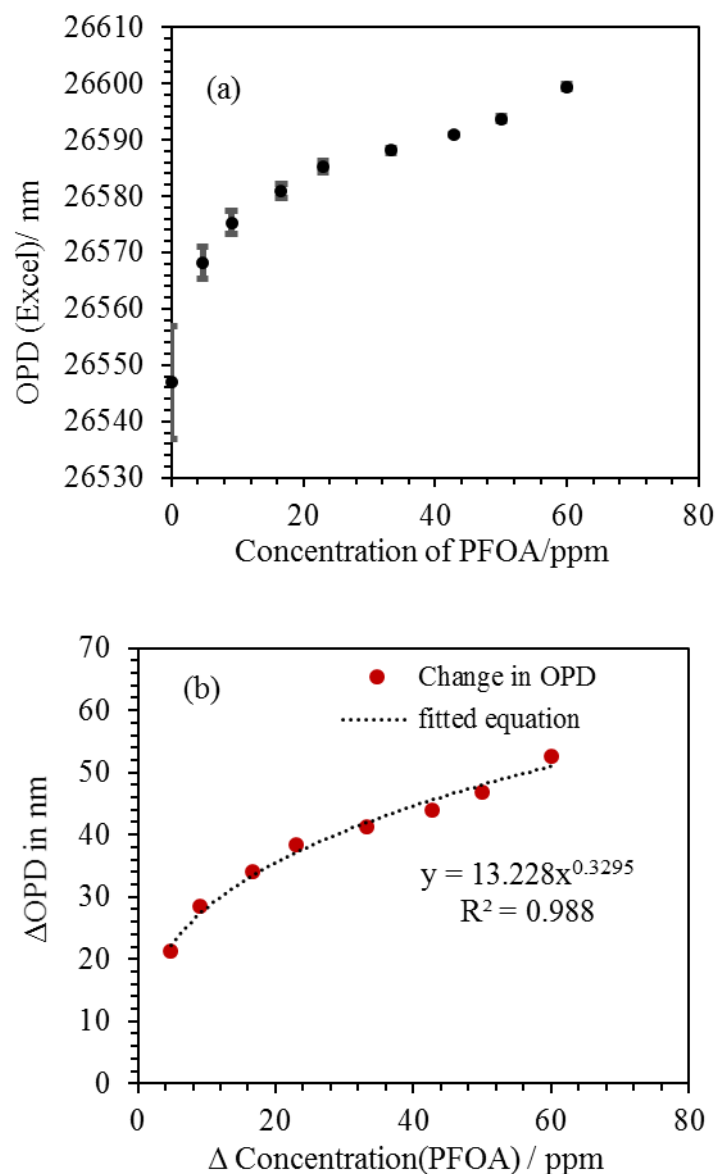


**Figure 5.13 (a) Variation of OPD (Excel) with PFOA concentration**  
**(b) Change in OPD vs. change in PFOA concentration with respect to the reference in water.**

It was ascertained from the OPD data that the PVDF coated fibre's sensitivity to PFOA varies from approximately 5 nm/ppm to 0.9 nm/ppm over the limited range of concentration chosen for investigation. Based on the observations presented above, it has been established that a higher concentration may cause instantaneous saturation of the

binding sites and render the PVDF coated fibre as a two-state device, almost switch-like in nature that would only indicate the presence or absence of PFOA.

In this experiment PFOA concentration lower than 4.76 ppm were not used as it was seen that the coated fibre did not produce significant wavelength shift below that level (Figure 5.14). A range of low PFOA concentrations between 0.1 ppb and 1ppb were tested in light of the finding that a MIP receptor based plasmonic fibre sensor for PFAS sensing was sensitive to 0.13–0.15 ppb[65]. It has been assumed that the lack of sensitivity of the PVDF coated fibre at the low concentrations depicted in Figure 5.14 is due to insignificant change in the OPD. Functionalization of the coating was thought to be a possible remedy to this situation and has been discussed in Chapter 7.

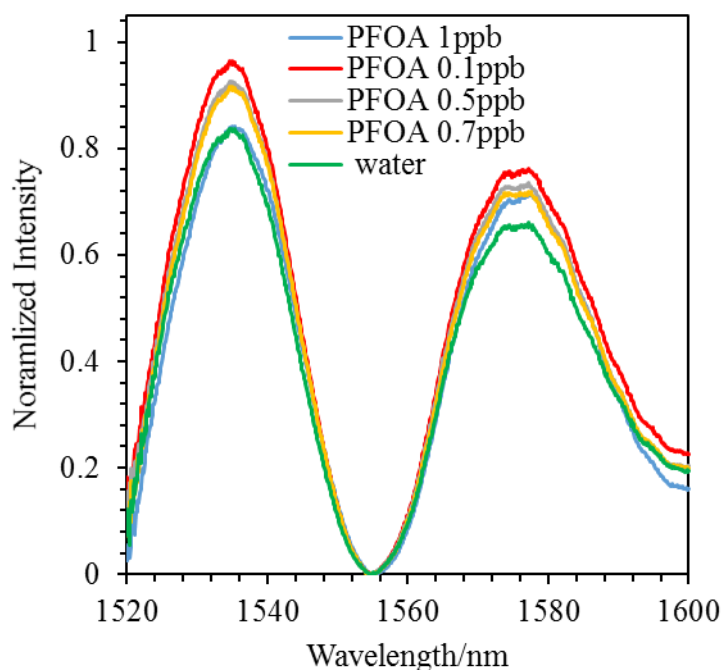


**Figure 5.14** PVDF coated fibre response to PFOA in the parts per billion (ppb) concentration range.

### 5.4.5 Coated Fibre Response to PFOA in Saline Water

It has been seen that the PVDF coated fibre is able to respond to PFOA in saline environments (i.e. in the presence of NaCl). The normalized spectral data which illustrates this are shown in Figure 5.15. The raw spectral data obtained using the experimental set up shown in Figure 5.1 were initially normalized against the reflection spectrum of a cleaved fibre end-face in water. After that each data set was normalized to itself. The highest value in each data set was considered 1 and the lowest was considered 0. In Figure 5.15 it can be seen that there is considerable difference in the way the PVDF coating on the optical fibre end-face responds to salt and PFOA. The reflection spectra of the stabilized coated fibre in water has been presented here to highlight this difference. The shifts in peak positions exist on either side of this spectrum.

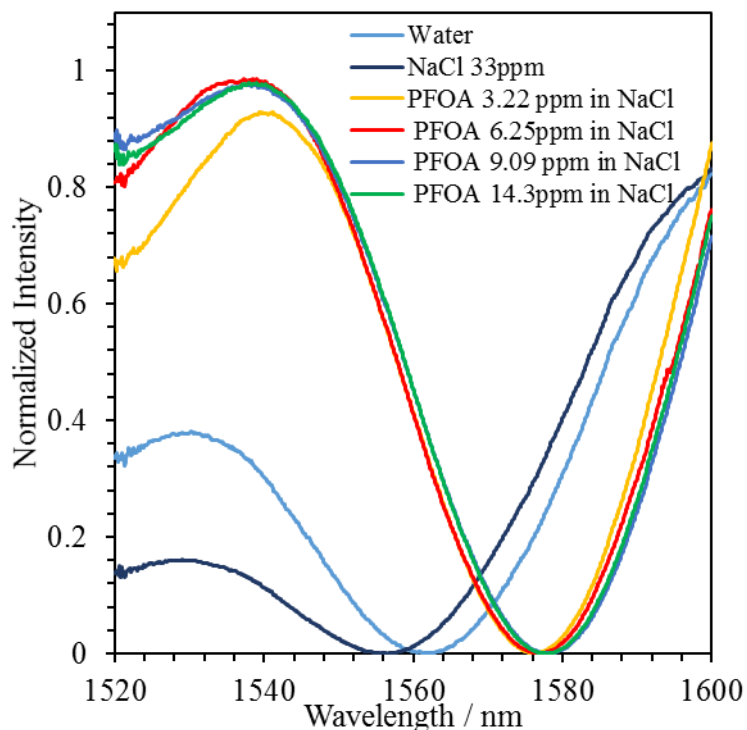
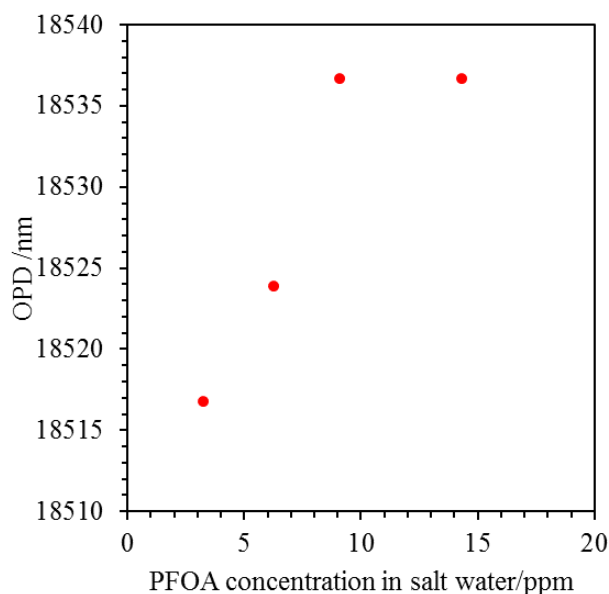


Figure 5.15 PVDF coated fibre's spectral response to PFOA in saline water.

It can be observed that the spectrum in NaCl solution appears on the lower wavelength side of the coated fibre's reference signal in water, whereas the spectra of PFOA in the salt solution mixture appears towards the right of the reference. Based on this observation it was assumed that the PVDF coating, which absorbed water during the initial stabilization process, released it when the salt solution was first added. This phenomenon was thought to cause a decrease in the physical thickness of the thin film and the refractive index (OPD), which resulted in a spectral shift towards the lower wavelength region. When PFOA was added to the salt solution, it was assumed that, the molecules attached themselves to the binding sites on the surface of the coating, which caused an apparent increase in the OPD and produced a spectral redshift. From this observation it can be inferred that salinity of the environment does not affect the capability of the PVDF coating adversely in PFOA sensing, at the concentrations that has been used in this experiment. The OPD, calculated from curve fits in Excel, have been plotted against the PFOA concentration in the salt water (NaCl solution). Figure 5.16 shows that with increase in PFOA concentration the OPD also increases. The data indicates an abrupt saturation beyond a PFOA concentration of 9.09 ppm. As can be noted from Figure 5.16 there are too few data points to obtain a reliable fit to assess sensitivity of the PVDF coated fibre with considerable accuracy. Therefore, it has been assumed that a linear relationship between the OPD and the measurand might only exist over a small range of concentration. It is unclear why the PVDF coated fibre saturates at the level shown here and the probable cause has been presumed to be linked to the availability of the binding sites.



**Figure 5.16 Variation in OPD with changing PFOA concentration in aqueous salt solution.**

If PVDF adsorbs sodium or chloride ion in the solution, then the number of available binding sites for PFOA to attach to decreases and as a result the saturation is reached at a lower concentration level than what was observed in non-saline aqueous solutions. Alternatively, it is also possible that the coating had a fewer number of binding sites to begin with and NaCl does not interact with PVDF at all. Thus, the only conclusion that can be derived from the presented results is that with proper calibration a PVDF coated optical fibre can be made to detect PFOA in salt water over a limited concentration range.

#### **5.4.6 Coated Fibre Response to PFAS in Wash Water from Fire-fighting Trucks**

One of the major causes of PFOA contamination in Australia was the use of fire-fighting foams containing this fluorosurfactant among other PFAS. In reality, the contaminated water or soil samples are likely to have a combination of PFOA and other PFAS, which is why the remarkable observation recorded with the PVDF coated optical fibre discussed in this section is so important.

The residual water from cleaning Australian fire-fighting trucks in Melbourne, which will be referred to as wash water here, was collected and tested by the designed OFS. The PVDF coated fibre has shown a positive response to PFAS wash water acquired from the fire-fighting trucks in the form of spectral red shift. In Figure 5.17, it can be seen that the probe is sensitive to PFAS in the parts per billion range, which means that its sensitivity to the wash water is 1000 times better than its sensitivity to only PFOA solution. This outcome hints at the PVDF coating being more sensitive to other perfluoroalkyls in the wash water, such as PFOS, which is another equally toxic substance. Even though this observation does not explicitly confirm whether the response was derived from a specific PFAS like PFOS or PFOA in the wash water or other contaminants, it highlights that in practical situations where combinations of PFAS are present, the PVDF coated fibre would be responsive and can potentially indicate their concentration level as a whole. Further analysis through curve fitting has shown that there is a linear relationship between PFAS concentration and OPD (Figure 5.18) over the chosen range. From Figure 5.18 it can also be seen that the trend line has an equation relating the OPD to PFAS concentration, where the gradient of the line is approximately 178 nm/ppb. This value is in essence the sensitivity of the PVDF coated fibre to PFAS in the wash water and is significantly large compared to the sensitivity of other sensors reported so far [65] within this range of concentration.

Investigating sensitivity of the PVDF coated fibre to all the chemicals present in the wash water from fire-fighting trucks was out of scope for this research but it can be a future work to determine the specific element to which the polymer PVDF reacts so strongly for sensor optimization purposes.

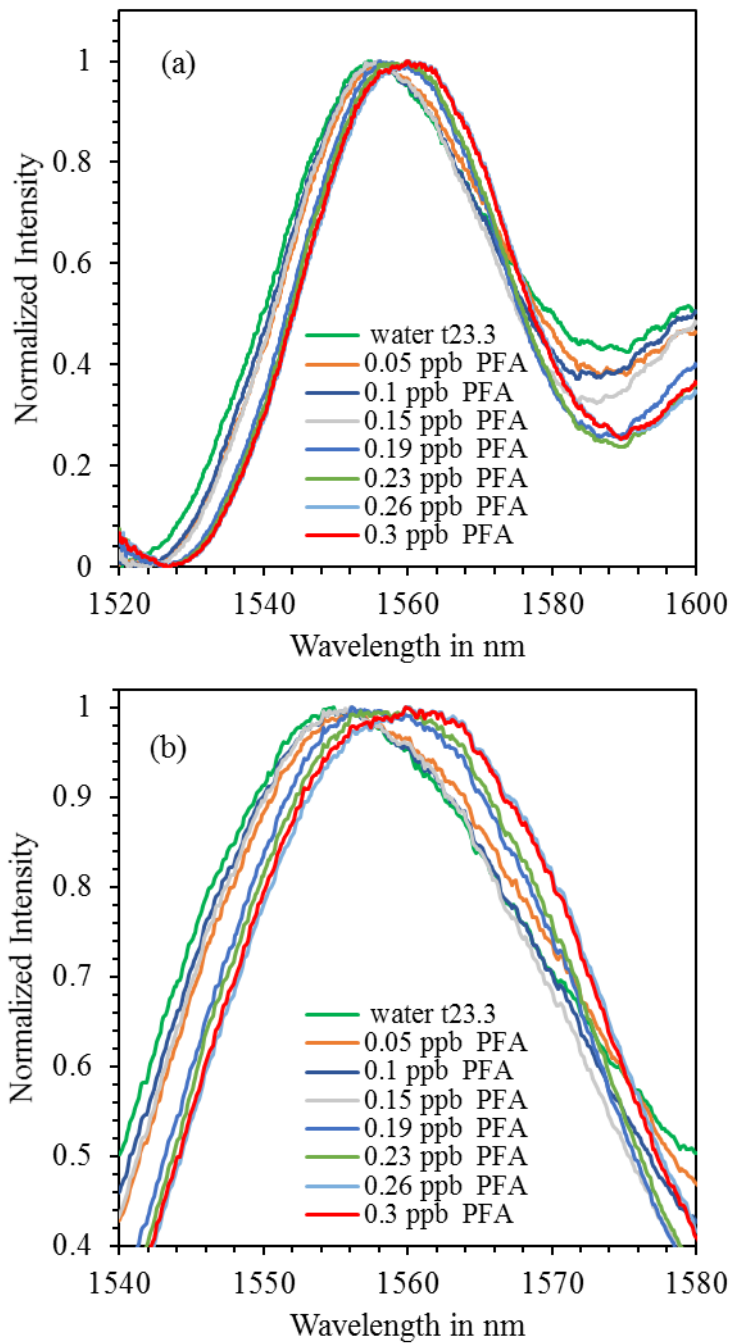


**Figure 5.17 (a) PVDF coated optical fibre's spectral response to PFAS in wash water.**

**(b) Magnified section of the graph shown in (a).**

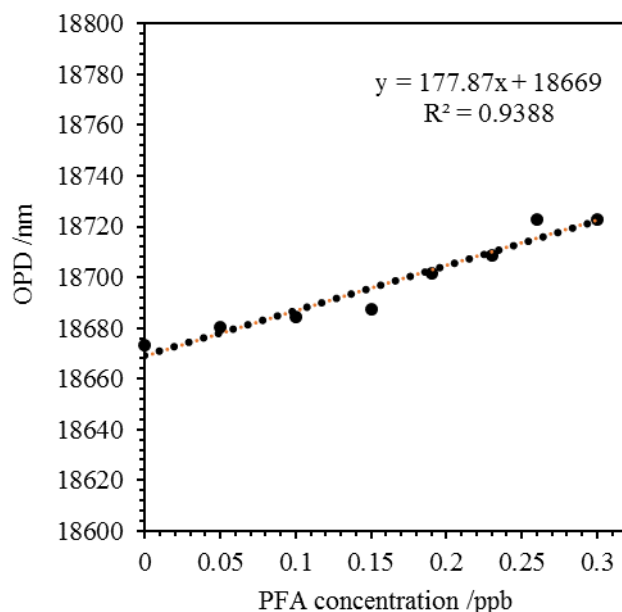


Figure 5.18 Variation in OPD with change in PFAS concentration in the parts per billion (ppb) range.

## 5.5 Overall Performance of PVDF Coated Fibre

The FP interferometry-based detector, which was created by forming a PVDF thin film at the end-face of a freshly cleaved optical fibre using immersion precipitation technique demonstrates positive response to PFOA in aqueous solutions and shows a very high sensitivity to PFAS wash water (from fire-fighting trucks), resembling real life contaminated samples. The sensitivity of the PVDF coated fibre shows a decreasing trend with increasing PFOA concentration in the neutral, and saline environment, which is as per expectation. Based on OPD analysis it can be suggested that the binding sites on the PVDF membrane fill up with increase in PFOA concentration and slows down the change in thickness and refractive index of the PVDF thin film on the fibre end-face as a result of which the sensitivity reduces. Experimental results also showed that the PVDF coated fibre is an effective tool for measuring variation in PFOA concentration, as well as, temperature but not both simultaneously. It was observed that the temperature sensitivity

in water is 3.9 nm/°C, whereas the PFOA sensitivity is different in different aqueous media. While the sensitivity value was seen to decrease from 5 nm/ppm to 0.9 nm/ppm with rise in PFOA concentration in a neutral environment (i.e. PFOA solution in ultra-pure water), it was found to be 178 nm/ppb in PFAS wash water obtained from fire-fighting trucks.

The temperature sensitivity, which seems quite low compared to some of the PFOA sensitivity values mentioned above, is in reality an important figure. It has to be considered for accurate calculation or uncertainty measurement of the PFOA sensitivity values i.e. cross temperature sensitivity has to be eliminated for accurate PFAS sensitivity measurement.

Crude analysis of the PVDF coated fibre characteristics defined by response time, linearity and hysteresis that were not primary concepts for investigation in this project show the coated fibre's response to be as follows:

- quick and almost switch-like, which in other words mean that a designed OFS from this material would be ideal for detecting the presence or absence of PFOA within a few seconds (approximately 10-50), for a relatively high and therefore unsafe concentration of the analyte, as established by relevant standards.
- non-linear, sensitivity varies non uniformly over a wide concentration range (178 nm/ppb to 5nm/ppm) in different aqueous environments.
- non-repeatable, the same coated fibre cannot be reused efficiently for measurement once it is cleaned using alcohols.

## **5.6 Chapter Summary**

This chapter has provided an overview of the PVDF coating formation technique and discussed the FPI identification and characterization procedure of the coated fibre. It has also listed the outcome from the probe's temperature sensitivity in water and compared the PFOA sensitivity in different aqueous media. The chapter has discussed the extremely high PFAS wash water sensitivity (178 nm/ppb) of the PVDF coated optical fibre, which shows a good prospect for optimization in the future and practical use in real situation. This chapter has described the OPD determination technique through curve fitting and has discussed the differences in the method of analysis used by the software Excel and Table curve used in the process. It has provided new knowledge regarding the polymer's use as a PFAS detector, which will be further investigated in the next chapter. To the best of the authors' knowledge, this is the first report on PFOA detection by PVDF. Moreover, there are no other reports of a PVDF coating at the end-face of an optical fibre, which has adopted an easier fabrication process than the one mentioned here.

## 6 Alternative Methods of PFOA Detection

---

### 6.1 Overview

This chapter discusses both direct and indirect analytical approaches and alternative optical methods for PFOA detection measurements that have been undertaken in this research alongside the FPI technique that was presented in the previous chapter. These include two refractometry based methods, one employing a bare optical fibre and the other an etched fibre Bragg grating (EFBG) containing optical fibre. Information on PFOA adsorption by PVDF was also obtained via a confirmatory analytical test using a standard HPLC technique.

In the previous chapters it was established, based on experimental data, that a coating developed from PVDF undergoes hydrophobic or dipole-dipole interactions with PFOA in aqueous solution, which leads to the adsorption of the contaminant on the surface of the developed thin film. In the precinct of this assumption it is expected that if the PVDF coating adsorbs PFOA then some of the molecules from the solution would be removed thereby reducing its concentration, which would affect the refractive index of the solution. Thus, sample solutions of known concentration of PFOA were formed in which flat PVDF thin films, cast on glass slides, were soaked for observation of PFOA adsorption. Data obtained from the samples were monitored for changes in PFOA concentration through comparison of reflection intensity and refractive index data.

## 6.2 Background of Methods

### 6.2.1 Refractive Index Measurement

A very simple method for undertaking refractive index measurements of liquids using an optical fibre is based on monitoring the Fresnel reflection from a freshly cleaved fibre end-face. Reflection signals from the fibre's tip at the liquid–fibre interface can be compared with reflection signals from an air–fibre interface to obtain information about the medium's refractive index. The spectra would illustrate a drop in power with increasing refractive index. Similarly, etched Bragg gratings containing fibres can also be used to monitor variation in the refractive index of different liquids by observing wavelength shifts in the spectra, with much increased sensitivity.

Fibre Bragg Gratings (FBG) are a type of selective or narrow-band high-reflectance partial reflectors or wavelength selective filter that is formed by inducing a permanent change in the refractive index of the photosensitive core of an optical fibre [219]. The Bragg or reflected wavelength, which is detected by an Optical Spectrum Analyser (OSA) or an Optical Sensor Interrogator (OSI) to identify a change in the measured parameter, is dependent on the grating structure, refractive index of the fibre core and grating period. These parameters are related by the following equation:

$$\Delta\lambda_B = 2n\Lambda \quad 6.1$$

where,  $\lambda_b$  is the Bragg wavelength,  $n$  is the effective refractive index of the fibre core, and  $\Lambda$  is the spacing between the gratings or the grating period. Any change in the measured parameter brings about a wavelength shift that can be compared to the reference wavelength value for determining the change in the desired factor. However, this typical

FBG configuration is not suitable for measuring refractive index variation due to the presence of the cladding over the fibre core that ensures light propagation through the optical waveguide by total internal reflection and also makes the grating less responsive to external changes in refractive index. This is not the case for long period FBGs, where the grating is formed in the cladding region as well and therefore evanescent fields are present at the cladding air interface [220]. Thus, to enable a FBG to detect refractive index variation in the surrounding environment, the cladding material is removed through a chemical etching process to produce a thinned FBG containing fibre. Usually the process involves submerging the FBG in a hydrofluoric acid bath for a certain time and is specific for a particular application [221].

An Etched Fibre Bragg Grating (EFBG) containing fibre enables interaction of the evanescent fields with the surrounding media due to the removal of the fibre cladding region. If the fibre cladding diameter is reduced symmetrically along the grating region, the effective refractive index (RI) of the FBG gets affected by the external refractive index, which in turn modulates the reflected Bragg wavelength. A shift in the Bragg wavelength of the EFBG combined with a modulation of the reflected amplitude is given by:

$$\Delta\lambda_B = 2\Delta n\Lambda\Delta\eta_P \quad 6.2$$

where  $\Delta\lambda_B$  is the change in wavelength of the Bragg reflection,  $\Delta n$  is the difference between the cladding refractive index and the surrounding refractive index,  $\Lambda$  is the period of the grating, and  $\Delta\eta_P$  is the variation of the fraction of the total power of the unperturbed mode that exists in the etched region [221].

The Bragg wavelength of an EFBG undergoes a red shift [221, 222] with increase in the surrounding refractive index and may sometimes be accompanied with changes in reflected power level.

### **6.2.2 Analytical Test for Determining Chemical Concentration**

Analytical laboratory test for determining chemical concentration present in trace levels involve HPLC-MS or GC-MS techniques. General descriptions of these methods are provided in Chapter 2, where the procedures used to separate, identify and quantify compounds in a sample have been discussed. Details on ionization and mass analysis techniques are provided, which help to understand how unknown substances can be identified based on the mass to charge ratio once they have been separated using a suitable chromatography technique. Quantification of a sample, after identification, is done using calibration curves. A protocol has been discussed below for general understanding of the quantification process in HPLC- MS.

During an HPLC experiment, a high-pressure pump takes the mobile phase from a reservoir through an injector to a packed column for sample component separation. When the mobile phase moves into a detector cell, the absorbance is measured along with the retention time, which is the amount of time it takes for a component to travel from the injector port to the detector [223]. Absorption spectroscopy is done at a specific wavelength compatible with the detector's specification to produce sample peaks on a chromatogram.

Initially peaks of standard solutions of known analyte concentrations are acquired for calibration purpose. Peak area is obtained by multiplying height by the full width at half maximum and a plot of peak area versus concentration graph of the standard solutions is

drawn [223]. A least square fit is obtained for the calibration curve following this. When the peak area of the desired analyte from an unknown sample is obtained, it is looked up on the calibration curve to obtain the corresponding concentration of the analyte.

### **6.3 Experimental Methods of PFOA Detection**

#### **6.3.1 Materials and Chemicals**

The PFOA solution used in this experiment was prepared using ultrapure water and PFOA from Sigma-Aldrich (Australia). The flat PVDF membrane that was soaked in a known concentration of the PFOA solution was prepared using Solef 1015, the PVDF grade from Solvay, N,N-dimethylformamide (DMF) from Sigma-Aldrich (Australia), polyvinyl butyral (Butvar) and chloroform from Sigma-Aldrich (Australia). Ethanol, methanol and isopropyl alcohol and some oils with known refractive indices were used in the refractive index measurement test with the bare optical fibre and etched FBG.

#### **6.3.2 Refractive Index Measurement Test with Bare Optical fibre**

An experimental set up consisting of a PXIe-4844 Optical Sensor Interrogator (OSI) (Figure 6.1) was first used to observe the reflection spectra in ethanol, methanol, isopropyl alcohol and some oils. Then, the set up was used to observe the spectra of different types of PFOA solutions with known concentrations but unknown refractive indices. The bare fibre was connected to one of the four channels of the OSI. The PXIe-4844 OSI was interfaced to a processor/computer with specialized LabVIEW programming achieved through the use of NI-OSI Explorer platform, and was used to acquire the spectral data consisting of the intensity versus wavelength data of the reflected light in dB scale over the 1510 to 1590 nm operating range with an accuracy of 1 pm.

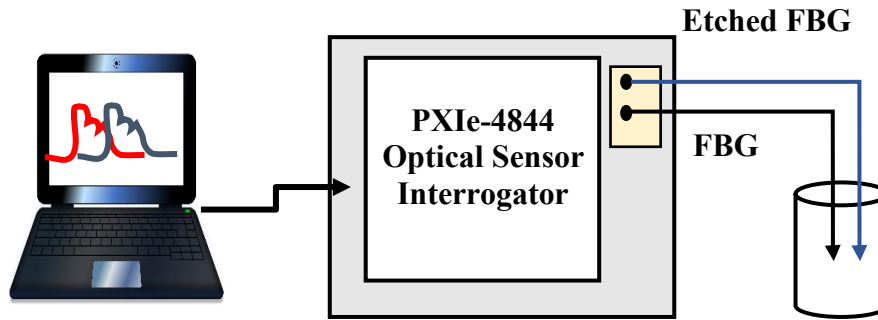


Figure 6.1 Experimental set up for observing wavelength shift using an etched FBG.

The PXIe-4844 is a dual-slot data acquisition module for fibre Bragg grating (FBG) optical sensors. It features an optical core, which combines a high-power, low-noise swept wavelength laser with fibre Fabry-Perot tunable filter technology from Micron Optics that offers a spectral resolution of 1pm. The NI PXIe-4844 was configured using the NI-OSI Explorer that scans the optical wavelength range to identify all connected FBG sensors and automatically parse the data into individual sensor measurements with appropriate scale [224]. The range and scaling equations needs to be specified before the scans and can be changed according to user's requirements. In case a bare fibre is used the scan shows a steady reflection signal of specific intensity.

In the refractive index measurement experiment, a clean and cleaved optical fibre was immersed in ethanol, methanol, isopropyl alcohol and some oils whose refractive index values were known and the reflection spectra were recorded. In a similar way spectral data was obtained for different concentrations of PFOA solution with unknown refractive index values at room temperature.

A stock solution of PFOA with a concentration of 100 ppm was prepared by dissolving 0.01g of PFOA in 100 mL of ultrapure water. Subsequent dilution of the stock solution was then performed to produce the sample PFOA solutions (30 and 40 ppm). A flat

membrane was formed from the polymer solution mixture containing PVDF, DMF, butvar and chloroform using the phase inversion process discussed in Chapter 3. The sample, which has been referred to as **soak water**, was formed by submerging a  $3 \times 1$  mm piece of the membrane in a bottle of the 100 ppm PFOA solution for several hours and then removing it.

Since the refractive indices of the PFOA solutions were unknown, the trend observed in the refractive index measurement test of the different alcohols mentioned above, besides evidence found in literature, were used to interpret the outcome of the refractive index measurement experiment with PFOA solutions. The normalized intensity of the reflected signal in a medium (alcohol, oil or PFOA solution) was calculated by measuring the total area under the intensity versus wavelength graph and then dividing it by the total area under intensity vs. wavelength plot of the reference, which was either air or water. The normalized area plots demonstrated the change in overall reflected power with a change in refractive index of the media, which helped to implicitly describe the relationship between concentration of different PFOA solutions and their corresponding refractive index values.

### **6.3.3 Refractive Index Measurement Test with Etched Fibre Bragg Grating**

The experimental set up shown in Figure 6.1 was used in this experiment for monitoring wavelength shifts of the EFBG as a function of changes in the sample solution's refractive index. The interrogator was used to scan the entire wavelength range from 1510 to 1590 nm to obtain reflection signals in different sample solutions. The intensity versus wavelength data were acquired using a LabVIEW platform and saved for further analysis.

A pre-fabricated etched FBG that was formed using a special technique mentioned in the work of Bal [221] has been used in this work to observe wavelength shift with changing refractive index of surrounding medium, using the set up shown in Figure 6.1. The EFBG spectra were recorded in air, water, methanol, ethanol, isopropyl alcohol, 1000 ppm, 125 ppm and 50 ppm PFOA solutions and the shifts in the respective spectra were compared based on the refractive indices of the liquids used. In addition to these, the spectrum of a soak water sample prepared from 100 ppm PFOA was also obtained.

During this experiment, the influence of temperature variation was monitored using a FBG that had an intact cladding. Shift in wavelength in the FBG denoted a temperature difference, which was taken into consideration for adjusting the wavelength shift of the EFBG to obtain the correct value. Due to the high spectral resolution (1 pm) of the OSI relatively small temperature differences could be monitored with the device. The absolute value of wavelength difference with respect to the reference spectrum (i.e. the FBG spectrum in water) was either added to the EFBG peak wavelength data or subtracted from it based on the direction of the shift. If the temperature of the solution was stabilized and the shift in the FBG spectra was insignificant the wavelength shift of the EFBG as observed on the display was considered for analysis. The normalized intensity of the reflected signal in a medium was calculated by measuring the total area under the intensity versus wavelength graph and then dividing it by the total area under intensity vs. wavelength plot of the reference signal in water.

#### **6.3.4 Quantification of PFOA Adsorption on PVDF Film**

A sample of 1 mg/L PFOA solution was prepared and a section of PVDF film was soaked for several hours. Samples of the PFOA solution before and after soaking in PVDF were

sent to ALS Water (Scoresby Victoria) where they were subjected to quantitative analysis in accordance with NATA accredited ALS Method EP231X.

## **6.4 Results and Discussion**

### **6.4.1 Refractive Index Measurement with Bare Optical Fibre**

The result from the refractive index measurement test with the bare optical fibre and the alcohol and oils with known concentration show that with increasing refractive index value of the media the intensity of the reflected signal decreases. The latter is in direct agreement with Fresnel equations, where in the case of an optical fibre end-face the angle of incidence is close to normal and therefore the intensity of reflected light, in reference to transmitted light, is given by the equation.

$$R = \left( \frac{n_1 - n_2}{n_1 + n_2} \right)^2 \quad 6.3$$

Where R is the reflected intensity and  $n_1$  and  $n_2$  are the refractive indices of the core of the optical fibre and the surrounding medium respectively. Figure 6.2 shows the plot of reflection intensity in dB scale versus refractive index, which illustrates the finding and serves as a point of reference for assessing refractive index of PFOA solutions of different concentrations. Figure 6.3 presents the normalized areas under the reflection intensity graph against various media that indicate a change in overall reflected power with change in refractive index. In addition Figure 6.4 shows the plot of reflected intensity of the media illustrated in Figure 6.2 in linear scale (mW) versus their refractive indices, which is characteristic of the observed Fresnel reflections.

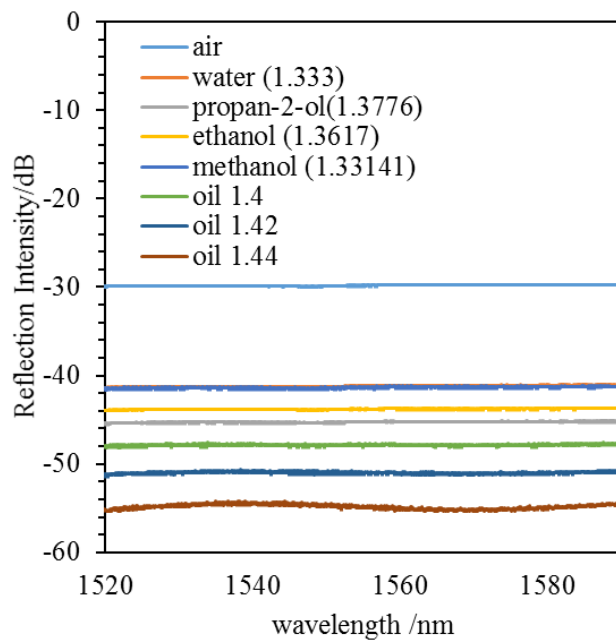


Figure 6.2 Reflection intensity of bare fibre in different media.

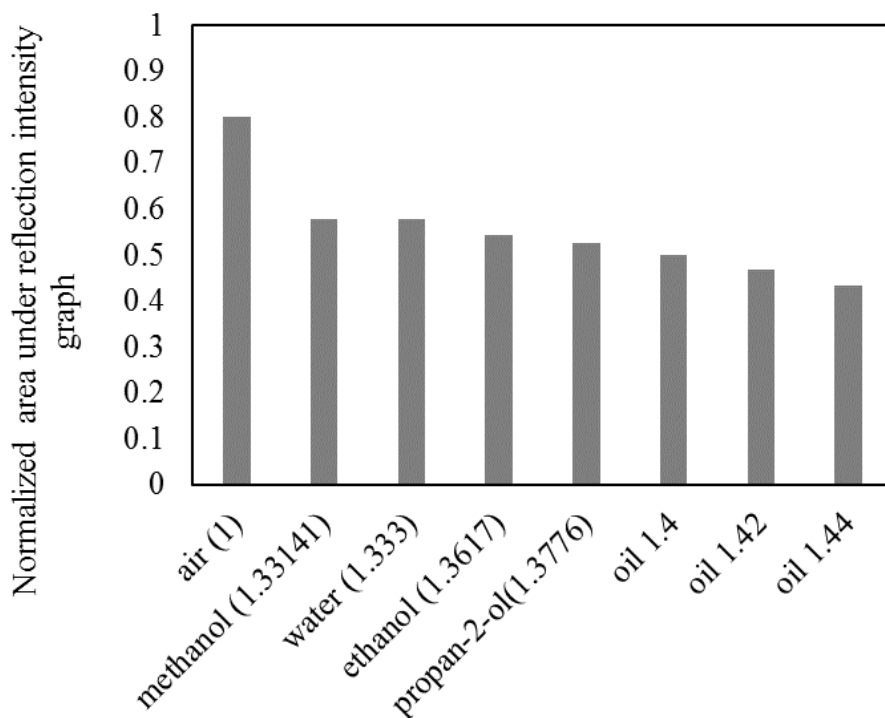
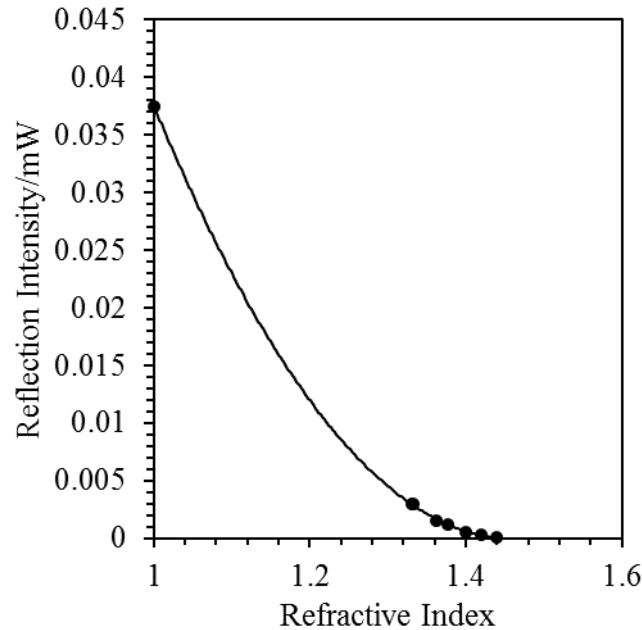
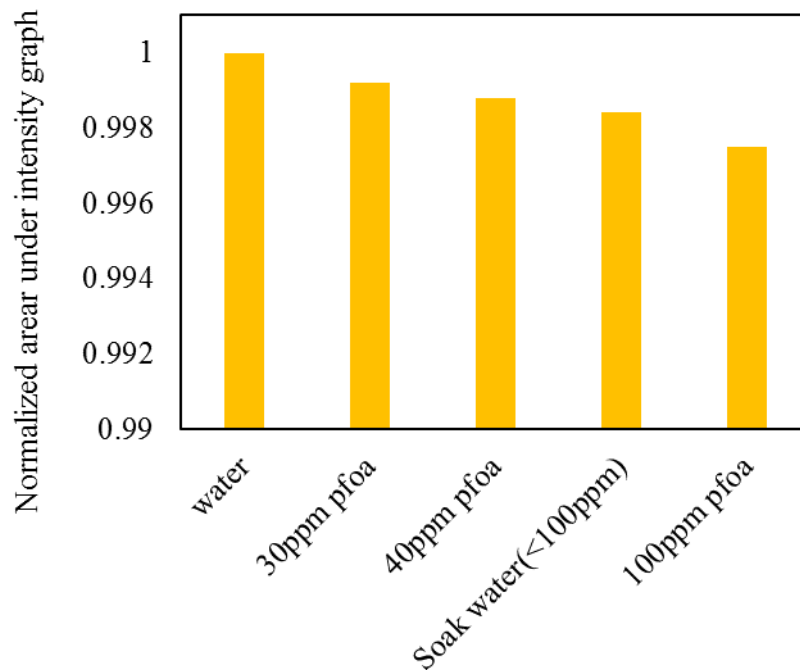


Figure 6.3 Normalized area graph of different media.



**Figure 6.4** Plot of reflection intensity in linear scale with changes in refractive index of the media shown in Figure 6.2.

The result of the refractive index measurement test for the PFOA solutions using a bare optical fibre is shown in Figure 6.5. The change in the normalized area under reflected intensity graph implies a change in refractive index of the sample solutions. The lower the concentration of the PFOA solution, the closer its overall intensity (indicated by the normalized area) is to that of water, which has a refractive index of 1.33. As the concentration of the solution increases, the total reflected intensity from the bare fibre end-face decreases indicating an increase in refractive index of the solution. As shown in Figure 6.5, the soak water intensity level is greater than that of 100 ppm but less than that of the 40 ppm PFOA solution. This suggests that the PVDF membrane absorbed some of the PFOA for which the concentration of the solution decreased, resulting in a decrease in refractive index and a corresponding increase in the intensity of reflected light. It should be noted that the initial concentration of the PFOA from which the soak water was prepared was 100 ppm as mentioned in earlier discussions.



**Figure 6.5 Intensity vs. concentration graph of PFOA samples of different concentration. The higher the value of the normalized area or total reflected intensity the lower the refractive index. The soak water sample hints at having a refractive index value in between that of 40 and 100 ppm PFOA.**

#### **6.4.2 Refractive Index Measurement with Etched Fibre Bragg Grating**

Figure 6.6 shows the response of the etched FBG to methanol, ethanol, propan-2-ol, ultrapure water and air, whose refractive indices were known. It is evident from Figure 6.6 that the Bragg wavelength undergoes a red shift with increasing refractive index, which is according to expectation [225]. The reflection intensity spectrum of methanol seems to be very similar to that of water as their refractive index values are quite close. Furthermore, it can be distinguished that the methanol spectrum peak at 1543.1 nm is positioned slightly towards the left of the water peak, indicating that the refractive index value of the medium is slightly less than that of water. It is also obvious from the normalized area versus refractive index plot in Figure 6.7 that the overall intensity of the reflected signal decreases with the increase in refractive index of the medium. Figure 6.8

shows similar response of the EFBG to PFOA solutions of different concentrations. As the refractive indices of the PFOA solutions used were unknown, the spectral data were analysed in perspective of the findings shown Figure 6.6.

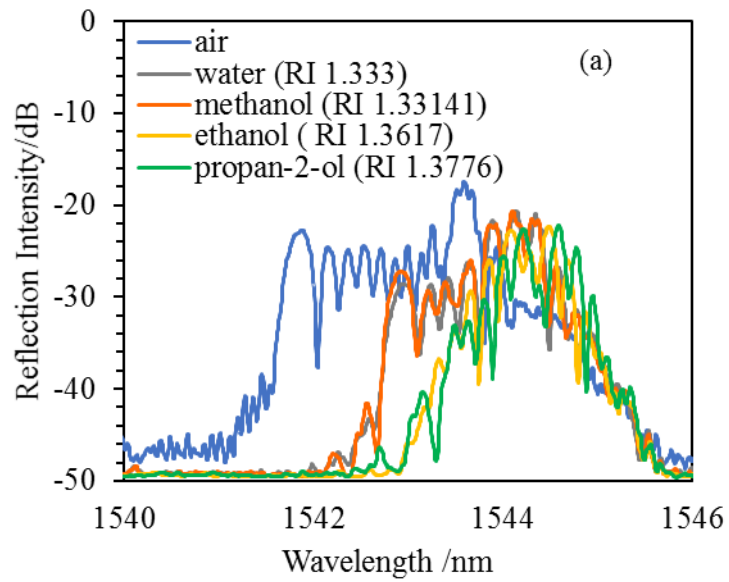
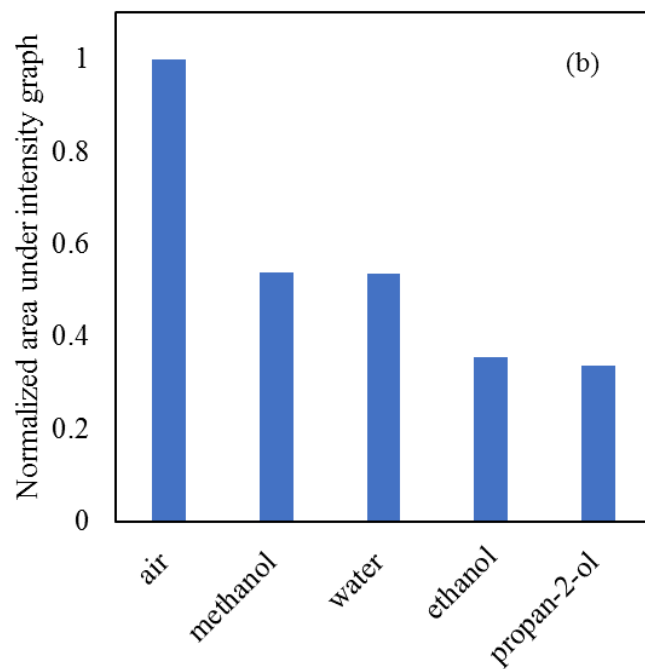
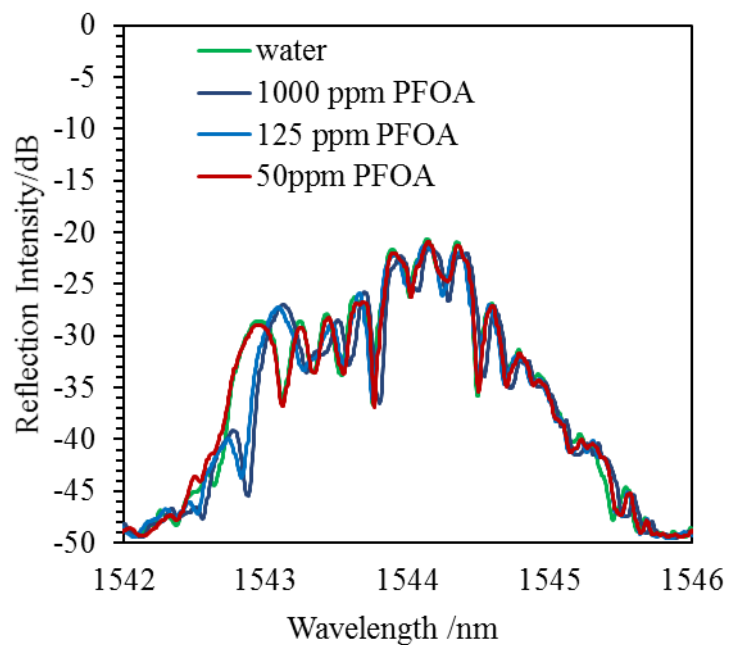


Figure 6.6 Wavelength shift of EFBG with change in refractive index of medium.



**Figure 6.7** Normalized area of graph of EFBG showing decrease in overall intensity with increase in refractive index.



**Figure 6.8** Response of EFBG to PFOA solution of varying concentrations.

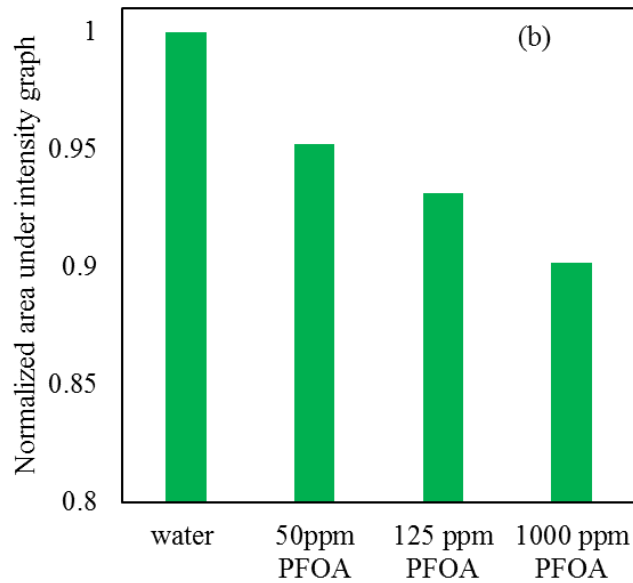


**Figure 6.9 Normalized area graph of intensity in PFOA solution of different concentrations.**

From the spectra presented in Figure 6.8, it can be observed that with increasing concentration of PFOA, the peak wavelength position in the 1543 nm region shifts prominently to a higher value. This implies that with increasing concentration, the refractive index of the solution increases. It is also observed that the spectrum of 50 ppm PFOA almost overlaps with that of water indicating that their refractive indices are very close. The normalized area under the graph versus PFOA concentration (Figure 6.9) shows a decrease in overall reflected intensity with increase in PFOA concentration.

Additionally, Figure 6.10 shows how the EFBG responds to the PFOA solution in which PVDF membrane was soaked (i.e. the soak water solution). Figure 6.11 shows the normalized area (i.e. with respect to the area of water) versus the PFOA concentration graph in which it can be seen more clearly that the PFOA soak water solution has an overall reflected intensity value between that of water and the 100 ppm PFOA solution. This suggests that PVDF adsorbed the per-fluoro compound from the 100 ppm PFOA

solution. It is assumed that as a result of this adsorption, the concentration of PFOA in the solution decreased along with its refractive index. The finding therefore indicates that the soak water solution has a refractive index value closer to that of water and less than the stock solution (100 ppm PFOA) from which it was made.

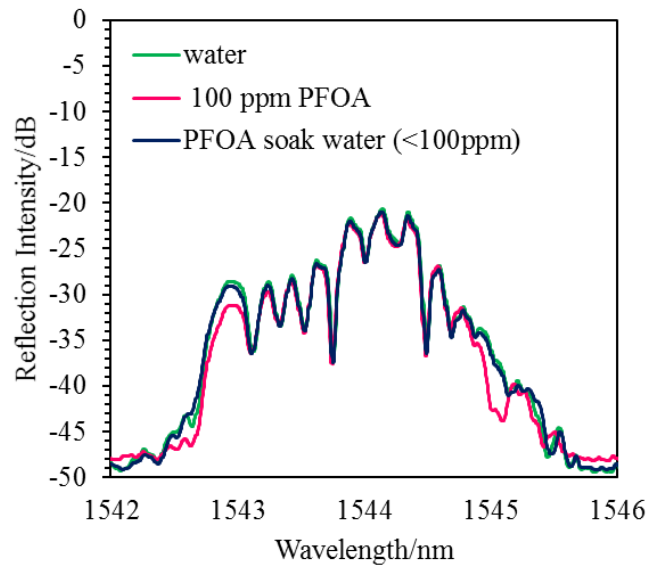


Figure 6.10 Response of EFBG to PFOA solution in which PVDF membrane was soaked.

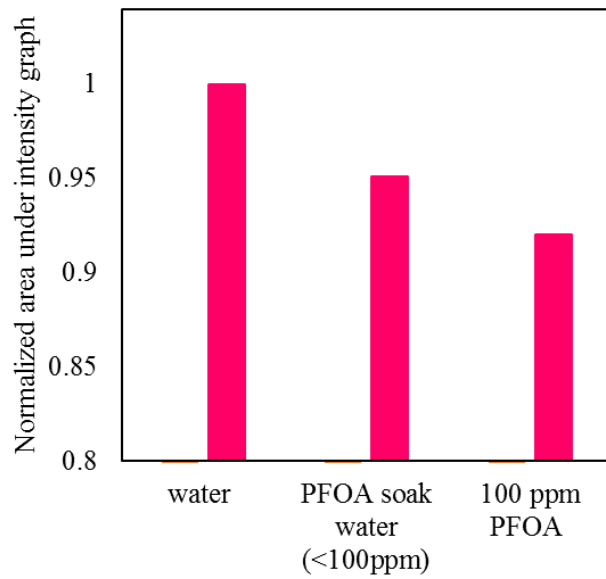


Figure 6.11 Normalized area graph of reflected intensity showing soak water having overall reflected intensity and refractive index closer to that of water.

### **6.4.3 Quantification of PFOA Adsorption**

The external laboratory test conducted by ALS Water showed that the concentration of the PFOA solution was significantly decreased after the addition of the PVDF membrane to the stock solution. These test results confirmed that 10% of PFOA was adsorbed on to PVDF film and it has been assumed that the amount of adsorption is restricted by the available surface area. Overall, the laboratory test results support the notion that the change in RI observed by the bare optical fibre and EFBG in the soak water is due to the reduced concentration of PFOA. More importantly, these results confirm the principle of operation of the PVDF coated optical fibre sensor scheme proposed in this project.

The findings also have implications for water treatment whereby PVDF membranes may be effective in removing PFAS compounds. As is evident from this study, it is the first time that this polymer has been investigated in relation to PFAS sensing. Further water research can look into functionalized PVDF membranes or adsorbents for PFAS removal. The next chapter discusses a potential dopant which can enhance PFAS adsorption from aqueous solutions.

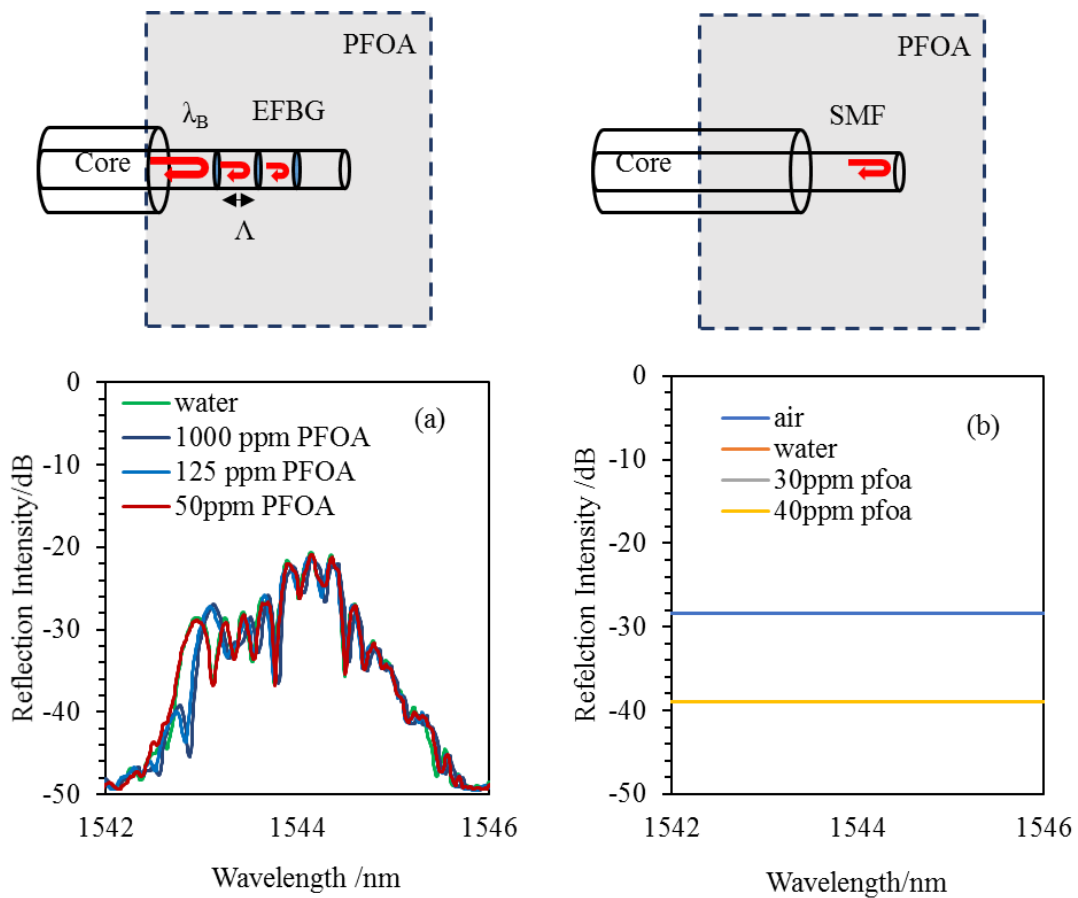
### **6.5 Comparison of the Optical PFAS Detection Techniques**

Table 6.1 summarizes the advantages and disadvantages of the different techniques that were used to detect PFOA in this research. The methods employed by the EFBG and the cleaved bare fibre end-face in detecting PFOA concentration involved measuring change in refractive index of the surrounding medium and producing a response to that. In case of the etched FBG a wavelength shift was observed in addition to changes in reflected intensity levels and in the bare fibre only a change in the reflected intensity level was seen in response to refractive index change. Figure 6.12 below depicts this phenomenon.

**Table 6.1 Comparison of PFOA sensing techniques utilizing OFS.**

Sensing Techniques/Sensors	Advantage	Disadvantage
Optical fibre refractive index sensor: <ul style="list-style-type: none"> <li>▪ Etched FBG (EFBG)</li> <li>▪ Bare Fibre</li> </ul>	<ul style="list-style-type: none"> <li>▪ Portable</li> <li>▪ Convenient</li> <li>▪ Economic</li> <li>▪ Offers remote sensing and real time continuous monitoring options</li> <li>▪ Light weight</li> </ul>	<ul style="list-style-type: none"> <li>▪ Lacks specificity</li> <li>▪ Low sensitivity (~0.002nm/ppm-EFBG)</li> <li>▪ Not robust</li> </ul>
PVDF coated FPI based OFS	<ul style="list-style-type: none"> <li>▪ Portable</li> <li>▪ Convenient</li> <li>▪ Economic</li> <li>▪ Offers remote sensing and real time continuous monitoring options</li> <li>▪ Versatile sensing capability</li> <li>▪ Robust</li> <li>▪ Easily optimized</li> <li>▪ Light weight</li> </ul>	<ul style="list-style-type: none"> <li>▪ Susceptible to temperature variation and denatures beyond 160° C.</li> <li>▪ Stabilizes slowly in aqueous solution (~2-3 hours initially in water and once stabilized 10-15 minutes in PFAs solution considering temperature influence)</li> <li>▪ Functionalization procedures are time consuming (~ 3-5 hours)</li> </ul>

Both of these methods are good at indicating a change in PFOA concentration levels when the tests are carried out in a controlled laboratory setting but inherently, they are non-selective and cannot differentiate between any chemical when measuring a change in refractive index. Thus, these techniques are not suitable for use in the natural environment but for this research they were extremely convenient alternative methods to prove that PVDF absorbs PFOA in aqueous solution.



**Figure 6.12 Comparison of PFOA sensing technique of (a) EFBG and (b) bare optical fibre showing fundamental differences in working principle. While an EFBG indicate changes in intensity level as well as wavelength shift a SMF only indicates a change in intensity level in response to a change in the measurand.**

The analyte's concentration reduces in the solution and causes a change in refractive index and associated reflected intensity or Bragg wavelength when a piece of PVDF membrane is soaked in a sample of known concentration of PFOA. This is evident from the figures shown above and the detailed discussion presented earlier in this chapter.

The PVDF coated fibre demonstrating FPI, which was examined in this work (Chapter 5) is also sensitive to refractive index change in its surrounding as it operates on a similar principle to thin film interference. When the coated fibre transitions from air to water or vice versa a change in the power level of the reflection spectrum indicates the differences

in the refractive index of the media. While the intensity of the reflected light from the PVDF coating is affected by the refractive index of the surrounding medium the shift in the spectrum is affected by the change in refractive index of the polymer and its physical thickness due to the change in the surrounding environment.

The difference in the sensing technique of the PVDF coated fibre with the EFBG and the bare optical fibre is that its performance is not directly dependent on the refractive index of the environment but the refractive index of the PVDF coating and its physical thickness. A combination of change in the refractive index and thickness of the film brings about a change in the optical path difference and a phase shift in the resulting FPI spectrum with PFOA concentration change as discussed in Chapter 5.

## **6.6 Chapter Summary**

This chapter has discussed alternative methods implemented in the research to confirm that PVDF absorbs PFOA. It presented results of refractive index measurements obtained by monitoring either the reflected signal from a cleaved optical fibre end-face or the wavelength shift of EFBGs. In both occasions it was observed that PVDF absorbs PFOA. In addition to this it reported an independent analytical laboratory test, which further validated the findings from the refractrometry based tests with the bare fibre and EFBG. This chapter also provided an account of the similarities and variances between the three different optical methods of PFOA detection used in this research and highlighted the advantage of a PVDF coated optical fibre in PFAS sensing. Subsequently, it created the scope to investigate functionalized coatings for enhanced and selective detection or absorption of PFAS.

## 7 Zeolite Doped Functionalized PVDF in PFAS Sensing

---

### 7.1 Overview

The performance analysis of a PVDF coated fibre for PFOA detection through demonstration of spectral shift and OPD change was done in the previous chapters. This chapter follows on to discuss the performance of zeolite incorporated PVDF coating for PFOA detection in aqueous solution. Functionalization has been reported to impact selectivity and also absorption. Therefore, investigations were carried out by doping the PVDF coating with zeolite nanoparticles to see if there is any change in the coated fibre's performance. The method of embedding zeolite particles in the PVDF thin film and subsequent experiments undertaken for assessing PFOA detection is presented here. Comparison of the zeolite doped and non-doped PVDF coatings are made using FTIR analysis to show differences between the synthesized coatings. In addition, SEM images of the zeolite embedded PVDF film surface before and after soaking in PFOA solution are presented in this chapter along with EDX spectra and detailed discussions on the findings.

### 7.2 Background on Zeolite Functionalized Membranes

Zeolites are naturally occurring aluminosilicates, where  $\text{AlO}_4$  and  $\text{SiO}_4$  form a tetrahedral framework by sharing the oxygen that give it an appearance of interconnected cages and channels [226]. They are commercially used as adsorbents in water purification to remove heavy metals and dissolved organics [227, 228]. Since zeolites allow incorporation of new functional groups (cations) in their structure, which help in altering their selectivity, they are also useful in applications involving anion uptake from effluents

[228]. There are reports of functionalized zeolite doped PVDF membranes for water treatment, which have high permeability and good fouling resistance that can be formed via the phase inversion process [229]. As Zeolite doped PVDF membrane samples show significant presence of the elements carbon, fluorine, silicon, oxygen and aluminium [134] in an EDX spectrum, the functionalized coating/membrane samples exposed to PFOA solution often need alternative tests such as HPLC-MS to verify the amount of absorbance.

In this chapter, zeolite doped PVDF membrane formation technique using immersion precipitation is discussed. The morphology and composition of samples characterized using SEM, FTIR and EDX have been reported here in comparison with a pristine or non-doped PVDF membrane. In addition, outcome of the coated fibre's characterization and stabilization experiments, undertaken following the same protocol discussed in Chapter 5, are presented, which reflect upon its ability to become a PFAS sensor.

### **7.3 Materials and Methods**

The first stage in the formation of zeolite doped PVDF membrane/coating involved preparation of the polymer solution with zeolite nanoparticles. The PVDF grade Solef 1015 was used in the process along with the solvent DMF and the zeolite powder was obtained from Govindan, et al. [230]. Approximately 1.67 g of PVDF was dissolved in 14 mL DMF under continuous stirring and heating at 80 °C, after which around 0.1 g of powdered zeolite was dispersed in the polymer solution using an ultrasonic bath for one hour. After a homogenous mixture was obtained, freshly cleaved and cleaned optical fibre end-faces were coated using the immersion precipitation technique discussed in Chapter 4. Additional samples were prepared by casting a thin film of the zeolite doped

polymer solution on a glass slide for FTIR analysis, SEM imaging and SEM/EDX elemental analysis. Fabry-Perot interference from the coated fibres was identified using the same method described in Chapter 5 and data analysis was performed using the software MATLAB and Excel.

A Perkin-Elmer Frontier FTIR spectrometer was used for characterization of the PVDF film and identifying the phase composition. The spectrum of the dry sample was collected before it was soaked in the 100 ppm (100 mg/L) PFOA solution. After soaking and allowing the PVDF to dry, the spectra of the sample were acquired and the results were compared.

Clean PVDF samples and some exposed to the PFOA solution (100 ppm) were air dried for 24 h, before small sections  $3 \times 3$  mm were cut and mounted on aluminium stubs with double-sided conductive carbon tape for SEM studies. The samples were then coated with iridium using a Cressington 208HR sputter coater and imaged using a Hitachi TM3030 Plus Tabletop SEM using the same settings as discussed in Chapter 4 and 5.

In EDX, to initiate the emission of X-rays from a specimen, a high-energy beam of charged particles such as electrons or protons, or a beam of X-rays, is focused into the sample being studied. The incident beam excites an electron in an inner shell (in ground state), ejects it from there and creates a hole where the electron was. An electron from an outer, higher-energy shell then fills the hole, and the difference in energy between the higher-energy shell and the lower energy shell is released in the form of an X-ray. The number and energy of the X-rays emitted from the specimen is measured by an energy-dispersive spectrometer. As the energies of the X-rays are characteristic of the difference

in energy between the two shells and of the atomic structure of the emitting element, EDX allows the elemental composition of the specimen to be measured [231].

A scanning electron microscope (SEM) produces images of a sample by scanning the surface with a focused beam of electrons in a raster scan pattern [232]. The position of the beam is combined with the intensity of the detected signal (consisting of both secondary and back scattered electrons) to produce an image. In the most common SEM mode, secondary electrons are detected using an Everhart-Thornley detector [232].

## **7.4 Results and Discussion**

### **7.4.1 FTIR Spectra of Zeolite Doped PVDF Thin Films**

The FTIR spectra of the zeolite doped PVDF membrane and a non-doped PVDF membrane are shown in Figure 7.1. The presence of a spectral shift and peak broadening between 850-750  $\text{cm}^{-1}$  and 1278-950  $\text{cm}^{-1}$  shows the difference between the two membrane structures. The FTIR spectra of a non-doped PVDF membrane and a zeolite doped membrane soaked in PFOA are shown in Figure 7.2 and Figure 7.3 respectively. It is interesting to note that direct comparison of these spectra with those of the dry samples do not show significant differences. As the structures of PVDF and PFOA are very similar (see Figure 1.2), and since 100 ppm PFOA has no outstanding signature in aqueous solution, adsorption of the analyte on the membrane surface could not be distinguished clearly through FTIR analysis. The results of this analysis therefore did not confirm whether the zeolite doped coating was better at absorbing PFOA compared to the non-doped coating. As a result, further analysis involving a different technique was used to test this hypothesis.

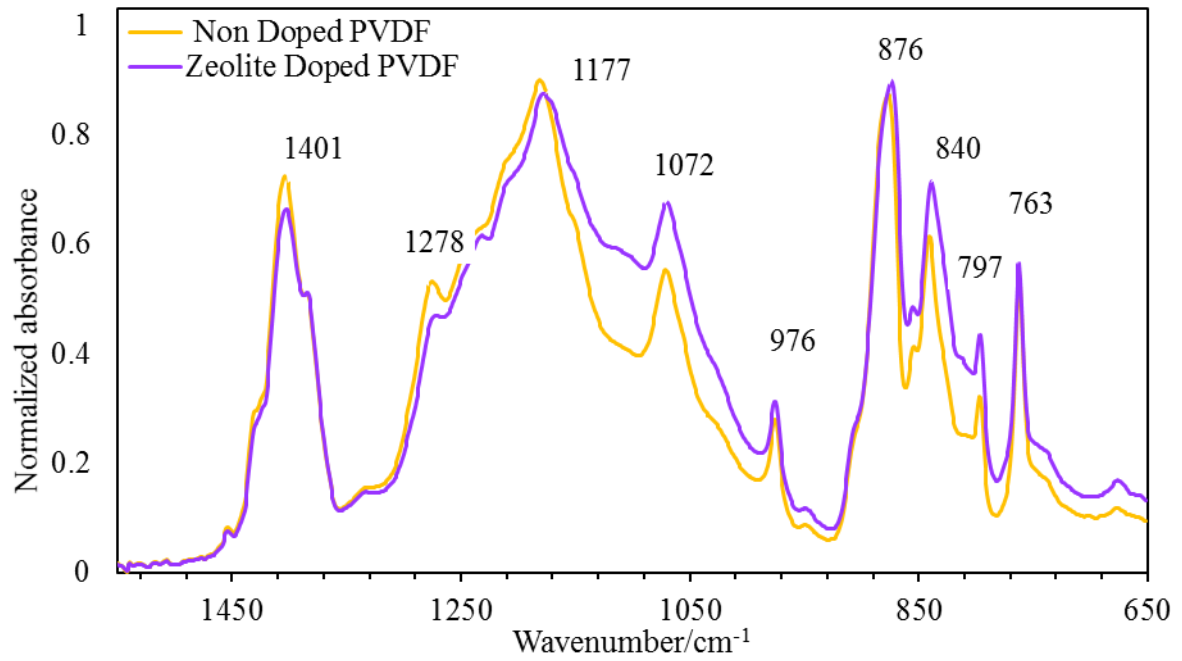


Figure 7.1 FTIR spectra of Zeolite doped PVDF coating and a non-doped PVDF coating.

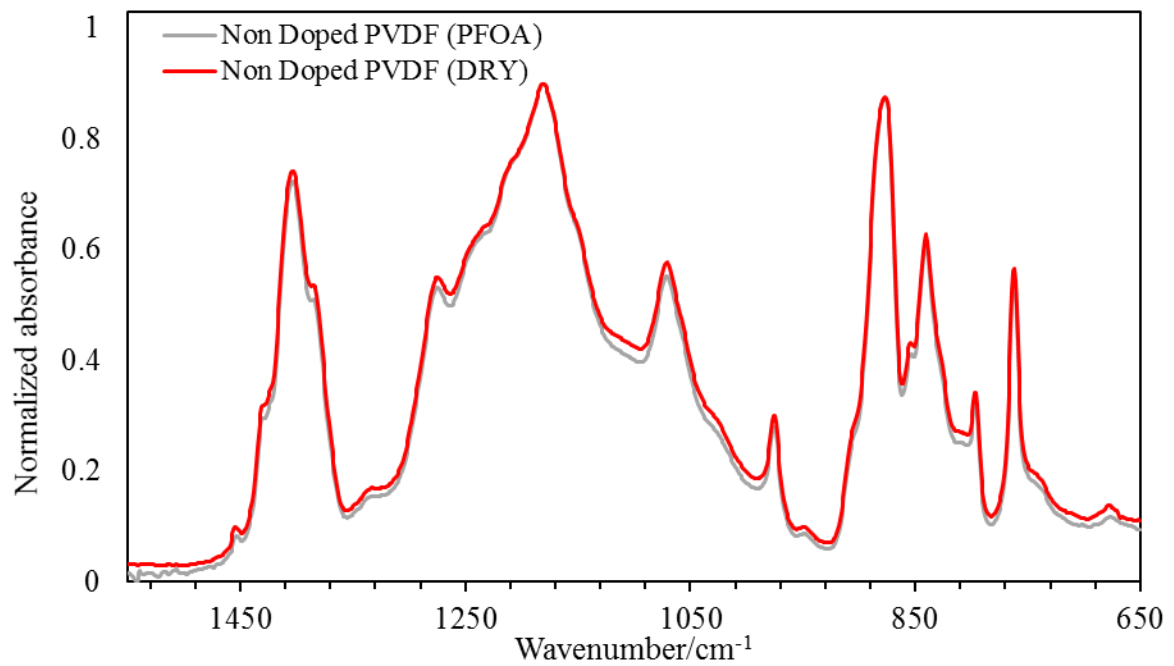


Figure 7.2 FTIR spectra of non-doped dry and PFOA soaked PVDF membranes.

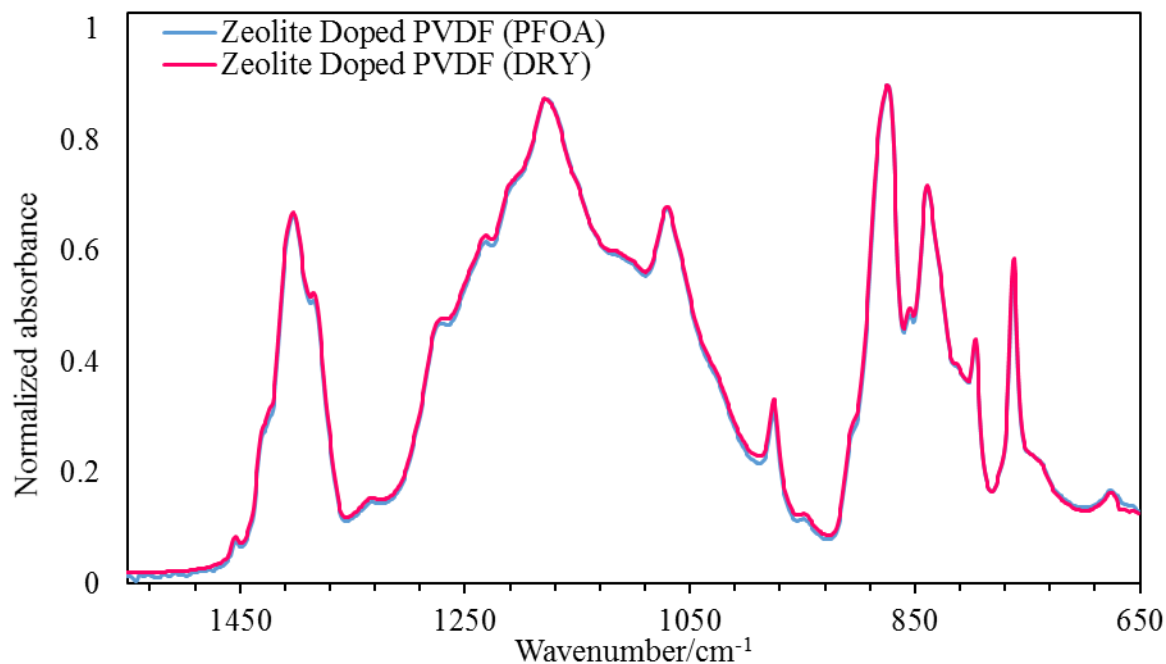


Figure 7.3 FTIR spectra of zeolite doped dry and PFOA soaked membrane.

#### 7.4.2 PFOA Adsorption by Zeolite Doped PVDF Thin Film

Confirmation of increased PFOA absorbance with presence of zeolite in the PVDF membrane prepared using Solef 1015 was obtained from an analytical laboratory test performed by an external lab. A sample of 1 mg/L PFOA solution was prepared by diluting the 100 ppm PFOA solution in which a piece of zeolite doped PVDF film was soaked. Samples of the PFOA solution before and after soaking in the zeolite doped PVDF membrane, i.e. the stock and soak water, were sent to ALS Water (Scoresby Victoria), where they were subjected to quantitative analysis in accordance with NATA accredited ALS Method EP231X. The concentration of PFOA in the stock solution was seen to be 94%, whereas that in which the zeolite doped PVDF membrane was soaked was found to be 83% indicating a 12% absorbance by the zeolite doped PVDF coating. Compared to a non-doped membrane which was subjected to the same test this absorbance value is 2% higher. Thus, it was observed that the functionalized PVDF

membrane has slightly better absorbance than the pristine or non-functionalized membrane. It has also been assumed that the amount of absorbance is subjected to the available surface area on the membrane. The following table shows the amount of PFOA adsorbed per unit area of the thin films that were used in the experiment. The description of the sample indicates the solutions tested. Sample #1 is the 1 mg/L PFOA stock solution prepared by diluting an original solution of concentration 100 mg/L. Sample #2 Solef, indicates the thin film and soak water solution tested. The result showed the concentration of the diluted solution in which the thin film prepared from Solef was soaked. Similarly, sample #3 Solef+zeolite, indicates the doped PVDF thin film formed from Solef and zeolite and the corresponding soak water sample tested. The ALS test result for this sample gives the concentration of PFOA in the diluted soak water sample. For both samples #2 and #3 the height and width for the respective rectangular pieces of thin films, which were submerged in known volumes of the stock solution (i.e. 16.2 and 17.1 mL respectively), were measured for determining the surface area exposed to PFOA. These values were then used to calculate the absorbance per unit area as shown in the table.

**Table 7.1 Perfluorooctanoic acid adsorption on rectangular PVDF thin film pieces.**

Sample	Description	ALS result (mg/L)	Undiluted (mg/L)	Adsorbed (mg/L)	Mass Adsorbed mg	Mass per unit area mg/m <sup>2</sup>
1	PFOA stock diluted (~1 mg/L)	0.94	94	-	-	-
2	Solef	0.85	85	9	0.1458	0.020
3	Solef+zeolite	0.83	83	11	0.1881	0.031

The amount of PFOA adsorbed on the surface of the thin film is the difference between the stock and the test solution. For sample #2 and #3 these values were obtained by subtracting the undiluted values of the test solutions from that of the stock solution. The total surface area of each of the rectangular pieces of thin films used, were calculated by adding the surface areas of both the exposed sides. Individual area calculation was done by multiplying the height and width of the thin films. The mass of PFOA adsorbed was obtained from the product of undiluted solution volume and the undiluted absorbance value. The amount of PFOA adsorbed per unit area was obtained by dividing the mass of PFOA adsorbed by the total surface area of the thin film.

The SEM images of the non-doped and zeolite doped PVDF thin films and their EDX spectra are shown in Figure 7.4 to Figure 7.10. The non-doped thin film images and the corresponding EDX data are illustrated from Figure 7.4 to Figure 7.7, while the zeolite doped coating and its SEM images are shown through Figure 7.8 to Figure 7.10.

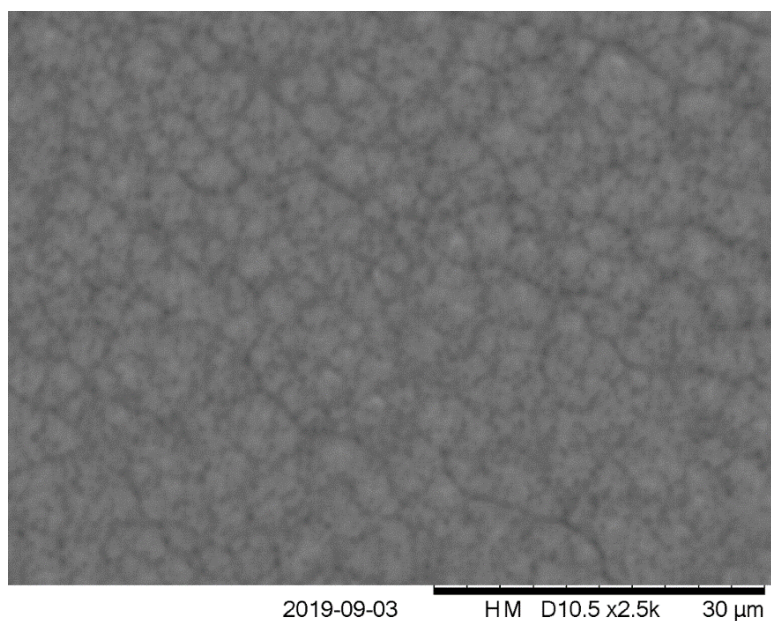


**Figure 7.4 SEM image of dry PVDF thin film surface formed from Solef 1015), Butvar and DMF at a magnification of  $\times 2500$ .**

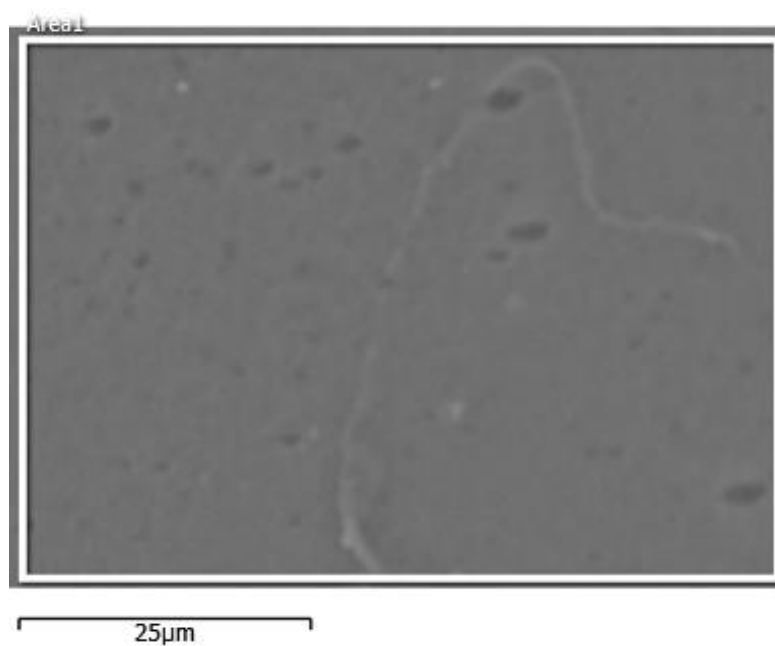


**Figure 7.5 SEM image and EDX data of selected area on a dry PVDF thin film.**

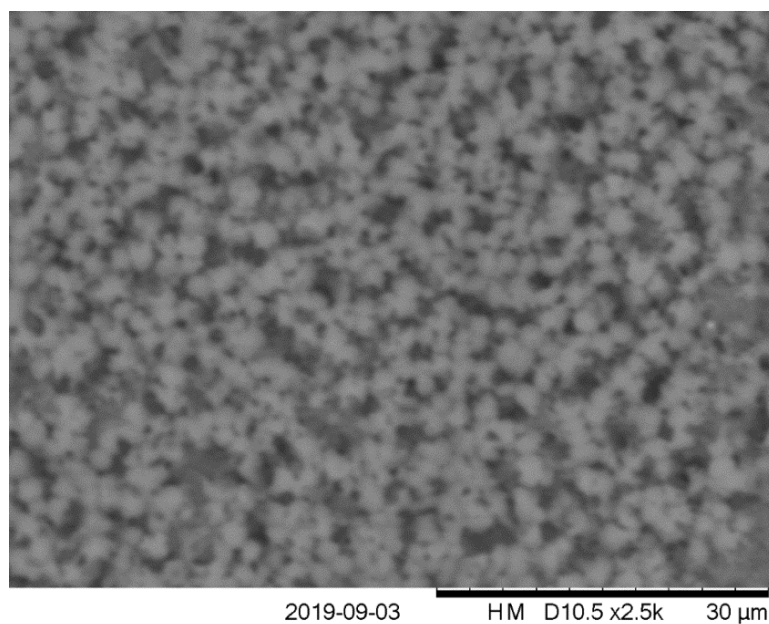


Figure 7.6 SEM image of the surface of a PVDF thin film after it was soaked in PFOA solution.

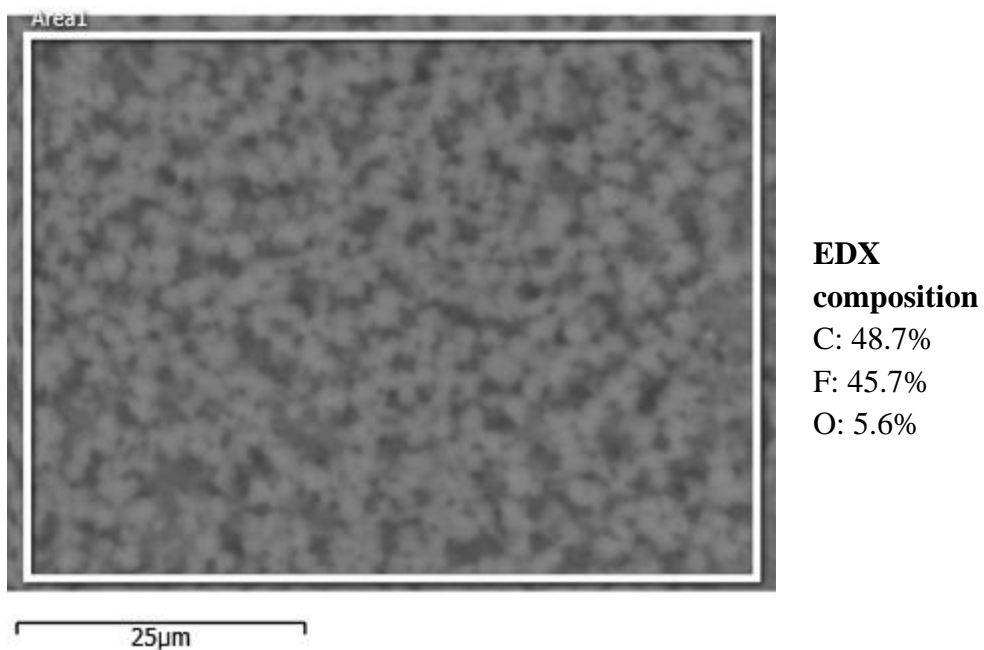


Figure 7.7 SEM image and EDX data of selected surface area on a PVDF thin film exposed to PFOA.

It can be observed from the images shown above that there are differences in the surface morphologies of the PVDF thin films, which have not been exposed to PFOA (dry samples) and those which have been exposed to PFOA solutions. Figure 7.4 displays the texture of the surface of a dry sample of PVDF thin film formed from the polymer grade Solef 1015 from Solvay, the solvent dimethylformamide (DMF) and the cross linker Butvar. On the other hand, Figure 7.6 displays the surface texture of the same (non-doped) thin film sample, which has been soaked in PFOA solution. Some nodule like structures can be seen on the latter image, which suggests that the change might be due to the presence of clusters of PFOA attached to the surface of the thin film. This is likely as the ALS test report confirm adsorption of PFOA onto PVDF membranes. While EDX cannot distinguish between PVDF and PFOA, it shows that both films (i.e. the dry one and the one subjected to PFOA) are comprised mainly of C, F, and O (Figure 7.5 and Figure 7.7). Similarly, the SEM images (Figure 7.8 and Figure 7.9) and EDX data (Figure 7.10) of the zeolite doped PVDF membranes formed from the same polymer grade and solvent as mentioned above show clear differences, as illustrated below. The composition of the zeolite doped PVDF thin film shows the presence of the Si and Al in addition to C, F and O in the EDX spectrum. Besides showing the elemental composition, Figure 7.10, also shows their even distribution throughout the membrane surface. In case of Si, a slight agglomeration or clustering is observed near the lower edge. However, no significant change in the texture of the membrane was observed due to this uneven distribution of Si in Figure 7.9 that has been used for mapping. It was further seen that the zeolite incorporated PVDF coating on an optical fibre end-face responds differently compared to a non-doped coating as outlined in the next section.

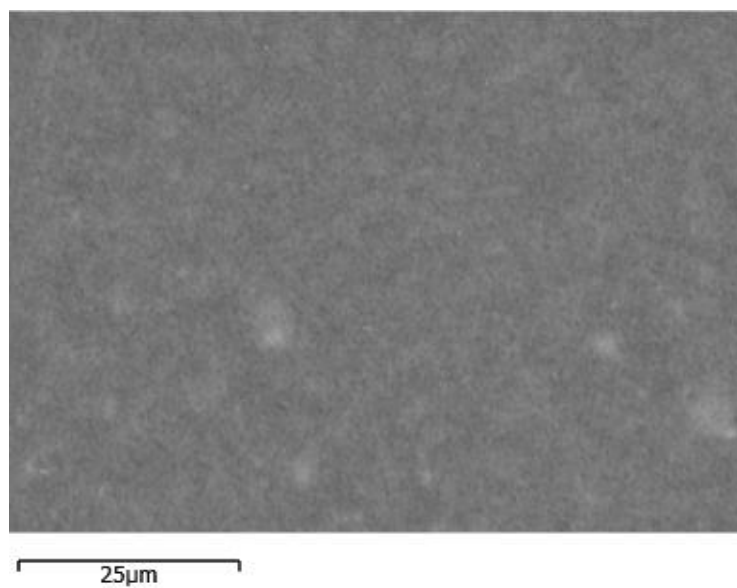


Figure 7.8 SEM image of zeolite doped PVDF thin film surface texture in dry state.

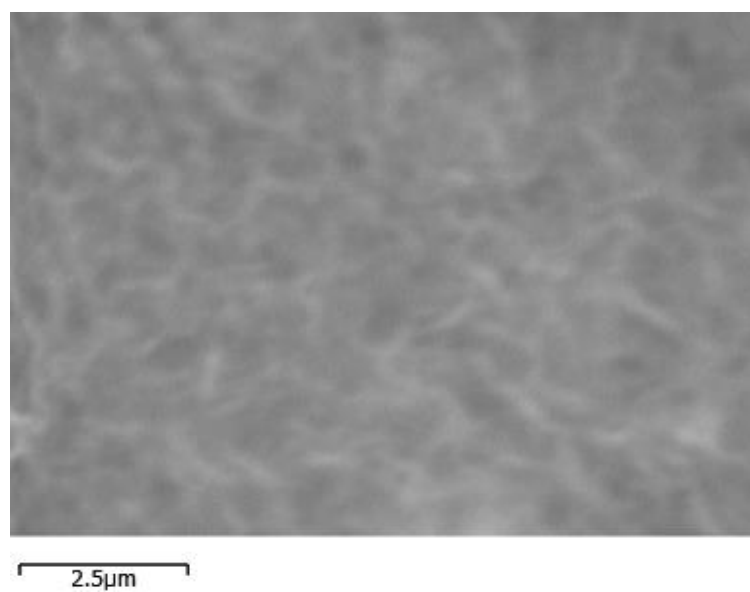
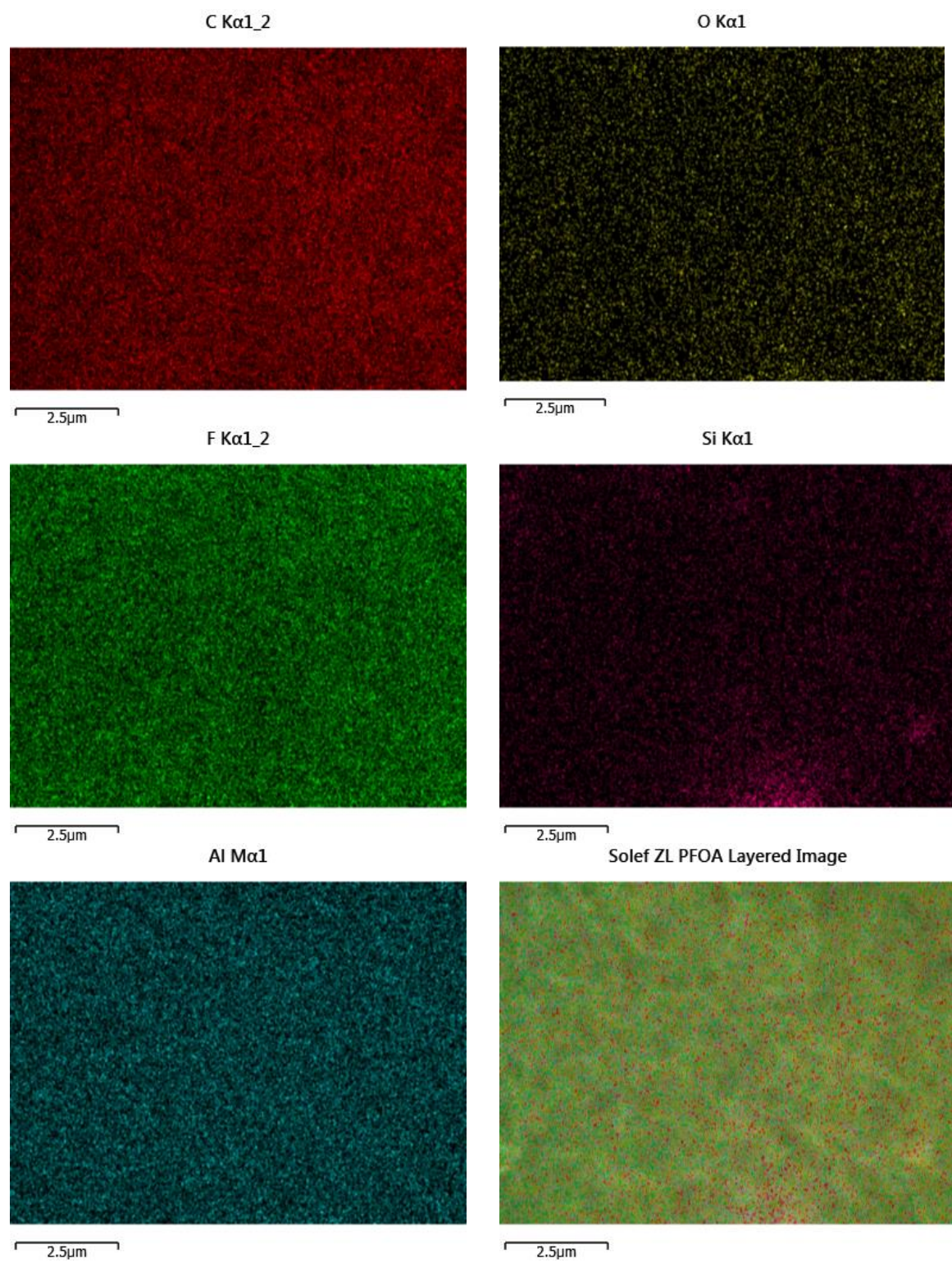


Figure 7.9 SEM and EDX data of zeolite doped PVDF thin film exposed to PFOA.



**Figure 7.10** EDX spectra showing composition of zeolite doped PVDF thin film exposed to PFOA.

### **7.4.3 Response of Optical Fibre with Zeolite Doped Coating to PFOA**

The reflection spectra of a zeolite doped PVDF coated optical fibre submerged in water for nine hours at constant temperature is shown in Figure 7.11. In this case, the spectrum was observed to evolve overtime without stabilizing. It is suggested that the zeolite causes the coating to become more hydrophilic and increases its water uptake over time. When the coating on the end-face swells, the OPD increases and causes a shift in the peak wavelength position in the spectra. The SEM image of a zeolite doped PVDF coating on an optical fibre end-face in its dry state is shown in Figure 7.12.

Optimization of the coating is necessary for a thorough investigation of its response to PFOA/ PFAS and as this task requires determination of the appropriate dopant content in the thin film through trial and error it has been deemed more suitable for a future work.

Therefore, this research only reports the success of a functionalized PVDF thin film in absorbing more PFOA compared to a non-functionalized coating based on an analytical test and forms the basis of future investigations. Moreover, this may offer new insights into the development of functionalized adsorbents for PFAS using both PVDF and zeolites.

## **7.5 Chapter Summary**

This chapter has presented results of the analysis of zeolite-doped PVDF in order to highlight the variation in the composition of non-doped PVDF and zeolite doped PVDF thin films. Analytical data from an external lab has demonstrated the ability of the doped membrane to absorb more PFOA than a non-doped membrane. In addition to this, it has briefly discussed the adverse effect of the dopant on the stability of the FPI reflection

spectra that impeded further studies in PFOA sensing with the proposed zeolite doped PVDF coated fibre while creating opportunity for more future work in this area.

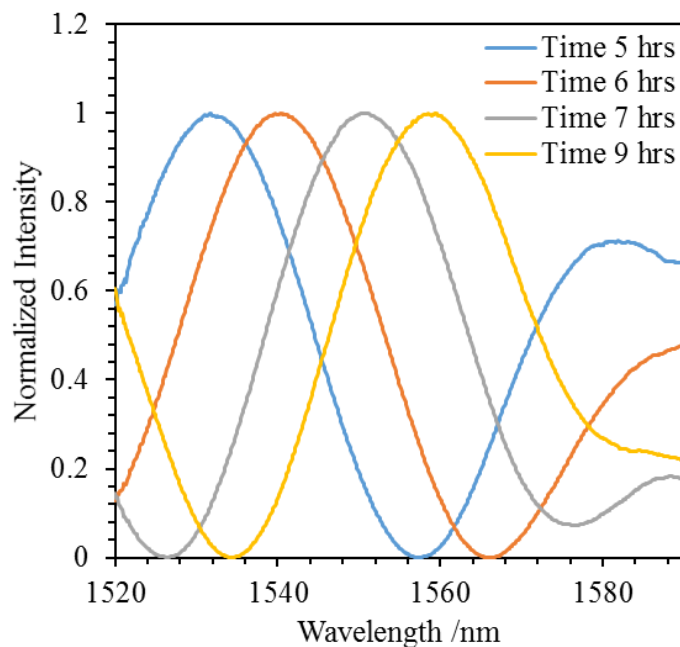


Figure 7.11 Zeolite doped PVDF coating on optical fibre end-face showing spectral response in water during stabilization phase.

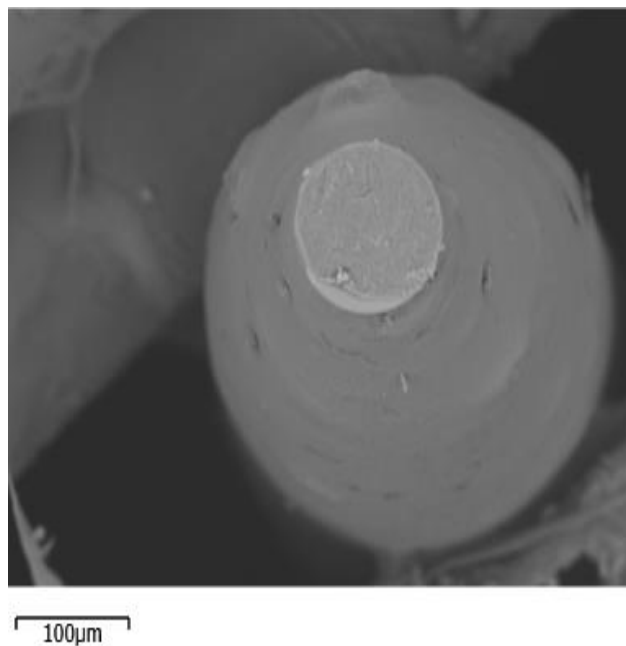


Figure 7.12 Optical fibre end-face with zeolite incorporated PVDF coating, in dry state.

## 8 Conclusions and Recommendations

---

### 8.1 Thesis Summary

This chapter concludes the thesis by summarizing the current context of PFOA detection and the findings from all the chapters. It also discusses further scope of research.

In the literature review chapter, it was established that PFOA is a toxic perfluoroalkyl compound, whose increasing presence in the natural environment in Australia and other countries is being perceived as a threat to well-being. The reported conventional analytical methods such as LC-MS and GC-MS are expensive but currently are the only reliable laboratory-based techniques used for PFAS analysis. Existing methods that address challenges with portability face specificity issues and limitations due to cross contamination and sensitivity to various environmental factors, including temperature. Therefore, researchers are exploring alternative technologies to quantify the chemical concentration precisely in its natural environment to make the process of identification and elimination of PFAS more effective.

A strong contender for *in situ* PFAS sensing comes in the form of optical fibre sensor (OFS) technology, which has attracted considerable interest in recent decades due to many advantages over traditional electrical sensors. Optical fibre sensors are known for their small size, immunity to electromagnetic interference, passiveness and intrinsic safety, high sensitivity and bandwidth, multiplexing capability, chemical inertness, and robustness to hostile environments. These advantages along with the declining cost of production and availability of better signal detection and interrogation systems, are increasingly making the optical fibre sensors commercially successful. Additionally,

sensors based on optical fibres are suitable for remote sensing operations and are compatible with online continuous monitoring applications. As the technology is portable, it can be easily configured to provide real time information on any physical, chemical or biological measurand in a field test. More importantly, chemical sensing functionality of OFS can be further enhanced by coating chemically selective optical materials at the end-face of optical fibres.

Using this strategy, a PVDF coated optical fibre that operates on the principle of Fabry-Perot interferometry was designed in this work to determine PFOA concentration in aqueous solution. This research demonstrated, for the first time, that PVDF absorbs PFAS and presented experimental evidence that supports *in situ* measurement of PFAS with a PVDF coated optical fibre by demonstrating changes in Fabry-Perot interference pattern. It further discussed alternative optical techniques based on refractive index measurement with etched FBG and bare optical fibre to provide additional evidence of PFOA adsorption onto PVDF.

Besides the above, this work has contributed new knowledge that infers that PVDF can be used as a sensing material as well as an adsorbent for filtering PFAS in aqueous solutions. Its selectivity and PFAS absorption capability can be further enhanced through incorporation of zeolite nanoparticles.

## **8.2 General Conclusions**

The PVDF coated optical fibre that was developed using the immersion precipitation technique in this project combined the advantages of PVDF with those of the optical fibre to form a very sensitive optical PFAS detector. The dip coating technique employed in fabricating the detector in this research was shown to be the simplest method currently

available to form a potential sensor and the experimental set up used was demonstrated to be both portable and appropriate for remote sensing and continuous real time monitoring operations.

Through this research, PVDF coated fibres were also shown to be potential temperature sensors with good linearity over a specified range. Based on experimental results it was demonstrated that the sensitivity of such a sensor might vary between 1.6 and 7.5 nm/°C between 21 °C and 160 °C. Although it was an important finding in general it also was a cause of concern for reliable PFOA detection. Consequently, a temperature compensated protocol for PFOA sensing was developed, where the steps involved stabilization of the coated fibre in water at a fixed temperature inside an incubator and acquisition of all spectral response under constant temperature conditions. This helped minimize error and maximize accuracy of the outcome of the tests besides addressing a gap in literature.

The data analysis technique that was applied to the interferograms in this work, following the acquisition of the spectra, was a convenient and straightforward process. It used mathematical modelling and curve fitting to determine changes in optical path difference as a measure of PFOA sensitivity. Performance analysis of the PVDF coated fibre which was dependent on this OPD analysis involved determination of a trend through plotting changes in OPD vs PFOA concentration. Results generated by the method of curve fitting using Excel and Table Curve, to determine the OPD values, were further analysed and validated with the help of microscopic images to determine their accuracy/reliability. The SEM image of a cross section of a cleaved PVDF coated fibre confirmed that the OPD values obtained through numerical modelling were all within an acceptable range.

As it was observed that the coated fibre is capable of responding to PFAS wash water having concentration in the ppb range, its actual limit of detection was assumed to be in the  $\mu\text{g/L}$  range, for certain perfluoroalkyl compounds other than PFOA. The difference in the sensitivity levels has been assumed to be caused by that the lack of available binding sites and structural variations of the thin film. However, as further investigation of the thin film morphology was out of scope for the undertaken project, the aforementioned hypothesis was not tested in this work. Thus, examining the required molecular interactions and chemical processes of PVDF and PFOA/PFAS has been considered a highly suitable future work for understanding sensor operation and optimization.

In addition to establishing the fact that a non-doped or pure PVDF thin film on an optical fibre end-face can detect PFOA present in saline and freshwater environment, the research also investigated the performance of a zeolite doped PVDF coated fibre. Analytical tests provided evidence on increased absorption of PFOA in zeolite doped membranes that creates prospect for numerous other research both in sensor development and water treatment.

Thus, to put in perspective which goals have been achieved the following list is provided in line with the aims and objectives mentioned in Chapter 1:

- Successful demonstration of the PVDF coated fibre as a potential sensing scheme to address *in situ* measurement of PFOA in aqueous solutions:
- Extremely thorough evaluation of current literature in the field and determination of new techniques to advance the field.

- Presentation of proof that PVDF absorbs PFOA in aqueous solution through standardized tests and demonstration of the robustness for establishing PVDF as a potential and effective sensor material.
- Creation of a simple coating fabrication technique to develop a PVDF thin-film on an optical fibre end-face such that it would demonstrate Fabry-Perot interference.
- Demonstration of a comprehensive sensor characterization protocol that provides proof of concept, while considering effect of cross-sensitivity to temperature and other environmental conditions.
- Use of a numerical modelling and graphical analysis technique to address some of the complexities of existing data interpretation process.
- Publication of results of the work done in the international literature, to inform the community of the successes of the research.

While the thesis has contributed many noteworthy findings and has reported several ways to overcome challenges in PFAS detection, it has also created numerous opportunities to further enhance the performance of the envisioned OFS. It ranges from optimising the procedure to carry out sensor cleansing operation and restoration, to addressing reusability and repeatability of measurements. Investigation of material properties and chemical reactions to design a recovery procedure and other such possible future works are suggested in the next section to provide a possible direction for the next stage of research that can build upon the findings of this work.

### 8.3 Recommendations for Future Work

New ideas or scope for enhancing performance of a potential OFS for instantaneous measurement of PFAS in aqueous samples can be explored based on the reported observations of the undertaken research. As such, some fundamental aspects of sensor development related to linearity, response time, reusability, accuracy of measurement, range of operation etc. can be examined. Thus, future work can involve:

- Designing methods to ensure reusability of the sensor and good repeatability: One of the ways to address this can be by developing a dry-cleaning technique that can help restore the binding sites. Cleansing with alcohol was found to be very harsh on the polymer and detrimental to sensitivity. Thus, instead of a wet cleaning procedure a photochemical cleaning technique can be potentially investigated for ensuring reusability without causing a loss of functionality.
- Carrying out molecular modelling to showcase interaction of the polymer and the specific analyte: A procedure that can help determine how functionalized and non-functionalized PVDF thin films react with PFOA/PFAS can help develop systems with better designs and higher sensitivity. Therefore, computational model using appropriate software can be built and examined for this purpose.
- Automating PVDF coating based sensor fabrication and thin film optimization process for higher accuracy: This work can accelerate the coating process and help control a multitude of parameters in thin film structure development and design to make the data analysis process easier. Different combination of hardware and software control can be investigated here to make the sensor fabrication process more efficient.

- Developing selective sensors for specific PFAS detection: Some surfactants like PFOS and PFOA are more harmful than others. Therefore, to be able to detect their individual concentration accurately without cross sensitivity to any other chemicals would be crucial for designing a highly sensitive and reliable OFS. Different dopants including nanoparticles can be explored in this regard apart from suitable polymer composites.
- Miniaturization and possible development of lab on a chip: To make a field sensor portable and easy to use it is necessary to make it compact and compatible with existing technology. Thus, options which look into possible IC formation can be explored.

All these propositions can be pursued further for developing a commercial PVDF based OFS for conducting field tests of perfluoroalkyl substances, the foundations for which was laid by the undertaken research discussed in this thesis.

## REFERENCES

- [1] J. Gardiner, "Fluoropolymers: Origin, production, and industrial and commercial applications," *Australian Journal of Chemistry*, vol. 68, no. 1, pp. 13-22, 2015.
- [2] Markets and Markets. (2019, 23.10.2019). *High Performance Fluoropolymer Market by Type (PTFE, FEP, PFA/MFA, ETFE), Form (Coating, Film & Membranes, Tubing) End-Use Industry (Industrial Processing, Transportation, Electrical & Electronics, Medical), and Region (North America, APAC, Europe) - Global Forecast to 2024*. Available: <https://www.marketsandmarkets.com/Market-Reports/fluor-polymer-market-497.html>
- [3] J. G. Drobny, "Fluoropolymers in automotive applications," *Polymers for Advanced Technologies*, vol. 18, no. 2, pp. 117-121, 2007.
- [4] A. Facchetti and T. Marks, *Transparent electronics: From synthesis to applications*. John Wiley & Sons, 2010.
- [5] M. Uno, Y. Tominari, and J. Takeya, "Fabrication of high-mobility organic single-crystal field-effect transistors with amorphous fluoropolymer gate insulators," *Organic Electronics*, vol. 9, no. 5, pp. 753-756, 2008.
- [6] H. Teng, "Overview of the development of the fluoropolymer industry," *Applied Sciences*, vol. 2, no. 2, pp. 496-512, 2012.
- [7] S. Ebnesajjad and P. R. Khaladkar, *Fluoropolymer applications in the chemical processing industries: The definitive user's guide and handbook*. William Andrew, 2017.
- [8] J. R. Fleming, D. Kemkes, R. G. Chatten, L. Creshaw, and J. Lmbalzano, "Material of construction for pharmaceutical and biotechnology processing: moving into the 21st century," *Pharmaceutical Engineering*, pp. 1-6, 2001.
- [9] B. J. Place and J. A. Field, "Identification of novel fluorochemicals in aqueous film-forming foams used by the US military," *Environmental Science & Technology*, vol. 46, no. 13, pp. 7120-7127, 2012.
- [10] Australian Health Protection Principal Committee. (2016). *Per- and poly-fluoroalkyl substances (PFAS) FactSheet* Available: [https://www.health.gov.au/internet/main/publishing.nsf/Content/A12B57E41EC9F326CA257BF0001F9E7D/\\$File/PFAS-factsheet-15June2016.pdf](https://www.health.gov.au/internet/main/publishing.nsf/Content/A12B57E41EC9F326CA257BF0001F9E7D/$File/PFAS-factsheet-15June2016.pdf)
- [11] S. Lerner, "The U.S. military is spending millions to replace toxic firefighting foam with toxic firefighting foam," in *The Intercept*, ed. online, 2018.

- [12] R. Turner, "Firefighting foam contamination: DFES confirms chemicals found in bore near training site," in *ABC News* vol. 2019, ed. Online, 2016.
- [13] R. Renner, "EPA finds record PFOS, PFOA levels in Alabama grazing fields," *Environmental Science and Technology*, vol. 43, no. 5, pp. 1245-1246, 2009.
- [14] C. F. Harvey *et al.*, "Groundwater arsenic contamination on the Ganges Delta: biogeochemistry, hydrology, human perturbations, and human suffering on a large scale," *Comptes Rendus Geoscience*, vol. 337, no. 1-2, pp. 285-296, 2005.
- [15] M. Kampa and E. Castanas, "Human health effects of air pollution," *Environmental Pollution*, vol. 151, no. 2, pp. 362-367, 2008.
- [16] E. Fabbri and S. Franzellitti, "Human pharmaceuticals in the marine environment: focus on exposure and biological effects in animal species," *Environmental Toxicology And Chemistry*, vol. 35, no. 4, pp. 799-812, 2016.
- [17] M. Guarnieri and J. R. Balmes, "Outdoor air pollution and asthma," *The Lancet*, vol. 383, no. 9928, pp. 1581-1592, 2014.
- [18] M. F. Naujokas *et al.*, "The broad scope of health effects from chronic arsenic exposure: update on a worldwide public health problem," *Environmental Health Perspectives*, vol. 121, no. 3, pp. 295-302, 2013.
- [19] K. Steenland, T. Fletcher, and D. A. Savitz, "Epidemiologic evidence on the health effects of perfluorooctanoic acid (PFOA)," *Environmental Health Perspectives*, vol. 118, no. 8, p. 1100, 2010.
- [20] J. C. De Witt, S. J. Blossom, and L. A. Schaider, "Exposure to per-fluoroalkyl and polyfluoroalkyl substances leads to immunotoxicity: epidemiological and toxicological evidence," *Journal of Exposure Science & Environmental Epidemiology*, p. 1, 2018.
- [21] J. Liang, X. Deng, and K. Tan, "An eosin Y-based "turn-on" fluorescent sensor for detection of perfluorooctane sulfonate," *Spectrochimica Acta Part A: Molecular and Biomolecular Spectroscopy*, vol. 150, pp. 772-777, 2015.
- [22] M. Maisonet *et al.*, "Maternal concentrations of polyfluoroalkyl compounds during pregnancy and fetal and postnatal growth in British girls," *Environmental Health Perspectives*, vol. 120, no. 10, pp. 1432-1437, 2012.
- [23] A. M. Vuong *et al.*, "Prenatal polybrominated diphenyl ether and perfluoroalkyl substance exposures and executive function in school-age children," *Environmental Research*, vol. 147, pp. 556-564, 2016.
- [24] Z. Liew *et al.*, "Attention deficit/hyperactivity disorder and childhood autism in association with prenatal exposure to perfluoroalkyl substances: a nested case-

- control study in the Danish National Birth Cohort," *Environmental Health Perspectives*, vol. 123, no. 4, pp. 367-373, 2014.
- [25] Agency for Toxic Substances and Disease Registry. (2016, 30.11.2017). *Per- and Polyfluoroalkyl Substances (PFAS) and Your Health*. Available: <https://www.atsdr.cdc.gov/pfas/>
- [26] W. Nicole, "PFOA and cancer in a highly exposed community: new findings from the C8 science panel," *Environmental Health Perspectives*, vol. 121, no. 11-12, p. A340, 2013.
- [27] C. Chang, "The places in Australia where you can't drink the water," in *News.com.au*, ed, 2016.
- [28] Z. Schlanger. (2019, 23.10.2019). *PFAS Costs Europe More than €50 Billion A Year in Health Problems*. Available: <https://qz.com/1575450/damaged-health-from-pfas-costs-europe-more-than-50-billion-euros-per-year/>
- [29] C. Chang, "Williamstown water contamination highlights dangers of PFOS and PFOA," in *News.com.au*, ed, 2016.
- [30] C. Fellner and P. Begley, "Toxic Secrets: Where the sites with PFAS contamination are near you," in *The Sydney Morning Herald*, ed, 2018.
- [31] D. Cuthbertson, "Is Fiskville the tip of an iceberg? PFAS detected across Victoria," in *The Age*, ed, 2018.
- [32] A. ABC Radio, "PFAS chemicals probe expanded around Adelaide's Edinburgh airbase," in *ABC News*, ed, 2018.
- [33] Australian Government Department of Health. (2016, 30.11.2017). *Health based guidance values for PFAS for use in site investigations in Australia*. Available: [https://www.health.gov.au/internet/main/publishing.nsf/Content/2200FE086D480353CA2580C900817CDC/\\$File/fs-Health-Based-Guidance-Values.pdf](https://www.health.gov.au/internet/main/publishing.nsf/Content/2200FE086D480353CA2580C900817CDC/$File/fs-Health-Based-Guidance-Values.pdf)
- [34] CRC Care. (2019, 12.03.2018). *PFAS practitioner guide*. Available: <https://www.crccare.com/knowledge-sharing/pfos-and-pfoa-guidelines>
- [35] J. L. Parker, "Lessons from the New York Waterfront: Addressing the risks of drinking water contamination from unregulated contaminants," *Environmental Claims Journal*, vol. 29, no. 3, pp. 242-252, 2017.
- [36] B. Baschuk, "UN Chemical Regulators Approve PFOA Ban, with Exemptions," in *Bloomberg Environment*, ed, 2019.
- [37] HEPA, DoEE. (2019). *PFAS National Environmental Management Plan*. Available: [https://www.epa.vic.gov.au/~/\\_/media/Files/Your%20environment/Land%20and%](https://www.epa.vic.gov.au/~/_/media/Files/Your%20environment/Land%20and%20)

[20groundwater/PFAS%20in%20Victoria/PFAS%20NEMP/FINAL\\_PFAS-NEMP-20180110.pdf](#)

- [38] R. Crawford, "Turnbull Government to fund \$13 million research program to tackle PFAS," in *South Coast Register*, ed, 2017.
- [39] C. A. Huset *et al.*, "Occurrence and mass flows of fluorochemicals in the Glatt Valley watershed, Switzerland," *Environmental Science & Technology*, vol. 42, no. 17, pp. 6369-6377, 2008.
- [40] K. Risha, J. Flaherty, R. Wille, W. Buck, F. Morandi, and T. Isemura, "Method for trace level analysis of C8, C9, C10, C11, and C13 perfluorocarbon carboxylic acids in water," *Analytical Chemistry*, vol. 77, no. 5, pp. 1503-1508, 2005.
- [41] W. M. Young, P. South, T. H. Begley, and G. O. Noonan, "Determination of Perfluorochemicals in Fish and Shellfish Using Liquid Chromatography–Tandem Mass Spectrometry," *Journal of Agricultural and Food Chemistry*, vol. 61, no. 46, pp. 11166-11172, 2013.
- [42] J. Gong, T. Fang, D. Peng, A. Li, and L. Zhang, "A highly sensitive photoelectrochemical detection of perfluorooctanic acid with molecularly imprinted polymer-functionalized nanoarchitected hybrid of AgI–BiOI composite," *Biosensors and Bioelectronics*, vol. 73, pp. 256-263, 2015.
- [43] S. Chu and R. J. Letcher, "Linear and branched perfluorooctane sulfonate isomers in technical product and environmental samples by in-port derivatization-gas chromatography-mass spectrometry," *Analytical Chemistry*, vol. 81, no. 11, pp. 4256-4262, 2009.
- [44] D. Benford *et al.*, "Opinion of the scientific panel on contaminants in the food chain on perfluorooctane sulfonate (PFOS), perfluorooctanoic acid (PFOA) and their salts," *EFSA Journal*, no. 653, pp. 1-131, 2008.
- [45] K. J. Hansen, H. Johnson, J. Eldridge, J. Butenhoff, and L. Dick, "Quantitative characterization of trace levels of PFOS and PFOA in the Tennessee River," *Environmental Science & Technology*, vol. 36, no. 8, pp. 1681-1685, 2002.
- [46] M. Takayose, K. Akamatsu, H. Nawafune, T. Murashima, and J. Matsui, "Colorimetric detection of perfluorooctanoic acid (PFOA) utilizing polystyrene-modified gold nanoparticles," *Analytical Letters*, vol. 45, no. 18, pp. 2856-2864, 2012.
- [47] H. Kawasaki *et al.*, "Functionalized pyrolytic highly oriented graphite polymer film for surface-assisted laser desorption/ionization mass spectrometry in environmental analysis," *Rapid Communications in Mass Spectrometry*, vol. 23, no. 20, pp. 3323-3332, 2009.

- [48] H. Kawasaki, Y. Shimomae, T. Watanabe, and R. Arakawa, "Desorption/ionization on porous silicon mass spectrometry (DIOS-MS) of perfluorooctane sulfonate (PFOS)," *Colloids and Surfaces A: Physicochemical and Engineering Aspects*, vol. 347, no. 1-3, pp. 220-224, 2009.
- [49] D. Cao *et al.*, "Quantitative detection of trace perfluorinated compounds in environmental water samples by Matrix-assisted Laser Desorption/Ionization-Time of Flight Mass Spectrometry with 1, 8-bis (tetramethylguanidino)-naphthalene as matrix," *Talanta*, vol. 85, no. 1, pp. 345-352, 2011.
- [50] J. E. Naile *et al.*, "Perfluorinated compounds in water, sediment, soil and biota from estuarine and coastal areas of Korea," *Environmental Pollution*, vol. 158, no. 5, pp. 1237-1244, 2010.
- [51] K. Senthilkumar, E. Ohi, K. Sajwan, T. Takasuga, and K. Kannan, "Perfluorinated compounds in river water, river sediment, market fish, and wildlife samples from Japan," *Bulletin of Environmental Contamination and Toxicology*, vol. 79, no. 4, pp. 427-431, 2007.
- [52] K. Wille *et al.*, "A validated analytical method for the determination of perfluorinated compounds in surface-, sea- and sewagewater using liquid chromatography coupled to time-of-flight mass spectrometry," *Journal of Chromatography A*, vol. 1217, no. 43, pp. 6616-6622, 2010.
- [53] C. L. Tseng, L. L. Liu, C. M. Chen, and W. H. Ding, "Analysis of perfluorooctanesulfonate and related fluorochemicals in water and biological tissue samples by liquid chromatography-ion trap mass spectrometry," *Journal of Chromatography A*, vol. 1105, no. 1-2, pp. 119-126, 2006.
- [54] B. Boulanger, J. Vargo, J. L. Schnoor, and K. C. Hornbuckle, "Detection of perfluorooctane surfactants in Great Lakes water," *Environmental Science & Technology*, vol. 38, no. 15, pp. 4064-4070, 2004.
- [55] A. Chauhan, M. K. Goyal, and P. Chauhan, "GC-MS technique and its analytical applications in science and technology," *Journal of Analytical and Bioanalytical Technology*, vol. 5, no. 6, p. 222, 2014.
- [56] D. J. Torres. (2019, 17.01.2019). *To Run or to Fly: A Comparison Between HPLC and GC*. Available: <https://bitesizebio.com/29109/run-fly-comparison-hplc-gc/>
- [57] K. L. Lynch, "Toxicology: Liquid Chromatography Mass Spectrometry," in *Mass Spectrometry for the Clinical Laboratory*: Elsevier, 2017, pp. 109-130.
- [58] P. Chaimbault, "The Modern Art of Identification of Natural Substances in Whole Plants," in *Recent Advances in Redox Active Plant and Microbial Products*: Springer, 2014, pp. 31-94.

- [59] C. Dass, *Fundamentals of contemporary mass spectrometry*. John Wiley & Sons, 2007.
- [60] R. S. Plumb, C. L. Stumpf, J. H. Granger, J. Castro-Perez, J. N. Haselden, and G. J. Dear, "Use of liquid chromatography/time-of-flight mass spectrometry and multivariate statistical analysis shows promise for the detection of drug metabolites in biological fluids," *Rapid Communications in Mass Spectrometry*, vol. 17, no. 23, pp. 2632-2638, 2003.
- [61] I. Ferrer and E. M. Thurman, "Multi-residue method for the analysis of 101 pesticides and their degradates in food and water samples by liquid chromatography/time-of-flight mass spectrometry," *Journal of Chromatography A*, vol. 1175, no. 1, pp. 24-37, 2007.
- [62] T. Kowalska and J. Sherma, *Preparative layer chromatography*. CRC Press, 2006.
- [63] C. J. McMurdo, D. A. Ellis, E. Webster, J. Butler, R. D. Christensen, and L. K. Reid, "Aerosol enrichment of the surfactant PFO and mediation of the water– air transport of gaseous PFOA," *Environmental Science & Technology*, vol. 42, no. 11, pp. 3969-3974, 2008.
- [64] C. Fang, X. Zhang, Z. Dong, L. Wang, M. Megharaj, and R. Naidu, "Smartphone app-based/portable sensor for the detection of fluoro-surfactant PFOA," *Chemosphere*, vol. 191, pp. 381-388, 2018.
- [65] N. Cennamo *et al.*, "A Molecularly Imprinted Polymer on a Plasmonic Plastic Optical Fiber to detect perfluorinated compounds in water," *Sensors*, vol. 18, no. 6, p. 1836, 2018.
- [66] J. T. Watson and O. D. Sparkman, *Introduction to Mass Spectrometry: Instrumentation, Applications, and Strategies for Data Interpretation*. John Wiley & Sons, 2007.
- [67] A. El Aneed, A. Cohen, and J. Banoub, "Mass spectrometry, review of the basics: electrospray, MALDI, and commonly used mass analyzers," *Applied Spectroscopy Reviews*, vol. 44, no. 3, pp. 210-230, 2009.
- [68] X. Zhao, J. Li, Y. Shi, Y. Cai, S. Mou, and G. Jiang, "Determination of perfluorinated compounds in wastewater and river water samples by mixed hemimicelle-based solid-phase extraction before liquid chromatography– electrospray tandem mass spectrometry detection," *Journal of Chromatography A*, vol. 1154, no. 1-2, pp. 52-59, 2007.
- [69] K. T. V. Grattan and T. Sun, "Fiber optic sensor technology: an overview," *Sensors and Actuators A: Physical*, vol. 82, no. 1-3, pp. 40-61, 2000.

- [70] B. Lee, S. Roh, and J. Park, "Current status of micro- and nano-structured optical fiber sensors," *Optical Fiber Technology*, vol. 15, no. 3, pp. 209-221, 2009.
- [71] M. Bosch, A. Sánchez, F. Rojas, and C. Ojeda, "Recent development in optical fiber biosensors," *Sensors*, vol. 7, no. 6, pp. 797-859, 2007.
- [72] H. Xai *et al.*, "Fiber optic sensor for detecting multiple parameters in a harsh environment," 2008.
- [73] S. J. Mihailov, "Fiber Bragg grating sensors for harsh environments," *Sensors*, vol. 12, no. 2, pp. 1898-1918, 2012.
- [74] K. Chan, H. Ito, H. Inaba, and T. Furuya, "10 km-long fibre-optic remote sensing of CH<sub>4</sub> gas by near infrared absorption," *Applied Physics B*, vol. 38, no. 1, pp. 11-15, 1985.
- [75] H. Naruse *et al.*, "Application of a distributed fibre optic strain sensing system to monitoring changes in the state of an underground mine," *Measurement Science and Technology*, vol. 18, no. 10, p. 3202, 2007.
- [76] S. Großwig, E. Hurtig, and K. Kühn, "Fibre optic temperature sensing: A new tool for temperature measurements in boreholes," *Geophysics*, vol. 61, no. 4, pp. 1065-1067, 1996.
- [77] M. Majumder, T. K. Gangopadhyay, A. K. Chakraborty, K. Dasgupta, and D. K. Bhattacharya, "Fibre Bragg gratings in structural health monitoring—Present status and applications," *Sensors and Actuators A: Physical*, vol. 147, no. 1, pp. 150-164, 2008.
- [78] S. M. Barnard and D. R. Walt, "A fibre-optic chemical sensor with discrete sensing sites," *Nature*, vol. 353, no. 6342, p. 338, 1991.
- [79] J. Liu, Y. Sun, and X. Fan, "Highly versatile fiber-based optical Fabry-Pérot gas sensor," *Optics Express*, vol. 17, no. 4, pp. 2731-2738, 2009.
- [80] C. Fang, Z. Chen, M. Megharaj, and R. Naidu, "Potentiometric detection of AFFFs based on MIP," *Environmental Technology & Innovation*, vol. 5, pp. 52-59, 2016.
- [81] N. Cennamo, L. Zeni, G. D. Agostino, G. Porto, and A. Biasiolo, "Optical chemical fiber sensor for the detection of perfluorinated compounds in water," in *2018 IEEE International Instrumentation and Measurement Technology Conference (I2MTC)*, 2018, pp. 1-5.
- [82] Resinex. (2019, 15.11.2018). *PVDF Kynar and Kynar Flex*. Available: <http://www.resinex.co.uk/products/kynar.html>

- [83] M. Tao, F. Liu, B. Ma, and L. Xue, "Effect of solvent power on PVDF membrane polymorphism during phase inversion," *Desalination*, vol. 316, pp. 137-145, 2013.
- [84] M. Batumalay, A. Lokman, F. Ahmad, H. Arof, H. Ahmad, and S. W. Harun, "Tapered plastic optical fiber coated with HEC/PVDF for measurement of relative humidity," *IEEE Sensors Journal*, vol. 13, no. 12, pp. 4702-4705, 2013.
- [85] P. C. Beard, A. Hurrell, E. Van Den Elzen, and T. N. Mills, "Comparison of a miniature, ultrasonic, optical fibre hydrophone with PVDF hydrophone technology," in *1998 IEEE Ultrasonics Symposium. Proceedings (Cat. No. 98CH36102)*, 1998, vol. 2, pp. 1881-1884: IEEE.
- [86] C. Pohlmann, "Visible light communication," in *Seminar Kommunikationsstandards in der Medizintechnik*, 2010, pp. 1-14.
- [87] C. H. Sterling, *Military Communications: From Ancient Times to the 21st Century*. Abc-clio, 2008.
- [88] N. Jones. (1937, 29.11.2019). *First'Radio'Built by San Diego Resident Partner of Inventor of Telephone: Keeps Notebook of Experiences With Bell, San Diego Evening Tribune, July 31, 1937*. Available: <http://www.aes-media.org/historical/html/recording.technology.history/images/PDRM0447d.jpg>
- [89] D. F. Welch, "A brief history of high-power semiconductor lasers," *IEEE Journal of Selected Topics in Quantum Electronics*, vol. 6, no. 6, pp. 1470-1477, 2000.
- [90] Vivek Alwayn. (05.05.2018). *Fiber-optic technologies*. Available: <http://www.ciscopress.com/articles/article.asp?p=170740>
- [91] D. Keck and P. Schultz, "Method of producing optical waveguide fibers," 1973.
- [92] P. M. Becker, A. A. Olsson, and J. R. Simpson, *Erbium-doped fiber amplifiers: fundamentals and technology*. Elsevier, 1999.
- [93] K. Kawano and T. Kitoh, *Introduction to Optical Waveguide Analysis*. Wiley Online Library, 2004.
- [94] The Fiber Optic Association. (2016, 29.11.2016). *Optical Fiber*. Available: <http://www.thefoa.org/tech/ref/basic/fiber.html>
- [95] G. Keiser, F. Xiong, Y. Cui, and P. P. Shum, "Review of diverse optical fibers used in biomedical research and clinical practice," *Journal of Biomedical Optics*, vol. 19, no. 8, p. 080902, 2014.
- [96] B. Mellish. (2019, 29.11.2016). *Single mode optical fiber*. Available: [https://commons.wikimedia.org/wiki/File:Singlemode\\_fibre\\_structure.svg](https://commons.wikimedia.org/wiki/File:Singlemode_fibre_structure.svg)

- [97] A. W. Snyder and J. Love, *Optical Waveguide Theory*. Springer Science & Business Media, 2012.
- [98] Newport. (2016, 29.11.2016). *Fiber Optics: Fiber Basics*. Available: [https://www.newport.com/medias/sys\\_master/images/images/hd5/ha2/8797095919646/Fiber-Basics.pdf](https://www.newport.com/medias/sys_master/images/images/hd5/ha2/8797095919646/Fiber-Basics.pdf)
- [99] W. Blanc *et al.*, "Fabrication of Rare Earth-Doped Transparent Glass Ceramic Optical Fibers by Modified Chemical Vapor Deposition," *Journal of the American Ceramic Society*, vol. 94, no. 8, pp. 2315-2318, 2011.
- [100] P. Peterka *et al.*, "Thulium-Doped Silica-Based Optical Fibers for Cladding-Pumped Fiber Amplifiers," *Optical Materials*, vol. 30, no. 1, pp. 174-176, 2007.
- [101] W. Blanc and B. Dussardier, "Formation and Applications of Nanoparticles in Silica Optical Fibers," *Journal of Optics*, vol. 45, no. 3, pp. 247-254, 2016.
- [102] G. P. Agrawal, *Fiber-optic communication systems*. John Wiley & Sons, 2012.
- [103] M. Blankenship and C. Deneka, "The outside vapor deposition method of fabricating optical waveguide fibers," *IEEE journal of Quantum Electronics*, vol. 18, no. 10, pp. 1418-1423, 1982.
- [104] C. K. Suzuki and D. Torikai, "Vitreous silica processing by vapor phase deposition for optical fiber preform," *Radiation Effects and Defects in Solids*, vol. 147, no. 1-2, pp. 55-63, 1998.
- [105] P. Geittner, D. Küppers, and H. Lydtin, "Low-loss optical fibers prepared by plasma-activated chemical vapor deposition (CVD)," *Applied Physics Letters*, vol. 28, no. 11, pp. 645-646, 1976.
- [106] R P Photonics Encyclopedia. (2019, 06.08.2019). *Fibre Fabrication*. Available: [https://www.rp-photonics.com/fiber\\_fabrication.html](https://www.rp-photonics.com/fiber_fabrication.html)
- [107] FIS The Solutionists. (2018, 18.06.2018). *How Fiber Optics Are Made?* Available: <http://www.fiberinstrumentsales.com/blog/how-fiber-optics-are-made>
- [108] How Products are Made. (2019, 24.10.2019). *Optical Fiber*. Available: <http://www.madehow.com/Volume-1/Optical-Fiber.html>
- [109] S. R. Nagel, J. B. MacChesney, and K. L. Walker, "An overview of the modified chemical vapor deposition (MCVD) process and performance," *IEEE Transactions on Microwave Theory and Techniques*, vol. 30, no. 4, pp. 305-322, 1982.
- [110] J. Hecht and L. Long, *Understanding Fiber Optics*. Prentice Hall, 1993.
- [111] R. C. Dorf, *Broadcasting and Optical Communication Technology*. CRC Press, 2006.

- [112] Y. J. Rao, D. J. Webb, D. A. Jackson, L. Zhang, and I. Bennion, "In-fiber Bragg-grating temperature sensor system for medical applications," *Journal of Lightwave Technology*, vol. 15, no. 5, pp. 779-785, 1997.
- [113] J. L. Gehrich *et al.*, "Optical fluorescence and its application to an intravascular blood gas monitoring system," *IEEE Transactions on Biomedical Engineering*, no. 2, pp. 117-132, 1986.
- [114] M. Epstein, "Fiber optics in medicine," *Critical Reviews in Biomedical Engineering*, vol. 7, no. 2, pp. 79-120, 1982.
- [115] B. P. Pal, *Fundamentals of Fibre Optics in Telecommunication and Sensor Systems*. Bohem press, 1992.
- [116] D. Singleton, G. Paraskevopoulos, R. Taylor, and L. Higginson, "Excimer laser angioplasty: Tissue ablation, arterial response, and fiber optic delivery," *IEEE Journal of Quantum Electronics*, vol. 23, no. 10, pp. 1772-1782, 1987.
- [117] G. Rajan, *Optical fiber sensors: advanced techniques and applications*. CRC press, 2015.
- [118] K. T. V. Grattan and B. T. Meggitt, *Optical Fiber Sensor Technology*. Springer, 1995.
- [119] M. N. O. Sadiku, *Optical and Wireless Communications: Next Generation Networks*. CRC Press, 2018.
- [120] S. Yin and P. Ruffin, "Fiber Optic Sensors," *Wiley Encyclopedia of Biomedical Engineering*, 2006.
- [121] B. Lee, "Review of the Present Status of Optical Fiber Sensors," *Optical Fiber Technology*, vol. 9, no. 2, pp. 57-79, 2003.
- [122] B. E. Jones, "Optical Fibre Sensors and Systems For Industry," *Journal of Physics E: Scientific Instruments*, vol. 18, no. 9, p. 770, 1985.
- [123] D. T. O. Joseph F. Benzoni. Military Applications of Fiber Optics Technology [Online]. Available: <http://www.dtic.mil/dtic/tr/fulltext/u2/a223825.pdf>
- [124] J. H. Ressia and J. L. Peck, "Fiber optics demonstrated use in space vehicles," in *Recent Advances in Space Technologies*, 2003, pp. 321-324: IEEE.
- [125] A. H. Hartog, *An Introduction to Distributed Optical Fibre Sensors*. CRC Press, 2017.
- [126] D. A. Krohn, T. M. Dougall, and A. Mendez, *Fiber Optic Sensors: Fundamentals and Applications*. SPIE Press Bellingham, Wa, 2014.

- [127] U. Roland, C. P. Renschen, D. Lippik, F. Stallmach, and F. Holzer, "A new fiber optical thermometer and its application for process control in strong electric, magnetic, and electromagnetic fields," *Sensor Letters*, vol. 1, no. 1, pp. 93-98, // 2003.
- [128] T. K. Gangopadhyay, "Non-Contact Vibration Measurement Based on an Extrinsic Fabry–Perot Interferometer Implemented using Arrays of Single-Mode Fibres," *Measurement Science and Technology*, vol. 15, no. 5, p. 911, 2004.
- [129] N. Furstenuau, M. Schmidt, H. Horack, W. Goetze, and W. Schmidt, "Extrinsic Fabry-Perot Interferometer Vibration and Acoustic Sensor Systems for Airport Ground Traffic Monitoring," *IEEE Proceedings- Optoelectronics*, vol. 144, no. 3, pp. 134-144, 1997.
- [130] K. Böhm, P. Marten, E. Weidel, and K. Petermann, "Direct Rotation-Rate Detection with a Fibre-Optic Gyro by using Digital Data Processing," *Electronics Letters*, vol. 19, no. 23, pp. 997-999, 1983.
- [131] D. I. Forsyth, S. A. Wade, T. Sun, X. Chen, and K. T. V. Grattan, "Dual Temperature and Strain Measurement with the Combined Fluorescence Lifetime and Bragg Wavelength Shift Approach in Doped Optical Fiber," *Applied optics*, vol. 41, no. 31, pp. 6585-6592, 2002.
- [132] J. Mandal, S. Pal, T. Sun, K. T. V. Grattan, A. T. Augousti, and S. A. Wade, "Bragg grating-based fiber-optic laser probe for temperature sensing," *IEEE Photonics Technology Letters*, vol. 16, no. 1, pp. 218-220, 2004.
- [133] S. Poeggel *et al.*, "Recent Improvement of Medical Optical Fibre Pressure and Temperature Sensors," *Biosensors*, vol. 5, no. 3, pp. 432-449, 2015.
- [134] D. H. Kang and H. W. Kang, "Surface energy characteristics of zeolite embedded PVDF nanofiber films with electrospinning process," *Applied Surface Science*, vol. 387, pp. 82-88, 2016/11/30/ 2016.
- [135] P. M. Tracey, "Intrinsic fiber-optic sensors," *IEEE Transactions on Industry Applications*, vol. 27, no. 1, pp. 96-98, 1991.
- [136] K. A. Fidanboylu and H. S. Efendioglu, "Fiber optic sensors and their applications," in *5th International Advanced Technologies Symposium (IATS'09)*, 2009, vol. 6.
- [137] S. M. John, "Evanescent wave fibre optic sensors: Design, fabrication and characterization," PhD Dissertation, Cochin University of Science & Technology, India, 2000.
- [138] A. Barrias, J. R. Casas, and S. Villalba, "A review of distributed optical fiber sensors for civil engineering applications," *Sensors*, vol. 16, no. 5, p. 748, 2016.

- [139] M. Nazari, "Nano-structured films on optical fibres as chemical sensors and actuators," PhD Dissertation, Victoria University, 2015.
- [140] O. S. Wolfbeis, "Fiber-optic chemical sensors and biosensors," *Analytical Chemistry*, vol. 80, no. 12, pp. 4269-4283, 2008.
- [141] X. D. Wang and O. S. Wolfbeis, "Fiber-optic chemical sensors and biosensors (2008–2012)," *Analytical Chemistry*, vol. 85, no. 2, pp. 487-508, 2012.
- [142] Water Quality Association. (2017, 17.12.2017). *Common Waterborne Contaminants*. Available: <https://www.wqa.org/learn-about-water/common-contaminants>
- [143] S. P. Kumar, T. S. Lee, C. P. G. Vallabhan, V. P. N. Nampoori, and P. Radhakrishnan, "Design and development of an LED based fiber optic evanescent wave sensor for simultaneous detection of chromium and nitrite traces in water," *Optics Communications*, vol. 214, no. 1, pp. 25-30, 2002/12/15/ 2002.
- [144] R. Verma and B. D. Gupta, "Detection of heavy metal ions in contaminated water by surface plasmon resonance based optical fibre sensor using conducting polymer and chitosan," *Food Chemistry*, vol. 166, no. Supplement C, pp. 568-575, 2015/01/01/ 2015.
- [145] Q. Wu and E. V. Anslyn, "Catalytic signal amplification using a heck reaction. An example in the fluorescence sensing of Cu (II)," *Journal of the American Chemical Society*, vol. 126, no. 45, pp. 14682-14683, 2004.
- [146] S. C. Warren Smith, S. Heng, H. Ebendorff Heidepriem, A. D. Abell, and T. M. Monroe, "Fluorescence-based aluminum ion sensing using a surface-functionalized microstructured optical fiber," *Langmuir*, vol. 27, no. 9, pp. 5680-5685, 2011.
- [147] Z. Zhujun and W. R. Seitz, "A Fluorescent Sensor For Aluminum(III), Magnesium(II), Zinc(II) And Cadmium(II) Based on Electrostatically Immobilized Quinolin-8-ol Sulfonate," *Analytica Chimica Acta*, vol. 171, no. Supplement C, pp. 251-258, 1985/05/01/ 1985.
- [148] R. Krska, K. Taga, and R. Kellner, "New IR fiber-optic chemical sensor for in situ measurements of chlorinated hydrocarbons in water," *Applied Spectroscopy*, vol. 47, no. 9, pp. 1484-1487, 1993/09/01 1993.
- [149] W. Cao and Y. Duan, "Optical fiber-based evanescent ammonia sensor," *Sensors and Actuators B: Chemical*, vol. 110, no. 2, pp. 252-259, 2005/10/14/ 2005.
- [150] S. K. Mishra, S. N. Tripathi, V. Choudhary, and B. D. Gupta, "SPR based fibre optic ammonia gas sensor utilizing nanocomposite film of PMMA/reduced

- graphene oxide prepared by in situ polymerization," *Sensors and Actuators B: Chemical*, vol. 199, no. Supplement C, pp. 190-200, 2014/08/01/ 2014.
- [151] O. S. Wolfbeis and H. E. Posch, "Fibre-optic fluorescing sensor for ammonia," *Analytica Chimica Acta*, vol. 185, no. Supplement C, pp. 321-327, 1986/01/01/ 1986.
- [152] F. Sidirolglou and T. Nguyen, "Synthesis of chitosan films on optical fibers for detection of ammonia vapors," in *Quantum Electronics Conference & Lasers and Electro-Optics (CLEO/IQEC/PACIFIC RIM), 2011*, 2011, pp. 1742-1744: IEEE.
- [153] R. Raghunandhan *et al.*, "Chitosan/PAA based fiber-optic interferometric sensor for heavy metal ions detection," *Sensors and Actuators B: Chemical*, vol. 233, pp. 31-38, 2016.
- [154] Y. J. Rao, "Recent progress in fiber-optic extrinsic Fabry–Perot interferometric sensors," *Optical Fiber Technology*, vol. 12, no. 3, pp. 227-237, 2006.
- [155] T. Yoshino, K. Kurosawa, K. Itoh, and T. Ose, "Fiber-optic Fabry-Perot interferometer and its sensor applications," *IEEE Transactions on Microwave Theory and Techniques*, vol. 30, no. 10, pp. 1612-1621, 1982.
- [156] M. R. Islam, M. M. Ali, M. H. Lai, K. S. Lim, and H. Ahmad, "Chronology of Fabry-Perot interferometer fiber-optic sensors and their applications: A review," *Sensors*, vol. 14, no. 4, pp. 7451-7488, 2014.
- [157] S. M. Tseng and C. L. Chen, "Optical fiber fabry-perot sensors," *Applied Optics*, vol. 27, no. 3, pp. 547-551, 1988.
- [158] M. G. Kim, J. Park, S. W. Kang, and B. K. Sohn, "Fiber optic Fabry-Perot pressure sensor with the Si<sub>3</sub>N<sub>4</sub>/SiO<sub>2</sub>/Si<sub>3</sub>N<sub>4</sub> diaphragm fabricated using micromachining technology," in *Smart Electronics and MEMS*, 1997, vol. 3242, pp. 347-354: International Society for Optics and Photonics.
- [159] L. H. Chen, C. C. Chan, W. Yuan, S. K. Goh, and J. Sun, "High performance chitosan diaphragm-based fiber-optic acoustic sensor," *Sensors and Actuators A: Physical*, vol. 163, no. 1, pp. 42-47, 2010/09/01/ 2010.
- [160] Y. J. Rao, Z. L. Ran, and Y. Gong, *Fiber-Optic Fabry-Perot Sensors: An Introduction*. CRC Press, 2017.
- [161] A. Perot and C. Fabry, "On the application of interference phenomena to the solution of various problems of spectroscopy and metrology," *The Astrophysical Journal*, vol. 9, p. 87, 1899.

- [162] J. J. Alcoz, C. Lee, and H. F. Taylor, "Embedded fiber-optic Fabry-Perot ultrasound sensor," *IEEE Transactions on Ultrasonics, Ferroelectrics, and Frequency Control*, vol. 37, no. 4, pp. 302-306, 1990.
- [163] F. J. Arregui, Y. Liu, I. R. Matias, and R. O. Claus, "Optical fiber humidity sensor using a nano Fabry-Perot cavity formed by the ionic self-assembly method," *Sensors and Actuators B: Chemical*, vol. 59, no. 1, pp. 54-59, 1999.
- [164] J. G. Vos, R. J. Forster, and T. E. Keyes, *Interfacial Supramolecular Assemblies*. John Wiley & Sons, 2003.
- [165] J. C. Love, L. A. Estroff, J. K. Kriebel, R. G. Nuzzo, and G. M. Whitesides, "Self-assembled monolayers of thiolates on metals as a form of nanotechnology," *Chemical Reviews*, vol. 105, no. 4, pp. 1103-1170, 2005.
- [166] M. Erwin, "Optical fiber coated with Nafion thin film for humidity sensing," in *11th Integrated Optics - Sensors, Sensing Structures and Methods*, 2016, vol. 10034, p. 6: SPIE.
- [167] T. Pustelny, E. Maciak, Z. Opilski, and M. Bednorz, "Optical interferometric structures for application in gas sensors," *Optica Applicata*, vol. 37, 2007.
- [168] L. H. Chen *et al.*, "Chitosan based fiber-optic Fabry-Perot humidity sensor," *Sensors and Actuators B: Chemical*, vol. 169, pp. 167-172, 2012.
- [169] D. Galbarra, F. J. Arregui, I. R. Matias, and R. O. Claus, "Ammonia optical fiber sensor based on self-assembled zirconia thin films," *Smart Materials and Structures*, vol. 14, no. 4, p. 739, 2005.
- [170] R. Weiser and G. L. Ross, "Teflon and human health: Do the charges stick?," in "Assessing the Safety of PFOA," 2005.
- [171] A. Volker. (2018, 27.08.2019). *Fabrication of Polymer Membranes*. Available: [https://iupac.org/cms/wp-content/uploads/2018/06/IUPAC\\_PolymEdu\\_EduWorkshop2018\\_PPT\\_VolkerAbetz.pdf](https://iupac.org/cms/wp-content/uploads/2018/06/IUPAC_PolymEdu_EduWorkshop2018_PPT_VolkerAbetz.pdf)
- [172] A. Salimi and A. A. Yousefi, "Conformational changes and phase transformation mechanisms in PVDF solution-cast films," *Journal of Polymer Science Part B: Polymer Physics*, vol. 42, no. 18, pp. 3487-3495, 2004.
- [173] R. Takayama, Y. Tomita, J. Asayama, K. Nomura, and H. Ogawa, "Pyroelectric infrared array sensors made of c-axis-oriented La-modified PbTiO<sub>3</sub> thin films," *Sensors and Actuators A: Physical*, vol. 22, no. 1-3, pp. 508-512, 1990.
- [174] A. Hossain and M. H. Rashid, "Pyroelectric detectors and their applications," *IEEE Transactions on Industry Applications*, vol. 27, no. 5, pp. 824-829, 1991.

- [175] C. R. Zamarreno, I. R. Matias, and F. J. Arregui, "Nanofabrication Techniques Applied to the Development of Novel Optical Fiber Sensors Based on Nanostructured Coatings," *IEEE Sensors Journal*, vol. 12, no. 8, pp. 2699-2710, 2012.
- [176] D. J. Lin, H. H. Chang, T. C. Chen, Y. C. Lee, and L. P. Cheng, "Formation of porous poly(vinylidene fluoride) membranes with symmetric or asymmetric morphology by immersion precipitation in the water/TEP/PVDF system," *European Polymer Journal*, vol. 42, no. 7, pp. 1581-1594, 7// 2006.
- [177] D. J. Lin, C. L. Chang, C. L. Chang, T. C. Chen, and L. P. Cheng, "Fine structure of poly(vinylidene fluoride) membranes prepared by phase inversion from a water/N-methyl-2-pyrrolidone/poly(vinylidene fluoride) system," *Journal of Polymer Science Part B: Polymer Physics*, vol. 42, no. 5, pp. 830-842, 2004.
- [178] L. P. Cheng, "Effect of temperature on the formation of microporous PVDF membranes by precipitation from 1-Octanol/DMF/PVDF and water/DMF/PVDF systems," *Macromolecules*, vol. 32, no. 20, pp. 6668-6674, 1999/10/01 1999.
- [179] T. H. Young, L. P. Cheng, W. M. You, and L. Y. Chen, "Prediction of EVAL membrane morphologies using the phase diagram of water–DMSO–EVAL at different temperatures," *Polymer*, vol. 40, no. 9, pp. 2189-2195, 4// 1999.
- [180] A. M. W. Bulte, M. H. V. Mulder, C. A. Smolders, and H. Strathmann, "Diffusion induced phase separation with crystallizable nylons. II. Relation to final membrane morphology," *Journal of Membrane Science*, vol. 121, no. 1, pp. 51-58, 1996/11/27 1996.
- [181] Y. W. Kho, D. S. Kalika, and B. L. Knutson, "Precipitation of Nylon 6 membranes using compressed carbon dioxide," *Polymer*, vol. 42, no. 14, pp. 6119-6127, 6// 2001.
- [182] W. Ma, J. Zhang, S. Chen, and X. Wang, "Crystalline phase formation of poly (vinylidene fluoride) from tetrahydrofuran/n, n-dimethylformamide mixed solutions," *Journal of Macromolecular Science, Part B: Physics*, vol. 47, no. 3, pp. 434-449, 2008.
- [183] W. Ma, J. Zhang, and X. Wang, "Formation of poly (vinylidene fluoride) crystalline phases from tetrahydrofuran/N, N-dimethylformamide mixed solvent," *Journal of Materials Science*, vol. 43, no. 1, pp. 398-401, 2008.
- [184] X. Zhao, J. Cheng, S. Chen, J. Zhang, and X. Wang, "Controlled crystallization of poly (vinylidene fluoride) chains from mixed solvents composed of its good solvent and nonsolvent," *Journal of Polymer Science Part B: Polymer Physics*, vol. 48, no. 5, pp. 575-581, 2010.

- [185] G. Mago, D. M. Kalyon, and F. T. Fisher, "Membranes of polyvinylidene fluoride and PVDF nanocomposites with carbon nanotubes via immersion precipitation," *Journal of Nanomaterials*, vol. 2008, p. 17, 2008.
- [186] Polyflour. (2019, 12.03.2018). *PVDF*. Available: <http://www.polyflour.nl/en/materials/pvdf/>
- [187] Porex Filtration Group. (2018, 12.03.2018). *Polyvinylidene Fluoride*. Available: <http://www.porex.com/technologies/materials/porous-plastics/polyvinylidene-fluoride/>
- [188] M. Buonomenna, P. Macchi, M. Davoli, and E. Drioli, "Poly (vinylidene fluoride) membranes by phase inversion: the role the casting and coagulation conditions play in their morphology, crystalline structure and properties," *European Polymer Journal*, vol. 43, no. 4, pp. 1557-1572, 2007.
- [189] C. Y. Kuo, H. N. Lin, H. A. Tsai, D. M. Wang, and J. Y. Lai, "Fabrication of a high hydrophobic PVDF membrane via nonsolvent induced phase separation," *Desalination*, vol. 233, no. 1, pp. 40-47, 2008.
- [190] Y. M. Zheng, S. W. Zou, K. G. N. Nanayakkara, T. Matsuura, and J. P. Chen, "Adsorptive removal of arsenic from aqueous solution by a PVDF/zirconia blend flat sheet membrane," *Journal of Membrane Science*, vol. 374, no. 1, pp. 1-11, 2011.
- [191] N. Lundquist *et al.*, "Polymer supported carbon for safe and effective remediation of PFOA-and PFOS-contaminated water," *ACS Sustainable Chemistry & Engineering*, 2019.
- [192] I. Ross *et al.*, "A review of emerging technologies for remediation of PFASs," *Remediation Journal*, vol. 28, no. 2, pp. 101-126, 2018.
- [193] CHROMacademy. (2018, 12.11.2018). *Mass spectrometry, fundamental LC-MS introduction*. Available: <http://www.ecs.umass.edu/eve/background/methods/chemical/Openlit/Chromacademy%20LCMS%20Intro.pdf>
- [194] National High Magnetic Field Laboratory. (2014, 12.11.2018). *Atmospheric Pressure Photoionization (APPI)*. Available: <https://nationalmaglab.org/user-facilities/icr/techniques/appi>
- [195] Emory College of Arts and Sciences. (2017, 14.11.2018). *Mass Spectrometry Ionization Methods*. Available: <http://chemistry.emory.edu/msc/tutorial/mass-spectrometry-ionization.html>
- [196] K. Blaum, "High-accuracy mass spectrometry with stored ions," *Physics Reports*, vol. 425, no. 1, pp. 1-78, 2006.

- [197] D. J. Douglas, A. J. Frank, and D. Mao, "Linear ion traps in mass spectrometry," *Mass Spectrometry Reviews*, vol. 24, no. 1, pp. 1-29, 2005.
- [198] K. H. Kingdon, "A method for the neutralization of electron space charge by positive ionization at very low gas pressures," *Physical Review*, vol. 21, no. 4, p. 408, 1923.
- [199] J. H. Gross, *Mass spectrometry: a textbook*. Springer Science & Business Media, 2006.
- [200] G. Siuzdak, *Mass Spectrometry for Biotechnology*. Elsevier, 1996.
- [201] J. F. Van Bocxlaer, K. M. Clauwaert, W. E. Lambert, D. L. Deforce, E. G. Van den Eeckhout, and A. P. De Leenheer, "Liquid chromatography—mass spectrometry in forensic toxicology," *Mass Spectrometry Reviews*, vol. 19, no. 4, pp. 165-214, 2000.
- [202] Thermo Nicolet. (2001, 22.09.2017). *Introduction to fourier transform infrared spectrometry*. Available: <https://www.chem.uci.edu/~dmitryf/manuals/Fundamentals/FTIR%20principles.pdf>
- [203] Solvay. (2019, 18.01.2019). *Solef 1015 Technical Data Sheet*. Available: <http://catalog.ides.com/datasheet.aspx?I=42041&FMT=PDF&E=111428>
- [204] S. Trpkovski, "Temperature and Strain Sensing using Rare Earth Fluorescence and Bragg Gratings in Optical Fibres " PhD Dissertation, Electrical Engineering Victoria University, Australia, 2005.
- [205] D. C. Pham *et al.*, "Strain-induced inverse magnetostriction measured on a single contacted Ni nanowire in a polymer matrix," *Materials Research Express*, vol. 1, no. 4, p. 045017, 2014.
- [206] J. Cheng, J. Zhang, and X. Wang, "Investigation on crystallization behavior and hydrophilicity of poly(vinylidene fluoride)/poly(methyl methacrylate)/poly(vinyl pyrrolidone) ternary blends by solution casting," *Journal of Applied Polymer Science*, vol. 127, no. 5, pp. 3997-4005, 2013.
- [207] EPA Victoria. (2017, 30.11.2017). *PFAS in Victoria*. Available: <http://www.epa.vic.gov.au/your-environment/land-and-groundwater/human-health-and-trichloroethylene-tce>
- [208] C. Kunacheva *et al.*, "Worldwide surveys of perfluorooctane sulfonate (PFOS) and perfluorooctanoic acid (PFOA) in water environment in recent years," *Water Science and Technology*, vol. 66, no. 12, pp. 2764-2771, 2012.
- [209] C. A. Moody, W. C. Kwan, J. W. Martin, D. C. Muir, and S. A. Mabury, "Determination of perfluorinated surfactants in surface water samples by two

- independent analytical techniques: liquid chromatography/tandem mass spectrometry and  $^{19}\text{F}$  NMR," *Analytical Chemistry*, vol. 73, no. 10, pp. 2200-2206, 2001.
- [210] C. A. Moody and J. A. Field, "Perfluorinated surfactants and the environmental implications of their use in fire-fighting foams," *Environmental Science & Technology*, vol. 34, no. 18, pp. 3864-3870, 2000.
- [211] X. Cai, T. Lei, D. Sun, and L. Lin, "A critical analysis of the  $\alpha$ ,  $\beta$  and  $\gamma$  phases in poly (vinylidene fluoride) using FTIR," *RSC Advances*, vol. 7, no. 25, pp. 15382-15389, 2017.
- [212] S. A. Wade, S. F. Collins, K. T. Grattan, and G. W. Baxter, "Strain-Independent Temperature Measurement by Use of A Fluorescence Intensity Ratio Technique in Optical Fiber," *Applied Optics*, vol. 39, no. 18, pp. 3050-3052, 2000.
- [213] G. W. Baxter, S. A. Wade, S. F. Collins, G. Monnom, and E. Maurice, "Rare-Earth-Doped Optical Fibers for Point Temperature Sensing," in *Doped Fiber Devices*, 1996, vol. 2841, pp. 249-256: International Society for Optics and Photonics.
- [214] F. Sidirolou, S. A. Wade, N. M. Dragomir, G. W. Baxter, and S. F. Collins, "Effects of High-Temperature Heat Treatment On Nd  $^{3+}$ -Doped Optical Fibers for use in Fluorescence Intensity Ratio Based Temperature Sensing," *Review Of Scientific Instruments*, vol. 74, no. 7, pp. 3524-3530, 2003.
- [215] S. F. Collins, G. W. Baxter, S. A. Wade, and P. M. Farrell, "Strain Dependence of Fluorescence from Rare-Earth-Doped Optical Fibres: Application to the Simultaneous, Co-Located, Measurement of Strain and Temperature," *Composite Structures*, vol. 58, no. 3, pp. 373-379, 2002.
- [216] S. Trpkovski, S. A. Wade, S. F. Collins, and G. W. Baxter, "Er $^{3+}$ : Yb $^{3+}$  Doped Fibre with Embedded FBG for Simultaneous Measurement of Temperature and Longitudinal Strain," *Measurement Science and Technology*, vol. 16, no. 2, p. 488, 2005.
- [217] J. Mandal, S. Pal, T. Sun, K. T. Grattan, A. T. Augousti, and S. A. Wade, "Bragg Grating-Based Fiber-Optic Laser Probe for Temperature Sensing," *IEEE Photonics Technology Letters*, vol. 16, no. 1, pp. 218-220, 2004.
- [218] D. A. C. Enríquez, A. R. da Cruz, and M. T. M. R. Giraldi, "Hybrid FBG-LPG sensor for surrounding refractive index and temperature simultaneous discrimination," *Optics & Laser Technology*, vol. 44, no. 4, pp. 981-986, 2012.
- [219] A. Othonos, "Fiber Bragg grating," *Review of Scientific Instruments*, Article vol. 68, no. 12, p. 4309, 1997.

- [220] V. Bhatia, "Applications of long-period gratings to single and multi-parameter sensing," *Optics express*, vol. 4, no. 11, pp. 457-466, 1999.
- [221] H. K. Bal, "Optical fibre refractive index, voltage and strain sensors: Fabrication and applications," PhD Dissertation, Victoria University, 2011.
- [222] A. Iadicicco, A. Cusano, A. Cutolo, R. Bernini, and M. Giordano, "Thinned fiber Bragg gratings as high sensitivity refractive index sensor," *IEEE Photonics Technology Letters*, vol. 16, no. 4, pp. 1149-1151, 2004.
- [223] JoVE Science Education Database. (2019, 17.09.2019). *High-Performance Liquid Chromatography (HPLC)*. Available: <https://www.jove.com/science-education/10156/high-performance-liquid-chromatography-hplc>
- [224] National Instruments. (2019, 20.03.2019). *PXIe-4844 (PXI Universal Input Module)*. Available: <http://www.ni.com/en-au/support/model.pxie-4844.html>
- [225] A. N. Chryssis, S. M. Lee, S. B. Lee, S. S. Saini, and M. Dagenais, "High sensitivity evanescent field fiber Bragg grating sensor," *IEEE Photonics Technology Letters*, vol. 17, no. 6, pp. 1253-1255, 2005.
- [226] A. H. Englert and J. Rubio, "Characterization and environmental application of a Chilean natural zeolite," *International Journal of Mineral Processing*, vol. 75, no. 1-2, pp. 21-29, 2005.
- [227] M. A. Barakat, "New trends in removing heavy metals from industrial wastewater," *Arabian Journal of Chemistry*, vol. 4, no. 4, pp. 361-377, 2011.
- [228] C. D. R. Oliveira and J. Rubio, "Adsorption of ions onto treated natural zeolite," *Materials Research*, vol. 10, no. 4, pp. 407-412, 2007.
- [229] H. Shi, F. Liu, and L. Xue, "Fabrication and characterization of antibacterial PVDF hollow fibre membrane by doping Ag-loaded zeolites," *Journal of Membrane Science*, vol. 437, pp. 205-215, 2013/06/15/ 2013.
- [230] M. Govindan, B. Zhu, M. Duke, S. Gray, and I. S. Moon, "Co<sup>3+</sup> homogeneous mediator generation efficiency in a divided tubular electrochemical reactor with MFI-type zeolite membrane," *Journal of Industrial and Engineering Chemistry*, vol. 52, pp. 28-34, 2017.
- [231] C. E. Lyman *et al.*, *Scanning electron microscopy, X-ray microanalysis, and analytical electron microscopy: a laboratory workbook*. Springer Science & Business Media, 2012.
- [232] L. Reimer, *Scanning Electron Microscopy: Physics of Image Formation and Microanalysis*. Springer, 2013.

# Appendix A

## Additional Spectral Data

Additional spectral data obtained from various trials have been provided below. The following figure shows the response of a PVDF coated fibre to different media under non-optimized conditions. The results were obtained under circumstances where the temperature was not constant and the coating chemistry was still evolving.

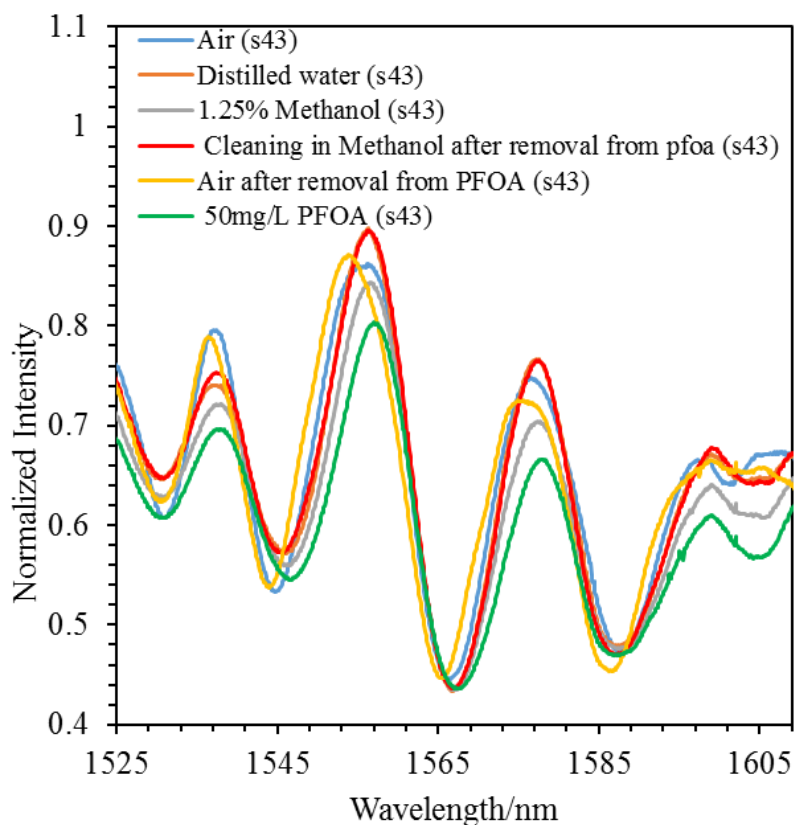
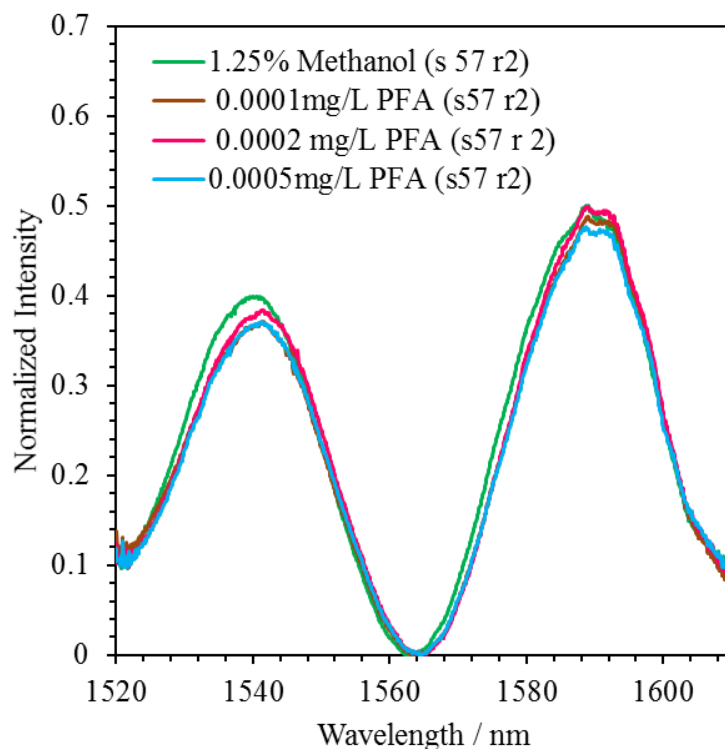
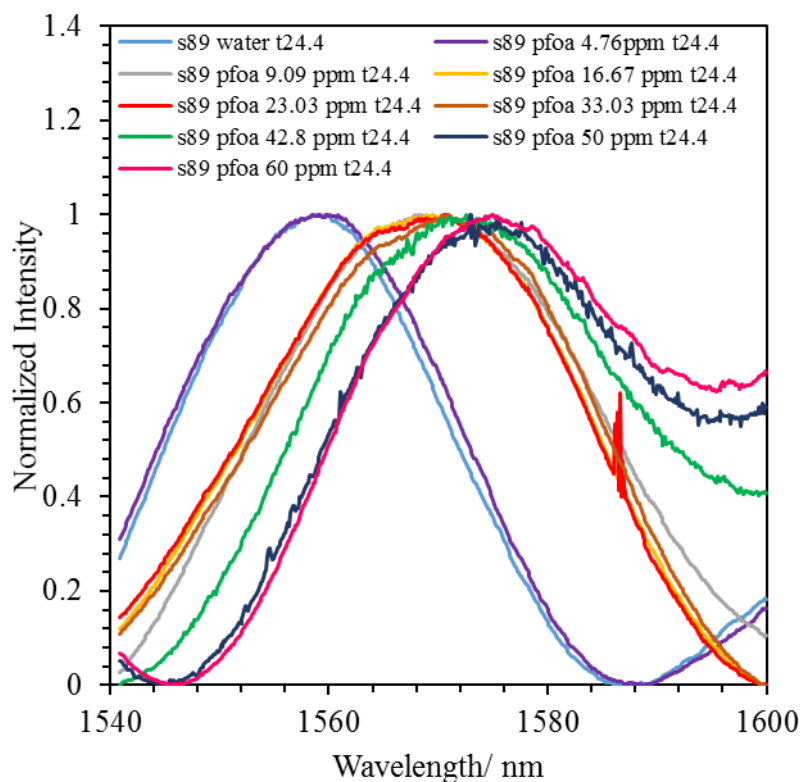


Figure 1 Response of PVDF coated fibre sample # 43 to different media under non-optimized experimental conditions.



**Figure 2 Response of PVDF coated fibre sample # 57 to PFAS wash water from fire-fighting trucks under non-optimized conditions. The use of methanol in addition to temperature variation was seen to affect sensitivity under non-optimized circumstances.**

In Figure 2 the response to PFAS wash water under non-optimized condition does not show significant changes when the concentrations are varied. There are various reasons behind this phenomenon one of which involves the impact of methanol on the polymer's sensitivity, surface structure and binding sites.



**Figure 3 Response of PVDF coated fibre sample # 89 to PFOA solutions of different concentrations at a constant temperature of 24.4 °C.**

The response of PVDF coated fibre sample #89 to PFOA under constant temperature and optimized conditions show significant changes indicated by the wavelength shift.

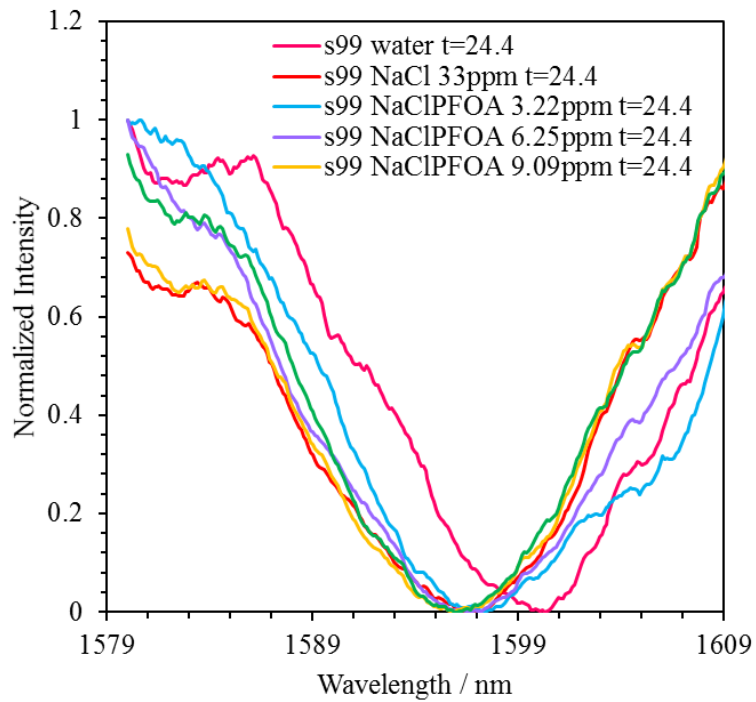


**Figure 4 Response of PVDF coated fibre sample #99 to PFOA in saline environment (i.e. in the presence of sodium chloride solution).**

Response of PVDF coated fibre sample # 99 to PFOA in saline environment under optimized conditions shows significant spectral shift. While a blue shift (lower wavelength) is observed upon addition of the NaCl solution to water, a red shift (higher wavelength) is seen to happen gradually upon subsequent addition of PFOA to the salt water.

## **Appendix B**

## Composition of PFAS Wash Water

The following table shows a list of the different perfluoroalkyl substances that were present in the wash water obtained from fire-fighting trucks. The sample tested by ALS Water (Scoresby Victoria) was prepared by adding 7 mL water to 20 mL wash water. The concentration of the diluted solution was determined by the external laboratory from which the undiluted concentration was obtained by multiplying the dilution factor as shown below.

<b>EP231A: Perfluoroalkyl Sulfonic Acids</b>	<b>ng/L</b>	<b>ug/L</b>
Perfluorobutane sulfonic acid (PFBS)	70	0.07
Perfluoropentane sulfonic acid (PFPeS)	40	0.04
Perfluorohexane sulfonic acid (PFHxS)	380	0.38
Perfluoroheptane sulfonic acid (PFHpS)	40	0.04
Perfluorooctane sulfonic acid (PFOS)	1780	1.78
<b>EP231B: Perfluoroalkyl Carboxylic Acids</b>		
Perfluorobutanoic acid (PFBA)		
Perfluoropentanoic acid (PFPeA)	30	0.03
Perfluorohexanoic acid (PFHxA)	90	0.09
Perfluorooctanoic acid (PFOA)	60	0.06
<b>EP231D: (n:2) Fluorotelomer Sulfonic Acids</b>		
6:2 Fluorotelomer sulfonic acid (6:2 FTS)	1570	1.57
8:2 Fluorotelomer sulfonic acid (8:2 FTS)	330	0.33
10:2 Fluorotelomer sulfonic acid (10:2 FTS)		
<b>EP231P: PFAS Sums</b>		
Sum of PFAS	4390	4.39
Sum of PFHxS and PFOS	2160	2.16
Sum of PFAS (WA DER List)	4310	4.31
13C4-PFOS	106%	
<b>Volume</b>	20 mL start+ 7mL= 27 mL	
<b>Dilution factor</b>	7/27= 0.26	
<b>Concentration of PFAS</b>	0.26*4.39=1.14 ug/L	